Food Structure

Volume 6 | Number 1 Article 1

1987

Food Microstructure

ISSN 0730-5419
CODEN – FMICDK
Vol. 6, No. 1, 1987

FOOD MICROSTRUCTURE

**An
International Journal
on the
Microstructure and Microanalysis
of
Foods, Feeds and their Ingredients**

Published semiannually by

Scanning Microscopy International
(Formerly Scanning Electron Microscopy, Inc.)
AMF O'Hare (Chicago), IL 60666-0507
U.S.A.

FOOD MICROSTRUCTURE

An International Journal on the Microstructure and Microanalysis of Foods, Feeds and their Ingredients

Annual Subscription Rates: U.S. $50.00 (U.S. delivery)
(including postage and handling by surface mail) U.S. $55.00 (elsewhere)

Business Communications:
Address all communications regarding subscriptions, change of address, etc. to Dr. Om Johari. (See below)

Editorial Correspondence and Inquiries:
Submit papers (see last page), news items, books for review, etc. to one of the editors or to:
Dr. Om Johari, Scanning Microscopy International
P.O. Box 66507, Chicago (AMF O'Hare), IL 60666, U.S.A.

FOOD MICROSTRUCTURE, Vol. 6 (1987), pp. 1-8
Scanning Microscopy International, Chicago (AMF O'Hare) , IL 60666 USA

0730-5419/87$3.00+.00

PRODUCT MORPHOLOGY OF FATTY PRODUCTS

I. Heertje, M. Leunis, W.J.M. van Zeyl, E. Berends

Unilever Research Laboratorium
P.O. Box 114
3130 AC Vlaardingen
The Netherlands

Abstract

In order to relate composition, processing and product properties of fat spreads, a proper description of the microstructure of these products is required. A technique for the observation of the three-dimensional product structure has been developed which allows free observation of the solid crystalline matrix by removing the liquid oil phase from a fat spread with a solvent system. To perform the different preparation steps required in a reproducible and efficient way, a special sample holder was constructed. Application of preformed sintered bronze elements allows free penetration of the organic solvents. In general, reproducible results are obtained with retention of the structural integrity of the solid crystalline matrix. The microstructure of fat spreads can now be studied in a more systematic way as it is possible to distinguish different types of structure elements, such as single crystals, crystal aggregates, globular clusters, crystalline shells and the way these elements interact.

Initial paper received February 11, 1987
Manuscript received May 05, 1987
Direct inquiries to I. Heertje
Telephone number: 31 10 4605513

Key Words: Fat spread, microstructure, product morphology, crystal, crystal agglomerate, crystalline matrix, crystalline shell, deoiling, margarine, butter.

Introduction

In the study of fat spreads such as margarine and butter, microstructural information plays an important role. A basic understanding of the relation between composition, processing and product properties, requires a proper description of the different aspects of the microstructure, such as the nature of the fat crystals and their interaction, the distribution of the oil phase and the water phase.

To observe the microstructure of fat spreads, different microscopical techniques have been applied (1-14) such as light microscopy and electron microscopy using thin sections or freeze fracture replicas. These techniques are well suited to show different aspects of the emulsion structure such as the size of the water droplets and the interface with the fat matrix, and, in favourable cases, some aspects of the fat distribution (e.g., the presence of globular structure elements in butter). However, when it comes to a proper description of the product morphology of a fat spread, in particular the three-dimensional network structure of the fat crystalline matrix, these techniques are insufficient. This is, in particular, due to the impossibility to properly observe the liquid oil phase separately from the solid fat phase by the current electron microscopical techniques and to the, in general, much higher liquid than solid fat content in fat spreads. Typical values for the fat phase of a margarine being 80% liquid and 20% solid.

In this context the product morphology should be distinguished from the crystal morphology which is concerned with the size and the shape of the individual fat crystals. Crystal morphology can be determined after separating the oil from the fat crystals, by suspending the product in a detergent solution (9) followed by the appropriate separation- and visualisation techniques. In doing so, however, product morphology is completely destroyed. Moreover, preparation of suspensions of single crystals is hampered by the presence of strongly clustered crystal aggregates.

Knowledge of the product morphology would be of paramount importance for a better understanding of the ultimate properties. As in this context crystal aggregates, rather than size, shape and number of the separate crystals, are the important structure elements, a new methodology had to be developed. This methodology should be able to remove the liquid oil from the product without disturbing the solid matrix. In order to observe the three dimensional solid matrix structure scanning

electron microscopy (SEM) techniques were considered to be the most appropriate. As attempts to separate oil from a product with a detergent solution (5) without disturbing the solid crystalline matrix, appeared to be unsuccessful, a technique has been developed which uses a solvent system and affects the crystal matrix only to an acceptable limit.

Methodology

Solvent and sample holder requirements

A possible way to remove the oil phase from a fat spread is treatment with a suitable solvent. Ideally such a solvent should dissolve the liquid oil without affecting the solid matrix. To this end, the solvent or the solvent mixture should have the right properties.

Best results were obtained with a mixture of 2-butanol and methanol (90/10;v/v). Treatment of a fat spread sample ultimately leads to a replacement of the nonvolatile liquid oil by the volatile solvent mixture. To make the sample amenable to SEM observation further preparation steps required are freezing, freeze drying, fracturing, coating and transfer to the SEM. In order to be able to perform these steps in a reproducible and efficient way, a special type of sample preparation holder is needed which integrates these preparation steps into one device. The design of such a sample holder should meet the following requirements:

- the deoiling should be as homogeneous as possible, i.e., all parts of the observable structure should preferentially be deoiled to the same extent;
- fracturing of the sample should occur in a well defined manner, without unacceptable fragmentation, in order to properly locate the position where measurements are made;
- during fracturing, coating and transfer of the sample, temperature fluctuations should stay within acceptable limits;
- on introducing a fat sample into the sample holder, deformation of the sample should be avoided;
- proper mechanical fixation of the sample in the sample holder should be allowed, in order to avoid charging phenomena. This applies in particular to the present, porous and fragile, strongly insulating fat specimen;
- accommodation of as many samples as possible in the holder.

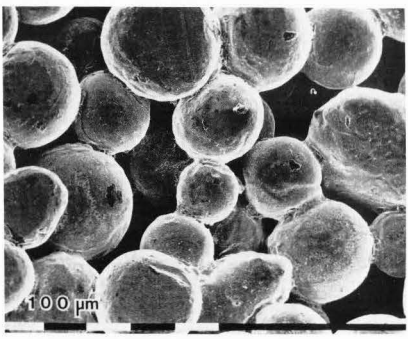

Figure 1. SEM Micrograph of sintered bronze (Accumatic Engineering Ltd.) showing porosity of the structure and sintering.

Design and construction of the sample holder

In order to integrate the deoiling with the other preparation steps a special construction material is needed, allowing free penetration of organic solvent combined with good thermal- and electrical conductivity properties. As such sintered bronze (Accumatic Eng. Ltd) appeared to be a good choice. A SEM micrograph of the material is given in Fig. 1. This material can further be machined into any desirable shape by the manufacturer. In the newly developed device preformed elements of sintered bronze have been incorporated.

Fig. 2 shows a cutaway section of the sample holder during the main stages of the sample preparation. The holder consists of two almost identical dovetail shaped parts (a and b) made of brass, held together by a pair of hinges (c and d) and leaf springs (j) of stainless steel. Two porous discs (e) made of sintered bronze, having three conical holes (diameter: 4mm), are fixed into these parts. The fat sample is introduced into these conical holes by means of a sampling tube (f) (Fig. 3). The holes are conical in order to avoid shear on the sample during filling. After filling (i) and removal of excess sample (ii), the holder is closed (iii) with porous discs (g), provided with conical pins which penetrate into the sample, ensuring proper fixation of the sample. Coaxial alignment and fixation of the discs with the holder is made by a spring (h). In this set-up the sample is surrounded on all sides by the sintered porous bronze material.

In the next stage the actual oil extraction takes place by immersing the holder as such in the solvent (for details see sample preparation). The next step is freezing and freeze drying, followed by storage under liquid nitrogen (for details see sample preparation).

The last stage of the preparation comprises fracture of the sample and coating of the fracture faces in a Balzers BAF 400 Cryo system and transfer of the coated sample into the cold stage of a Philips 505 SEM, fitted with a Hexland Cryo transfer system CT 1000. The fracturing is accomplished as follows: by means of the mounting rod of the Hexland Cryo system which is screwed into the top hole (i), the sample holder is slid via an airlock system onto the cooled rotary table (1) of the Balzers equipment. The travel of the bottom part of the holder is limited by a small pin in the table, whereas the top part is allowed to shift further backwards against the force exerted by leaf springs (j) during insertion. This shift is determined by the clearance (0.5 mm) between one pair of hinges (d) and the connecting pin. In this manner a predefined cross-sectional fracture of the samples is obtained.

Now, by lifting the mounting rod with a hook and unscrewing the rod, the top part of the holder is released from the leaf spring lock (j) and swings to the indicated position (vii) by means of the torsion spring (k).

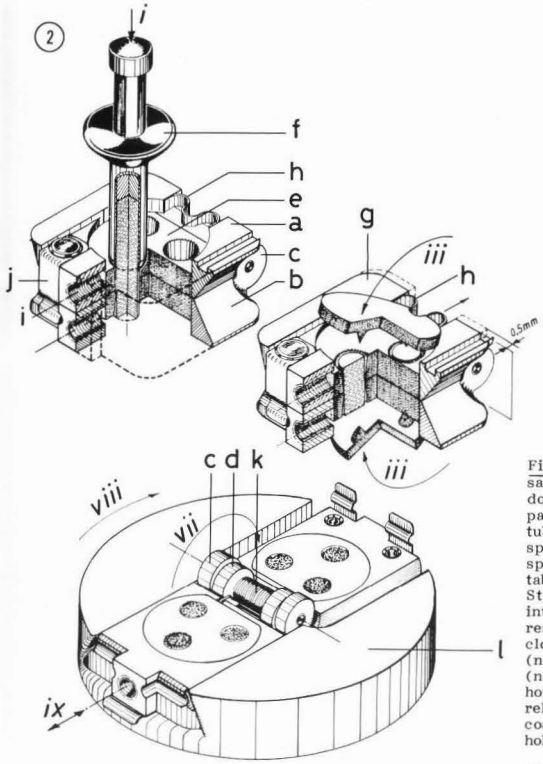

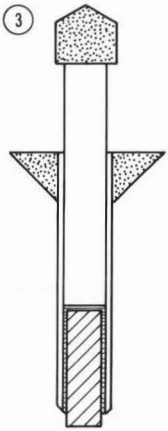

Figure 2. Sample holder and stages of sample preparation. Parts: a and b: dovetail-shaped brass elements; c and d: pair of hinges; e: porous discs; f: sampling tube; g: top- and bottom porous discs; h: spring; i: tophole of sample holder; j: spring lock; k: torsion spring; l: rotary table of the Balzers BAF 400 Cryo system. Stages of sample preparation: i): introduction of fat sample into holder; ii): removal of excess sample (not shown); iii): closing of holder with discs; iv): deoiling (not shown); v): freezing and freeze drying (not shown); vi): fracture of sample by horizontal movement (not shown); vii): release of top part from bottom part; viii): coating with rotation; ix): mounting of holder and transfer to SEM.

Figure 3. Sampling tube.

Table 1. Optimal deoiling time (h) of fatty products as a function of product characteristics and deoiling temperature

Product structure	Water content (%)	Deoiling temperature (°C)	
		10	15
Coarse (large crystals)	0	25-35	22-30
	20	18-24	17-22
	60	16-20	15-18
Fine (small crystals)	0	35-45	30-40
	20	25-35	22-30
	60	16-20	15-18

The fractured surfaces are coated (viii) (for details see sample preparation) and subsequently the holder is retracted (ix) into the airlock, by means of the mounting rod, transferred and slid into the Cryo chamber of the Hexland system, and inserted into the Cryo stage of the Philips 505 SEM for observation.

The different stages in the preparation procedure have been summarized in the legend to Fig. 2.

Details of sample preparation

Deoiling

Deoiling is performed in a 100 ml glass cylinder which is filled with 100 ml of a mixture of 2-butanol and methanol (90/10; v/v). The sample holder, containing the fat spread, is suspended in the upper part of the cylinder. The preferred temperature for deoiling is between 5 and 15°C. The optimal deoiling time depends on the characteristics of the product as well as on the deoiling temperature (Table 1). The

higher the water content of the product, the shorter the deoiling time. Similarly, decreasing crystal size and lower temperatures require longer deoiling times.

During the deoiling step the liquid oil is replaced by the mixture of 2-butanol and methanol. Next, this liquid mixture should be removed, in order to allow free observation of the solid fat matrix. This is done by first replacing the solvent mixture by pure methanol, followed by freezing and freeze drying. To this end the deoiled sample is transferred into a 100 ml glass cylinder containing pure methanol, and stored for 1 day at the same temperature as that applied for deoiling. Subsequently the sample is frozen in liquid nitrogen and freeze dried overnight at a temperature of 173°K in a Balzers FDU freeze drying system. This temperature is critical, as it allows the evaporation of the still solid methanol at a reasonable rate, without disturbing the fat crystalline matrix by melting phenomena of the methanol.

Coating and observation

Samples are coated with platinum/carbon in the Balzers 400 system using electron beam induced evaporation. Coating is carried out under angles of 45 and 90° with rotation (viii) of the sample (Fig. 2). Layer thickness is about 15 nm. After this step the sample is transferred to the Philips SEM for observation at 10 kV with a spot size of usually 20 nm. Magnification ranges from 250 to 10,000 times.

Results and Discussion

Performance of the new sample holder

In most cases a well defined flat fracture face is obtained, just between the plane of the porous discs (Fig. 4). Over the whole fracture plane the same structure is observed, indicating that deoiling is homogeneous. Apparently, the construction of the holder situating the permeable sintered bronze around the sample on all sides, results in equal deoiling in all directions. Further favourable aspects are:

- the different preparation steps are integrated into one holder;
- three samples (which means six fracture faces) can be introduced into a single holder;
- the fractured sample can be properly fixed in the sample holder by means of the specially designed pins. This also ensures good electrical contact in order to avoid charging phenomena;
- deformation of the sample is limited.

Separation of solid and liquid phases

A sharp separation between the solid and the liquid fat phase by treatment with a solvent is not to be expected since triacylglycerols in the solid phase will partly dissolve during the solvent extraction. Indeed, it is found that, apart from loss of solid phase, retention of liquid phase also occurs. In favourable cases, in margarines, 30% loss of solid phase is accompanied by 10% retention of the liquid phase.

In other cases, when very small crystals are present, separation between solid and liquid becomes very difficult, and losses of up to 50% of the solid phase may occur with a retention of 20% of the oil phase. In those cases, proper observation of the fat crystalline matrix is strongly hampered by the attached oil. In most cases, however, the disturbing influence of the attached oil is restricted and proper observations of the product morphology can be made.

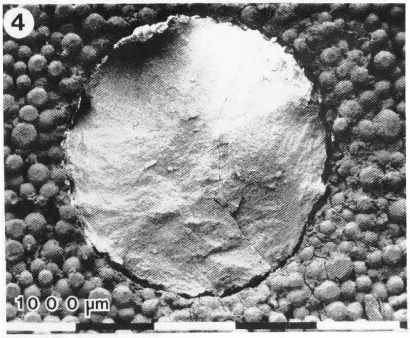

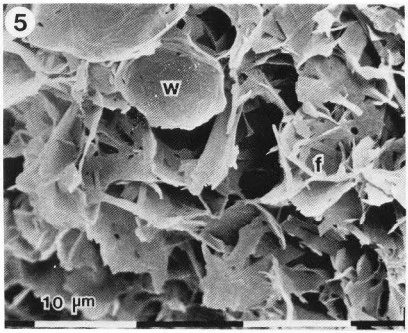

Fig. 4. The fat sample enclosed in the sintered bronze of the sample holder, showing fracture in the plane between the porous discs and good contact between the sample and the bronze.
Fig. 5. Typical margarine structure showing water droplet shells (w) and fat crystalline network (f).

Some observations

Figs. 5 - 14 show examples of product morphology for margarine and butter samples as examples of results obtainable by present technique. A typical margarine structure is shown in Figs. 5 and 6. Shells of water droplets are clearly discernible as well as a continuous fat matrix which appears to be an interconnected network structure composed of single crystals and sheetlike crystal aggregates. Such a sheetlike aggregate is composed of strongly clustered single crystals (Fig. 7). The latter micrograph, obtained via replication, shows a more detailed view of such an aggregate. The proper preservation of the water droplet structure indicated that the applied methodology is sufficiently mild to retain the structural integrity of the solid matrix. It needs further to be stressed, that for a proper impression of the three-dimensional product structure, stereomicrographs are essential (Fig. 6).

Figure 6. Stereomicrographs of a typical margarine showing water droplet shells and fat crystalline network.

Figure 7. Sheetlike crystal aggregate pointing out into space obtained by replication.

Figure 8. Example of butter structure showing many globules. Frequent occurrence of hollow spheres.

Figure 9. Example of butter structure showing few intact globules and interglobular crystal structure.

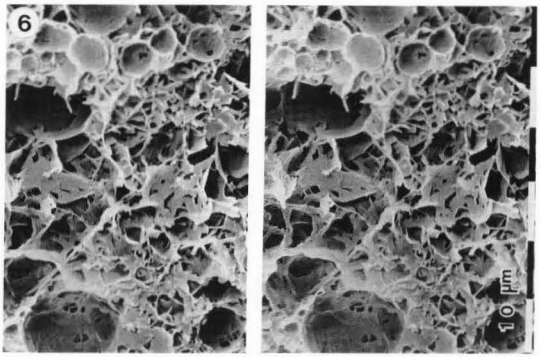

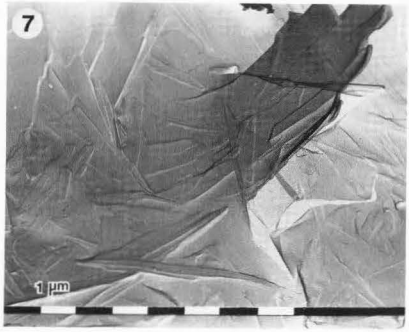

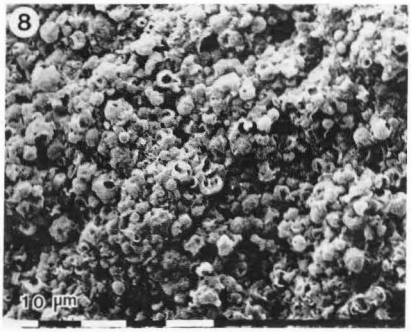

Figs. 8 and 9 show examples of the structure of butter. The typical butter globules (10,13) are clearly discernible. Butters differ in the amount of globules. The butter sample in Fig. 8 contains many more globules than the one in Fig. 9, which shows much more interglobular crystal structure (10). Butter globules consist of an outer crystalline layer composed of high melting fat, surrounding liquid oil inside (2,10,13). This becomes more pronounced after processing involving cold-warm-cold ripening of the original cream (13,14). The crystalline shell structure, made visible by the deoiling process, is well demonstrated in Fig. 8 by the frequent occurrence of hollow spheres. A typical example of such a hollow sphere is shown in Fig. 10.

Although in general margarines show a structure as presented in Figs. 4 and 5, sometimes larger crystal agglomerates can be detected. Figs. 11 and 12 show more or less globular crystal aggregates of a size of about 15-20 µm. Apart from the influence of the fat composition these agglomerates may be induced by post crystallisation after votator processing. These types of clusters resemble the spherulite type of clusters observed by light microscopy (7).

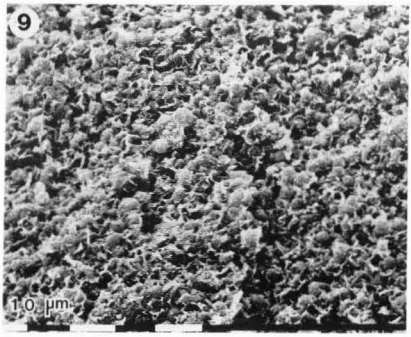

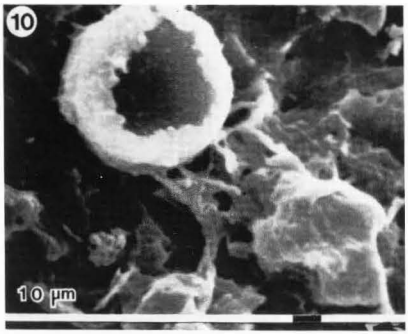

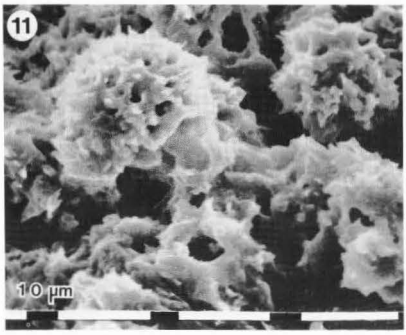

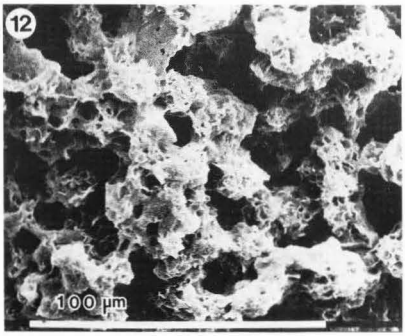

A further aspect of the product morphology of a fat spread is the structure of the interface between the water and the fat phase. Often a crystalline shell around the water droplets is clearly visible (e.g., Fig. 6) which can be traced to processing conditions and the type of emulsifier applied. An example of strong shell formation is given in Fig. 13, whereas shells are virtually absent in the micrographs shown in Fig. 14.

The examples show that the present method offers a new approach in the observation of product morphology of fat spreads. In general reproducible results are obtained with retention of the structural integrity of the solid crystalline matrix. The microstructure of fat spreads can now be studied in a more systematic way as it is possible to distinguish different types of structure elements, such as single crystals, crystal aggregates, globular clusters, crystalline shells and the way these elements interact.

References

1. Berger KG, Jewell GG, Politt RJM. (1979). Oils and fats. In: Food Microscopy. Vaughan JG (Ed.), Academic Press London, New York, San Francisco, 445-497.

2. Buchheim W. (1970). Verteilung hochschmelzender triglyceride in Fettkugelchen der milch. Naturwissenschaften 57, 41.

3. Buchheim W, Precht D. (1979). Electron microscopic study on the crystallisation processes in fat globules during the ripening of cream. Milchwissenschaft 34, 657-662.

4. deMan JM. (1982), Microscopy in the study of fats and emulsions. Food Microstruc. 1, 209-222.

5. Jewell GG, Meara ML. (1970). A new and rapid method for the electron microscopic examination of fats. J. Am. Oil Chem. Soc. 47, 535-538.

6. Kalab M. (1985). Microstructure of dairy foods. 2. Milk products based on fat. J. Dairy Sci. 68, 3234-3238.

7. Meara M, Evans GG, Jewell GG, Davies DP. (1974). British Food Manufacturing Industries Research Association; Research Report 204.

8. Mouwen DWC. (1974). Electron microscopy of margarine. Abstracts in program of 48th Annual Fall Meeting of the American Oil Chemists' Society, Philadelphia, August 1974. Available from the AOCS, 508 S. Sixth Ave, Champaign, IL. 61820, U.S.A.

9. Poot C, Dijkshoorn W, Haighton AJ, Verburg CC. (1975). Laboratory separation of crystals from plastic fats using detergent solution. J. Am. Oil Chem. Soc. 52, 69-72.

10. Precht D, Buchheim W. (1979). Electron microscopic studies on the physical structure of spreadable fats. I. The microstructure of fat globules in butter. Milchwissenschaft 34, 745-749.

Figure 10. Example of deoiled butter globule showing hollow sphere structure.

Figure 11. Example of spherical crystal agglomerates in a margarine.

Figure 12. Interconnected structure of crystal agglomerates in a fat blend.

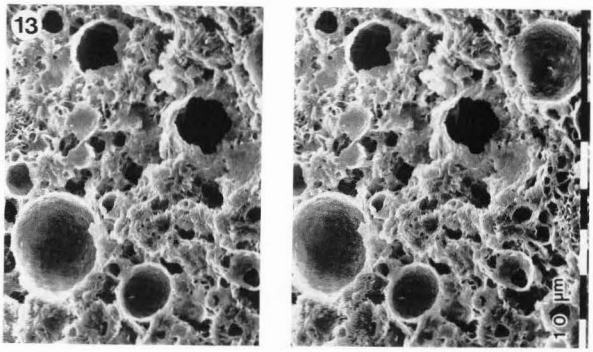

Figure 13. Water droplets with strong crystalline shell formation. Stereomicrographs.

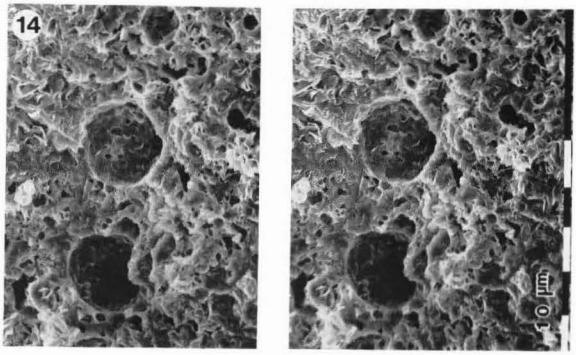

Figure 14. Water droplets without strong shell formation. Stereomicrographs.

11. Precht D, Buchheim W. (1980). Electron microscopic studies on the physical structure of spreadable fats. II. The microstructure of the interglobular fat phase in butter. Milchwissenschaft 35, 393-398.

12. Precht D, Buchheim W. (1980). Electron microscopic studies on the physical structure of spreadable fats. III. The aqueous phase in butter. Milchwissenschaft 35, 684-690.

13. Precht D, Peters, KH. (1981). The consistency of butter. I. Electron microscopic studies on the influence of different cream ripening temperatures on the frequency of definite fat globule types in cream. Milchwissenschaft 36, 616-620.

14. Precht D, Peters KH (1981). The consistency of butter. II. Relationships between the submicroscopic structures of cream fat globules as well as butter and the consistency in dependence of special physical methods of cream ripening. Milchwissenschaft 36, 673-676.

Discussion with Reviewers

K. Larsson and L. Hernqvist: As the different fat polymorphic forms have so different morphology they might behave quite differently at interfaces. Do you have information from X-ray diffraction on the fat crystal forms present, for example in samples corresponding to Figs. 5 and 8?

Authors: In these particular cases we have not measured the crystal modifications by X-ray diffraction. However, it is known that in normal margarine samples (Fig. 5), β'-crystals are present and virtually no β-crystals. Consequently we also consider the water-fat interface to be composed of β'-crystals. A different situation exists for butter (Fig. 8). Normally both β and β'-crystal modifications are observed. In particular the outer crystalline shell of high melting fat appears to be composed of β-crystals (Precht D, (1980), Fette, Seifen. Anstrichmittel 82, 142-147). It would therefore certainly be interesting to investigate, whether after deoiling, enrichment of the β phase has occurred.

J.M. deMan: The micrograph of margarine shows a leaf-like structure which seems to be different from

the established idea of individual crystals joining to form a network. These sheetlike structures are also fairly large for a normal margarine. How would the authors reconcile such a very interwoven structure with the traditional view of many small crystals loosely interacting?

Authors: On the basis of our experience we consider the normal margarine structure to be a network of single crystals and sheetlike aggregates. Depending on conditions (composition, processing) the sheetlike- or the single crystal character can be enhanced. A network of pure single crystals is not very common. Under extreme processing conditions many small, loosely interacting crystals do occur. Indeed, the presented margarine pictures show a rather coarse network structure. 3-D observation is essential to get a proper impression of the structure.

J.M. deMan: The crystal sheetlike formation in Fig. 7 seems to be larger than what is usually seen in polarized light microscopy. Is there a reason for this apparent discrepancy?

Authors: The intention of Fig. 7 is to show a typical example of a sheetlike aggregate. The size of this aggregate, composed of single crystals, is about 5-10 μm. The single crystals are smaller. It is these crystals which, in the first instance, will show up in polarized light. When clusters do exist, the outlines of these clusters are imaged by those (single) crystals, which are in the proper orientation. Clusters, observed in polarized light, with sizes between 5 and 20 μm occur frequently in normal margarines, although there are margarines having such small crystals, that no polarized light image is obtained.

W. Buchheim: In Figs. 8 and 9 the fine structure of two types of butter is demonstrated showing varying degrees of globular fat particles. It would be also of interest to know what the aqueous phase of butter looks like. Is it possible to differentiate unequivocally between a water droplet and a globular fat particle? Did you also find a crystalline shell around the water droplets in butter as demonstrated, e.g., in your Fig. 6 for margarine?

Authors: This is a very interesting issue. Indeed, in margarine, we find the water droplet shell structure, whereas, in general, this is not the case in butter. As in shown in the presented material, it is possible to distinguish between a water droplet and a globular fat particle. Water droplets show an open structure, indicating cross fracture through the shell structure, whereas the globular fat particles show surface fracture over the shell structure. Apparently, the crystal structure stabilizing the water droplets in butter, if present, is very easily lost in the applied deoiling procedure. It suggests that, in general, shell formation around water droplets in butter is not very prominent. However, in some special cases we have observed more pronounced shell formation.

FOOD MICROSTRUCTURE, Vol. 6 (1987), pp. 9-16
Scanning Microscopy International, Chicago (AMF O'Hare) , IL 60666 USA

0730-5419/87$3.00+.00

SCANNING ELECTRON MICROSCOPY STUDIES OF THE CELLULAR CHANGES IN RAW, FERMENTED AND DRIED COCOA BEANS

A. S. Lopez*, P. S. Dimick and R. M. Walsh

Department of Food Science, The Pennsylvania State University,
116 Borland Laboratory, University Park, PA 16802

*Current Address: Cacao Research Center, CEPLAC/CEPEC, 45600 Itabuna Brazil

Abstract

Cocoa beans are submitted to a curing process of fermentation and drying to develop flavor precursors. The beans must have reached maturity; otherwise, no amount of processing can produce the desired flavor. Early work with cacao cell cultures showed that only when the cells have "matured" could a chocolate or cocoa flavor result from further processing. Fermentation is therefore required because unfermented beans may develop little chocolate flavor when roasted. Likewise, the outcome of excessive fermentation may also result in unwanted flavor. Thus, the first major post-harvesting phase to have an impact on flavor development is that of fermentation. During this phase of curing, the mucilaginous pulp surrounding the beans undergoes an ethanol, acetic and lactic fermentation. The acid and heat generated kill the beans with a resulting change in cell membranes. This facilitates enzyme and substrate movement with notable swelling of the bean. Changes induced in the beans during the process affect the texture and flavor quality. This paper relates texture of the bean to cellular and subcellular transformations observed by scanning electron microscopy.

Initial paper received April 18, 1986
Manuscript received April 06, 1987
Direct inquiries to P.S. Dimick
Telephone number: 814 863 2962

KEY WORDS: Theobroma cacao, scanning electron microscopy of cocoa seeds, cellular changes, fermentation.

Introduction

Chocolate, which is manufactured from the seeds of Theobroma cacao owes its popularity and world-wide appeal to its unique and characteristic flavor. Prior to being processed into chocolate, the seeds from the ripe fruits, immediately following harvesting, are subjected to a fermentation and drying process during which the flavor precursors are developed. Only after undergoing such a process do the seeds (commonly referred to as beans) possess those attributes necessary and desirable for the manufacture of chocolate. The term, 'fermentation', is misleading when applied to the curing of cocoa because, although typical alcohol, lactic and acetic fermentations occur in the pulp that surrounds the seed, the reactions that are responsible for the formation of the flavor precursors are reactions between the seed enzymes and their substrates (Lopez, 1986). In the intact bean these substrates are separated and compartmentalized by biological barriers which break down during the fermentation treatment. The liberation and intermixing of enzymes and substrates lead to spontaneous reactions which are governed by the physicochemical conditions of fermentation. They are influenced by the external microflora of fermentation and the method used. Thus the fermentation process and the biochemical transformations that it provokes inside the bean are of major importance in the development of chocolate flavor. The majority of investigations aimed at elucidating the nature of chocolate flavor have been directed at the chemistry of fermentation and the manufacturing process in contrast to the few reports on the micro-structure of the seed (Roelofsen, 1958; Duncan and Todd, 1972; Vaughan 1970) and that provoked by fermentation (Biehl, 1973; Hoskin et al., 1984). The present study attempts to address this subject utilizing scanning electron microscopy (SEM) techniques.

Materials and Methods

Ripe fruit of Theobroma cacao of the Forastero variety were obtained from the Cacao Research Center of CEPLAC (Comissao Executivo do Plano da Lavoura Cacaueiro). Immediately after removal from the fruits, samples of the seeds

including the testa cotyledon and the embyronic axis, were prefixed in 3% glutaraldehyde in 0.1M Sorensen's buffer, (pH 7.1) and post-fixed in 1% OsO_4 in 0.1M Sorensen's buffer for 1 h. The samples were then dehydrated through a gradient ethanol series, frozen in liquid nitrogen and cryofractured to expose a surface unaffected by the initial cutting (Humphreys et al., 1974). Samples were critical point dried in a Polaron E3000 with CO_2 as a transitional fluid, mounted on aluminum stubs with silver adhesive and gold-coated in a Polaron PS-2 sputter coater on a cold stage with 280 to 420A of gold. When fat, which was liberated from the sample, recrystallized on the surface it obscured the field. These samples were then refractured, immersed over-night in acetone, air-dried and recoated with gold. Fermented beans (seeds) of mixed Trinitario-Forestero crosses, were obtained from the Hummingbird Hershey farm in Belize, Central America. These fermentations were carried out in a series of shallow and deep boxes currently being used on the farm. The fermenting seeds were aerated after 24, 48, 96 and 120 h during the 6-day fermentation. Bean samples were obtained after 3 and 6 days of fermentation and were prepared as in the case of the fresh control beans, except that vacuum infiltration was applied at the initial fixing step to insure thorough penetration throughout the sample. Prepared samples of unfermented and fermented beans were viewed using an ISI-60 SEM at 10kV. Photomicrographs were taken with a Polaroid 545 Land Camera and Polaroid 52 film (ASA-400) or with a 50mm Tahkumar lens and Plus X 35mm film (ASA 125).

Observations

In this study, the identification of cell types and the cellular inclusions relied upon the descriptions of cocoa seed tissue provided by Roelofsen (1958), Vaughan(1970), Duncan and Todd (1972) and Jaenick (1973). No staining for identification at the light microscope was undertaken in this phase of the study. There is a considerable amount of ambiguity with respect to the terminology used to describe the cocoa seed or bean. For our purpose, the interpretation used by Duncan and Todd (1972), Jaenick (1973) and Esau (1977) whereby the embryo is regarded as consisting of the embryonic axis and the two cotyledons was adopted. The embryo of the cocoa seed is somewhat oval in shape and flattened. It is comprised of two irregularly formed cotyledons and the embryonic axis to which they are attached. These are enclosed in a fibrous testa, the seed coat or shell which itself is enveloped in a mucilagenous pulp. Only the cotyledons are utilized in the manufacture of chocolate and although at this step, both the embryonic axis and the testa with remnants of the pulp are discarded, they serve a very important role in the fermentation process which is a prerequisite for the manufacture of chocolate.

The mucilagenous pulp or endocarp of the fresh intact cocoa seed comprises large tubular parenchyma cells (Figs. 1,2). These, together with the underlying spongy parenchyma contain the substrates for the microorganisms during fermentation. The pulp is separated from the rest of the testa by a single layer of smaller epidermal cells (Fig. 2) beneath which are found the large slime or mucilage cells which measure from 100 to 400 µm. These cell types are embedded in a mass

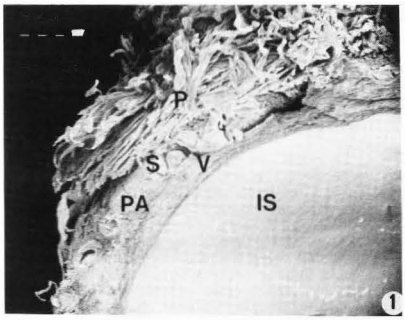

Fig. 1. SE micrograph of a cross section of the unfermented cacao seed testa showing the tubular pulp cells (P) and the spongy parenchyma below it, the large slime or mucilage cells (S) embedded in the parenchyma of the testa (PA) which also contains the vascular bundles (V). IS = internal surface of the testa. Bar = 100 µm.

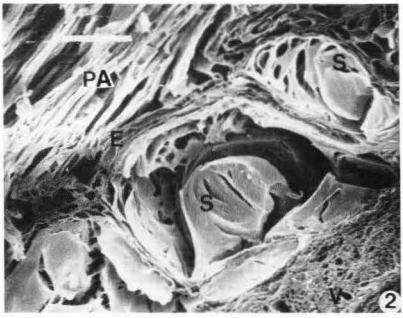

Fig. 2. Details of the slime cells (S) separated by a layer of epidermal cells (E) from the spongy parenchyma (PA) above. Below the slime cells are vascular bundles (V) embedded in the parenchyma. Bar =100 µm.

of thin-walled parenchyma cells which also contain scattered bundles of vascular tissue generally running in the direction of the long axis of the seed (Figs. 1-2). The parenchyma cells of this layer nearest the cotyledon are compressed (Fig. 3). Between the testa and the cotyledons is a thin 'bees wing' or endosperm (Duncan and Todd, 1972) which is also referred to as the perisperm (Roelofsen, 1958; Vaughan, 1970). This is a film of thin-walled, flattened cells that completely surround the cotyledons, and also protrude into the cotyledonary folds (Figs. 4 and 14).

Fig. 3. Portion of the testa parenchyma containing the vascular bundles (V) and flattened parenchyma layer at the inner surface (PA). Bar = 10 μm.

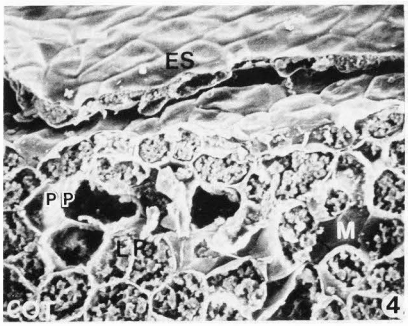

Fig. 4. Unicellular sheet of endosperm or perisperm (ES) which lies between the testa and the cotyledon (Cot) of the seed. Lipid/protein storage cells (LP), polyphenol cells (PP) and mucilage filled cells (M) are also evident. The smaller, uniseriate epidermal cells in contact with the endosperm do not bear trichomes. Bar = 10 μm.

Fat globules and crystals (Hoskin et al., 1980) were not observed on the endosperm surface. The epidermal cells (Figs. 4-5), form a uni-seriate layer of tubular cells which completely surround the cotyledons and are continuous with the epidermis of the embryonic axis. These cells are not uniform and those on the abaxial surfaces are larger than those of the adaxial surfaces. Cuticle and starch granules are also evident and some of the cells have multi-cellular trichomes arising from their surfaces (Fig. 5). The surface formed by the cotyledon's epidermal cells was smooth but undulating and interrupted only by the occasional presence of trichomes.

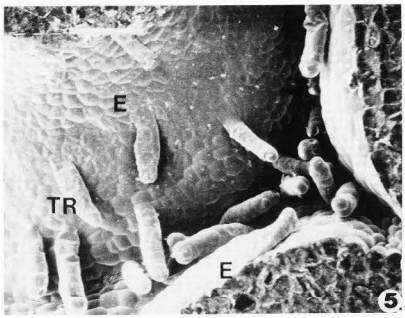

Fig. 5. Multicellular trichomes (TR) arising from the surface of epidermal cells in the cotyledon folds. The epidermal cells (E) form an undulating surface; no superficial wax-like secretions were noted. Bar = 100 μm.

The ground parenchyma (Figs. 4 and 6), which constitutes the major part of the cotyledon tissue, consists of two types of thin walled cells. These are closely packed in an irregular fashion with virtually no spaces between them. The most abundant cell types are the smaller lipid/protein storage cells (Fig. 6). They contain a large number of lipid vacuoles or globules embedded in cytoplasm which also contains starch granules and protein bodies. Scattered among these cells and often occurring in groups are larger cells whose interiors are filled almost entirely by a large vacuole (Fig. 6). These cells are recognized as polyphenol cells and contain virtually all of the seed's polyphenolic material and alkaloids (Roelofsen, 1958; Vaughan, 1970). In the Forestero cocoa, under low power of the light microscope, they appear as violet streaks due to the presence of anthocyanin pigments which give the cotyledons their characteristic violet or purple color. Vascular tissue of composite bundles of xylem and phloem is also present within the cotyledons (Fig. 7).

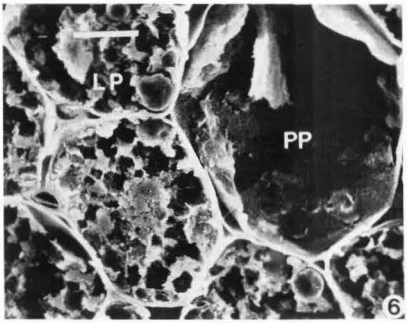

Fig. 6. Cotyledon section showing lipid/protein storage cells (LP) and polyphenol cells (PP) containing remnants of cytoplasm and starch and other embedded inclusions. Bar = 10 µm.

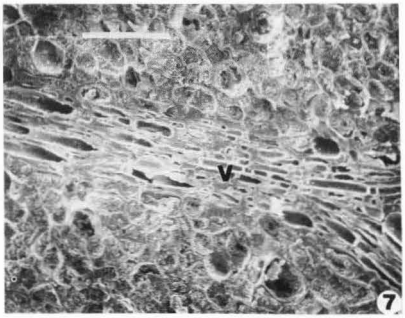

Fig. 7. Vascular tissue within the cotyledon (V). Bar = 100 µm.

In longitudinal sections of the embryonic axis, the morphological differentiation in the epicotyl described by Duncan and Todd (1972) was not evident. This may be due to the plane of the fracture during sample preparation. However, epidermis, cortex, procambium and pith were well defined in the hypocotyl and root cap regions (Figs. 8-9). No stoma were seen although they have been reported (Duncan and Todd, 1972). Starch granules and cuticle were observed in the epidermis. Vascular tissue was also evident in the procambium region. The innermost cells of the pith show extensive mucilage (Fig. 10).

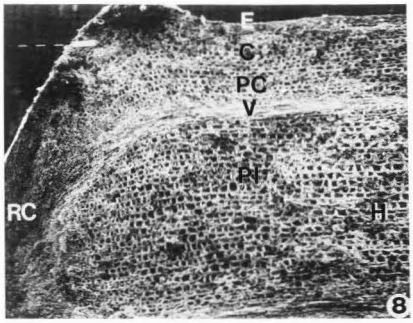

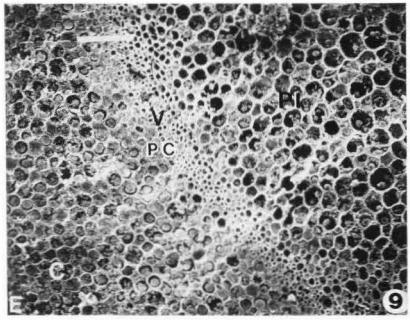

Fig. 8. LS, and Figure 9 CS of the embryonic axis showing the root-cap (RC) and hypocotyl (H) region. (E) = epidermis, (C) = cortex, (PC) = procambium, (Pi) = pith and (V) = vascular region. Bar = 100 µm.

In the fermented cacao seed structural changes resulting from the treatment are minimal. The most noticeable change is in the testa, precisely in the pulp layer where most of the tubular cells have flaked away. Those few remaining cells show masses of bacilli and yeasts occupying intercellular spaces (Figs. 11-12). Examination of the testa of freeze dried beans showed the presence of polyhedral crystals similar to those of calcium oxalate seen in the parenchyma of many plant tissues (Fig. 13).

The perisperm or endosperm that lies between the testa and the cotyledon did not appear to undergo structural changes. In the unfermented seeds, however, it closely adheres to the cotyledon surface while in the fermented

Fig. 10. CS of embryonic axis showing mucilage cells (M) in the pith. Bar = 10 μm.

Fig. 11. CS of the testa of the fermented seed showing the remnants of the pulp (P), the vascular tissue (V), the flattened parenchyma (PA) and the mucilage cells (S). Bar = 100 μm.

Fig. 12. CS of testa showing detail of compressed pulp cells with bacilli and yeast embedded between cells. Bar = 10 μm.

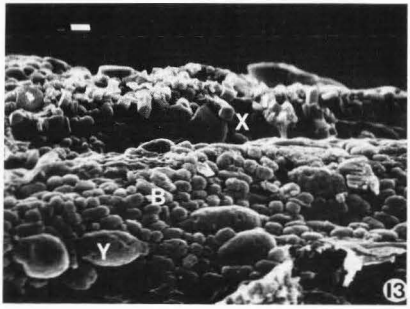

Fig. 13. Microflora embedded in the pulp of the fermented testa shows yeast cells (Y), bacilli (B) and crystalline bodies (X). Bar = 1 μm.

seeds it is often found loose or attached to the testa. It still remains attached to the cotyledons however, where it dips into the cotyledonary folds (Fig. 14).

Since the testa protects the cotyledons from the microflora during fermentation, changes such as cell lysis that might be expected to be provoked by microbial action, are not noted. Nor is there evidence in the literature that suggests that microbial enzymes produced in the testa and capable of lysing cellular components are actually transported into the cotyledon. The enzymatic changes in the seed during fermentation are intracellular and involve the hydrolysis and mobilization of proteins and polyphenols, and the redeposition of fat within the cell. The starch is believed to remain unchanged (Schmeider and Keeney, 1980). Except for the fat, changes in the other components are not manifested as obvious structural modifications detectable with the SEM.

As mentioned above, the lipids and proteins are stored in cells apart from the polyphenols. In general, the appearance of the sections of the fermented seed appear denser than those of unfermented seeds. This apparent difference in density mainly involves the lipid/protein cells whose cytoplasm in the fermented seed appears to be reticulate and riddled with holes (Figs. 15-16). This is most likely due to the removal of fat during the dehydration step.

Other discernible changes are in the polyphenol cells. In the sections from the unfermented seeds, they were generally void except for part of the cytoplasm lining of the vacuole (Fig. 6). In the fermented seeds however, the

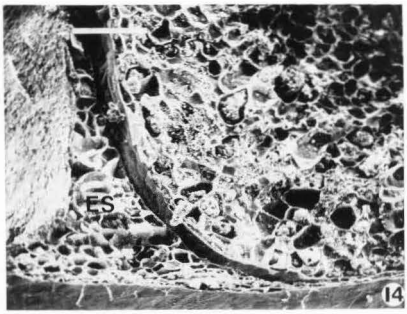

Fig. 14. The fermented seed endosperm (ES) at a point where it enters the cotyledon fold. Bar = 100 μm.

cellular contents appear to have solidified (Fig. 14) and when not fractured, the solidified mass gave the appearance of having remnants of the cytoplasm and other spherical bodies embedded in it. This suggests that some fat protein and starch may also be contained in the polyphenol cells (Fig. 16). However, empty polyphenol cells were most frequently observed. Dispersed throughout the cotyledon tissue, there were cells filled with what appeared to be dehydrated mucilage. No obvious changes in the structure of the embryonic axis of the fermented samples were noticed but sharper sections were obtained. This could be the result of the interaction between proteins and polyphenols (Fig. 17).

Conclusion

During the initial phase of fermentation, the seed undergoes changes typically associated with germination. However these orderly biochemical reactions give way to spontaneous enzymatic and chemical changes on the death of the seed. Polyphenols diffuse throughout the tissue and combine with proteins and other compounds in complex chemical reactions.

The cotyledon and the enzymatic transformations that they undergo during fermentation are of interest to chocolate processors. However, the other components of the seed, though often ignored, play important, though indirect, roles in the curing process. The testa, for example, serves not only in providing substrates for the microbial fermentation and a barrier against the entry of microorganisms and insect pests, but also has a direct bearing on the fermentation process. The permeability of the testa to the microbial metabolites produced in the pulp, which are necessary for the curing of the seed, determine the rate of fermentation and therefore the quality of the product (Lopez, 1986). The observations in this study confirm that the microflora of fermentation do not penetrate the testa to invade the seed but are confined to the periphery. The role of the

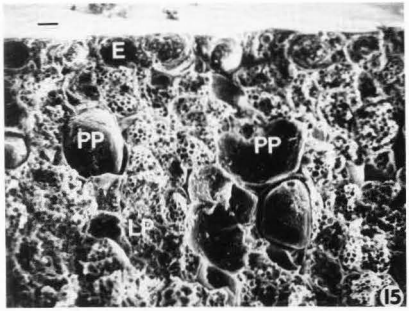

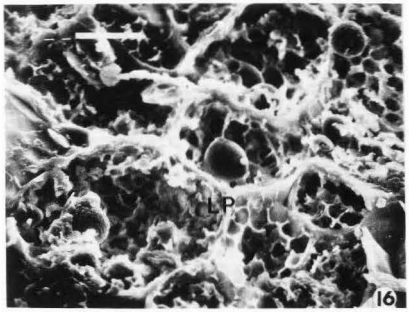

Figs. 15, 16. Fermented cacao seed cotyledon. (E) = epidermal layer, (LP) = lipid/protein cells and (PP) = polyphenol cells with cytoplasm remnants or solidified interior. Bar = 10 μm.

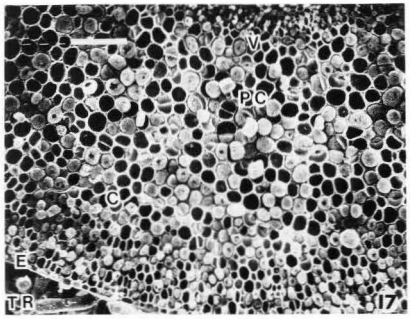

Fig. 17. CS of the embryonic axis of the fermented seed. (TR) = trichomes, (E) = epidermis, (C) = cortex, (PC) = procambium, (V) = vascular tissue. Bar = 100 μm.

embryonic axis in flavor precursor development is not clear although incipient germination of the seed is believed necessary for flavor development. There is however, some evidence that suggests that germination determines the texture of the cured seed as well as influences the oxidative phase during the latter stages of fermentation. It has been observed for example (Lopez, 1984), that in fermentations where conditions that encourage germination prevail, the cured seeds generally have an open and plump appearance that chocolate manufacturers prefer (Anon., 1968). On the other hand, when germination is inhibited or halted by the rapid development of heat and acetic acid of fermentation, the seeds are more likely to be compact and cheesy (Lopez, 1986). Plump beans are preferred because they are easier to dehull and there is less carry-over of shell into the product. Furthermore, the open structure of the seed allows for better oxidation of the cotyledon polyphenols and therefore a greater reduction in the astringency and bitterness. The reason for the occurrence of compact seeds was not obvious from the samples examined in this study. Changes in the cotyledons resulting from fermentation and responsible for flavor precursor formation are still not clear (Lopez, 1986). However, it is well established that among the more important of these are the changes in the proteins and the polyphenols. Both are fragmented into numerous smaller units which themselves interact to form a large number of complex substances. Evidence from SEM suggesting that protein bodies undergo changes was not conclusive mainly due to the interference of the lipid fraction. Biehl (1973) believes that under certain circumstances the fat isolates hydrophilic constituents in the seed, preventing them from mixing and reacting. Fat coating of cellular material was observed in some samples but it was not conclusive that this had occurred during fermentation and that enzymatic changes had been prevented. Confirmation of this as well as other chemical transformations will be possible during the next phase of the study which aims at investigating intracellular reactions with differential stains and light microscopy, in conjunction with SEM.

Acknowledgements

Authorized for publication as Paper No. 7399 in the journal series of the Pennsylvania Agricultural Experimentational Station.

References

Anon. (1968). Raw cacao: Manufacturers' quality requirements, Alliance, Vale, Surry. 12 p.

Biehl, B. (1973). Veranderungen der subcellularen struktur in keimblattern von kakaosamen (Theobroma cacao) wahrend der fermentation und trocknung. Z. Lebensm. Unters. Frosch. 153:137-150.

Duncan, F. J. and Todd, A. W. (1972). Structure of the mature embryo of Theobroma cacao L. Ann Bot. 36:939-945.

Esau, K. (1977). Embryo and seedling. In: Anatomy of Seed Plants. John Wiley and Sons Inc., N.Y. 475-476 p.

Hoskin, J. M., Dimick, P. S. and Daniel, R. R. (1980). Scanning electron microscopy of the Theobroma cacao seed. J. Food Sci. 45:1538-1540 and 1545.

Humphreys, W. J., Spurlock, B. O. and Johnson, J. S. (1974). Critical point drying of ethanol-infiltrated, cryofractured biological specimens for scanning electron microscopy. Scanning Electron Microsc. 1974:275-282.

Jaenick, J. (1973). Elektronenmikroskopische untersuchungen an embryonen von Theobroma cacao L. (Kakao) wahrend der embriogenese und semenkeimung. Dessertation, Tieraztliche Hochschule Hannover.

Lopez, A. S. (1984). Difusao de substancia quimica da testa de amendoas de cacau. Informe Tecnico, CEPEC/CEPLAC. Ilheus Ba, Brasil. 168-171 p.

Lopez, A. S. (1986). Chemical changes occurring during the processing of cacao. Proceedings of the Biotechnology Symposium. (Ed). P. S. Dimick. The Pennsylvania State University. 19-54 p.

Roelofsen, P. A. (1958). Fermentation, drying and storage of cacao beans. Adv. Food Res. 8:225-296.

Schmeider, R. L. and Keeney, P. G. (1980). Characterization and quantification of starch in cacao beans and chocolate products. J. Food Sci. 45:555-557.

Vaughan, J. G. (1970). Sterculiaceae-cacao. In: Structure and Utilization of Oil Seeds. Chapman and Hall Ltd. London. 241-243 p.

Discussion with Reviewers

J. F. Heathcock: Have the authors made any observations on the differences in structure between the inner and outer portions of the cotyledons?

Authors: Yes. The cotyledons are the convoluted laminae of the first pair of "leaves" which function as storage organs during growth. They do develop some chlorophyll too,but later fall off when the radicle has emerged and the first three "true" leaves have formed. (The cellular composition of the surface of the cotyledon and the interior are similar in that they are composed of the same type of cells.)

However, the layers are different in that there is a distinct cuticular layer which carries the multicellular trichomes. These are more numerous on the underside of the cotyledons.

J. F. Heathcock: Could you comment further on the appearance of fat crystals on the preparations? This may suggest inadequate fixation. What differences would you expect to see between well fixed tissue and tissue in which the fat has been solvent extracted?
Authors: It is possible that inadequate fixation was responsible for some of the aberrations seen in the micrographs. In the unfermented cacao seed two types of cells have been described: the protein storage cells and the polyphenolic cells. The former contain starch grains and agglomerates, protein vacuoles and nucleic material surrounded by fat globules (1-6 μm in diameter), which form the bulk of the cell contents. Fermentation produces changes that cause the fat globules to coalesce and form larger bodies, surrounded by a hydrophilic protein phase (Biehl, personal comm.). The starch is believed to be unchanged. The polyphenolic cells contain a single large polyphenol vacuole surrounded by a thin cytoplasmic layer which contains starch grains, protein bodies and the nucleus. The polyphenol cells would appear as empty cells because of the extraction of the polyphenols by acetone during preparation.

J. F. Heathcock: What changes do you think are going on in the polyphenol cells to produce the "solidified" contents that you describe?
Authors: During fermentation, hydrolysis of proteins and polyphenols occur. Besides these enzymatic degradative processes, recombination and condensation reactions between the polyphenolic fragments and also between them and the proteins occur. It is believed that these reactions will produce insoluble polyphenol-protein complexes which are probably those observed in the polyphenol-protein cells of fermented cotyledon tissue.

J. F. Heathcock: Could you describe further what you think are the structural similarities and differences between germination and fermentation and do you have any evidence that some cocoa beans may start germinating prematurely before they are even fermented?
Authors: The fermentation of cocoa may be defined as encompassing all the changes that occur in the seed during the curing process. These are both the external microbial and the intercellular enzymatic fermentations as well as the pregermination changes that would occur prior to the death of the embryo. This germination may be expected to begin even in the mature fruit on the tree and is governed by an inhibitor contained in the pulp of the seed. Physiological stress is believed to cause a destruction of the inhibitor and provoke premature germination in the case of drought and frost damage.

FOOD MICROSTRUCTURE, Vol. 6 (1987), pp. 17-24
Scanning Microscopy International, Chicago (AMF O'Hare) , IL 60666 USA

0730-5419/87$3.00+.00

MICROBIAL CELL DIVISION AND SEPARATION: EFFECT OF CITRATE ON THE GROWTH OF GROUP N STREPTOCOCCI

S. Ito, T. Kobayashi, K. Ozaki, T. Morichi[1], M. Saitoh

Dept. of Microbial Engineering, Tochigi Res. Laboratories of Kao Corporation, 2606 Akabane, Ichikai, Haga, Tochigi 321-34, Japan

[1]National Institute of Animal Industry, Tsukuba, Norindanchi, P.O. Box 5, Ibaraki 305, Japan

Abstract

In the presence of citrate, some strains of lactic streptococci grow as long chains of innumerable cells. The results with citrate-negative and citrate-resistant variants suggest that citrate is involved in the cell separation system of the streptococci. Observations of the long chains under scanning and transmission electron microscopes suggest that citrate inhibits a certain step near the final cell separation, or that citrate can stimulate initiation of cell division at multiple sites, thereby leading to the cells in long chains.

Initial paper received January 30, 1987
Manuscript received March 14, 1987
Direct inquiries to S. Ito
Telephone number: 81-2856-82131x5604

Key Words: Lactic starter, Streptococcus, long chain formation, citrate, cell division, autolysin, dechaining enzyme, flavor.

Introduction

The streptococci represent a group of fastidious microorganisms which exhibit remarkable heterogeneity with respect to their biochemical and genetic characteristics. Group N streptococci occupy an important position as lactic starters in the fields of dairy and food technology. Various strains of these organisms have been used for the flavor enhancement of milk, butter and cream (Mocoquot & Hutel, 1970). However, little is known about the morphology of the lactic streptococci under different growth conditions.

Recently, we observed abnormally long chains of citrate-fermenting lactic streptococci in broth, with the lengths of the chains dependent upon the concentration of citrate. We have attempted to clarify the effect of citrate upon the length of the chains of cells. We believe that our results provide clues that will help to elucidate the mechanism of certain phases of cell division in lactic streptococci.

Materials and Methods

Bacteria and media

All bacterial strains used were group N streptococci. Among them, Streptococcus sp. KSM-1106 was isolated from a sample of cream by S.I., and Streptococcus sp. KSM-1112 from a lactic starter by T.M.. Our strains were of an intermediate type, and were neither typical S. cremoris nor S. lactis. All strains were propagated in 12% reconstituted nonfat dry milk (NFDM, Difco) at 26°C, and incubations were continued in quiescent state until the medium coagulated. The coagulated medium was kept at 4°C by monthly transfers in the NFDM. The protease activity (Prt) of each organism was checked anaerobically by the ability to form clear zones around the colonies on agar plates, which contained 12% NFDM, 1% glucose and 1.5% agar (pH 6.8). The ability to utilize citrate (Cit) was checked by anaerobic growth on the citrate agar plates described by Kempler and McKay (1980). The lactose fermenting ability (Lac) was checked by the growth in a standard medium containing 1% lactose. The standard medium for growth contained the following ingredients (g/liter): glucose or an alternate sugar (10); polypeptone (10, acid-hydrolyzed soy bean digest of Daigo Eiyo Co. Ltd., Japan); yeast extract (5, Difco); and distilled water; the pH was adjusted to 6.8 with NaOH. The medium was sterilized by autoclaving. The citrate medium was prepared by adding disodium citrate at

varied concentrations to the above-mentioned standard medium. Media were supplemented with filter-sterilized inorganic ions, organic acids, amino acids and antibiotics as required.

Isolation of mutants

The gene coding for the Cit phenotype was plasmid-linked in our strains (our laboratory, unpublished data). The Cit phenotype of the KSM-1106 strain was highly unstable and was readily lost when the strain was transferred several times, successively, as a stab in the agar medium of Yashima et al. (1970) at 30°C. The cured cells were incubated in 12% NFDM at 26°C for 3 days and then plated on the citrate agar plates of Kempler and McKay (1980). A citrate-negative (Cit^-) mutant grew up as the white colony on the citrate agar plate and its relevant phenotype was $Lac^+Prt^+Cit^-$ (designated KSM-1106C$^-$). The Cit^- mutant lacked a citrate permease (unpublished data).

A citrate-resistant (Cit^r) mutant derived from the KSM-1106 strain was prepared as follows. The KSM-1106 strain was grown at 26°C in a 20-ml test tube containing 5 ml of standard medium. Cells were harvested after 16 h of growth, washed twice in chilled saline and then resuspended in 5 ml of chilled deionized water. The resulting cell suspensions were treated with N-methyl-N'-nitro-N-nitrosoguanidine (10μg/ml) for 90 min at 30°C with gentle agitation. The treated cells were diluted, immediately transferred to 12% NFDM, and incubation was continued without shaking, at 26°C until the medium coagulated. An aliquot was then resuspended in medium that contained 150 mM citrate. After incubation at 26°C for 3 days, the culture was spread plated on the citrate agar plates (Kempler & McKay, 1980) and incubated anaerobically in order to check the phenotype of Cit. Blue colonies grew up, indicative of the Cit^+ phenotype, and were purified. By this procedure, the mutant strain, KSM-1106C^r ($Lac^+Prt^+Cit^+$) was isolated.

Culture conditions and measurement of growth

Usually, cells used for experiments were prepared from the cultures in the early stationary phase of growth, reached after 14 to 16 h of incubation at 26°C in standard medium. The cultures, containing an inoculum of a 1:100 dilution of the same preculture, were grown anaerobically on standard medium in capped test tubes. At intervals, samples with appropriate dilution were transferred into 3.0 ml cuvettes and absorbance at 590 nm (A_{590}) was measured, using a Hitachi 220 spectrophotometer.

Determination of chain length

The test strains were harvested all in the early stationary phase of growth for counting cell numbers per each chain. The cultures, after 14 to 16 h of growth at 26°C, were mixed by gently inverting the capped test tube twice. A loopful of the culture was placed on a glass slide and covering it with a coverslip. The cells were observed under a light microscope with an oil immersion lens (phase contrast optics, x 1,000 magnification). The cell numbers in 100 to 150 chains were counted and the average chain length, in number of cells/chain, was calculated.

Scanning electron microscopy (SEM)

For SEM, cell pastes were fixed in 4% glutaraldehyde in 0.1 M cacodylate buffer (pH 7.2) at 4°C for 2 h. Specimens were postfixed in OsO_4, buffered with cacodylate as above, at 4°C for 1 h, washed with cacodylate buffer and then dehydrated by two immersions for 5 to 10 min each in 50, 60, 70, 80, 90, 95 and 100% ethanol. Specimens were then put in isoamyl alcohol for 10 min and critical-point dried in liquid CO_2. Dried specimens were mounted on stubs and coated with gold for 4 to 5 min by vacuum evaporation. A JSM-35C electron microscope (JEOL Ltd., Japan) was operated at 10 or 15 kV.

Transmission electron microscopy (TEM)

Specimens were fixed with glutaraldehyde and postfixed with OsO_4, as described above. Fixed specimens were dehydrated in a graded alcohol series (3 times each in 50, 70, 90 and then in 100% ethanol). Specimens were washed twice with propylene oxide for 10 min and infiltrated with 1:1, 3:1 and 7:1 portions of epoxy resin (Epon 812):propylene oxide for 2 h each. Specimens were infiltrated with 100% resin overnight and then embedded in fresh resin. Thin sections (50 to 80 nm in thickness) were stained with uranyl acetate and Reynolds' lead acetate solutions (Reynolds, 1963) for 10 min and examined under a JEM-100CX electron microscope (JEOL Ltd., Japan) operated at 80 kV.

SEM by Robinson backscattered electron detector (WET-SEM)

The culture, after 14 to 16 h of growth at 26°C, was transferred onto a cover glass and observed directly in a WET-SEM WS-250 (Akashi Seisakusho Ltd., Japan) (Shimakura & Inoue, 1985) equipped with the wide angle backscattered electron detector developed by Robinson (1975). The accelerating voltage used was 15 kV in a vacuum of from 0.2 to 0.3 Torr.

Results

Citrate-induced growth of chains of lactic streptococci

In general, group N streptococci grow as pairs or, in some cultures, as short chains (Teuber & Geis, 1981). During studies on the biochemistry and genetics of the catabolism of citrate, we found that Streptococcus sp. KSM-1106 grew as very long chains in the presence of citrate, as seen by WET-SEM. This strain grew predominantly as pairs of cells or as short chains in standard medium (Fig. 1). The chain length of the organism increased with increasing concentration of citrate. When the concentration of citrate reached 15 mM, the chains of cells became tangled clumps in which the numbers of cells were too great to be counted (Figs. 2 and 3). When the culture was transferred to fresh standard medium, the chain length was reduced again to 2 or 4 cells per chain, indicating a reversion to the more usual pattern of growth.

If one is solely interested in visualizing "untreated" specimens of the chains of streptococci, the WET-SEM method may be the fastest and simplest method since it involves the fewest manipulative procedures. For information that relates to surface structure or ultrastructure, experiments that employ SEM and TEM are necessary, as described below.

Lactic streptococci with the ability to grow as long chains were identified by growth at 30°C for 2 days in medium that contained citrate. Of 26 strains examined, 5, including strain KSM-1106, grew as long chains in the presence of citrate, i.e., Streptococcus sp. KSM-1112, S. diacetylactis DRC-2, S. diacetylactis D-16 and S. cremoris AHU 1083. In contrast, taxonomic strains of S. lactis ATCC 19435 ($Lac^+Prt^+Cit^+$) and S. cremoris ATCC 19257 ($Lac^+Prt^+Cit^-$) occurred in pairs or short chains (about 4 cells/chain) whether citrate was present or absent. Hereafter, Streptococcus sp. KSM-1106 and its

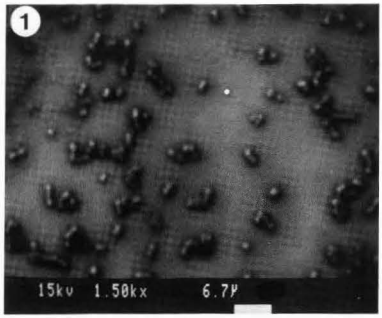

Fig. 1. WET-SEM micrograph of Streptococcus sp. KSM-1106, grown in standard medium. Bar=6.7μm.

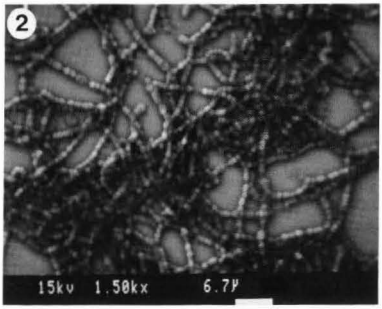

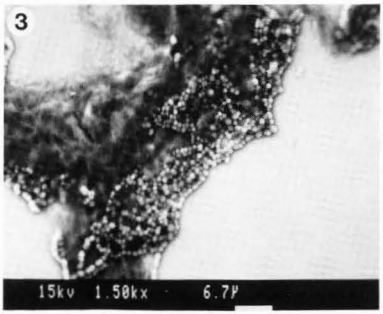

Figs. 2 and 3. WET-SEM micrographs of the cells, grown in medium supplemented with 15 mM citrate. Bar=6.7μm.

mutant stains were used extensively.

Effects of growth conditions on the chain length

Effect of several additives were examined on the chain length of Streptococcus sp. KSM-1106, as summarized in Table 1.

Supplementation of standard medium with various organic acids (15 mM or 30 mM) allowed the growth of the test strain; the compounds tested were citrate, oxalacetate, succinate, malate, fumarate, cis-aconitate, isocitrate, tartarate and itaconate. These naturally-occurring organic acids could not replace citrate as a trigger for the formation of long chains. The possibility existed that citrate might act to chelate inorganic ions present in standard medium, thereby potentiating the formation of long chains. This possibility was evaluated by growing the test strain with powerful chelating agents, such as EDTA, tripolyphosphate (STPP) (Cutler, 1972) or Zeolite (Schwuger & Smolka, 1976). These chelating agents were added to give over 50% inhibition of the growth after 16 h of incubation, but no sign of chain elongation was observed by use of these additives. D-Cycloserine, bacitracin, ampicillin, cephazolin, vancomycin and ristocetin, antibiotics inhibitory against the synthesis of bacterial cell walls, did not potentiate the formation of long chains by the strain. Glycine (Gly) and/or isoleucine (Ileu), which are known to alter the bacterial cell wall (Miyashiro et al., 1980), also had no effect upon chain length. In addition, the growth of cells as long chains, induced by 10 mM citrate, was not arrested by addition of the building blocks of bacterial cell wall, such as lysine (Lys), diaminopimelic acid (DAP), glutamic acid (Glu), alanyl-alanine (Ala-Ala), glucosamine ($GluNH_2$) and N-acetyl-glucosamine (N-Ac-$GluNH_2$) (for instance, Johnson & McDonald (1974), who used S. cremoris HP).

The chain length of the test strain did not change when the temperature of incubation was varied between 14 and 34°C. At 37.9°C, the upper limit for growth, the chains (in standard medium, in the absence of citrate) were slightly longer (6 to 8 cells/chain). Variation of the initial pH of standard medium from 4.5 to 7.7 did not cause the formation of long chains, nor did the substitution of any sugars, added in place of glucose, such as fructose, galactose, lactose, maltose, trehalose or salicin. In the presence of citrate, the organism grew as long chains, independently of added sugars.

Function of inorganic ions

Various cations, added as sulfates or chlorides, were tested for their effects on the chain length of Streptococcus sp. KSM-1106. In standard medium that contained 15 mM citrate (over 50 cells/chain), a dramatic destabilization of the chains of cells was observed upon addition of divalent cations, in the order: $Mn^{2+} > Ca^{2+} > Mg^{2+} > Fe^{2+} > Zn^{2+}$. At 15 mM citrate, the shortest chain length of cells of strain KSM-1106 was observed at 5 mM Mn^{2+} (5.0 ± 0.3 cells/chain) and at 15 mM Ca^{2+} (8.8 ± 0.8 cells/chain). Al^{3+}, Co^{2+}, Na^{+}, K^{+} and NH_4^{+} could not interrupt the formation of long chains by citrate (over 50 cells/chain).

Growth characteristics of Cit variants

When the concentration of citrate was raised from zero to 15 mM, the yield of growth of a mutant strain KSM-1106C^{-}, after 16 h of incubation at 26°C, was increased up to 130% of the control yield (in standard medium, in the absence of citrate), but above 15 mM

Table 1. Effect of additives on the chain length of Streptococcus sp. KSM-1106

Exogenous additives	A_{590} after 16 h	PCLC* (%)	ANCC**
In standard medium			
No addition	0.89	52	4.0 ± 0.1
Citrate (15 mM)	1.05	8.3	> 50
Oxalacetate (15 mM)	0.64	56	4.2 ± 0.3
Succinate (30 mM)	0.59	57	3.8 ± 0.7
Malate (30 mM)	0.59	53	3.9 ± 0.9
Fumarate (15 mM)	0.52	52	3.8 ± 0.6
cis-Aconitate (15 mM)	0.59	58	4.2 ± 0.3
DL-Isocitrate (30 mM)	0.64	51	4.2 ± 0.3
Pyruvate (15 mM)	0.52	49	4.6 ± 0.3
Tartarate (15 mM)	0.48	55	4.3 ± 0.3
Itaconate (15 mM)	0.62	49	4.4 ± 0.2
Gly (20 mM)	0.88	56	3.8 ± 0.2
Leu (20 mM)	0.84	54	4.1 ± 0.1
Ileu (20 mM)	0.66	49	4.0 ± 0.2
Gly(10 mM)+Ileu(10 mM)	0.48	53	4.0 ± 0.4
D-Cycloserine (0.1 mM)	0.44	58	4.0 ± 0.1
Bacitracin (0.05 mM)	0.52	44	3.8 ± 0.4
Ampicillin (0.9 mM)	0.44	47	4.2 ± 0.2
Cefazolin (0.5 mM)	0.46	52	4.0 ± 0.1
Vancomycin (0.1 mM)	0.39	53	3.6 ± 0.3
Ristocetin (0.1 mM)	0.44	52	3.8 ± 0.4
EDTA (0.5 mM)	0.42	55	4.6 ± 0.6
STPP*** (20 mg/ml)	0.43	51	4.3 ± 0.1
Zeolite 4A (120 mg/ml)	0.37	48	4.7 ± 0.2
In standard medium containing 10 mM citrate			
No addition (10 mM citrate only)	0.98	9.2	38 ± 2.6
Asp (20 mM)	0.92	8.2	35 ± 4.3
L-Lys (20 mM)	0.96	5.2	36 ± 2.1
DAP (30 mM)	0.88	9.1	38 ± 1.8
Glu (20 mM)	0.98	8.4	36 ± 3.0
L-Ala (20 mM)	0.96	8.0	39 ± 1.6
D-Ala (20 mM)	0.90	7.7	39 ± 2.4
Ala-Ala (20 mM)	0.88	6.9	37 ± 3.2
N-Ac-$GluNH_2$ (20 mM)	0.94	8.2	36 ± 1.5
$GluNH_2$ (20 mM)	0.84	7.8	36 ± 1.9
$GalNH_2$ (10 mM)	0.91	6.8	38 ± 2.4

*% of chains with 4 or less cells. **Average number cells/chain. ***Sodium tripolyphosphate.

growth was retarded. Concentrations of citrate greater than 40 mM completely inhibited the growth of this mutant (and also of the parent). In contrast, another mutant strain KSM-1106C^r could grow in standard medium containing 220 mM citrate. The yield of growth of this mutant, after 16 h of incubation at 26°C, was higher between 5 and 170 mM citrate, and the maximum yield was observed between 30 and 50 mM citrate at which concentrations the yield was 160% of the control yield without citrate. However, the susceptibilities to EDTA, STPP and Zeolite were the same among Cit$^-$ and Cit^r strains.

As the concentration of citrate was increased, the Cit$^-$ mutant occurred as long chains with increasing numbers of cells per chain. When the concentration of citrate was brought up to 15 mM, the chains became tangled clumps of innumerable cells, as observed with the parent. In contrast, the Cit^r mutant occurred as short chains (2 to 6 cells/chain) over the range of concentrations of citrate from zero to 40 mM, but above 40 mM it abruptly occurred as long chains.

Observations with the electron microscope

Figures 4 to 8 show SEM micrographs of Streptococcus sp. KSM-1106 and S. cremoris ATCC 19257, grown in the presence or absence of citrate. Cells of Streptococcus sp. KSM-1106 usually occurred in pairs or short chains of ovoid cells, 0.6 to 0.8 by 0.8 to 1.2 μm in size (Fig. 4). Long chains with very many cells were formed in standard medium that contained citrate (Fig. 5). The wall of some cells had burst, demonstrating that the walls of cells in long chains are fragile. In addition, citrate changed the morphology of cells of this strain from ovoid to a mixture of ovoid and rod-shaped cells of irregular size and shape, 0.4 to 1.0 by 1.0 to 1.7 μm. With 5 mM Mn^{2+} present in medium supplemented with 15 mM citrate, the cells of this strain were revealed to be in a well-separated coccoid cell form, about 0.6 to 0.8 μm in diameter (Fig. 6).

Ovoid cells of the typical taxonomic ATCC strain, S. cremoris and S. lactis, grew in pairs or short chains, regardless of the presence or absence of citrate. Normal cells of S. cremoris had many small protrusions on the cell surface (Fig. 7). However, when citrate was present, cracks were often observed in the cell surface (Fig. 8). The cell surface of S. lactis was smooth, independently of the addition of citrate over a range of concentrations.

To gain further insight, we prepared SEM micrographs of the Cit$^-$ and the Cit^r mutants of strain KSM-1106, grown in the presence of 15 mM citrate. The Cit$^-$ strain, lacking a citrate permease, grew as long chains with a mixture of ovoid and rod-shaped cells (Fig. 9). The chain length of the Cit^r strain, grown in standard medium, was very short (about 2 cells/chain) with ovoid and rod-shaped forms (0.6 by 0.6 to 2.2 μm, Fig. 10). Even when grown with 30 mM citrate, this mutant grew as short chains of cells with well-separated coccoid cell form (about 0.6 μm in diameter, Fig. 11).

We next prepared TEM micrographs of thin sections of chaining cells of the KSM-1106, grown in the presence of 15 mM citrate (Figs. 12, 13 and 14). The micrographs obtained suggest apparently that the organism in long chain has undergone a cell division and/or growth cycle without complete formation of cross wall. In fact, the cross wall was not synthesized completely in some cells in the long chain.

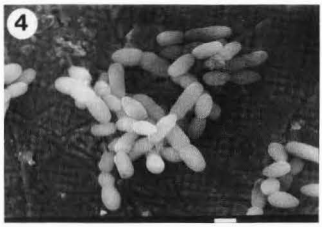

Fig. 4. SEM micrograph of Streptococcus sp. KSM-1106, grown in standard medium. Bar=1.0 μm.

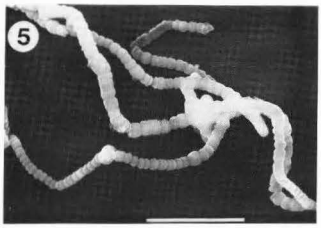

Fig. 5. SEM micrograph of Streptococcus sp. KSM-1106, grown in medium supplemented with 15 mM citrate. Bar=10 μm.

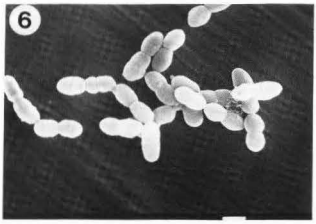

Fig. 6. SEM micrograph of Streptococcus sp. KSM-1106, grown in medium supplemented with 15 mM citrate and 3 mM Mn^{2+}. Bar=1.0 μm.

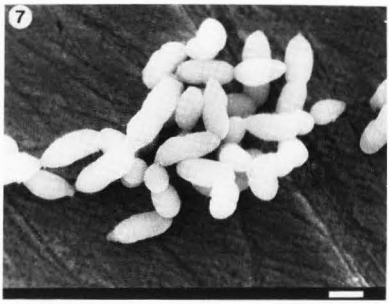

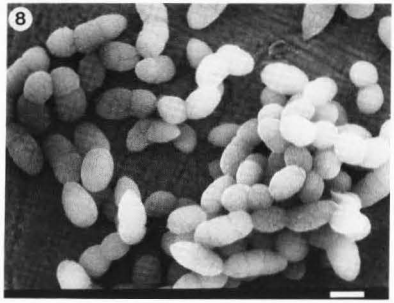

Fig. 7. SEM micrograph of S. cremoris ATCC 19257, grown in standard medium. Bar=1.0 μm.

Fig. 8. SEM micrograph of S. cremoris ATCC 19257, grown in medium supplemented with 15 mM citrate. Bar=1.0 μm.

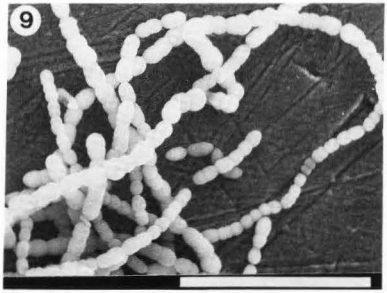

Fig.9. SEM micrograph of the mutant KSM-1106C⁻, grown in medium supplemented with 15 mM citrate. Bar=10 μm.

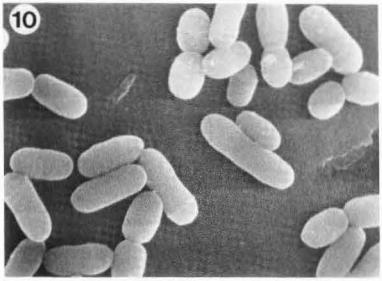

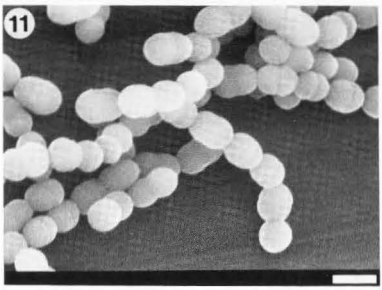

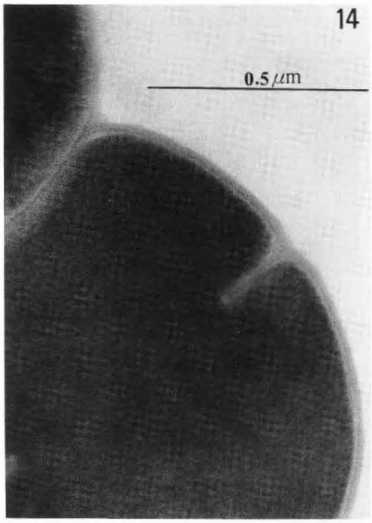

Fig. 10. SEM micrograph of the mutant KSM-1106Cr, grown in standard medium. Bar=1.0 μm.

Fig. 11. SEM micrograph of the resistant mutant cells, grown in medium supplemented with 30 mM citrate. Bar=1.0 μm.

Figs. 12 - 14. TEM micrographs of thin sections of Streptococcus sp. KSM-1106 grown in medium supplemented with 15 mM citrate.

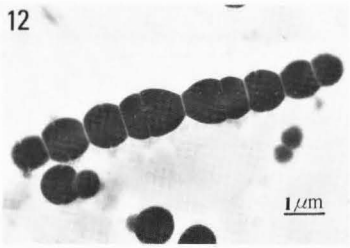

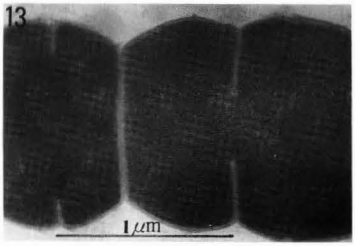

Discussion

SEM and TEM are useful techniques for studying the microstructure of a variety of microorganisms including a group of prokaryotes having no distinct organelle. Experimentally we used WET-SEM for morphological studies of streptococci. This technique is not useful at present for making comparisons of the microstructural appearance of bacterial specimens but can be used to obtain much information about the wet appearance of specimens, free from drying artifacts.

Morphology of bacterial cells has been reported to be changeable under different environmental conditions such as pH (Rhee & Pack, 1980) and temperature (Goel & Marth, 1969). The streptococci characteristically tend to grow as pairs or short chains, but sometimes they grow in chains of variable length, dependent, for instance, on the strain (McDonald, 1971; Shaikh & Steward-Tull, 1975), addition of immune antisera (Ekstedt & Stollerman, 1960) or contact with suramin, a lysozyme inhibitor (Lominski & Gray, 1961). Whitehead and Hunter (1949)

observed so-called "involution" forms of S. cremoris, on cultivation at 37°C, which had very long chains of flattened cocci. McDonald (1971) also isolated long chains of S. cremoris and S. lactis from growths in the orifices of chemostat medium inlet tubes.

In this paper, we have reported that citrate induces the formation of long chains of cells of group N streptococci. The observations obtained with the SEM may be interpreted to indicate that the formation of long chains occurs as the result of a failure of cells to separate after division and not of a failure of cross wall formation. It also raises a possibility that citrate can stimulate initiation of cell division at multiple sites, resulting in greater fragility of cells in long chains. However, the TEM micrographs of thin sections of chains of cells of the KSM-1106 strain showed that the cross walls were not synthesized completely in several cells in the chain. This result alternatively suggests that citrate inhibits an intermediary step between cross wall formation and cell separation but not the final step of cell separation. As our results have been obtained from cells during an unbalanced growth, it is inadequate at present to elucidate the details by which some strains of group N streptococci grew as long chains in the presence of citrate.

In medium supplemented with citrate, a Cit^r mutant, capable of growing at high concentrations of citrate, grew as very short chains, but Cit^-, a mutant missing a citrate permease, grew as very long chains. These results suggest that citrate must be a specific trigger for the growth of long chains of cocci, but this abnormal morphology may be unrelated to their ability to metabolize citrate. Inhibition of the formation of long chains by divalent cations further suggests that these cations are essential for normal growth as short chains. We hypothesized that the cations in the growth medium might be sequestered by citrate and, in fact, the separation of bacterial cells has been reported to require divalent cations (Webb, 1949; Kojima et al., 1970). Especially, McDonald (1957) has demonstrated that lactic streptococci require divalent cations for growth in the presence of citrate. However, the mechanism of the effect of citrate on chain length cannot readily be explained by its chelating of the essential divalent cations since strong chelating agents, such as EDTA, STPP and Zeolite, exerted no effect on the morphology or chain length of the cells.

Involvement of an enzyme or a set of enzymes (autolysin(s)) responsible for division and separation (dechaining) of streptococcal cells has been studied (Lominski et al., 1968; Shockman et al., 1967; Higgins et al., 1970). Fein and Rogers (1976) presented direct evidence for the mechanism of the formation of long chains of bacterial cells, using an autolysin-deficient strain of Bacillus subtilis. Therefore, the formation of long chains of group N streptococci may be related to inhibition of the dechaining enzyme by citrate. Inhibition of dechaining activities has frequently been reported to induce the formation of long chains of some streptococci (for instance, Soper & Winter (1973)) and other organisms (Chatterjee et al., 1969; Tomasz, 1968; Fan, 1970). Recently, we found a dechaining activity in cell free extract of Streptococcus sp. KSM-1106 (Ito et al., 1984). The dechaining enzyme which was extracted from the parent was inhibited by citrate, but the enzyme obtained from the Cit^r mutant was not affected by citrate. It seems likely that such an enzyme in the Cit^r mutant is one that has been genetically altered to have a lower affinity for citrate. These preliminary results might tend to eliminate the possibility that citrate stimulated initiation of cell division at multiple sites of the test strain, as described earlier in Discussion. We suggest that this dechaining enzyme may have a specific binding or affinity site for citrate and, hence, the essential role of divalent cations in normal growth might be nullified in some way, with the net result that long chains of cells are generated. Recently, we have obtained the data which suggest that the dechaining enzyme of Streptococcus sp. KSM-1106 locates on the outer membrane or in the periplasmic space of the cells, using spheroplasts of the parent and the Cit^- strains. We are now engaged in attempts to purify this enzyme in order to compare it with the previously reported autolysins with respect to catalytic nature and physiological meaning involved in cell division system.

Acknowledgments

We thank the Application Center of Akashi Seisakusho, Ltd., for providing facilities, and Mr. S. Shimakura, Director of the Center, for valuable discussion concerning the WET-SEM micrograph.

References

Chatterjee AN, Mirelman D, Singer, HJ, Park JT. (1969). Properties of a novel pleiotropic bacteriophage-resistant mutant of Staphylococcus aureus H. J. Bacteriol. 100, 846-853.

Cutler WG. (1972). Surfactant Science Series, Vol. 5 (Part 2). (eds). Cutler WG, Davis RC, Marcel Dekker, New York, p. 453-729.

Ekstedt RD, Stollerman GH. (1960). Factors affecting the chain length of group A streptococci. I. Demonstration of a metabolically active chain splitting system. J. Exp. Med. 112, 671-686.

Fan DP. (1970). Autolysin(s) of Bacillus subtilis as dechaining enzyme. J. Bacteriol. 103, 494-499.

Fein JE, Rogers HJ. (1976). Autolytic enzyme-deficient mutants of Bacillus subtilis 168. J. Bacteriol. 127, 1427-1442.

Goel MC, Marth EH. (1969). Chain length of Leuconostoc citrovorum modified by dilution and shaking procedures of the plate count. J. Dairy Sci. 52, 1941-1947.

Higgins ML, Pooley HM, Shockman GD. (1970). Site of initiation of cellular autolysis in Staphylococcus faecalis as seen by electron microscopy. J. Bacteriol. 103, 504-512.

Ito S, Kobayashi T. Saitoh M, Morichi T. (1984). Citric acid-induced long chain formation of Streptococcus sp.. Agric. Biol. Chem. 48, 2205-2210.

Johnson KG, McDonald IJ. (1974). Peptidoglycan structure in cell walls of parental and filamentous Streptococcus cremoris HP. Can. J. Microbiol. 20, 905-913.

Kempler GM, McKay LL. (1980). Improved medium for detection of citrate-fermenting Streptococcus subsp. diacetylactis. Appl. Environ. Microbiol. 39, 926-927.

Kojima M, Suda S, Hotta S, Hamada K, Suganuma A. (1970). Necessity of calcium ion for cell division in Lactobacillus bifidus. J. Bacteriol. 104, 1010-1013.

Lominski I, Cameron J, Wyllie G. (1968). Chaining and unchaining Streptococcus faecalis—a hypothesis of the mechanism of bacterial cell separation. Nature (London) 181, 1477.

Lominski I, Gray S. (1961). Inhibition of lysozyme by 'Suramin'. Nature (London) 192, 683.

McDonald IJ. (1957). Effect of acetate, citrate, and bivalent metal ions on utilization of sodium caseinate by lactic streptococci. Can. J. Microbiol. 3, 411-417.

McDonald IJ. (1971). Filamentous forms of Streptococcus cremoris and Streptococcus lactis. Observations on structure and susceptibility to lysis. Can. J. Microbiol. 17, 897-902.

Miyashiro S, Enei H, Takinami K, Hirose Y, Tsuchida T, Udaka S. (1980). Stimulatory effect of inhibitors of cell wall synthesis on protein production by Bacillus brevis. Agric. Biol. Chem. 44, 2297-2303.

Mocoquot G, Hutel C. (1970). The selection of some micro-organisms for the manufacture of fermented and acidified milk products. J. Soc. Dairy Tech. 23, 130-146.

Reynolds ES. (1963). The use of lead citrate at high pH as an electron-opaque stain in electron microscopy. J. Cell Biol. 17, 208-212.

Rhee SK, Pack MY. (1980). Effect of environmental pH on chain length of Lactobacillus bulgaricus. J. Bacteriol. 144, 865-868.

Robinson VNE. (1975). Wet stage modification to a scanning electron microscope. J. Microsc. 103, 71-77.

Schwuger MJ, Smolka HG. (1976). Sodium-aluminium-silicates in the washing process Part I: Physico-chemical aspects of phosphate substitution in detergents. Colloid & Polymer Sci. 254, 1062-1069.

Shaikh MR, Stewart-Tull DES. (1975). Streptococcus faecalis chain-disruption. J. Gen. Microbiol. 91, 195-197.

Shimakura S, Inoûe T. (1985). WET-SEM and its application. DENSHIKENBIKYO 19, 172-174.

Shockman GD, Thompson JS, Conover MJ. (1967). The autolytic enzyme system of Streptococcus faecalis. II. Partial characterization of the autolysin and its substrate. Biochemistry 6, 1054-1065.

Soper JW, Winter CG. (1973). Role of cell wall autolysin in chain formation by a mutant strain of Streptococcus faecalis. Biochim. Biophys. Acta 297, 333-342.

Teuber M, Geis A. (1981). The Prokaryotes, Vol. 2. (Eds.) Starr MP, et al., Springer-Verlag, New York. p. 1614.

Tomasz A. (1968). Biological consequences of the replacement of choline by ethanolamine in the cell wall of Pneumococcus: Chain formation, loss of transformability, and loss of autolysis. Proc. Natl. Acad. Sci. U.S.A. 59, 86-93.

Webb M.(1949). Influence of magnesium on cell division. II. The effect of magnesium on growth and cell division of various bacterial species in complex media. J. Gen. Microbiol. 3, 410-417.

Whitehead HR, Hunter GJE. (1949). A note on morphological differences between strains of Streptococcus cremoris. J. Gen. Microbiol. 3, 43-45.

Yashima S, Kawai K, Okami Y, Sasaki Y. (1970). Effect of oxygen on glucose dissimilation by heterolactic bacteria. J. Gen. Appl. Microbiol. 16, 543-545.

Discussion with Reviewers

R.A. Holley: Could the surface cracks of S. cremoris be artifacts of preparation?
Authors: It is not clear whether these cracks were artifacts or not. However, the cracks of S. cremoris, induced by citrate, were observed in repeated experiments.

I.J. McDonald: Did the pH of citrate-containing media have any effect on chain length of Streptococcus sp. KSM-1106?
Authors: Any effect was not observed at pH values between 5.0 and 7.5. At these pH values, our strain occurred as long chains in the presence of 30 mM citrate.

FOOD MICROSTRUCTURE, Vol. 6 (1987), pp. 25-33
Scanning Microscopy International, Chicago (AMF O'Hare) , IL 60666 USA

0730-5419/87$3.00+.00

THE CRYSTALLIZATION OF CALCIUM PHOSPHATE AT THE SURFACE OF MOULD-RIPENED CHEESES

B.E. Brooker

AFRC Institute of Food Research, Reading Laboratory
Shinfield, Reading, Berkshire RG2 9AT, U.K.

Abstract

Samples of several different types of mould-ripened cheese were examined by light and electron microscopy for evidence of calcium phosphate crystallization near their surfaces, which, it was predicted, should result from the pH changes that take place in the rind during ripening. Transmission electron microscopy showed that characteristic convoluted crystals appeared in the rind as mould growth developed and that there was good evidence that at least some of the crystal nucleation was taking place inside effete hyphae. Light microscopy showed that this coincided with the appearance of birefringent, phosphate-rich crystals in the cheese rind which were tentatively identified as calcium phosphate. This was confirmed by a series of experiments in which frozen and fractured cheese was examined by scanning electron microscopy in conjunction with digital X-ray spectrometry. This showed that the rind contained very high levels of calcium and phosphorus which could not be attributed to surface drying because in the same area, there was no corresponding concentration of other elements, such as chlorine.

It is proposed that the high pH generated by the surface flora causes the precipitation of calcium phosphate from the continuous aqueous phase. In addition, the inhibitory effect of casein on the phase transformation to crystalline calcium phosphate is probably removed by the action of extracellular proteases from the mould. The resulting depletion of calcium phosphate in the aqueous phase establishes a gradient which is responsible for the diffusion of more of the salt from deeper parts of the cheese and the progressive concentration in the rind.

Initial paper received February 10, 1987
Manuscript received May 05, 1987
Direct inquiries to B.E. Brooker
Telephone number: 44-734-883103x2283

KEY WORDS: Calcium phosphate, crystallization, cheese, mould-ripened, mould, ammonia, casein, X-ray analysis, freezing stage, scanning electron microscopy.

Introduction

It has been known for some time that during the maturation of cheese, microscopic aggregates of calcium phosphate crystals (up to 25 μm diameter) soon appear in the protein matrix and gradually increase in number with time (Laxa, 1926; Swiatek and Jaworski, 1959; Brooker et al., 1975). Although these aggregates appear throughout the protein matrix, the microscopical study of hard cheeses has shown that they occur in largest numbers along the curd junctions and it has therefore been assumed that calcium phosphate crystallizes from pockets of residual whey. Since milk is saturated with respect to a number of calcium phosphate salts, it can be expected that, during the development of acid in renneted milk, part of the micellar calcium phosphate will dissolve to give a supersaturated solution in the subsequent curd or cheese serum. This appears to be borne out by the results of a recent study of 1 month old Cheddar cheese by Morris et al. (1987), in which the aqueous phase was isolated from the cheese by pressing and then found on analysis to be supersaturated with respect to various calcium phosphate salts and to tricalcium citrate. However, there still exist problems in explaining the precipitation of calcium phosphate from an aqueous phase at the low pH's which predominate in young cheeses and in understanding the subsequent crystal nucleation and growth in a casein and peptide-rich environment which, according to previous observations (Termine and Posner, 1970; Termine et al., 1970; Visser et al., 1986) should inhibit such phase transformation. The observation that bacteria are often closely associated with the crystalline material in cheese, and indeed sometimes contain crystals, has suggested to some authors (Knoop and Peters, 1971; Kalab, 1980) that a local rise in pH caused either by the lysis and release of cell contents from dead bacteria or by microbial activity, is sufficient to initiate crystallization of calcium phosphate from the nucleation sites presented by the bacteria.

In the case of hard cheeses, obvious practical problems confront any attempt to demonstrate the minute local changes in pH required by this hypothesis, but it is obvious that similar yet very profound and well established changes do take place over the entire surface of mould-ripened

cheeses such as Camembert and Brie. For example, Le Graet et al. (1983) have demonstrated that pH changes take place at the surface of Camembert-like cheeses during maturation. According to these authors, the pH of the original cheese curd is 4.6 but by day 6 a sharp rise takes place at the cheese surface such that at day 17 the pH has reached 7.6.

On the basis of what has been said above, it can be predicted that in a zone near the surface of soft, mould-ripened cheeses where there is a sharp rise in pH as the flora develops, extensive crystallization of calcium phosphate from the aqueous phase can be expected to occur. In the present work, a number of mould-ripened cheeses were examined for evidence of such changes. This was done using transmission electron microscopy (TEM) and by exploiting the benefits of the low temperature stage of the scanning electron microscope (SEM) which, in addition to preserving natural structural detail, allows the quantification and spatial distribution of relevant elements to be determined in fully hydrated specimens using X-ray spectrometry.

Materials and Methods

Coulommier cheeses were made from pasteurised milk according to the factory method given by Scott (1986) and their surface sprayed with an aqueous suspension of spores of Penicillium candidum (supplied by Eurozyme, U.K.). At least 2 days were allowed to elapse between salting and the earliest microscopical examinations. Mature and immature samples of French Camembert, German and English (Lubborn cheese) Brie and white Lymeswold (Dairy Crest) were purchased from retail outlets.

Light microscopy

Slices of cheese 3 mm thick and normal to the surface were taken from mould-ripened cheeses and frozen by immersion in iso-pentane cooled with solid carbon dioxide. Frozen sections, 3 µm thick, were cut using a Reichert sledge microtome fitted with a Peltier cooling stage and attached to slides. After drying, they were immersed in xylene, mounted unstained in a neutral medium and examined with a Zeiss WL microscope between crossed polarizer and analyzer filters. Other sections were stained by the von Kossa technique (after Carleton and Drury, 1957) for phosphate groups and examined by bright field microscopy. Using these methods, the volume fraction of birefringent and phosphate-rich particles in the rind of ripe Coulommier cheese was determined using a modification of the point counting method of Glagoleff (1933).

Transmission electron microscopy

Samples of each of the above soft cheeses were taken from near the surface to include the layer of mould together with 2 - 3 mm of the underlying cheese matrix. They were fixed for 3 - 4 h in unbuffered 2% glutaraldehyde and then washed for 1 h in 0.1 M cacodylate-HCl (pH 6.8) buffer before transfer to 1% osmium tetroxide buffered with 0.1 M cacodylate-HCl to pH 6.8. After 2 h, they were washed in water and dehydrated in a graded series of acetone-water mixtures and 100% acetone before embedding in Araldite. Sections were cut on a Reichert OmU3 ultramicrotome and stained in lead citrate before examination in a Hitachi 600 transmission electron microscope at an accelerating voltage of 100kV.

Scanning electron microscopy and X-ray analysis

All specimens were examined by SEM whilst still fully hydrated and were prepared and handled using an EMscope SP2000 cryo-preparation unit with transfer device and microscope cold stage. A slice of soft cheese, 2 mm thick, was taken at right angles to the surface so that it included the whole thickness of the layer of mould and some 3 - 4 mm of the underlying protein matrix. It was then placed in a grooved copper holder (or carbon if X-ray analysis was to be performed) where, if necessary, it was secured using a solution of carboxymethyl cellulose and frozen by plunging into nitrogen slush. The sample was transferred to the preparation unit under vacuum, fractured using a pre-cooled blunt rod and then coated in situ either with gold, when purely morphological information was required, or with carbon when X-ray spectrometry was to be performed in conjunction with the structural observations. When coating had been done, the frozen sample was transferred to the cold stage (maintained at -185°C) of a Hitachi S570 SEM and examined. In some cases however, where more detail of the organic matrix was required, the samples were etched by subliming some of the surface ice before coating with gold. This was done in a controlled fashion by observing the uncoated specimen in the microscope at low accelerating voltage (1 - 2 kV) whilst raising the temperature of the sample by means of a stage heater. Sublimation was allowed to occur for 5 min at temperatures as high as -50°C until sufficient detail could be seen. When this was completed and the sample had once more been cooled down to liquid nitrogen temperature, it was transferred to the preparation unit and coated with gold before examination once again in the SEM at higher accelerating voltages.

All X-ray microanalysis was done using a Link Analysis AN 10/85 spectrometer with a standard windowed detector fitted to the specimen chamber of the SEM. When areas of frozen specimens had been selected for elemental analysis, the lowest possible accelerating voltage consistent with the excitation potentials of the selected elements was used to reduce unnecessary penetration of the specimen. The spatial distribution of a number of elements including calcium (Ca), phosphorus (P) and chlorine (Cl) was determined using a semi-quantitative digital X-ray mapping procedure (Digimap) with a screen resolution of 128 x 128 pixels. Fully quantitative determination of the levels of elements in different parts of the cheese was performed using the ZAF-PB analyser software for rough surfaces (Link Analysis) on multiple site (>30) spot analysis with standards (Statham and Pawley, 1978; Statham, 1979).

Results

Light microscopy and TEM

The ultrastructural appearance of Coulommier cheese before its surface had been inoculated with mould spores was similar to that previously described by Knoop and Peters (1971). Uniformly distributed throughout the entire cheese in small numbers, aggregates of needle-like crystals (up to 20 µm diameter) were found which were identical to those reported elsewhere from a variety of soft and hard cheeses (Knoop and Peters, 1971; Brooker et al., 1975; Kalab, 1977,1980; Bottazzi et al., 1982). These crystal aggregates were birefringent when examined in polarized light and when stained by the von Kossa technique, appeared intensely black. When the spatial distribution of Ca and P was determined in frozen specimens by digital X-ray mapping, the coordinates of focal concentrations of both elements coincided and it was therefore concluded that the material at these points was composed of calcium phosphate. Because the distribution and numbers of these bodies was similar to that of the crystalline aggregates, it was concluded that the latter were composed of calcium phosphate, as indeed did Bottazzi et al. (1982) in their study of Grana cheese. Detected levels of Ca and P in the surrounding protein matrix were relatively uniform and low.

When the rind (surface 150 µm) was examined from the same cheese on which the inoculated mould had been growing for 1 week, it was evident from TEM that large convoluted crystals had started to appear alongside the existing crystal aggregates (Fig. 1). This coincided with an obvious increase in the number of birefringent particles which were also found to be rich in phosphate groups from their intense staining after the von Kossa technique (Fig. 2). Examined by TEM, the morphology of these particles was quite distinct from that of the crystal aggregates, but it was tentatively concluded that they also were composed of crystalline calcium phosphate in view of their optical activity and their high phosphate content.

In the case of Coulommier cheese, there was a gradual and noticeable increase in the number of these crystals during ripening. Similarly, in all of the other varieties of ripe cheese examined, enormous numbers of calcium phosphate crystals were observed by light microscopy but there was also a gradual reduction in their diameter, the deeper in the cheese they were found (Fig. 2). As expected, the mean volume fraction of birefringent particles in the surface 150 µm of ripe Coulommier was 21.81% ± 7.92 (n = 4000) compared well with 24.50% ± 8.34 (n = 4000) for the phosphate-rich bodies visualised by the von Kossa technique. In comparable areas of the cheese surface, the corresponding values for uninoculated cheese which had no mould growth were 0.06% ± 0.04 for birefringent particles and 0.09% ± 0.03 after von Kossa staining.

By TEM, crystals were usually found associated with the surface of the closely packed hyphae in the rind (Fig. 3) and on very many occasions, crystal growth could be seen to extend across the cell wall into the dispersed contents of a dead hypha (Fig. 4). However, in such cases it was not clear whether crystal growth had originally started within the hyphae or from the aqueous phase of the cheese. Profiles such as those given in Fig. 5 demonstrate that in many instances, the nucleation site for crystal growth was inside the moribund hyphae. Since it is impossible to infiltrate crystals with resin in order to section them, it is important to note that the structures viewed by TEM and referred to here as crystals, actually refer to the spaces vacated by crystalline material during processing. Such spaces were visible by negative contrast because of the presence of the surrounding protein.

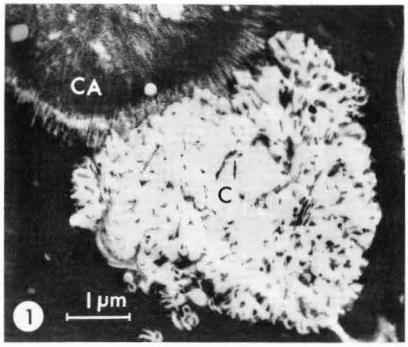

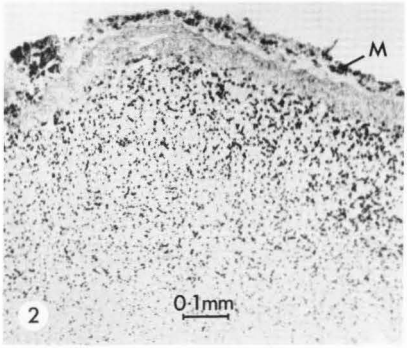

Fig. 1. A convoluted crystal (C) in the rind of a 3 week old Coulommier cheese lying adjacent to a crystal aggregate (CA). TEM.
Fig. 2. Frozen section through the surface of 3 week old Coulommier cheese stained by the von Kossa technique. Beneath the mould (M), numerous phosphate-rich particles are visible. Light microscopy.

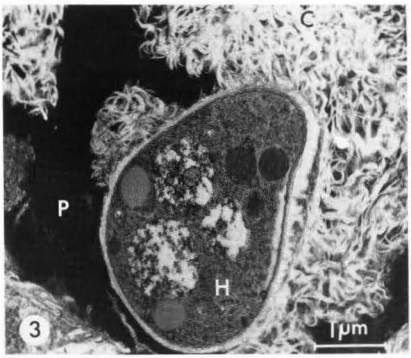

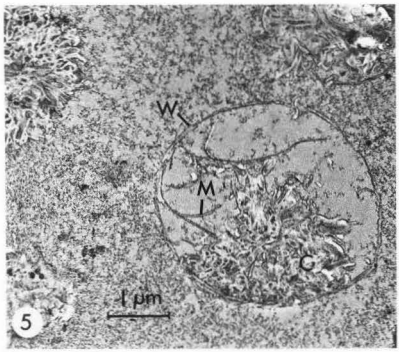

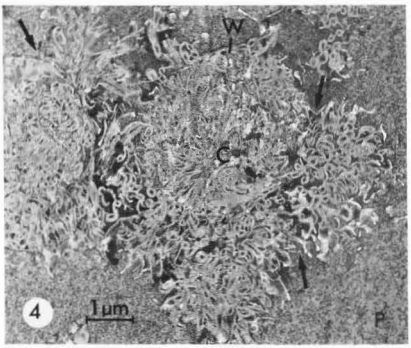

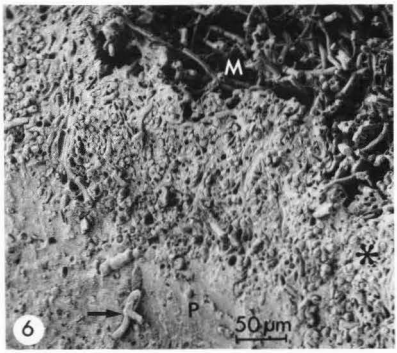

Fig. 3. Transverse section of a hypha (H) of Penicillium candidum in the rind of Camembert cheese surrounded by several convoluted crystals (C). P = protein matrix. TEM.
Fig. 4. Convoluted crystals (C) growing inside the cell walls (W) of two effete hyphae in Brie cheese. The crystals extend through the cell walls (at arrows) into the surrounding cheese matrix (P). TEM.

Fig. 5. Transverse section of a single moribund hypha in which only a few membrane remnants remain (M). The growth of a convoluted crystal (C) has not yet extended beyond the cell wall (W). From the rind of Brie. TEM.
Fig. 6. Ten day old Coulommier cheese rind frozen and fractured showing the growth of mould (M) on the protein matrix (P). The most superficial layer (*) of the cheese contains a tangled mass of hyphae. Below this (arrows), hyphae are less common. SEM cryo stage.

SEM and X-ray analysis

When frozen cheese samples were fractured normal to the mould covered surface and examined by SEM, a clearly defined superficial layer (150 - 250 µm thick depending on cheese variety) was visible in which a tangled mass of mould hyphae had burrowed into the cheese matrix (Fig. 6). This corresponded to the layer seen by TEM but because of the tight packing of structures, and the lack, at this resolution, of any characteristic morphology on the part of the calcium phosphate crystals, the latter could not be positively identified in this type of preparation. Digital X-ray mapping of a fracture face such as that shown in Fig. 7 showed the individual crystal aggregates of calcium phosphate in the region below the cheese rind as described above (Figs. 8,9,10 and 11) but it also showed very high levels of Ca and P in a layer 75 - 250 µm thick (depending on age and variety of cheese) which always corresponded to that part of the rind containing the tightly packed

Fig. 7. Camembert cheese rind frozen and fractured showing the growth of mould (M) on the surface of cheese matrix (P). Figs. 10 and 11 are digital X-ray maps of this same area. SEM cryo stage.

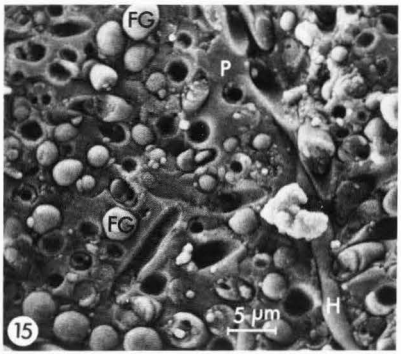

Fig. 15. Lymeswold cheese frozen and fractured. In the lower part of the rind (500 µm from surface) numerous fat globules (FG) protrude from the surface. Note the exposed hyphae (H). P = protein matrix of the cheese.

hyphae and convoluted crystals (Figs. 10 and 11). The distribution of Ca and P was continuous in this zone so that the X-ray emission from individual crystals could not be separated from that of their neighbours. X-ray maps of the same area viewed at low magnification (up to x30) showed, in addition, gradually diminishing levels of Ca and P from the rind to the deeper parts of the cheese matrix (Figs. 12 and 13). This gradient could not be regarded as an artefact caused by the surface topography of the specimen because a digital X-ray map of Cl in the same area showed a comparatively uniform distribution both in the rind and in the much deeper parts of the cheese (Fig. 14). This important observation also demonstrated that the very high levels of Ca and P in the cheese rind were not caused by drying of the cheese surface, for such desiccation would also have led to a concentration of the sodium chloride in the aqueous phase and, correspondingly, high levels of Cl in the X-ray map.

Similar observations were made with all of the other mould-ripened cheeses examined. However, Lymeswold was unlike any other cheese because when frozen and fractured, the fracture plane passing through the rind showed many spherical objects projecting from the surface whose dimensions were similar to those of the convoluted calcium phosphate crystals observed by TEM (Fig. 15). However, when multiple spot analyses were done on these objects, they contained no more Ca and P than background and therefore probably represented fat globules embedded in the protein matrix.

Quantitative data on the relative levels of Ca and P in the surface rind and the deeper areas of Camembert and Coulommier cheeses were obtained using spot analysis of at least 30 randomly assigned points in each zone by X-ray spectrometry. The results presented in Table 1 are those obtained from Camembert cheese and show that the average concentration of Ca and P in the rind was almost 20 times greater than in the body. Similar figures were obtained using Coulommier cheese. In some places, there was a 100 fold difference between the highest values of Ca (4.94 g%) and P (4.12 g%) in the rind and their minimum values in the cheese body (Ca 0.04 g%: P 0.03 g%). The wider spread of values obtained for Ca and P concentrations in the body of the cheese (Table 1) is not entirely unexpected because a proportion of these random point analyses would be expected to impinge on some of the many crystalline aggregates of calcium phosphate and can thus be expected to give much higher values than those derived solely from the background protein matrix.

Discussion

In many surface ripened cheeses, the deamination of amino acids by the mould and its associated flora produces ammonia (Hemme et al., 1982) which diffuses into the rind and raises the pH (Le Graet et al., 1983), thereby creating conditions in which soluble calcium phosphate might be expected to precipitate and then crystallize from the aqueous phase. However, because casein and peptides have an inhibitory effect not only on the formation of amorphous calcium phosphate but also on its transformation to the crystalline form (Termine and Posner, 1970; Termine et al., 1970), the extracellular proteases produced by the mould which degrade cheese protein to peptides and amino acids, probably have a part to play in crystallization by removing the local source of inhibition.

Figures 8 - 14 (color plate) are on pp. 32-33.

The results of the present study show that during the maturation of mould-ripened soft cheeses, calcium phosphate crystallizes and becomes concentrated in a thin layer near the cheese surface. Since crystalline, phosphate-rich bodies appear in the rind at the same time, it is concluded that they are composed of calcium phosphate and from their numbers, that they are largely responsible for the observed high levels of Ca and P near the cheese surface. However, it cannot be excluded that in the digital X-ray maps, there is a significant contribution from amorphous calcium phosphate dispersed throughout the aqueous phase of the rind which has not yet crystallized. This would help explain the near continuous distribution of Ca and P seen in the X-ray maps. It seems clear from the number and distribution of calcium phosphate crystal aggregates observed throughout the cheese that they contribute little to the total levels in the rind. Profiles such as that in Fig. 5 are reminiscent of those obtained by Kalab (1980) in the case of lactic acid bacteria and demonstrate clearly that nucleation and growth of crystals frequently takes place inside hyphae and that their cell walls are freely permeable to the soluble calcium phosphate of the cheese. Such nucleation sites have the advantage that the pH is high enough to initiate precipitation of calcium phosphate whilst, at the same time, being remote from the inhibitory effect of casein on its subsequent crystallization. In spite of this, it is still doubtful how much of the total crystal growth is initiated in this way compared with other sites in the rind. However, it appears highly likely that the escape of cell contents from moribund hyphae contributes not only to the rise in pH of the cheese surface but that hyphae also release cell organelles which may act as nucleating centres in the aqueous phase.

Although the concentration of Ca and P in the surface of Camembert has been noted by other authors using atomic absorption spectrometry (Metche and Fanni, 1978; Le Graet et al., 1983), the values for Ca and P in the rind given by these workers were considerably lower than those obtained in the present study. This was because the sampling procedure of removing relatively large pieces of cheese for analysis necessarily included the deeper zone of Ca and P - depleted cheese which therefore had the effect of lowering the average levels throughout the sample.

Whilst these considerations explain crystallization of the calcium phosphate that already exists in the aqueous phase near the cheese surface, the pronounced concentration of this salt, apparent from the digital X-ray mapping, requires a further explanation. A diagrammatic representation of the events that could be involved in this process are shown in Fig. 16. It can be seen that as the pH of the cheese surface begins to rise and crystallization begins, the aqueous phase becomes depleted and a chemical gradient is established with respect to calcium phosphate. Soluble calcium phosphate in the aqueous of deeper parts of the cheese then diffuses towards the surface where, eventually, that too is precipitated by the prevailing conditions of high pH. In this way, calcium phosphate gradually accumulates in the cheese rind where it reaches (and can probably surpass) the high levels detected in this study. Although diffusion rates for calcium phosphate through the aqueous phase of cheese have not been measured, Geurts et al. (1974) have determined the effective diffusion coefficient for sodium chloride and found it to be in the order of 0.2 cm^2/day. Since similar rates of diffusion can be expected for calcium phosphate, concentration to the observed levels is quite feasible by this mechanism.

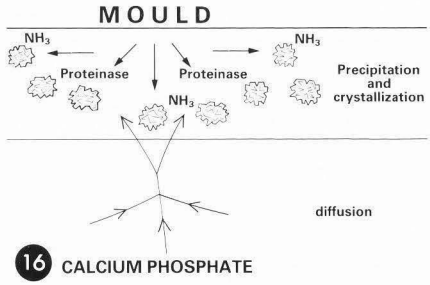

Fig. 16. Diagrammatic representation of the events involved in the crystallization and concentration of calcium phosphate in the rind of mould-ripened cheeses.

Table 1. Mean concentrations of Ca and P (g%) ± SD in 30 randomly assigned points of Camembert rind and cheese body in cheese of 53% water content. Determinations by X-ray spectrometry.

	Ca	P
Rind	3.50 ± 0.77	2.86 ± 0.64
Cheese body	0.19 ± 0.17	0.16 ± 0.15

Acknowledgements

The author extends grateful thanks to Mrs. Jill Webb for her technical assistance in parts of this work.

References

Bottazzi V, Battistotti B, Bianchi F. (1982) The microscopic crystalline inclusions in Grana cheese and their X-ray microanalysis. Milchwissenschaft, 37, 577 - 580.

Brooker BE, Hobbs DG, Turvey A. (1975) Observations on the microscopic crystalline inclusions in Cheddar cheese. Journal of Dairy Research, 42, 341 - 348.

Carleton HM, Drury RAB. (1957) Histological technique. 3rd Ed. Oxford University Press, London. pp 62 - 66.

Geurts TJ, Walstra P, Mulder H. (1974) Transport of salt and water during salting of cheese. 1. Analysis of the processes involved. Netherlands Milk and Dairy Journal, 28, 102 - 129.

Glagoleff AA. (1933) On the geometrical methods of quantitative mineralogic analysis of rocks. Trudy Institute Prikladnoi Mineralogic i Metallurgic, 59, 1 - 47.

Hemme D, Bouillanne C, Métro F, Desmazeaud M-J. (1982) Catabolisme microbien des acides aminés au cours de l'affinage des fromages. (Microbial catabolism of amino acids during the ripening of cheese). Sciences des Aliments, 2, 113 - 123.

Kalab M. (1977) Milk gel structure. VI. Cheese texture and microstructure. Milchwissenschaft, 32, 449 - 457.

Kalab M. (1980) Decayed lactic bacteria - a possible source of crystallization nuclei in cheese. Journal of Dairy Science, 63, 301 - 304.

Knoop A-M, Peters K-H. (1971) Submikroskopische Strukturveranderungen im Camembert-Käse während der Reifung. (Electron microscopy of the structural changes in Camembert cheese during ripening). Milchwissenschaft, 26, 193 - 198.

Laxa O. (1926) L'examen microscopique des fromages. (The microscopical examination of cheeses). Le Lait, 6, 885 - 903.

Le Graet Y, Lepienne A, Brule G, Ducruet P. (1983) Migration du calcium et des phosphates inorganiques dans les fromages à pâte molle de type Camembert au cours de l'affinage. (Migration of calcium and inorganic phosphates in soft cheeses of the Camembert type during ripening). Le Lait, 63, 317 - 332.

Metche M, Fanni J. (1978) Rôle de la flore fongique dans l'accumulation du calcium et du phosphore à la surface des fromages du type camembert. (Role of the fungal flora in the accumulation of calcium and phosphorus at the surface of cheeses of the Camembert type). Le Lait, 58, 336 - 354.

Morris HA, Holt C, Brooker BE, Banks JM, Manson W. (1987) Extraction and analysis of juice from a one-month old Cheddar cheese. Journal of Dairy Research (In Press).

Scott R. (1986) Cheesemaking Practice. 2nd ed. Elsevier Applied Science p. 431.

Statham PJ. (1979) Measurement and use of peak-to-background ratios in X-ray analysis. Mikrochimica Acta, Suppl. 8, 229 - 242.

Statham PJ, Pawley JB. (1978) A new method for particle X-ray micro-analysis based on peak to background measurements. Scanning Electron Microscopy, 1978; I: 469 - 476.

Swiatek A, Jaworski J. (1959) Histochemische Untersuchungen uber die Verteilung von Mineralsalzen im Kaese. (Histochemical study of the distribution of mineral salts in cheese). 15th International Dairy Congress, London. Clay & Co. Ltd. 3, 1509 - 1518.

Termine JD, Posner AS. (1970) Calcium phosphate formation in vitro. I. Factors affecting initial phase separation. Archives of Biochemistry and Biophysics, 140, 307 - 317.

Termine JD, Peckauskas RA, Posner AS. (1970) Calcium phosphate formation in vitro. II. Effects of environment on amorphous-crystalline transformation. Archives of Biochemistry and Biophysics, 140, 318 - 325.

Visser J, Minihan A, Smits P, Tjan SB, Heertje I. (1986) Effects of pH and temperature on the milk salt system. Netherlands Milk and Dairy Journal, 40, 351 - 368.

Discussion with Reviewers

M. Kalab: Did not the relatively high temperature of -50°C used during freeze-etching lead to ice crystal formation ?
Author: Ice crystal growth certainly does occur at this temperature but in practice this presents no great problem. Specimens of the size used in this study always contain some ice crystals but the time for which they are held at this temperature does not allow significant growth to occur. It is interesting to note that such high temperatures are required with some specimens in which the water is tightly bound.

M. Kalab: What was the source of the ZAF-PB Analyser software ? Are references available ?
Author: This is a standard software package available from Link Analysis, High Wycombe, U.K. It is especially useful for the quantitative determination of elements in samples with a 'rough' surface and its special feature is the measurement of peak to background (PB) ratios to do this accurately. Of the many references available, I have given two by Statham.

Figs. 8 - 14. Digital X-ray maps of frozen and fractured samples of Camembert cheese showing the distribution of various elements. SEM. M = mould.
Fig. 8. Distribution of Ca in a zone just beneath the rind. The focal concentrations represent crystal aggregates.
Fig. 9. Distribution of P in the same area as that in Fig. 8. Focal concentrations correspond in position to those in Fig. 8.
Fig. 10. Distribution of Ca in the area shown in Fig. 7 near the cheese surface. Very high levels occur in a layer of the rind. Note also the multiple focal concentrations (arrows) in deeper parts which correspond to aggregates of crystalline calcium phosphate. There is little or no activity in the area occupied by the surface mould.
Fig. 11. Distribution of P in the same field as Fig. 10. A similar layer in which levels are very high can be seen in the rind. The co-ordinates of the focal concentrations in the deeper areas coincide with those for Ca in Fig. 10. Note the reasonably high levels of P in the mould.
Fig. 12. Low magnification elemental map showing the distribution of Ca. The high concentration in the rind is clearly seen but the individual crystal aggregates are invisible at this magnification. Note the zone of reduced Ca levels below the rind and beneath this, lower levels still.
Fig. 13. Distribution of P in the same field as Fig. 12. A gradient similar to that in Fig. 12 is less clear but the high levels in the rind are obvious.
Fig. 14. Distribution of Cl in the same field as Figs. 12 and 13. There is no concentration of Cl in the rind (R) and no indication of the gradient seen in Figs. 12 and 13.

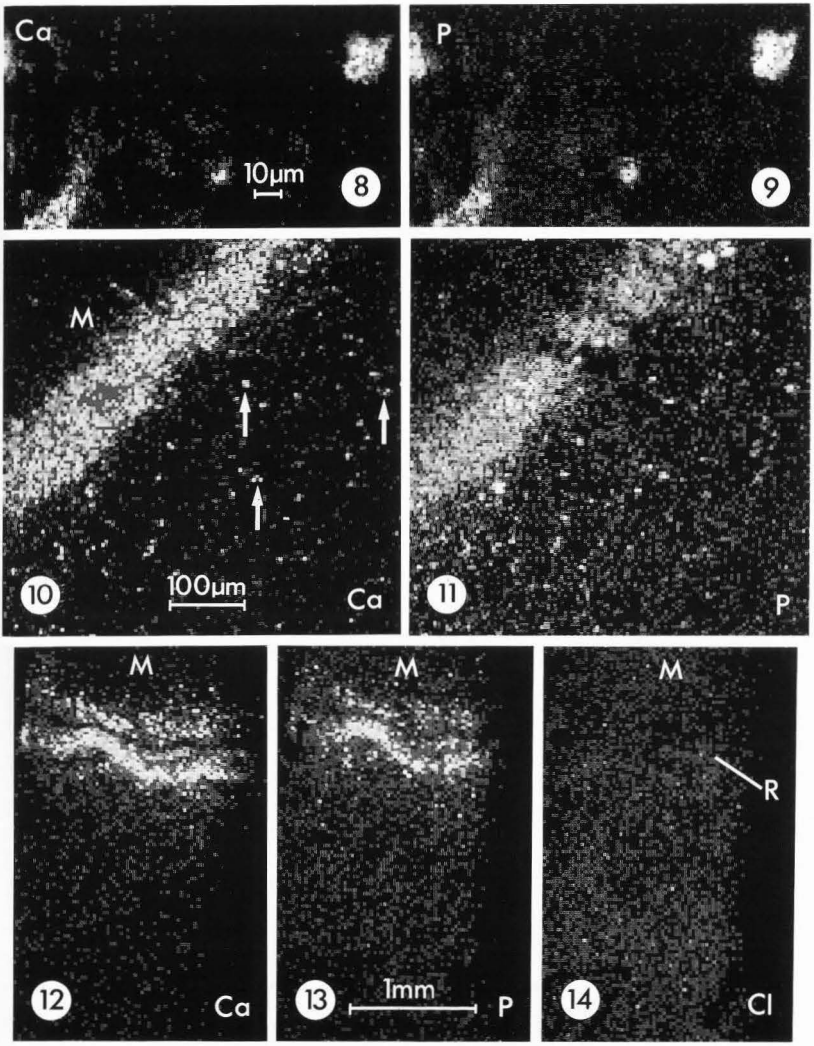
Ca
10µm
8
P
9
M
10
100µm
Ca
11
P
M
12
Ca
M
13
1mm
P
M
R
14
Cl
INCREASING CONC.

FOOD MICROSTRUCTURE, Vol. 6 (1987), pp. 35-46
Scanning Microscopy International, Chicago (AMF O'Hare) , IL 60666 USA

0730-5419/87$3.00+.00

THE SIZE DISTRIBUTION AND SHAPE OF CURD GRANULES IN TRADITIONAL SWISS HARD AND SEMI-HARD CHEESES

M. Rüegg and U. Moor

Federal Dairy Research Institute
3097 Liebefeld, Switzerland

Abstract

Curd granule junction patterns in hard (Emmentaler, Gruyere, Sbrinz) and semi-hard cheeses (Appenzeller, Tilsiter, Raclette) were visualized on slices and examined using light microscopy and digital image analysis. Horizontal and vertical sections were cut in different zones of the loaves, in order to obtain information on the orientation of the flattened curd granules.

The frequency histograms of the cross section areas could in most cases adequately be described as a log-normal distribution. The median values ranged from 0.97 to 1.15 mm^2 and, from 1.31 to 1.68 mm^2 for hard and semi-hard cheeses, respectively.

An elliptical form factor was used as a measure of the deformation of the granules. The average ratio of the elliptical axes was in the range of 0.41 to 0.56 in horizontal and 0.33 to 0.48 in vertical sections. The difference between the form factors in the orthogonal sections was less pronounced in the Appenzeller and Tilsiter cheeses than in the other varieties. Significantly different junction patterns were observed in regions of the edges and sides of the original billets of curd. The micrographs revealed interesting features around the eyes and in the cheese rind.

Semi-mechanized and traditionally manufactured Appenzeller and Tilsiter cheeses had different curd granule junction patterns, mainly because of different moulding and pressing arrangements.

Initial paper received December 12, 1986
Manuscript received March 26, 1987
Direct inquiries to M.W. Ruegg
Telephone number: 41-31-598 166

Key words: Cheese, curd granules, light microscopy, digital image analysis, size distribution, sample preparation technique, microstructure.

Introduction

The importance of both the size and uniform size distribution of curd granules for cheese quality has always been emphasized, in old and modern text books on cheese (e.g., Steinegger, 1904; Fleischmann and Weigmann, 1932; Mair-Waldburg et al., 1974; Scott, 1981). The approximate size of the granules is given in the recipe of each cheese variety. It depends on the way in which the coagulum is cut and on the subsequent thermal and mechanical treatment in the vat and press. Stirring and heating causes the protein matrix to shrink and expel whey (syneresis). Syneresis continues to some extent during pressing. Several studies assessed the significance of the size of the granules and the curd dust for factors such as syneresis (Kammerlehner, 1974), eye formation (Clark, 1918; Koestler, 1933; Hostettler, 1943; Schulz, 1953; Bolliger and Burkhalter, 1957; Flüeler and Kaufmann, 1985), cheese yield (Schwarz and Mumm, 1951; Bolliger and Burkhalter, 1957), moisture, fat content and acidification (Koestler, 1933; Bolliger and Burkhalter, 1957; Flüeler and Kaufmann, 1985). The separation of differently sized particles before pressing and its influence on the quality of Emmental cheese has been studied by Dorner and Ritter (1942) and Bolliger and Burkhalter (1957). Bohac (1970) used frozen sections to study the orientation of the flattened curd granules in hard cheese after pressing. The grain boundaries in curd and cheese, which are known to have a low fat content (King, 1958; Mulder et al., 1966; Hansson et al., 1966), have been studied by various authors and with different techniques including microscopy of frozen or embedded thin sections (e.g., review by Heinrich, 1968; Fricker and Meyer, 1960), sanded preparations of dehydrated slices (Kalab, 1977; Kalab et al., 1982; Rüegg et al., 1985) and electron microscopy (Fricker and Meyer, 1960; Hostettler, 1961; Annibaldi and Nanni, 1979; Rüegg et al., 1980). Effects of various manufacturing processes and equipment on junction patterns in cheddar cheese have been investigated by Emmons et al. (1980), Kalab et al. (1982) and Lowrie et al. (1982).

With very few exceptions, the work on size

and size distribution conducted in the past was of a qualitative nature. Very few quantitative data on the shape and size of granules after cutting or within the cheese body after pressing are available. Dorner and Ritter (1942) most probably were the first who studied systematically the size and shape of curd granules throughout loaves of Emmental cheeses. They took into account the elongation of the curd granules after pressing and measured the diameters on differently oriented cross sections (horizontal, vertical, 45° angle). The small size of frozen sections and the manual measurements permitted the collection of only a limited number of data. Using techniques similar to those introduced by Kalab (1977) and Kalab et al. (1982) together with digital image analyzers, greater surface areas can be observed and the acquisition of a large number of data for stereological and statistical analyses becomes possible (Rüegg et al., 1985).

In the present work, the size-distribution, shape and orientation of curd granules in some important Swiss hard- and semi-hard type cheeses were examined by means of light microscopy and digital image analyses. The primary aim was to obtain reference data for normal first quality cheeses and to investigate the extent to which these were affected by different manufacturing equipment. The micrographs also revealed useful information about the fine structure around the eyes and in the cheese rind.

Materials and Methods

Cheese samples

Mature Emmentaler, Gruyere, Sbrinz, Appenzeller, Tilsiter and Raclette cheeses were obtained directly from different Swiss factories. Raclette cheese was produced from pasteurized milk. The other cheese varieties were manufactured traditionally from raw milk according to procedures described in various textbooks (Muggli et al., 1959, Peter and Zollikofer, 1966, Mair-Waldburg et al., 1974, Steffen et al., 1987). The size distribution of the freshly cut curd particles was as described in standard recipes and varied between approximately the size of hazelnuts (4 - 8) mm and wheat grains (2-4 mm; e.g., Mair-Waldburg et al., 1974). Loaves of each variety were purchased from 5 to 8 different manufacturers and samples were taken from the outer and central zone as indicated in Fig. 1. Vertical (nr. 1 to 6) and horizontal sections (nr. 7 to 12) were cut to obtain information about the orientation of the curd granules inside the cheese body. The curds of Appenzeller, Tilsiter and Raclette cheeses were prepressed in rectangular blocks before filling into the regular round hoops. Sections were therefore taken in these cheeses in the region of the original edge and side part of the billets of curd as shown in Fig. 2. For survey purposes near the rind, slabs were cut through the whole loaf near the hoop side and prepared for microscopical observation as described in the next paragraph.

Typical diameters and heights of cheese loaves were: Emmentaler 85/20, Gruyere 55/12, Sbrinz 55/15, Tilsiter 25/7, Appenzeller 33/9 and Raclette 33/7 cm.

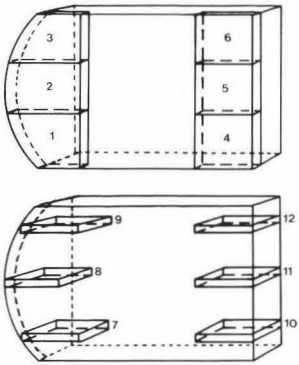

Fig. 1. Schematic drawing of cheese showing the sampling zones for vertical (1 to 6) and horizontal (7 to 12) sections.

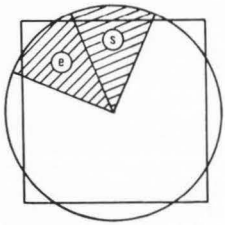

Fig. 2. Sampling zones for semi-hard cheeses in the region of the former edge (e) and side (s) part of the billets of curd.

Preparation of specimens and microscopy

A procedure similar to that proposed by Kalab et al. (1982) was used. The horizontal and vertical sections, 35 x 25 x 2 mm, were fixed, stained, dehydrated and defatted successively with the following solutions and solvents:

- glutaraldehyde/acrolein (6%, 3%), 2-4 d at 5°C
- citrate/phosphate buffer pH = 5.4 (0.005, 0.011 mol/l), 2 x 30 min
- ethanol (95%), 2 x 1h

- methyleneblue (0.05% in ethanol), 5-10 min
- ethanol (95%), 2 x 30 min
- diethylether, 2 x 4h
- n-hexane, 2 x 2 h

The solutions were stirred during each treatment. Overlapping of the sections was prevented by means of specially developed glass holders.

The prepared sections were dried at room temperature overnight between filter paper and glass plates to prevent deformation. One surface was finally sanded with carborundum paper, grade P320, using a sanding disk rotated by an electric stirrer (Heidolph, model 741.00, Kelheim, West Germany). Cheese samples shrunk by about 10% in all directions after drying. A mean factor was determined for each variety together with the magnification factor as described below.

Sections were photographed using a Wild-Leitz Fotomakroskop M400, equipped with a reducing lens (0.5 times) and an automatic 35-mm camera MPS55 (Wild-Leitz AG, Heerbrugg, Switzerland). Illumination was from one side at an angle of 30^0 by means of a low voltage microscopy lamp. Final magnification on the prints used for image analysis was 4.5-5.0 times. The exact magnification was determined for each variety by measuring cheese samples of known original dimensions on the final prints. The effect of shrinkage was thus included.

Digital image analysis

The visualized curd granule junctions were traced on the digitizer tablet of a Mop-Videoplan image analysis system (Kontron Bildanalyse GmbH, München, West-Germany). About 100 connected granules were measured on each photomicrograph. If granules were completely folded to spherical or elliptical particles only the outer contours were traced. The system was programmed to calculate the area (A), the major and minor diameters (a,b), the elliptical form factor or elongation factor (b/a) and the center of mass coordinates. To approximate the axis a and b the data acquisition program calculated an ellipse with the same moment of inertia as the traced structure.

The non-parametric U-test as available in the standard Mop-Videoplan statistical software was applied for testing the significance of differences between the measured distributions within a cheese and between different cheeses. Because of the asymmetry of the distributions of most of the measured parameters the median-value (50%-value) and the interquartil-range (lower and upper 25% values) were used to characterize the data. The shape of the distribution curves was compared with Gauss and log-normal distributions by means of the Kolmogoroff-Smirnow-test included in the Mop-Videoplan program for particle size analysis (TGA program).

The estimation of the number, size and shape of particles by using information only from two-dimensional sections is a well known problem (Weibel, 1979). The section profile distribution is more or less distorted when compared to the true particle size distribution. Only under the strict assumption that all particles have the same known simple shape it is possible to correct the biased distribution of cross-sections and to estimate precisely, the particle number and size (Wicksell, 1925). The apparent diameters are usually smaller than the true diameters and random sections actually contain a relatively greater number of large particles than small ones. The two causes work in opposite directions thus having a chance to balance each other. The average curd granule diameters derived from cross-sections probably slightly underestimate the true dimensions. For comparison, spheres with a size distribution similar to that of curd granules would show in cross sections an average diameter which is about 5% smaller than the true mean diameter. (This difference was estimated by the method of Goldsmith (1967)) . Nevertheless, the principle of Dellesse shows that the volume density of particles is equal to the areal density of the profiles on sections (Weibel, 1979). In this study the approximate elliptical axes have mainly been considered to be a measure of the deformation of the curd granules.

Results and Discussion

Hard cheeses

Curd granule junction patterns in vertical sections typical for Emmentaler, Gruyere and Sbrinz cheese are shown in Figs. 3, 4 and 5, respectively. These sections were cut through the whole loaves near the hoop side including the rinds. Pressing of the fresh cheese, pressure from the gas inside the eyes and to some extent plastic deformation during ripening, leads to characteristic deformation and orientation of the granules. A region around an eye in an Emmentaler cheese is shown at higher magnification in Fig. 6. The regions near the rind and eyes were not considered for the determination of the size distributions of the curd granules. As an example of the increasing deformation in the rind, Fig. 7 shows the elliptical form factor as a function of the distance from the bottom rind of an Emmentaler cheese. The slope of the regression line indicates the increasing elongation of the granules near the rind. Only at a distance of about 10 - 15 mm from the rind do the form factors remain constant within a certain bandwidth.

A pronounced difference could be observed between the patterns on vertical and horizontal sections. Pressing of the cheese loaves and some plastic deformation during ripening flattened the granules. In vertical sections the curd granule boundaries therefore appeared elongated and the maximum diameter was oriented preferentially in the horizontal direction. The difference between the extreme diameters was less pronounced in horizontal sections and there was no preferential orientation. In Fig. 8 are examples of vertical (8a) and horizontal (8b) sections from Sbrinz cheese. The diameters of the cross sections of the curd granules ranged from about 0.5 to 5.0 mm. Typical frequency

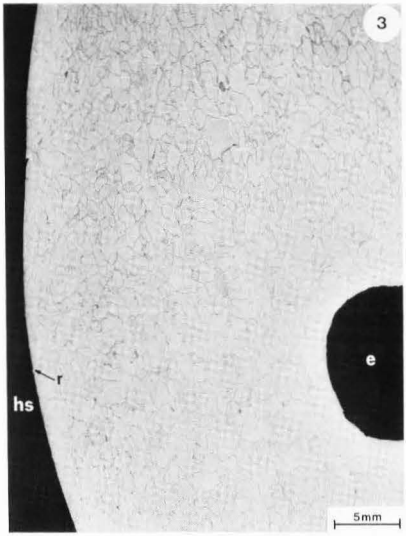

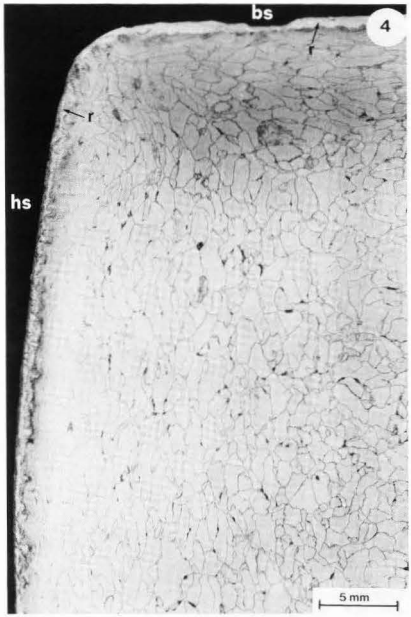

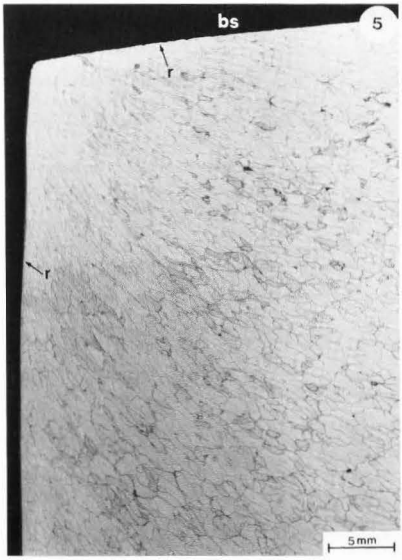

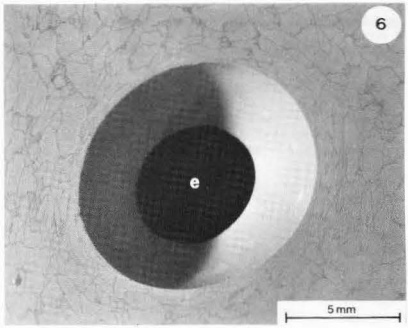

Symbols in photographs: a, artifact from sanding paper; bs, bottom of loaf after filling; e, eyes; hs, hoop side of loaf; i, intensively stained, protein rich zones or curd dust (particles smaller than about 1 mm after cutting of coagulum); r, rind; s, slits.

distributions of the elliptical axes on horizontal and vertical sections are shown in Fig. 9. The median values for the major axis were similar for horizontal and vertical sections in the three types of hard cheeses (1.6 - 1.7 mm, Table 1). The median values for the minor axis ranged from 0.72 to 0.77 mm in vertical and from 0.84 to 0.93 in horizontal sections. It should be remembered that these axes do not correspond to the extreme diameters of the curd granules but represent the calculated axes of an ellipse which has the same moment of inertia as the cross section of the granule. The average form factors determined from the ratio of the elliptical axes on horizontal and vertical sections differed significantly. Fig. 10 shows the frequency distributions of the form factors obtained for Gruyere cheese. The shape of the histogram for the horizontal sections is indicated by the dotted distribution curve. The

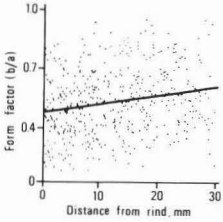

Fig. 7. Deformation of curd granules near the rind in Emmentaler cheese. Elliptical form factor in vertical sections as a function of the distance from the bottom rind of the cheese.

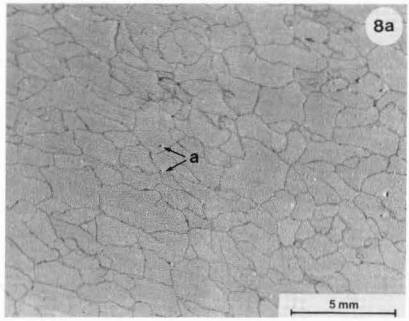

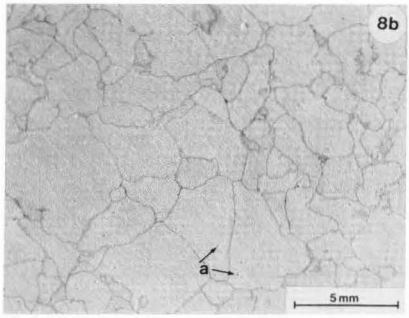

Fig. 8. Typical curd granule junction patterns in vertical (8a) and horizontal (8b) section of Sbrinz cheese indicating deformation due to pressing.

Fig. 3. Vertical section near the hoop side of Emmentaler cheese showing orientation of flattened granules near the rind.

Fig. 4. Vertical section through the loaf of a Gruyere cheese. Dark spots probably indicate zones of incomplete fusion of curd particles or curd dust. Note smear on rind.

Fig. 5. Curd granule junction pattern in vertical section through the loaf of a Sbrinz cheese. Pressure from bottom and hoop side leads to characteristic orientation of flattened granules.

Fig. 6. Deformation of curd granules around eyes in Emmental cheese.

dotted curve and the continuous line correspond to the calculated normal distributions. The actual distributions differ somewhat from the ideal Gauss distribution. Similar results were obtained for the other hard cheeses. The average f-values ranged from 0.557 to 0.561 and 0.436 to 0.475 in horizontal and vertical sections, respectively (Table 1). Sbrinz cheese had higher average form factors than Emmentaler and Gruyere cheese. The lower degree of deformation in Sbrinz cheese can partially be explained by the lower moisture content of this variety, which increases the viscosity of the cheese body and decreases its deformability. Lower temperature during the curing process also decreases the flattening of the cheese loaves.

As outlined in the experimental section the best measure of the size of the curd granules is the area of their cross section. The

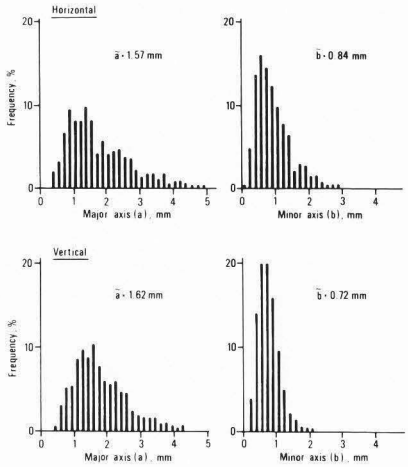

Fig. 9. Frequency distributions of the calculated elliptical axes of cross sections of curd granules in Gruyere cheese. Each histogram is based on 720 values (6 cheeses and 6 zones according to Fig. 1).

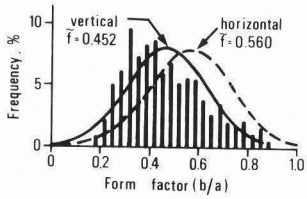

Fig. 10. Frequency histograms of elliptical form factors in vertical and horizontal sections of Gruyere cheese. 720 data from 6 cheeses. The bars for the horizontal sections are not shown. The curves indicate the shape of a normal distribution. The actual distributions differ from an ideal Gauss distribution.

area values revealed an asymmetric distribution. Fig. 11 shows the distribution pattern obtained for Gruyere cheese. Similar histograms of the area frequencies were obtained for Emmentaler and Sbrinz cheese. The shape of the histograms can adequately be described by a log-normal distribution. In Fig. 11, nineteen of the total of 720 values measured in horizontal sections were greater than 6 mm^2. In Emmentaler and Sbrinz cheese, 5 and 3% respectively of the surface areas in horizontal sections were greater than 6 mm^2. As summarized in Table 1 the median values of the area ranged from 0.9 to 1.2 mm^2. The interquartil range, which covers 50% of the values, was from about 0.5 to 2.2 mm^2. The differences between the 3 varieties were small. The only statistically significant difference was between Emmentaler (1.15 mm^2) and Gruyere (0.97 mm^2).

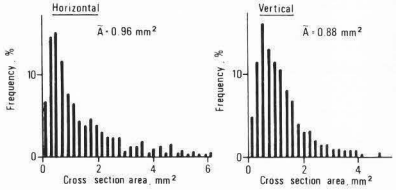

Fig. 11. Size distribution of curd granules in Gruyere cheese. Cross section area frequencies on horizontal and vertical sections through the loaf according to the sampling scheme in Fig. 1.

Within the cheese loaves, small but significant differences could be observed between the size distribution profiles and average form factors. However, the differences between the parameters determined on the sections according to Fig. 1 were not systematic and did not indicate separation of differently sized particles. Only in Gruyere cheese were the form factors near the hoop side (sections nr. 1 + 2 + 3) systematically larger than in the central part of the loaf (sections nr. 4 + 5 + 6), indicating a different deformation in the middle of the loaf.

Different moulding and pressing arrangements were used by some manufacturers. However, the differences between the cheeses of a particular variety were in most cases of the same order of magnitude as the differences within the cheese loaves. A greater number of samples from each manufacturer would therefore be needed for an evaluation of the effect of equipment on the junction patterns. Emmentaler cheese had the largest and Gruyere cheese the smallest dispersity (see interquartil ranges in Table 1).

Semi-hard cheeses

Appenzeller, Tilsiter and Raclette cheeses are prepressed in rectangular curd billets before filling into round hoops. The extra mass of curd near the edges led to different deformations and thus granule junction patterns near the former edges and sides of the billets. Fig. 12 shows a horizontal cross section near the edge of an Appenzeller

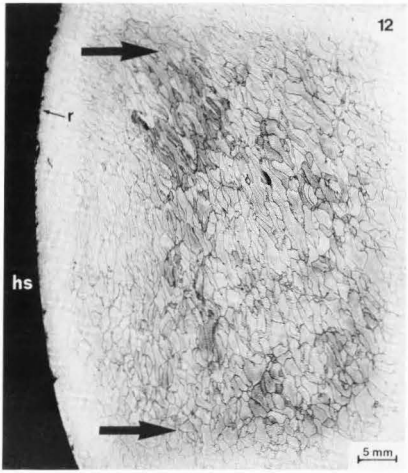

Fig. 12. Horizontal section through loaf of Appenzeller cheese in the zone of the former edge of the billet. Arrows symbolize the pressure from the hoop side in this region.

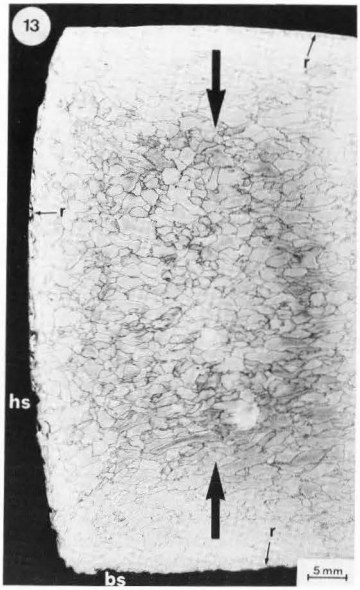

Fig. 13. Typical pattern of curd granule junctions in a vertical section through the loaf of an Appenzeller cheese in the region of side of the former curd billet. Arrows symbolize the pressure from the upper and lower side.

cheese. The junction pattern looks like that of a vertical section of a hard cheese because of the flattening of the granules. The arrows indicate the radial pressure from the hoop side. This radial pressure, together with the vertical pressure in the cheese press (Fig. 13), leads to rod-shaped granules. As shown in Figs. 12 and 14 the granules therefore also appear flattened in horizontal sections. Fig. 14 shows typical patterns observed near the edges and sides of the billets of Appenzeller and Tilsiter cheese. A schematic drawing of the situation is given in Fig. 15. The relatively small values of the form factors in horizontal sections as well as the smaller surface areas in vertical sections, observed for Appenzeller and Tilsiter cheese, can be explained by the preferential orientation of the elongated curd granules (Table 1). In Raclette cheese the difference between the junction patterns near the edges and sides of the curd billets were less pronounced. However, the difference between the vertical and horizontal sections was again similar to that observed in hard cheese, as can be seen from Fig. 16. Comparison of Figs. 14 and 16 with corresponding micrographs of the other varieties also shows that Raclette cheese was manufactured with larger curd granules. The average granule size as well as the width of the size distribution in semi-hard cheeses were generally greater than those in the hard cheeses. It follows from the data in Table 1 that Raclette cheese had the largest granules and the broadest size distribution of all the varieties tested.

As illustrated in Fig. 17, semi-hard cheeses sometimes showed special junction patterns in the edge zones. The example shows dark areas which represent regions of incomplete fusion of curd granules. The interstices were most probably filled with whey and possibly curd dust. Inhomogeneous "whirling" structures can be caused by uneven filling of the cheese moulds and nonuniform addition of curd remnants.

Some of the Appenzeller and Tilsiter cheeses were manufactured using cheesemaking machines, pumping and automatic pressing equipment. These cheeses differed significantly in their curd granule junction pattern from those manufactured traditionally using smaller vats, cloths and manual presses. The vertical sections in Fig. 18 show that flattening of curd granules was less pronounced in cheese loaves which were manufactured in a traditional

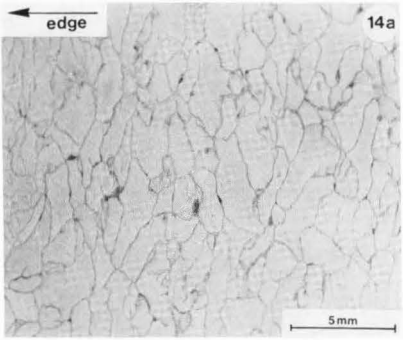

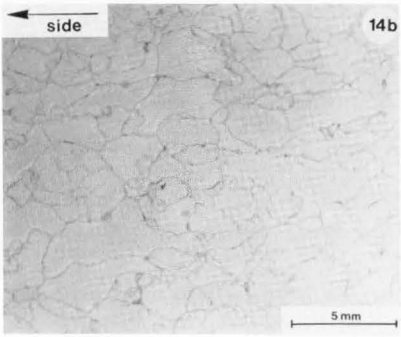

Fig. 14. Comparison of the junction patterns in Tilsiter cheese near the edge (14a) and side (14b) of the original curd billet. Horizontal sections.

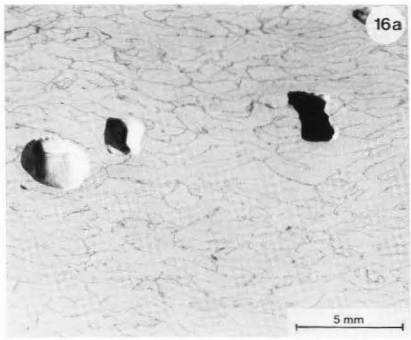

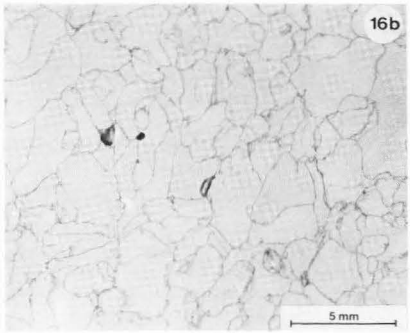

Fig. 16. Typical patterns on vertical (16a) and horizontal (16b) sections of Raclette cheese.

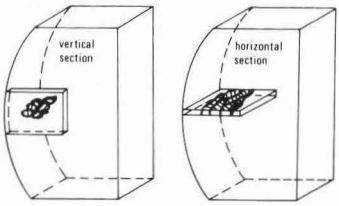

Fig. 15. Schematic model showing cross-sections of curd granules in the region of the original edges of the curd billets in Appenzeller and Tilsiter cheese. Radial and vertical pressure leads to rod-shaped curd granules.

Fig. 17. Vertical section through Tilsiter cheese in the region of an edge of the former curd billet. Larger arrows point to regions of abnormal orientation, incomplete fusion and inclusion of curd dust or whey.

Fig. 18. Difference between curd granule junction patterns of Appenzeller cheese manufactured traditionally (18a; vat, cloth) and cheesemaking machine (18b; pump, automatic pressing equipment).

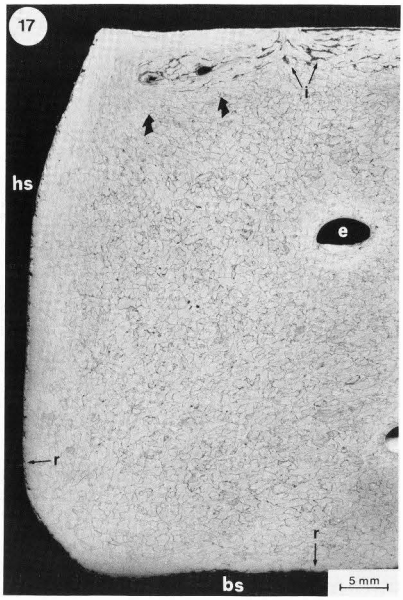

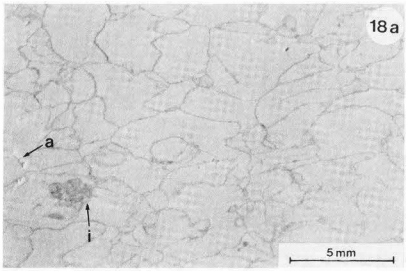

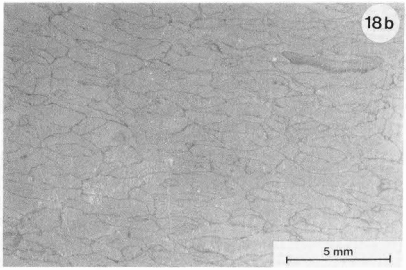

Table 1: Average size and elongation of curd granules in horizontal and vertical sections of some traditional Swiss hard and semi-hard cheeses (median values, x, and interquartil ranges r_x)[1)]

Parameter		Emmentaler	Gruyere	Sbrinz	Appenzeller	Tilsiter	Raclette
a) **horizontal**							
Area, mm^2	A	1.15	0.97	1.07	1.31	1.42	1.68
	r_A	0.56-1.27	0.48-2.04	0.46-2.18	0.65-2.67	0.69-2.75	0.73-4.01
Major axis, mm	a	1.68	1.56	1.62	1.95	2.22	2.22
	r_a	1.23-2.38	1.05-2.35	1.09-2.35	1.33-2.85	1.45-3.28	1.39-3.38
Minor axis, mm	b	0.93	0.84	0.89	0.93	0.89	1.05
	r_b	0.62-1.32	0.55-1.23	0.56-1.30	0.61-1.33	0.61-1.21	0.66-1.74
Form factor,b/a	f	0.557	0.559	0.561	0.497	0.405	0.509
	r_f	0.44-0.69	0.43-0.67	0.45-0.69	0.37-0.62	0.30-0.53	0.38-0.65
b) **vertical**							
Area, mm^2	A	1.00	0.89	0.93	1.02	1.06	1.34
	r_A	0.54-1.61	0.54-1.46	0.49-1.66	0.53-1.91	0.53-1.93	0.66-2.34
Major axis, mm	a	1.69	1.62	1.62	1.78	1.73	2.28
	r_a	1.21-2.40	1.19-2.26	1.10-2.25	1.22-2.68	1.22-2.58	1.53-3.45
Minor axis, mm	b	0.77	0.72	0.77	0.76	0.80	0.77
	r_b	0.57-1.02	0.54-0.93	0.56-1.02	0.54-1.04	0.56-1.10	0.57-1.01
Form factor,b/a	f	0.448	0.436	0.475	0.436	0.459	0.334
	r_f	0.34-0.60	0.34-0.58	0.37-0.62	0.32-0.60	0.34-0.60	0.23-0.48

1) 800-1000 measurements for each variety (5 to 8 different loaves, 6 (hard cheeses) or 12 zones (semi-hard cheeses) per loaf as shown in Figs. 1 and 2, and 10-20 granules per zone)

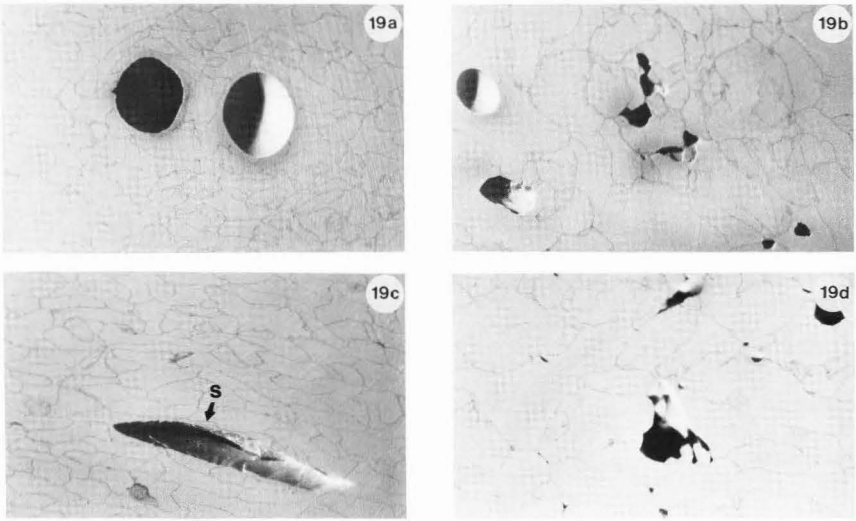

Fig. 19. Different types of eyes in Raclette cheese (see text for explanation).

manual fashion. The higher pressure used in the automatic pressing equipment is probably the main reason for the the different junction patterns in the vertical sections.

The micrographs of the cheese sections also revealed structural features around holes. In Raclette cheese, for example, three different types of holes could be distinguished on the basis of the deformation of adjacent granules, inner surface and shape (Fig. 19). A first group consisted of eyeholes having smooth surfaces and circular contours. The diameters ranged from about 1 to 3 mm. On the inner surface, the curd granule junctions appeared as a network of dark lines. In the section plane, the contours did not follow the junction lines. It could not be deduced from the micrographs whether the inital germ at the beginning of eye formation was located between granules or inside a granule. On the basis of their shape we may conclude that the eyes of this first group were formed by gas pressure in homogeneous zones, where the curd granules were completely fused together. Examples are in Fig. 19a and the left side of Fig. 19b.

Openings with contours following the original curd granule borders could be considered as a second group of eyes. The largest diameters of the openings were in the approximate range of 1 - 8 mm. This type of opening most probably was formed between unfused granules, where whey inclusion favoured growth of microorganisms (Fig. 19b, right half and Fig. 19d).

Slits or cracks following not only the original curd granule borders but also cutting through granules formed a third group of eyes (Fig. 19c). In the Raclette cheeses tested the slits were usually 2 to 5 mm long. They occurred less frequently than the other types of openings. The slits must have been formed at a relatively late stage of maturation, when the cheese texture was less elastic ("short") and broke during gas development.

In conclusion, the technique used to visualize junction patterns over large areas of cheese is valuable for characterizing the type and quality of a cheese, for studying cheese defects and eye formation. From the quantitative analysis of the size, size distribution, deformation and orientation of the curd granules, data characteristic for manufacturing processes and equipment are obtained.

Acknowledgments

The authors wish to thank J. Schnider, A. Kessler, F. Rentsch and H. Schär for providing the cheese samples and to Dr. M. Casey for his linguistic assistance.

References

Annibaldi S, Nanni M (1979) Osservazioni preliminari sulla microstruttura del formaggio parmigiano reggiano (Preliminary observations of the microstructure of Parmigiano Reggiano cheese). Sci.techn. Lat.-cas. 30, 191-198.

Bohac V (1970) Microstructure et rheologie du fromage a pâte dure (Microstructure and rheology of hard type cheese). XVIII. Int. Dairy Congr., Austr. Nat. Dairy Committe, A.4.6., Vol. ID, 393.

Bolliger O, Burkhalter G (1957) Der Einfluss der Bruchkorngrösse auf den Lochansatz beim Emmentalerkäse (Influence of curd granule size on eye formation in Emmental cheese). Schweiz. Milchzeitung, Wiss. Beilage Nr. 52, 3 - 26.

Clark WM (1918) On the formation of "eyes" in Emmental cheese. J. Dairy Sci. 1, 91-112.

Dorner W, Ritter P (1942) Ueber die Verteilung der Bruchkörner verschiedener Grösse im Emmentalerkäse und ihr Einfluss auf den Käseausfall (On the size distribution of curd granules in Emmental cheese and its influence on cheese quality). Schweiz. Milchzeitung 27,1-3.

Emmons DB, Kalab M, Larmond E (1980) Milk gel structure X. Texture and microstructure in cheddar cheese made from whole milk and from homogenized Coco-fat milk. J. Texture Studies 11, 15-34.

Fleischmann W, Weigmann H (1932) Lehrbuch der Milchwirtschaft (Dairy Science text-book). Paul Parey, Berlin, 7th ed., 689-692.

Flüeler O, Kaufmann H (1985) Einfluss der Bruchkorngrösse auf die Qualität (Influence of curd granule size on cheese quality). Schweiz. Milchzeitung 111 (40), 353.

Fricker A, Meyer F (1960) Beitrag zur Struktur des Edamerkäses (On the structure of Edamer cheese). Milchwissenschaft 15, 281-286.

Goldsmith PL (1967) The calculation of true particle size distributions from the sizes observed in a thin slice. Brit. J. Appl. Phys. 18, 813-830.

Hansson E, Olsson H, Sjöström G (1966) Mikrofotographie der Käsestruktur (Microphotography of cheese structure). Milchwissenschaft 21, 331- 334.

Heinrich C (1968) Physikalische Eigenschaften der Käse (Physical properties of cheese). In: Handbuch der Lebensmittelchemie. Band 3, Teil 1, F. Kiermeier (ed.) Springer Verlag, Berlin, 628-634.

Hostettler H (1943) Die gärungschemischen Vorgänge im Hartkäse (The chemistry of fermentation in hard cheese). Landw. Jahrbuch der Schweiz, Paul Haupt, Bern, 65-75.

Hostettler H (1961) Die Struktur des Milchkaseins und ihre Bedeutung für die Emmentalerkäsefabrikation (The structure of casein in milk and its significance for the manufacture of Emmental cheese). Schweiz. Milchzeitg. 87, 545-547, 557-559.

Kalab M (1977) Milk gel structure VI. Cheese texture and microstructure. Milchwissenschaft 32, 449-453.

Kalab M, Lowrie RJ, Nichols D (1982) Detection of curd granule and milled junctions in cheddar cheese. J. Dairy Sci. 65, 1117-1121.

Kammerlehner J (1974) Ueberprüfung verschiedener Einflüsse auf die Lab-Gerinnungszeit und Molkensynärese von Labkäsebruch und von Käse sowie seine Feuchtigkeitsabgabe im Reifungsprogramm (Examination of various factors influencing clotting time and syneresis of curd and cheese and loss of moisture during curing). Deutsche Molkerei-Ztg. (Kempten-Allgäu) 11, 342-350.

King N (1958) Observations by fluorescence microscopy of casein in milk, curd and cheese . J. Dairy Res. 25, 312-319.

Koestler G (1933) Zur Kenntnis der chemischen Grundlagen der Gärungen im Emmentalerkäse (The basis of the fermentation processes in Emmental cheese). Landw. Jahrbuch der Schweiz, Paul Haupt, Bern, 156-199.

Lowrie RJ, Kalab M, Nichols D (1982) Curd granule and milled curd junction patterns in Cheddar cheese made by traditional and mechanized processes. J. Dairy Sci. 65, 1122-1129.

Mair-Waldburg H, Bürk H, Hefele B, Lübenau-Nestle R, Wanner J, Dilger G (1974) Bearbeitung und Behandlung von Bruch und Käse. (Processing and treatment of curd and cheese). In: Handbuch der Käse. Mair-Waldburg H, (ed.) Volkswirtschaftlicher Verlag GmbH, Kempten (Allgäu), West Germany, 167-186.

Muggli J, Schällibaum V, Diethelm W (1959) Lehrbuch der Tilsiter- und Appenzellerkäserei (Textbook for Tilsiter- and Appenzeller cheese factories). KJ Wyss Erben AG, Bern, 15-43.

Mulder H, De Graaf JJ, Walstra P (1966) Microscopical observations on the structure of curd and cheese. XVII. Int. Dairy Congr. D, Th. Mann GmbH, Hildesheim, 413-420.

Peter A, Zollikofer E (1966) Lehrbuch der Emmentalerkäserei (Textbook for Emmental cheese factories). 11th edition. K.J. Wyss Erben AG, Bern, 27-70, 125-128, 132-135.

Rüegg M, Moor U, Blanc B (1980) Veränderungen der Feinstruktur von Greyerzerkäse im Verlauf der Reifung. Eine Studie mit dem Raster-Elektronenmikroskop (Changes in the fine structure of Gruyere cheese during ripening. A scanning electron microscopic study). Milchwissenschaft 35, 329-335.

Rüegg M, Moor U, Schnider J (1985) Ueber die Grössenverteilung und Form der Bruchkörner im Emmentalerkäse (The size distribution and shape of curd granules in Emmental cheese). Schweiz. Milchw. Forsch. 14, 3 - 7.

Schulz ME (1953) Die Käsestruktur als qualitätsbestimmender Faktor (The structure of cheese as quality factor). Kieler Milchw. Forschungsberichte 5, 379-395.

Schwarz G, Mumm H (1951) Einfluss der Bruchgrösse auf die Ausbeute an halbfettem Tilsiterkäse (Influence of curd granule size on the yield of semi fat Tilsiter cheese). Molkerei-Ztg. Hildesheim 5,786.

Scott R (1981) Cheesemaking practice. Applied Science Publ. Ltd., London, 171-176.

Steffen C, Flückiger E, Bosset JO, Rüegg M (1987) Swiss-type varieties. In: Developments in dairy chemistry-4, Cheese. Fox PF (ed.), Applied Science Publishers, Londen (in press).

Steinegger R (1904) Der praktische Schweizer Käser (Practical Swiss cheese making). Verlag KJ Wyss, Bern, 231.

Weibel ER (1979) Stereological methods. Vol.1. Practical methods for biological morphometry. Academic Press, London, 26-27, 162-203.

Wicksell SD (1925) The corpuscle problem. I. Biometrica 17, 84-99.

Editor's Note: All of the reviewers' concerns were appropriately addressed by text changes, hence there is no Discussion with Reviewers.

FOOD MICROSTRUCTURE, Vol. 6 (1987), pp. 47-56
Scanning Microscopy International, Chicago (AMF O'Hare) , IL 60666 USA

0730-5419/87$3.00+.00

THE MORPHOLOGY OF BLACK TEA CREAM

R. D. Bee , M. J. Izzard, R. S. Harbron* and J. M. Stubbs

Unilever Research Laboratory, Colworth House,
Sharnbrook, Bedfordshire, ENGLAND, MK44 1LQ

* Department of Physical Chemistry, University of Bristol,
Cantocks Close, Bristol, ENGLAND, BS8 1TS
* Present Address : Department of Plant Biology, University
of Birmingham, P. O. Box 363, Birmingham, ENGLAND, B15 2TT

Abstract

The colloidal precipitate known as tea cream, which separates when a hot aqueous infusion of black tea is cooled, is investigated by electron microscopic (EM) techniques of shadowing, sectioning, freeze-etching and scanning and also by optical microscopy. These indicate tea cream to be an association colloid, the morphology of which depends on overall solids concentration. Dilute infusions (0.1% w/w) produce macromolecular aggregates of about 50 nm, but at higher tea solids concentrations secondary aggregation of the initial particles results in ill-defined clusters of approximately 1 μm in diameter. At 5% w/w, clear, spherical liquid droplets, typically 1-2 μm in diameter are observed. Increasing concentration to 40% w/w causes an increase in size of the individual colloidal droplets and an increase in the phase volume of this disperse phase. The colloidal phase contains 55-65% solids by weight, the total solids content appearing to be independent of overall composition of the solutions from which it is formed. The colloid may be separated from cooled tea infusions by centrifugation but individual particles display strong resistance to coalescence. At high tea cream phase volumes phase inversion can occur and dispersions of the dilute phase in a continuous cream phase are then observed.

Initial paper received February 10, 1986
Manuscript received March 27, 1987
Direct inquiries to R.D. Bee
Telephone number: 44-234-781781x2247

Key words : Black tea, tea cream, colloidal precipitate, association colloid, coacervate.

Introduction

Tea cream is a colloidal precipitate formed by black tea liquors as they cool. The composition of tea cream and the chemical factors causing its formation have been the subject of considerable investigation over the past twenty years. Previously, attention has been paid to the chemical causes of the separation of tea cream and to chemical composition but little significance has been placed on its physical nature. This paper reports the cream structures that are formed from tea infusions with solids concentrations between 0.1% and 60% w/w, indicates the phase volumes involved and describes phase inversion at high tea solids concentrations (>40%).

Chemical components

Tea cream composition is known to be complex. It has been reported by Roberts (8) to consist largely of a mixture of theaflavins, thearubigins and caffeine. It also contains other components such as bisflavanols, unoxidised flavanols, pectin (9), caffeic, gallic and ellagic acids, and several other compounds (14,18). In addition, non-caffeine nitrogen and chlorophyll-derived compounds have been identified in tea cream (14). Specific interactions between caffeine and polyphenols resulting in their incorporation into the tea cream phase have also received much attention (9,14).

Roberts (8) has claimed that thearubigins are by far the most abundant polyphenolic oxidation products in black tea and that they are the major constituent of tea cream (approximately 66%). Roberts maintains that thearubigin fractions of black tea have molecular weights of the order of 700 and contain no nitrogen (8,10). Conversely, other authors have suggested them to be of much higher molecular weight (4). Vuataz et al. have shown in detailed work (17), that their preparation of thearubigin contained 0.55% nitrogen which could not be accounted for by caffeine or free amino acids and have suggested that molecular weights of up to 40,000 are involved. However, acid hydrolysis of the material produced a wide range of free amino

acids which led them to conclude the thearubigin fraction to be partly composed of substances related to humic acids. Recent work has suggested thearubigins to be pentameric flavon-3-ols and their gallates containing both hydrolysable and non-hydrolysable interflavanoid links. Such structures would be consistent with molecular weight of approximately 1,500 measured for these species (1).

It is clear from the above that the unresolved character of the thearubigins presents difficulties when attempting to rationalise the behaviour of the tea cream phase on a chemical basis. Also it is evident that the behaviour of the "cream phase" depends on the influence of a wide range of components.

Amount of tea cream formed

A colloidal precipitation process involving so many components may be expected to be extremely variable but some clear generalisations can be made. It has been shown that tea cream levels depend on infusion composition; particularly strong tea cream formation occurs in infusions high in polyphenols and caffeine (9). Other compositional factors influencing the quantity of tea cream have been identified as pH (14), concentration of various salts and other solutes (11). At constant composition, however, the principal variables are temperature and tea solids concentration. It seems that the amount of tea cream formed is inversely related to temperature whereas it is directly proportional to total solids concentration.

Nature and properties of tea cream

Despite the many investigations which produced the conclusions outlined above, relatively little attention has been paid to the physical form adopted by the precipitate. Rutter's work (11,12) is a notable exception. Smith (14) had reported that tea cream took the form of small spheres a few micrometers in diameter which formed at approximately 40°C on cooling but which did not disappear until approximately 55°C on reheating.

By optical and electron microscope studies, Rutter confirmed tea cream to be a suspension of polydisperse spheres with diameters in the range 0.3-2.0 μm. He also identified the presence of many smaller particles, the majority being approximately 0.04 μm in diameter in dilute solutions (<3% w/v total solids concentration).

Materials and Methods

So as to minimise the variability inherent in tea samples, this study has exclusively used a bulked sample of dried extract. The extract was prepared by hot water counter-current stripping of black Ceylon tea made initially at approximately 5% tea solids and then concentrated and spray dried to a fine flowing powder. All experimental samples were drawn from the single bulk sample which was stored at room temperature in sealed steel drums. All infusions were prepared with distilled water and are given as % w/w unless otherwise stated.

Cream phase preparation

Rutter (11) showed that the rate of cooling can affect particle size and stability to flocculation of the tea cream phase. Consequently, a routine procedure has been adopted for the tea cream phase preparation in this study. In all cases, reconstituted infusions were prepared by heating preparations of known concentrations at 95°C for 15 minutes in a conical flask fitted with a reflux condenser. The preparations were sealed in glass flasks, cooled against ambient temperature and aged for 4 h. The tea solids used contained 3% moisture and were contaminated with 3.3% of insoluble debris from the original leaf. In addition, a crystalline insoluble material was identified. This has traditionally been reported to be calcium oxalate (16) but shown in this case by powder X-ray diffraction and X-ray emission microanalysis to be principally magnesium oxalate. Where necessary, these figures have been taken into account in quoting soluble tea solids concentrations. The pH of the reconstituted infusions was 4.7.

Phase volume of tea cream

The volume of tea cream produced by a given liquor concentration has been estimated by centrifugal separation (10 cm^3 samples 20,000xg, 30 min, 20°C) of the two phases. This approach assumes that, under the centrifugal conditions employed, the tea cream is not compressed in such a way that it is changed from the equilibrium it has reached in free suspension. Secondly, it assumes that the interstitial liquor between droplets does not contribute significantly to the measured amount of the tea cream.

A second series of experiments, in which the relative volumes of the two phases were measured gravimetrically, (by density determinations on the supernatant liquid and the total liquor) supported the data obtained volumetrically. Gravimetric determinations of the solid material dissolved in the supernatant then permitted the determination of the concentration of species in the two phases to be established.

Optical microscopy

This was carried out on a Leitz Ortholux 2 optical microscope. Transmitted phase contrast and plane polarized light were used to examine the prepared infusions. No staining was necessary.

Transmission electron microscopy

Tungsten shadowing

Tea cream from each concentration was fixed in 1% w/v osmium tetroxide solution at room temperature for 30 min. Samples were then

centrifuged, resuspended in distilled water and then sprayed with a nasal atomiser onto a previously carbon covered EM grid. The grids were shadowed with tungsten at an angle of 45° in an Edwards 306 coating unit fitted with an electron beam gun. Finally, grids were examined in a J.E.M. 100C electron microscope at 80 kV.

Sectioning

Samples were prepared by fixing in 1% w/v osmium tetroxide solution at room temperature for 30 min. They were washed with two changes of distilled water, separated by centrifugation and then dispersed in 1% agar solution at just above the gelation temperature (40°C). On cooling, small blocks of the suspending gel were cut, dehydrated in ethanol and embedded in EPON 812 resin by the conventional schedule (2).

Thin sections were cut using a Reichert-Jung Ultracut microtome, stained with lead citrate and examined by transmission electron microscopy in a J.E.M. 100C electron microscope at 80 kV.

Freeze-etching

Tea cream was removed from suspension by gentle centrifugation and a small sample carried on a copper stud was frozen in Freon 22 which had been pre-cooled to its freezing point in liquid nitrogen. The frozen sample was then fractured with a cold knife (-180°C) under vacuum and held at -98°C for 30 seconds in a Polaron freeze-etching module. The etched surface was shadowed with carbon/platinum at 45° and the replica backed with carbon. The replica was cleaned from residual tea cream by floating it on chromic acid overnight and washing it with distilled water.

Scanning electron microscopy (SEM)

Fixed tea cream particles from a 5% infusion were examined in the form of a centrifuge pellet. The pellet was obtained by centrifuging an infusion, fixed with 1% w/v osmium tetroxide solution at room temperature for 30 min, at 1,500xg. The resultant pellet was rinsed with distilled water and dried in a vacuum desiccator. Once dried, the pellet was mounted on a SEM stub, sputter-coated with gold (~20 nm) and examined in a Cambridge Stereoscan 600 scanning electron microscope. The microscope was operated at 25 kV.

Results and Discussion

Optical microscopy

Infusions have been examined over the concentration range of 1-60% solids at 20°C. Tea cream has its most clearly defined form in the concentration range of 5-20% solids where it exists, for the most part, as a dispersion of spheres (Fig. 1). At 5% solids the mean particle diameter is approximately 1-2 μm and this increases to approximately 2-3 μm at a concentration of 10%. The tea cream phase at 5% solids appears homogeneous, but increasing concentration causes the droplets to become heterogeneous. The heterogeneous nature, or presence of inclusions, is particularly apparent in the largest droplets.

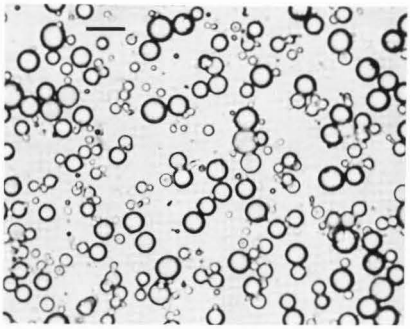

Fig. 1. Optical micrograph of a 20% infusion at 25°C.
Bar = 4 μm

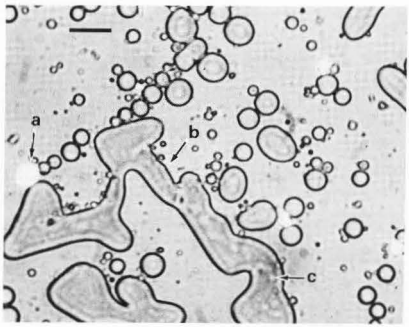

Fig. 2. Optical micrograph of a 31% infusion at 25°C
a - magnesium oxalate crystallite
b - irregular configuration of tea cream
c - inclusions of supernatant phase
Bar = 4 μm

Above 20% solids, the tea cream phase more easily loses its spherical form and can be distorted into rod-like shapes by shearing on the microscope slide. Under these conditions, individual droplets can be made to coalesce. Tea cream phase in infusions of solids concentrations greater than 25% adopts irregular configurations (Fig. 2), whilst on reaching 40% solids, the phase volume of the cream has increased significantly and the tea cream and supernatant phases have roughly similar volumes. It is clear at this concentration that the system is made up

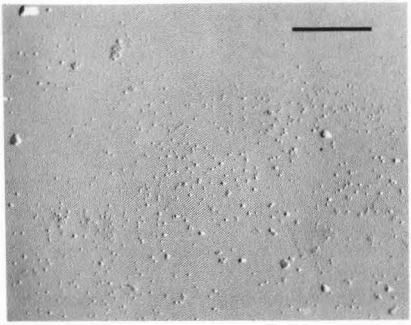

Fig. 3. Tungsten shadowed subunits from a 0.1% infusion at 25°C. Bar = 1 μm.

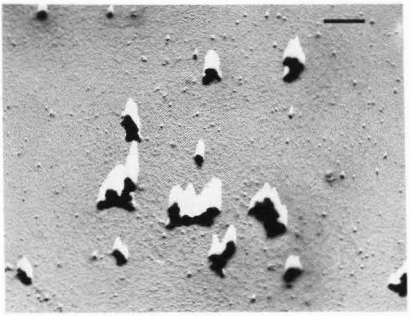

Fig. 4. Tungsten shadowed aggregates from a 1.0% infusion at 25°C. Bar = 1 μm.

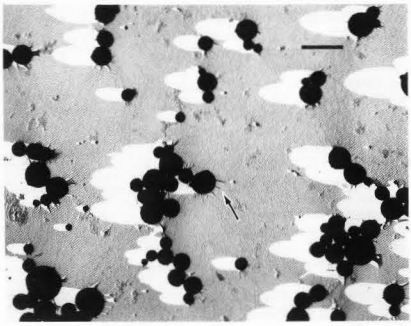

Fig. 5. Tungsten shadowed tea cream particles from a 5% infusion at 25°C. Bar = 2 μm. Arrow indicates fibrous material occluded to cream droplet.

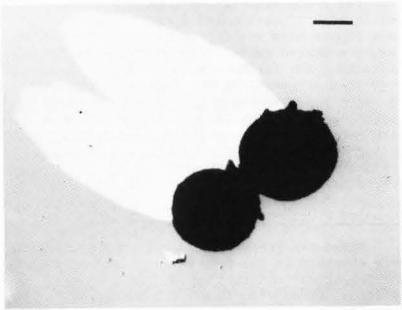

Fig. 6. Tungsten shadowed tea cream particles from a 20% infusion at 25°C. Bar = 2 μm.

of two liquid phases and observation of the flow patterns in the two phases indicate the tea cream phase to be by far the more viscous. The phases adopt no well defined shape and inclusions of supernatant phase can be seen in the cream phase (Fig. 2). In this overall composition, such droplets coexist with similar sized droplets of the cream phase. Neither phase is clearly a continuous phase though, as concentration is increased, the cream phase volume increases significantly and the tea cream becomes the supporting phase. At 40-45% solids only small amounts of the supernatant phase can be detected microscopically and at 60% solids the system appears to be a single phase.

Observations on preparations in the range 43-52% solids did not clearly show at what point all the supernatant phase was lost. Having shown that small droplets of the supernatant phase can exist as inclusions in the cream phase, it seems likely that these inclusions exist above the concentrations at which they can be observed microscopically. A composition, above which the system contains only the cream phase, has been estimated by electron microscopy to be approximately 55% solids.

Polarised light microscopy over the whole concentration range revealed no evidence of liquid crystallinity in either phase, though a significant level of the crystallites were present in the supernatant (Fig. 2).

Tea cream particles from low concentration infusions (approximately 1%) have less well defined shapes. At 1% solids, tea cream is produced as an irregular amorphous precipitate which gives the appearance of irregular granules built up from a finely divided precipitate. It does not adopt the spherical form characteristic of higher concentrations. The individual components of the flocculates are difficult to

characterise with the light microscope as they are at (or below) the limit of resolution. Only irregular flocculates (approximately 1-2 μm) are observed. At 2.5% solids, the phase has started to adopt the recognisable globular form.

Electron microscopy

Electron microscope studies have been made on cream phase formed from infusions of 0.1, 1.0, 5.0 and 20.0% solids. Micrographs of osmium-stained and tungsten-shadowed tea cream particles from each concentration are gathered in Figs. 3-6.

At low concentrations (0.1%) (Fig. 3), the small particles appear to be relatively loose aggregates of precipitated macromolecular material. Typically they are 170-200 nm in diameter as measured by the Coulter Nanosizer and have a relatively narrow size distribution. Measurements from electron micrographs of shadowed particles indicate a smaller size, approximately 30-60 nm with only a few particles up to 100 nm in diameter. It is likely that the particle diameter determined by electron microscopy represents the minimum value, considering that a high proportion of the tea cream droplet is water [at higher concentrations of total solids, water occupies approximately 45% by weight (Fig. 7) and this volume may be lost in preparation of the tea cream for electron microscopy]. On the other hand, the Nanosizer quasi-elastic light scattering technique detects an effective hydrodynamic volume. It does this by monitoring the fluctuations in intensity as they are subject to Brownian motion. In this experimental system, the method is likely to overestimate the size of particles which carry extensive polymer adsorbed to the surfaces or are coated with diffuse layers of polymer and which, therefore, may be relatively "anchored" in the aqueous suspension. Analogous discrepancies between these techniques have been noted previously in studies of casein micelles (13) which are similarly heavily hydrated polymeric particles.

Tea cream particles from 1% infusions (Fig. 4) are loose ill-defined aggregates approximately 0.5-1.0 μm in diameter, though some smaller particles characteristic of lower concentrations still remain.

At 5% solids (Fig. 5), particle sizes are of the order of 0.5-1.5 μm whereas larger particles of about 3 μm are typical of 20% infusions. Particles at 5% and 20% solids appear as single isolated spheres as expected from optical microscopy. They are fixed as spheres (probably during staining) and produce elliptical shadows indicating that the particles at the stage of electron microscopy are solid fixed units. On the exterior of tea cream from 20% infusions (Fig. 6) solid material is seen to be occluded, whereas tea cream from 5% infusions clearly has fibrous material projecting from the particles.

Micrographs of stained, embedded and sectioned creams from infusions of 1.0, 5.0 and 20.0% solids are shown in Figs. 8-13.

The sectioning technique confirms that the loose aggregates formed from 1% infusions are very heterogeneous (Figs. 8 and 9) and that they appear to be built up from the smaller particles which are observed at 0.1% and 1.0% by tungsten shadowing (Figs. 3 and 4). The staining behaviour suggests two types of principal component make up the tea cream particle, one heavily stained and the other more lightly stained. It appears that each particle builds up in a similar way and is a relatively even mixture of heavily and lightly stained components. The fact that aggregates are similar in size may indicate some specificity in their assembly. It is possible therefore, that these particles are the building blocks or subunits of the well-defined structure which is developed by the time the tea solids concentration is increased to 5% (Figs. 10 and 11).

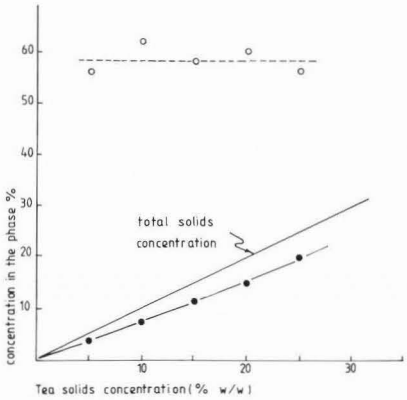

Fig. 7. Concentration of solids by weight in tea cream phase and supporting medium.
● supporting medium
o tea cream phase

With the sectioning technique, still more detail of the heterogeneity can be resolved. The two magnifications shown in Figs. 8 and 9 indicate clearly that under the conditions occurring in 1% infusions, the precipitate is made up of two components one of which stains only lightly. In all cases, material is present which stains only weakly on the surface leaving the interior unstained. It is unlikely that this material can be forming as hollow vesicles and it is thus suspected to be aggregated precipitate (probably polymeric) itself not susceptible to staining but which has adsorbed on it some stained material.

All micrographs at this concentration emphasise the heterogeneity of the precipitate, particularly with respect to its staining behaviour. Even the components taking stain strongly can be seen to be extremely heterogeneous with respect to staining sites.

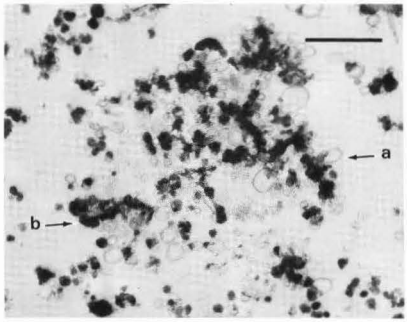

Fig. 8. Sectioned tea cream particles from a 1% infusion.
Bar = 1 μm.
a = surface stained component
b = heavily stained component

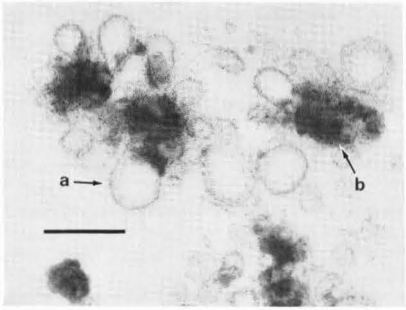

Fig. 9. Sectioned tea cream particles from a 1% infusion.
Bar = 400 nm.
a = surface stained component
b = heavily stained component

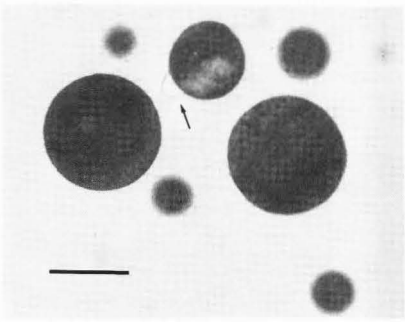

Fig. 10. Sectioned tea cream particles from a 5% infusion. Arrow indicates poorly stained, hollow structure.
Bar = 800 nm.

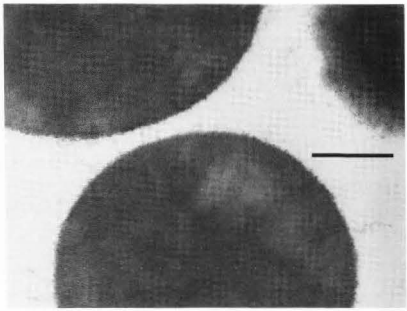

Fig. 11. Sectioned tea cream particles from a 5% infusion.
Bar = 200 nm.

The fixation and staining chemistry of osmium tetroxide have been described in some detail (7), but the actual staining mechanism of tea cream by osmium tetroxide is not understood. It is known to covalently bind at sites of unsaturation but is also reported to interact with species such as proteins, amino acids and sugars. It is likely that in addition to producing the differential staining shown in the present micrographs, the osmium tetroxide acts as a fixative for these particular structures.

As with the shadowing technique, tea cream from 5% infusions provides the simplest picture. Again, the particles appear dense and homogeneously stained, but now the diffuse and ill-defined nature of the surface of the sphere is more apparent. Each cream droplet has occluded to its surface an amorphous layer of precipitate which frequently extends into the supporting phase. This is shown in Fig. 11. In addition to cream droplets, some diffuse, suspended material is observed. This sometimes adheres to the cream and occasionally it is freely suspended. Frequently small, poorly stained, apparently hollow structures can be seen (Fig. 10).

The discrete spherical nature of tea cream from 5% infusions is clearly seen in scanning micrographs Figs. 14 and 15. That the individual cream droplets survive centrifugation and dehydration can probably be attributed, in some degree, to the fixing action of the osmium stain.

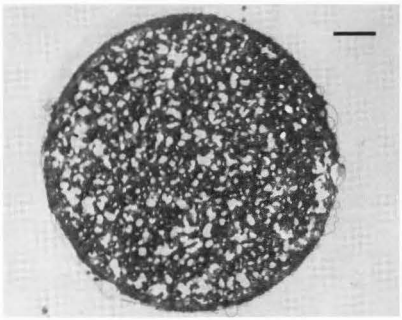

Fig. 12. Sectioned tea cream particle from a 20% infusion.
Bar = 500 nm.

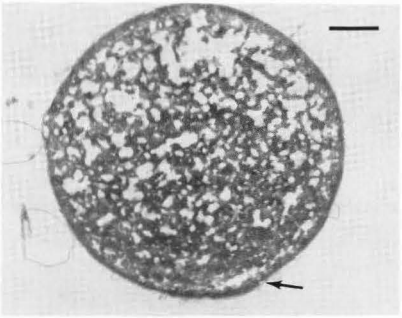

Fig. 13. Sectioned tea cream particle from a 20% infusion. Arrow shows heavily stained, detached surface.
Bar = 1 μm.

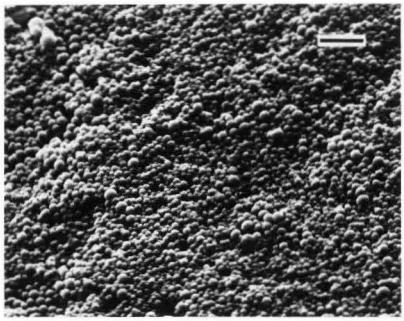

Fig. 14. Scanning electron micrograph of tea cream particles from a 5% infusion.
Bar = 10 μm.

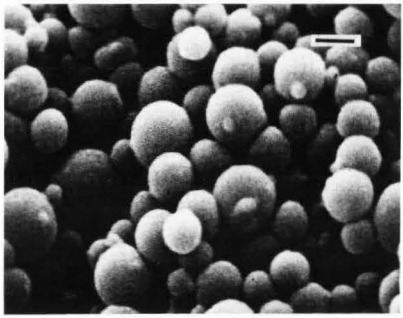

Fig. 15. Scanning electron micrograph of tea cream particles from a 5% infusion.
Bar = 2 μm.

On increasing total solids concentration from 5% to 20%, two major changes are observed. Most obviously, the particle loses the homogeneous internal structure (Fig. 11) and becomes heterogeneous, the internal material segregating into fractions, one heavily stained with osmium and the other unstained or, at most, weakly stained (Figs. 12 and 13). Furthermore, the particles now appear more densely consolidated than at 5% solids concentration. There are few cases of precipitated material extending long distances into the supporting phase and the particle surfaces are more distinct. It is noticeable that the more strongly stained material forms a continuous surface round the tea cream droplet. This surface, or skin, is occasionally pulled away from the remainder of the particle in some micrographs (Fig. 13). As with 5% preparations, apparently hollow structures can be seen and in many cases these are strongly occluded to the cream particle surface.

On increasing to 50-60% solids concentration, only the cream phase can be detected by optical microscopy. It may be assumed, however, that the type of internal segregation noted on the 20% cream particles also takes place at the higher solids levels.

Freeze-etching has been found to be the most reliable technique for estimating the total solids concentration at which the dilute phase disappears (Fig. 16). No supernatant phase has been distinguished in preparations at 60% solids and so we conclude that only the cream phase exists at this concentration. Micrographs of freeze-etched samples taken from the top and bottom of a pellet produced by centrifugation of unstained tea cream are shown in Fig. 17 and 18

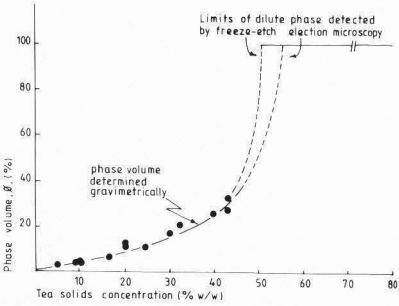

Fig. 16. Phase volume of tea cream as a function of tea solids concentration at 25°C.

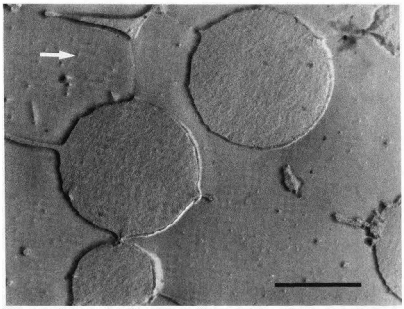

Fig. 17. Freeze-etched tea cream from a 5% infusion.
Arrow indicates direction of shadowing.
Bar = 1 μm.

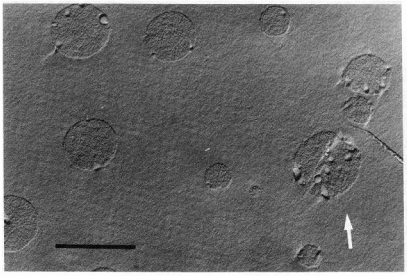

Fig. 18. Supernatant inclusions in tea cream pellet formed by centrifuging a 5% infusion.
Arrow indicates direction of shadowing.
Bar = 1 μm.

to illustrate how clearly the phases can be distinguished. At the top, tea cream droplets can still be clearly identified whereas at the bottom of the pellet, the cream phase is now continuous and spherical inclusions of the dilute phase are seen.

In Fig. 17 the cream droplets project above the background material (shadowed from left-to-right), as expected from the relative solids concentrations in the two phases (Fig. 7). Fig. 18 illustrates the reverse situation where the dilute phase is discontinuous and is etched below the level of the surrounding cream phase (shadowed from the bottom).

The sequence of events occurring with increasing tea solids is laid out schematically in Table 1. Taking the significant concentrations in order, in the region of 0.1%, (at least) two types of subunit are present. These presumably are composed of material which is inherently insoluble at this concentration or which is intrinsically soluble but has been rendered insoluble through formation of a complex with another soluble component. Whichever is the case, on increasing the concentration (above 1.0% solids), these subunits aggregate and finally knit closely together, the compaction to a sphere of heavily hydrated precipitate being completed between 1-5% solids. The progression is presumably accompanied by internal rearrangement within the tea cream droplet so that these polymeric materials carrying the highest percentages of hydrophilic groups are located towards the exterior with the least hydrophilic ones innermost.

Table 1

Tea solids concentration (% w/w)	Comments
Infinitely dilute	molecules in solution
0.1	subunits + solution
1	tea cream phase + solution
20	tea cream phase with internal segregation + solution
50-60	liquid tea cream phase only
100	tea glass

The processes in the above sequences could be explained by considering the primary polymeric solutes to have hydrophilic (ionic or polar) and hydrophobic regions. As solute levels are increased, the competition for the available water would be increased and the most hydrophobic parts of the molecules would be increasingly excluded from solution. This explanation of tea cream formation implies that the phase results from hydrophobic interactions (5,15) (cf. surfactant micelles). Alternatively, the cream

phase may separate as a result of complex coacervation - this arises from the mutual attraction of oppositely charged species (3, 6).

At concentrations greater than 20% solids, two separate structural elements can be clearly identified within the tea cream. Such separation may result from a negative heat of mixing two polymers and, whilst only detectable microscopically at these concentrations, similar effects may be contributing at much lower total solids to the overall phase behaviour.

As the chemistry of the components described is not yet resolved, these mechanisms cannot be progressed beyond speculation. However, it seems unlikely that tea cream formation takes place solely by hydrophobic bonding but that the process results from a combination of hydrophobic bonding and simple and complex coacervation of material onto a nucleus of the inherently insoluble species of tea.

Acknowledgements

The authors would like to thank, Mr. C. Clay and Mrs. L. Luddington for several of the electron micrographs produced during the course of this study. R.H. would like to acknowledge the SERC for the provision of a CASE studentship.

References

1. Cattell DJ, Nursten HE. (1976). Fractionation and Chemistry of Ethyl Acetate Soluble Thearubigins from Black Tea. Phytochemistry. 15, 1967-1970.

2. Glauert AM. (1974). Practical Methods in Electron Microscopy. North-Holland. Amsterdam 3 (1), 144-148.

3. Kruyt HR. (1949). Colloid Science - Irreversible Systems. Elsevier, Amsterdam. II, 230-258 and 433-482.

4. Millin DJ, Rustidge DW. (1967). Tea Manufacture. Process Biochem. 2, 9-13.

5. Mittal KL. (1976). Symposium on Micellisation, Solubilisation and Microemulsions. Albany, N.Y., Plenum Press, New York.

6. Overbeek JTG, Voorn MJ. (1957). Phase Separation of Polyelectrolyte Solutions. Theory of Complex Coacervation. J. Cell. Comp. Phys. 49, (Suppl. 1), 7-26.

7. Pearse AGE. (1980). Histochemistry : Theoretical and Applied. Churchill Livingstone. Edinburgh. 4th ed. 1, 114-119.

8. Roberts EAH. (1962). In Chemistry of Flavonoid Compounds. Pergamon, London. Geissman TA, (Ed.) 468-512.

9. Roberts EAH. (1963). The Phenolic Substances of Manufactured Tea X. The Creaming Down of Tea Liquors. J. Sci. Fd. Agric. 14, 700-705.

10. Roberts EAH, Cartwright RA, Oldschool M. (1957). The Phenolic Substances of Manufactured Tea. Fractionation and Paper Chromatography of Water Soluble Substances. J. Sci. Fd. Agric. 8, 72-80.

11. Rutter P. (1971). A Physicochemical Study of Tea Cream. PhD. Thesis. Leeds. UK.

12. Rutter P, Stainsby G. (1975). The Solubility of Tea Cream. J. Sci. Fd. Agric. 26, 455-463.

13. Schmidt DG, Walstra P, Buchheim W. (1973). The Size Distribution of Casein Micelles in Cow's Milk. Neth. Milk Dairy J. 27, 128-142.

14. Smith RF. (1968). Studies on the Formation and Composition of Cream in Tea Infusions. J. Sci. Fd. Agric. 19, 530-534.

15. Tanford C. (1973). The Hydrophobic Effect : Formation of Micelles and Biological Membranes. Wiley-Interscience, New York.

16. Thorpe's Dictionary of Applied Chemistry. Longmans. London. 4th ed. XI, 451.

17. Vuataz L, Brandenburger H. (1961). Plant Polyphenols III. Separation of Fermented and Black Tea Polyphenols by Cellulose Column Chromatography. J. Chromatog. 5, 17-31.

18. Wickremasinghe RL, Perera KPWC. (1966). Analysis of Cream of Tea. Tea Quarterly. 37, 131-133.

Discussion with Reviewers

R.J. Carroll: What is a fine thread-like material observed in the background of Figure 5?
Authors: Figure 7 shows there to be a significant concentration of tea solids dissolved or suspended, which is not incorporated into the tea cream phase. This can also be seen in Figure 11, where loosely aggregated material extends outside the tea cream phase. We take the fibrous material seen in Figure 5 to result from such polymeric material originally present in the dilute phase. Its chemical nature is not known.

W. Buchheim: How do the authors explain the fibrous material on Figure 5 and its absence in Figures 3, 4 and 6?
Authors: Figures 3 and 4 show tea cream particles from infusions of low concentrations (0.1 and 1.0 respectively). It is assumed that these concentrations are below that required for the necessary level of polymeric material to be

present in the dilute phase. At the higher concentration (20%), shown in Figure 6, it is possible that the material which produces the fibrous structure in Figure 5 has been precipitated from solution by build-up of the very soluble solutes and ions present in black tea. Indeed, such further precipitation could be responsible for the occluded solid material noted in Figure 6.

P. Walstra: Do the authors have any idea of the magnitude of the interfacial tensions between tea cream and the supporting medium as a function of concentration and temperature?
Authors: No, these data have not been measured. At present we have no idea of how clearly the interface is defined. As the tea cream contains a substantial proportion of water (~40%) the idea of a classical interfacial tension cannot be followed too rigorously. However, the droplets are naturally spherical and it is recognised that a study of the apparent interfacial tension may be useful in understanding the cohesive forces between the components of the tea cream phase.

P. Walstra: Do the authors agree that besides hydrophobic bonding and electrostatic interaction the conformational entropy of either phase and the interfacial free entry between them should be considered to explain the association?
Authors: Yes, the formation of tea cream is a highly complex process which is certainly controlled by many factors. The morphology we have described here is that which forms spontaneously on slow cooling and it should also be remembered that more rapid formation rates result, for example, in smaller tea cream droplets and particle flocculation (11).

D.P.Dylewski: How does time affect the morphology and chemistry of black tea cream?
Authors: Although tea cream particles settle out with time, provided there is no microbiological contamination, the infusions remain stable for several months and the suspensions can be redispersed by gentle shaking. The effect of time on the chemistry of black tea cream has not been examined, though it is assumed that further polymerisation of the polypherolic components is possible. Some increase in particle size seems to take place but the bulk of the increase has occurred in the first four days.

W. Buchheim: The osmium tetroxide stained cream droplets shown in Figure 10 and 11 differ decisively in their fine structure from those in Figures 12 and 13. Is this structural difference unequivocally related to compositional differences or could preparatory artifacts have occurred? What did the freeze-etched preparation of a 20% infusion look like?
Authors: We are confident that the internal structure of cream droplets from 5 and 20% infusions are different and that the areas of unstained and stained material in particles from 20% infusion represent segregation of material within the cream droplet. It can be speculated that these respective regions are built up from the strongly staining and poorly staining material noticed at lower concentrations (Figures 8 and 9). We have no freeze-etched preparations from 20% infusions.

FOOD MICROSTRUCTURE, Vol. 6 (1987), pp. 57-61
Scanning Microscopy International, Chicago (AMF O'Hare) , IL 60666 USA

0730-5419/87$3.00+.00

MICROSTRUCTURAL STUDIES OF TEXTURIZED VEGETABLE PROTEIN PRODUCTS: EFFECTS OF OIL ADDITION AND TRANSFORMATION OF RAW MATERIALS IN VARIOUS SECTIONS OF A TWIN SCREW EXTRUDER

S. GWIAZDA*, A. NOGUCHI and K. SAIO

National Food Research Institute, Yatabe, Tsukuba
Ibaraki, Japan 305

*Present address: Agricultural University of Warsaw
03-849 Warsaw, Poland, Grochowska 272

Abstract

In high-temperature short-time extrusion cooking with a twin screw extruder, effects of oil addition to defatted soybean flour and microstructural transformation of full-fat soybean flour during cooking, were investigated by use of a light microscope. At levels up to 15%, soybean oil was distributed in the protein and carbohydrate matrix as small, spherical drops under the experimental conditions used in this study. However, oil contents above 15% significantly prevented formation of well-aligned fibrous structures in the extrudates. During extrusion cooking, the starting materials began to break down by shearing and kneading forces in the feed section but gross cellular structures remained up to the cooking zone. After being introduced into the cooking zone, protein and carbohydrate were plasticized and appeared to be stream-like. Passage through the breaker plate and long cooling die induced formation of a fiber-like extrudate.

Initial paper received July 14, 1986
Manuscript received December 30, 1986
Direct inquiries to K. Saio
Telephone number: 81-2975-6-8008

Key words: Microstructure, soybean, texturized vegetable protein, extruder, extrudate, oil, protein, twin screw, barrel

Introduction

Extrusion cooking technology has been used to texturize many foodstuffs to produce expanded, texturized or fibrous structures. In the United States, such processes using a single screw extruder have found extensive application to prepare meat analogs mainly from defatted vegetable proteins, while in Europe, twin screw extruders have been primarily used to texturize cereals to produce bread analogs. These technologies were also introduced into the Japanese food industries and have been rapidly developed and applied in the Japanese market.

Over the past few years, the twin screw extruder has been especially appealing to the Japanese food industries because of its potential to operate for diverse purposes including compression, mixing, kneading, reaction, texturization, sterilization and inactivation of enzymes.

Because microstructural technologies have proven to be useful tools for studying the qualities and changes of texturized products, many researchers have examined effects of protein contents, protein solubility, pH, ionic strength and additives on texturized products prepared with single screw extruders (Faubion and Hoseney, 1982a; 1982b; Neumann et al., 1984; Noguchi et al., 1981; Rhee et al., 1981; Simonsky and Stanley, 1982). However, few papers have reported effects of lipid content (Faubion and Hoseney, 1982b), because a single screw extruder does not permit use of high lipid contents as a result of its design where materials are transported by frictional force between the barrel and screw. We have therefore examined the effects of oil addition on microstructure of soybean extrudates and describe our results here.

Secondly, this paper deals with microstructural transformations of the raw materials as they progress through the barrel of an extruder. Aguilera et al. (1976) set up 7 sampling points in a Wenger X-5 single screw extruder and investigated the progressive changes in soybean grits as they passed through the extruder. Our experiments were similar but used a Creusot-Loire BC-45 twin screw extruder with a long cooling die and our starting materials were full-fat soy meal plus a small amount of potato

starch in order to better understand the transformation or deformation of cellular structures and added starches.

Materials and Methods

Materials

Effects of oil addition on microstructure of extrudates were studied with defatted soybean meal (Nisshin FT) containing 55% crude protein and 10.5% moisture and having a Nitrogen Solubility Index (NSI) of 31.1. It was premixed with 5, 10 or 15% soybean oil in a kneader and chopper.

A full-fat soyflour-starch mixture used to determine the transformation of materials in the extruder was made by grinding whole soybeans, sieving to 0.5 mm, and then mixing with 5% potato starch.

Extrusion-cooking conditions

A Creusot-Loire BC-45 co-rotating twin screw extruder with a long cooling die attached was used. Screw speed was 60 rpm except for the defatted flour containing 15% oil which was extruded at 120 rpm. Feed rate was 15 kg/hr. The barrel temperature in normal operation was 180°C. Screw geometry was Reverse-Forward-Reverse-Forward-Forward from the die side as shown in Fig. 1. Moisture contents of the sample flours were 60%.

Preparation of microscopic specimens

The initial soybean flours were mixed with lukewarm agar sol and coagulated. A small piece of the agar was then fixed with 1% osmium tetroxide in phosphate buffer (pH 7), dehydrated with an ethanol series, and then embedded in Epon resin. The resin was sliced, placed on glass slides and stained with Coomassie Brilliant Blue (CBB) for protein or periodic acid Schiff reagent (PAS) for carbohydrates; the samples were examined under a light microscope. The extrudates were treated the same as the initial flours except for the embedding in agar gel. The extrudates were examined lengthwise (along the direction of extrusion) and crosswise (at right angles to the direction of extrusion). The extruder contents were removed at locations A-G shown in Fig. 1 at 5 to 7 min. after stopping the extruder. The extruder contents and extrudates were treated as described above.

Rheological measurement of extrudates

The extrudates were punched out in the form shown in Fig. 2, and used to measure the maximum breaking strength with a Fudo Rheometer (model NRM-300 2D). The deformation rate was 6 cm/min. The values obtained were averages of a minimum of 8 samples.

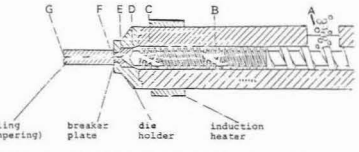

Fig. 1. Configuration of the extruder and sampling positions (A-G).

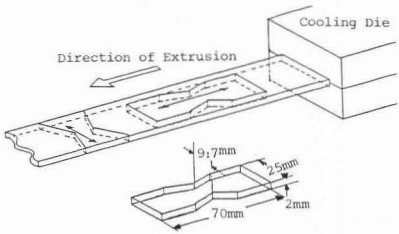

Fig. 2. Sample preparation for texture measurements.

Results and Discussion

Figure 3 shows micrographs of the initial defatted flours with varying levels of added soybean oil. Gross cell disruption including agglomerated protein bodies and cell walls as observed. Added oil was not associated with protein but was scattered in big and small amorphous drops.

After extrusion cooking, the extrudates observed in lengthwise sections show well aligned fiber-like structures as shown in Fig. 4 (A - D). However, the lengthwise orientation of the fibers decreased, thickness of the fibrils increased and size of the air cells increased as the oil content increased. The fat globules observed in the fibrous protein matrix were smaller and more spherical than oil droplets in the initial flours. Under these extrusion cooking conditions, all of the added oil existed in this state.

The microstructures in crosswise sections also clearly show fibrous-like networks (Fig. 4 E - H). As in the lengthwise sections, thickness of the fibrils increased and size of the air cells increased as oil content of the extrudates increased.

The maximum breaking strengths of the extrudates is shown in Fig. 5. The values of breaking strength of the extrudates in lengthwise samples, decreased rapidly as oil content increased. In contrast, the crosswise samples decreased slightly at 5 and 10% but increased significantly at 15% added oil. These results, obtained by rheological measurement, agree with the microstructural changes observed on varying oil content; namely, the orientation of fibrils changed from lengthwise to crosswise at more than 10% oil. Under the extrusion cooking conditions used in this experiment, oil was expressed during cooking when more than 20% oil was present and light micrographs showed large oil drops outside of the protein matrix (data not shown).

Figure 6 shows the full-fat flour before (A) and after it had progressed through the forward (long and short pitch) and reverse screws (B-1 and B-2). In the raw flour, the added potato starch granules were clearly observed, whereas after mixing and kneading by the screws, no

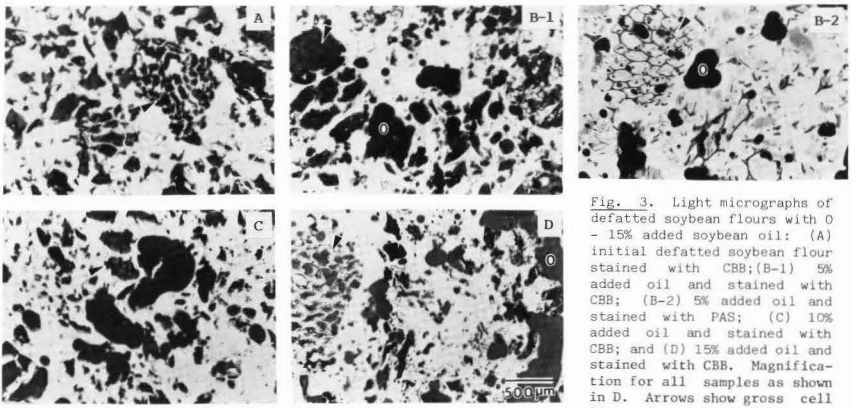

Fig. 3. Light micrographs of defatted soybean flours with 0 - 15% added soybean oil: (A) initial defatted soybean flour stained with CBB;(B-1) 5% added oil and stained with CBB; (B-2) 5% added oil and stained with PAS; (C) 10% added oil and stained with CBB; and (D) 15% added oil and stained with CBB. Magnification for all samples as shown in D. Arrows show gross cell disruption. O = oil droplets.

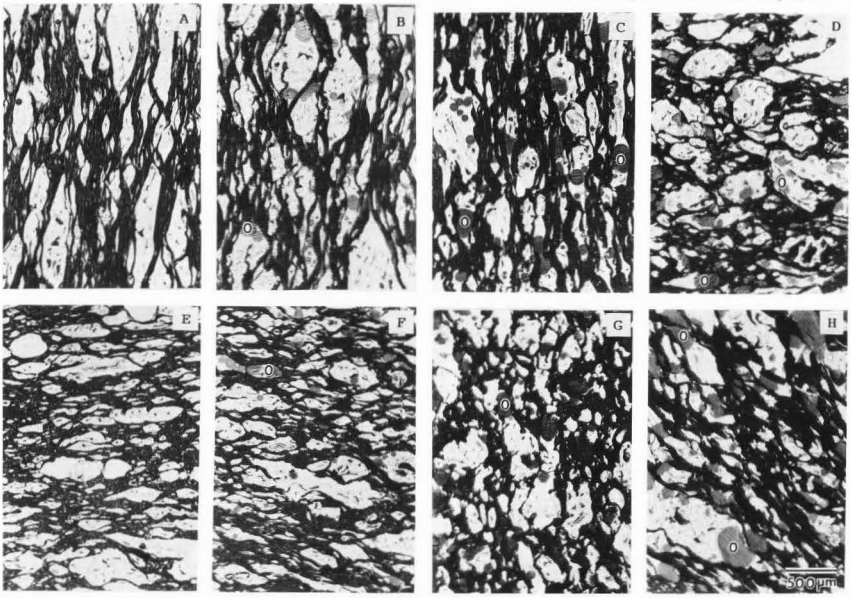

Fig. 4. Light micrographs of extrudates prepared from defatted soybean flours with 0 - 15% added soybean oil and stained with CBB.
A, B, C and D; extrudates in lengthwise sections with added soybean oil of 0, 5, 10 and 15%, respectively, stained with CBB. E, F, G and H; extrudates in crosswise sections with added soybean oil of 0, 5, 10 and 15%, respectively, stained with CBB.
O; oil droplets scattered throughout fibrous network. Magnification for all figures as shown in H.

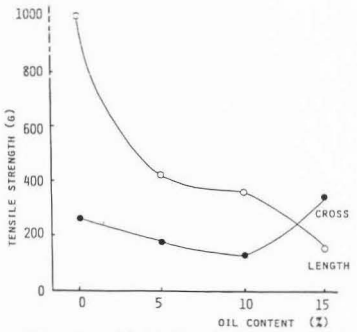

Fig. 5. Effect of oil addition on breaking strength of extrudates prepared from defatted soybean flour. Length-tensioned along the direction of extrusion and cross-tensioned at right angle to extrusion.

granules were found. However, the cellular materials retained their gross structures as shown by staining with CBB (B-1) and/or PAS reagent (B-2) and small oil droplets have begun to appear in the matrix. Both carbohydrate and protein were intertwined in "stream" formation. This agrees with Rhee et al. (1981) who reported that insoluble carbohydrate formed a matrix with plasticized protein in stream formation.

When the materials were introduced into the cooking zone (note location of induction heater in Fig. 1), protein and carbohydrate began to plasticize and the microstructure appeared to be more stream-like (Fig. 6, C - E). As the flour passed through the perforated breaker plate and the long die, fiber formation progressed to completion (Fig. 6 F, G). The results agree with the conclusion of Aguilera et al. (1976) that in a single screw extruder most of the structural changes, such as strand formation, occurred above 145°C and that plasticization took place just before the die.

Under this extrusion cooking condition, the solid fibrous structure obtained with defatted soybean (Fig. 4) could not be prepared from full-fat flour. However, when the extrudate was

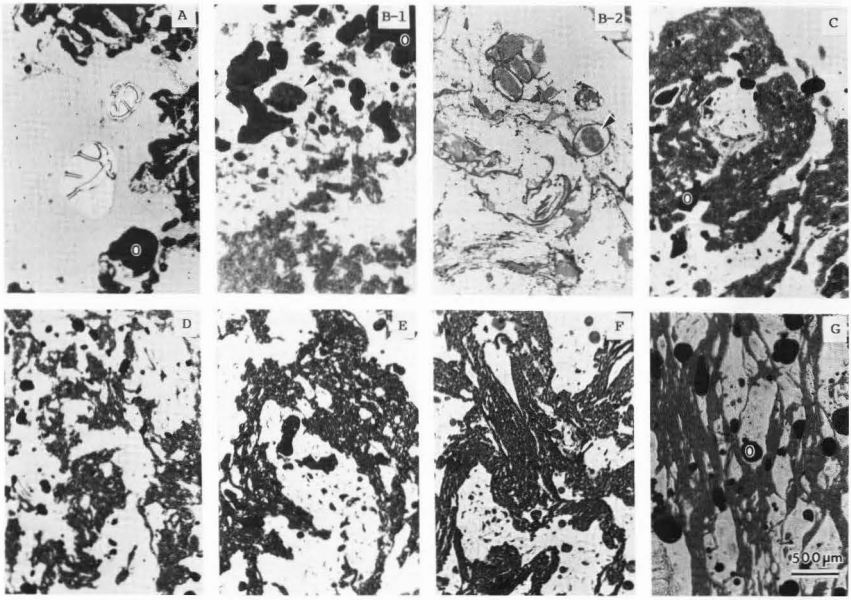

Fig. 6. Changes in microstructures of full-fat soybean flour and added starch during high-temperature short-time extrusion cooking; (A) initial full-fat soybean flour + potato starch; and (B - G) extrudates taken from positions B - G of the extruder (Fig. 1) Stained with CBB except for B - 2 which was stained with PAS. O = oil droplets.

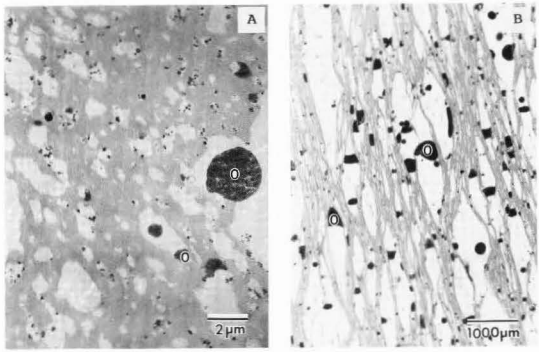

Fig. 7. Electron (A) and light (B) micrographs of extrudate prepared from the one-to-one mixture of full-fat soybean flour and defatted soybean flour. O: oil droplets. Small black spots scattered throughout fibrous matrix in Fig. 7-A are also oil globules.

prepared under the same condition but by addition of defatted soybean flour to the full-fat flour in a 1:1 ratio, a highly fibrous structure could be extruded (Fig. 7). This fact suggests that oil inhibits formation of fibrous structure. However, more than 20% oil may be used by selecting more reverse or kneading screws in the higher length/diameter barrel of a twin screw extruder.

Acknowledgement

The authors sincerely thank members of the Food Engineering Laboratory of the National Food Research Institute for their kind help in operating the extruder.

References

Aguilera JM, Kosikowski FV and Hood LF (1976). Ultrastructural changes occurring during thermoplastic extrusion of soybean grits. J. Food Sci. 41, 1209-1213.

Faubion JM and Hoseney RC (1982a). High-temperature short-time extrusion cooking of wheat starch and flour. I. Effect of moisture and flour type on extrudate properties. Cereal Chem. 59, 529-533.

Faubion JM and Hoseney RC (1982b). High-temperature short-time extrusion cooking of wheat starch and flour. II. Effect of protein and lipid on extrudate properties. Cereal Chem. 59, 533-537.

Neumann PE, Jasberg BK and Wall JS (1984). Uniquely textured products obtained by coextrusion of corn gluten meal and soy flour. Cereal Chem. 61, 439-445.

Noguchi A, Kugimiya W, Haque Z and Saio K (1981). Physical and chemical characteristics of extruded rice flour and rice flour fortified with soybean protein isolate. J. Food Sci. 47, 240-245.

Rhee KC, Kuo CK and Lusas EW (1981). Texturization. ACS symposium series, 147, 51-88.

Simonsky RW and Stanley DW (1982). Texture-structure relationships in textured soy protein. V. Influence of pH and protein acylation on extrusion texturization. Can. Inst. Food Sci. Technol. J. 15, 294-301.

Discussion with Reviewers

A.-M. Hermansson: Can the authors speculate on the mechanisms behind the effect of the oil content on the alignment and formation of fibrous structures of the extruder?

Authors: Although the interactive reactions during extrusion cooking are still obscure, it has been speculated that hydrogen, ionic and hydrophobic bondings contribute as do disulfide bonds to intramolecular reactions between protein and carbohydrates. Intramolecular peptide bonds are also likely to form. Oil may interact with soybean protein by hydrophobic bonding and might prevent direct protein - protein reactions. But fundamental experiments are necessary to clarify this point.

W.J. Wolf: What is the evidence that all of the added oil was present in the form of globules or droplets? Can you rule out the possibility of protein - lipid interaction at the molecular level which would not be detected by light microscopy?

Authors: At present we cannot completely rule out protein-lipid interactions at the molecular level. However, Fig. 7-A, obtained with the electron microscope, likewise indicates that the lipid is dispersed as minute globules in the mesh-like structure.

FOOD MICROSTRUCTURE, Vol. 6 (1987), pp. 63-74
Scanning Microscopy International, Chicago (AMF O'Hare) , IL 60666 USA

0730-5419/87$3.00+.00

THE INFLUENCE OF INGREDIENTS AND PROCESSING VARIABLES ON THE QUALITY AND MICROSTRUCTURE OF HOKKIEN, CANTONESE AND INSTANT NOODLES

R. Moss*, P. J. Gore and I. C. Murray

Bread Research Institute of Australia
P O Box 7, North Ryde NSW 2113
Australia

Abstract

Light and scanning electron microscopy have been used as a part of a research program designed to study the influence of flour quality and processing variables on three of the noodle types that are popular in South East Asia. The noodles selected for study were Cantonese, Hokkien and modern instant. They represent the range of cooking and processing variables that are commonly encountered in these products. Flour particle size and the choice of alkaline ingredients influence protein development during the sheeting process. A continuous protein matrix is required in the raw noodle if it is to have good eating quality when cooked. The swelling of the starch granules during cooking disrupts the protein matrix and the extent of this disruption at the surface of the noodle is related to surface stickiness and cooking loss.

Initial paper received November 03, 1986
Manuscript received January 14, 1987
Direct inquiries to R. Moss
Telephone number: 61-2 888 9600

Key Words: Cantonese noodles, Hokkien noodles, Instant noodles, Kan swi, alkaline ingredients, noodle processing, flour quality, cryosections, light microscopy, scanning electron microscopy.

Introduction

Noodles form an important part of the diet in many of the countries of South East Asia, China and Japan. Hence, much of the wheat that is produced in the major exporting countries is used to produce flour for noodle manufacture. However, there has been relatively little published on the factors influencing noodle quality, and even less published on the microstructure of noodles. The situation is further complicated by the fact that there are a number of different kinds of noodles, each with different production requirements and quality attributes. The three types of noodles that are considered in this paper are : Cantonese noodles which are sold uncooked; Hokkien noodles which are sold partially cooked; and modern instant noodles which are steamed and fried before sale.

There are certain similarities between the microstructure of some noodles and pasta, due in part to the similarities of low dough moisture and cooking methods. Resmini and Pagani (20) have published a detailed review of the microstructure of pasta which contains an extensive bibliography. Oh et al. (15 - 19) have published several papers on Japanese noodles, some of which used scanning electron microscopy (SEM) techniques to elucidate the nature of various processing changes. Dexter et al.(4) have also used SEM to study the microstructure of Japanese noodles made from soft and durum wheat flours. Endo et al.(5) used SEM to study the effect of maturation on Chinese noodle quality. There do not appear to be any papers published relating microstructure to quality aspects of modern instant noodles.

Microscopy has been used, together with other techniques, in the noodle research program conducted at the Bread Research Institute of Australia and this paper attempts to relate the microstructure of Cantonese, Hokkien and modern instant noodles to processing and quality parameters.

Flours

Three straight run flours (73-75% extraction) of 9.0%, 12.0% and 18.7% protein were prepared for this study using a Buhler experimental mill. A sample of bread wheat (Triticum aestivum) semolina was milled on a Miag Vario-Roll mill and sieved to produce four flours of different particle sizes

Table 1 Cantonese Noodles

Effect of flour particle size and starch damage on eating quality

Flour		Noodle		
Particle Size	Maltose (% maltose)	Cooking Time (min)	Eating Quality	Cooking Loss(%)
<85 µm	3.3	7.0	Good	11.0
85-180 µm	2.0	6.5	Good	11.0
265 -355 µm	1.9	6.5	Inter.	12.3
>355 µm	0.8	7.0	Poor	12.6
High Starch Damage <85µm	5.0	8.25	Very poor, gummy	17.7

(Table 1). The final fraction was then subdivided and a portion remilled to increase the level of starch damage as indicated by the high maltose figure (Table 1). The protein contents of these five flours were similar (12.2 ± 0.1%) and thus would not significantly influence noodle quality. Two commercially milled flours (11.0% and 12.5% protein) were also used for certain trials as indicated in the text. Flours were analysed for protein content and diastatic activity by standard methods (1).

Noodle Preparation

There are slight differences in the formulation and processing techniques used to produce the three different kinds of noodles, and these are summarised in Tables 2 and 3. However, basically noodle doughs consisting of flour, alkaline salts (kan swi) or common salt and water (Table 2) were mixed in a Hobart N50 mixer as previously described (10). The crumbly mix was transferred to an Otake noodle machine and compressed four times, with various folds, into a coherent sheet (Table 3). The sheet was rested and then reduced in thickness by passage three times between the rollers at successively decreasing clearance. The dough was then cut into strips by passage between the cutting rolls. Instant noodles were formed into a wave pattern at this stage by the addition of a pair of rubber plates beneath the cutters.

Table 2 Noodle Formulae

	Cantonese			Hokkien	Instant
Flour (13.5% mb)	100	100	100	100	100
Water	32	32	32	31	31
Kan swi					
- amount	1	1	1	2	0.5
- type*	A:B (9:1)	C	D	D:A:B (10:9:1)	A:B (3:2)

* A = Na_2CO_3; B = K_2CO_3; C = NaOH; D = NaCl.

Table 3 Noodle Processing Variables

	Cantonese	Hokkien	Instant
Compression stage	3(0)*	3.8(0)	4(0)
	3(1)	3.8(1)	4(1)
	3(2)	3.8(2)	4(2)
	3(0)	3.8(0)	4(0)
Rest time	30 min	0 min	0 min
Reduction stage	2.2	3.0	2.0
	1.4	2.0	1.2
	0.95	1.0	0.8
Final dough sheet thickness	1.5	2.0	1.0
Cut noodle size (mm)	1.5 x 1.5	2.0 x 2.5	1.0 x 1.5

* Roller gap in mm and numbers of folds in parenthesis.

Noodle Cooking

All noodles were stored in plastic bags at 22°C prior to cooking. Cantonese noodles (10) were cooked on the day of preparation by immersion in boiling water until the uncooked core had just disappeared (Table 4).

Hokkien noodles (11) were pre-cooked in boiling water for 40 sec on the day of preparation. They were then oiled and on the following day they were fully cooked by boiling for 2.5 min.

Instant noodles were steamed for 1 min at 35 kilopascals followed by frying in palm oil at 150 °C for 45 sec. Instant noodles were sealed in a plastic bag and stored at 22°C for one month before organoleptic evaluation.

Table 4 Cantonese Noodles

Effect of flour protein content on optimum cooking time and eating quality

Flour Protein (%)	Optimum Cooking Time (Min)	Eating Quality
9.0	4.0	Soft
12.0	4.25	Firm
18.7	4.75	Rubbery

Noodle Evaluation

Noodle eating quality was determined by the method of Miskelly and Moss (10). Stickiness was subjectively assessed by a trained taste panel and its presence was identified by the noodles sticking to the teeth during mastication or by stickiness during handling. Noodle pH was determined by the method of Moss et al.(12). Cooking loss was determined by evaporating an aliquot (70ml) of cooking water to dryness in a tared pyrex dish. The dish plus residue was then weighed, the residue ashed at 600° C for 1 h and then weighed. Cooking loss was the amount of organic material removed during ashing and was expressed as mg dry matter per 100g raw noodles. Cooking water pH was measured on a separate aliquot of cooking water.

Microscopy

The samples were prepared for light microscopy (LM) as previously described (13) and stained for protein (8, 14), starch (6), fat (7), and bran (9) or germ (9). In the case of cooked products, the samples were prepared for sectioning by rapidly freezing in iso-pentane, cooled by liquid nitrogen to just above the freezing point of the iso-pentane. Some sections of these samples were allowed to dry in the cryostat and examined, unstained and mounted in a synthetic resin (Eukitt, Carl Zeiss, West Germany) using either polarised light or phase-contrast microscopy. This was done to avoid any further swelling of the gelatinised or partially gelatinised starch granules due to contact with aqueous solutions. Samples for scanning electron microscopy were rapidly frozen in a similar manner, freeze-dried and prepared for examination in a Cambridge S600 SEM as previously described (13).

Results and Discussion

Noodle Doughs

The same general microstructural changes took place for all types of noodle doughs during processing, but the rate of development of the dough was influenced by such factors as flour quality, other ingredients and the processing variables selected for each product.

In all types of noodle doughs there is very little gluten development in the mixing stage, which is in contrast to bread dough. In the latter the protein is pulled away from the starch granules in the early stages of mixing to form a coarse, discontinuous network (Fig. 1). Further mixing is then required to develop the desired fine continuous network. In noodle doughs the protein does not pull away from the starch granules during mixing and the microstructure resembles that of compacted flour, with many endosperm particles being clearly discernible (Fig. 2). This is due to the low moisture content of noodle doughs (31-32%) and is characteristic of such products as pasta, in addition to noodles.

In noodle manufacture, the main aims of mixing are, therefore, to uniformly distribute ingredients and to hydrate the flour particles. Dough development is carried out by passage through rollers.

After mixing, all noodle doughs are then compressed into a continuous sheet by repeated passage through pairs of rollers. Examination of dough microstructure during this process indicates that adjacent endosperm particles become "fused" together so that the protein matrix within one endosperm particle becomes continuous with that of adjacent particles. There is much less protein orientation in noodle doughs than in bread doughs that are passed through rollers. Only a few, sub-aleurone, protein masses show orientation in noodle doughs. At the end of the compression stage the visual appearance of the dough sheet looks quite uniform, but micro-structurally, fusion of endosperm particles is not complete. The outline of partially fused endosperm particles is still clearly recognisable (Fig. 3).

The reduction stage which follows further develops the gluten. To obtain the best quality

Legend to Figures.

All light micrographs are transverse sections. In colour micrographs of sections stained with periodic acid Schiff reagent (PAS)/Fast green the starch is stained magenta and the protein blue-green.

E - edge of noodle;
EP - endosperm particle;
GS - grossly swollen starch granules;
M - protein mass;
P - protein;
S - starch.

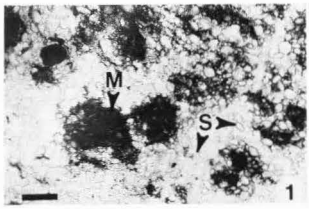

Fig. 1. Light micrograph of a section of bread dough during the early stages of mixing. Note the isolated protein masses formed by the pulling away of the protein from the flour endosperm particles. Stain Ponceau 2R. Bar = 70 µm.

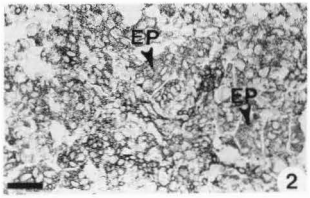

Fig. 2. Light micrograph of a Hokkien noodle dough at the end of mixing. The protein has not pulled away from the starch in the endosperm masses. Stain Ponceau 2R. Bar = 70 µm.

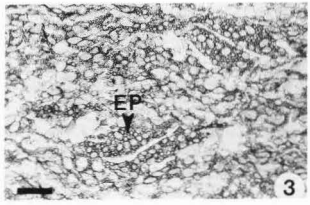

Fig. 3. Light micrograph of a Hokkien noodle dough at the end of the compression stage. Dough development is not complete as the outline of some of the endosperm particles is still clearly recognisable. Stain Ponceau 2R. Bar = 70 µm.

noodles, an extremely uniform protein matrix must be obtained, with no traces of endosperm particles being discernible. However, the upper and lower surfaces of the noodle sheet have a slightly less continuous protein matrix than that seen in the centre of the noodle. After the final reduction stage the noodles are cut, but this does not have any appreciable effect on the microstructure.

Cooked Noodles

The cooking process varies considerably for the 3 types of noodle under consideration. It is therefore difficult to generalise details of microstructural changes and more specific information will be given later. However, in boiled noodles softness is related either to the occurrence of voids in the noodle or the presence of highly swollen starch granules. It has been reported (5) that in Chinese noodles a 24 h maturation period prior to cooking improves eating quality and produces voids in the noodle. However, the improvement may be due to the effect of other factors that play a role during the maturation, rather than the production of voids per se. Surface stickiness is related to a breakdown of the protein matrix at the surface and to a wide outer core of grossly swollen starch granules. Cooking loss is also usually related to surface stickiness, as the disruption of the protein matrix at the periphery of the noodle allows particles to become detached from the bulk of the noodles due to the vigorous action of the boiling water.

Hokkien Noodles

General

All Hokkien noodles were prepared from the commercially milled flour of 11.0% protein content. Some of the major changes that take place during cooking can be illustrated considering the case of Hokkien noodles. After only 20 sec immersion in boiling water all the starch had started to swell and lose some birefringence (compare Figs. 4a, 4b, & 5). There was an outer zone of total gelatinisation that was 400 µm wide. The grossly swollen starch in this zone was held in place by a diffuse protein matrix and also probably by starch molecules that had leached out of the gelatinised starch granules (Fig. 5). The starch in the central region of the noodle had also started to swell and lose some birefringence (Fig.4b). The protein was still quite compact and there were some very small voids (20-50 µm wide). Pre-cooking for an additional 20 or 40 sec caused only a slight increase in width of the outer zone (max. width 600 µm) but internally, with longer cooking, the starch granule swelling was more apparent and the number and size of the voids increased (max. diameter 100 µm).

In the final cooking stage the pre-cooked noodles were reheated in boiling water until there was no longer a white core in the centre of the noodle. In the case of the 40 sec pre-cooked noodle this occurred after 2.5 min cooking. However, after 1 minute's final cooking there was only the slightest trace of birefringence in the centre of the noodle. Yet, the noodle still looked opaque, presumably due to the limited swelling and water up-take of the starch. There was only a very gradual transition in the appearance of the starch from the edge to the centre of the noodle. After 2.5 min final cooking there were no birefringent starch granules in the centre of the noodle, but an increase in size of the starch granules was not apparent. At the outer edge of the noodle, the surface was

Fig. 4a. Light micrograph of the centre of an uncooked Hokkien noodle, taken with polarised light and a 1/4 wave plate. Note the majority of the starch granules are strongly birefringent. Stain Ponceau 2R. Bar = 70 µm.

Fig. 4b. Light micrograph of the centre of a 20 sec pre-cooked Hokkien noodle, taken with polarised light and a 1/4 wave plate. Note that small voids have been formed (arrows) and that all the starch granules have started to lose some birefringence indicating that they are starting to gelatinise. Stain Ponceau 2R. Bar = 70 µm.

Fig. 5. Light micrograph of the edge of a 20 sec pre-cooked Hokkien noodle, taken with polarised light and a 1/4 wave plate. Note the non-birefringent, grossly swollen starch granules at the edge of the noodle and the diffuse protein matrix. This zone is approximately 400 µm wide, and the more central starch granules still show some degree of birefringence. Stain Ponceau 2R. Bar = 70 µm.

Fig. 6. Light micrograph of a Hokkien noodle (40 sec. pre-cook) cooked for 2.5 min (optimum). Although the swollen starch granules in the outer zone have partially disrupted the protein matrix, the outer edge of the section is smooth. Stain PAS/Fast green. Bar = 60 µm.

Fig. 7. Light micrograph of a Hokkien noodle (40 sec. pre-cook) cooked for 4.0 min (overcooked). Note the extensive disruption of the noodle surface due to the vigorous action of the boiling water and the excessive swelling of the starch granules. Stain PAS/Fast green. Bar = 60µm.

Fig. 8. Light micrograph of a Cantonese noodle made from the high protein (18.7%) flour. Note the thicker, more intensely stained protein matrix and the trapped air cells. Stain PAS/Fast green. Bar = 60 µm.

Fig. 11. Light micrograph of a Cantonese noodle, after the compression stage, made from the flour of coarse particle size (265-335 µm). Stain PAS/Fast Green. Bar = 60 µm.

Fig. 12. Light micrograph of a Cantonese noodle, after the compression stage, made from the flour of fine particle size (<85 µm). Stain PAS/Fast Green. Bar = 60 µm.

Fig. 18. Light micrograph of an Instant noodle, made from the 9.0% protein flour, after the frying process. There is no layer of fat at the surface of the noodle, and the fat is distributed uniformly throughout in the form of coarse globules which are stained red. Stain Sudan IV/Oil Red O. Bar = 50 µm.

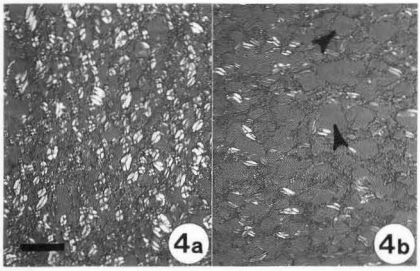
4a
4b

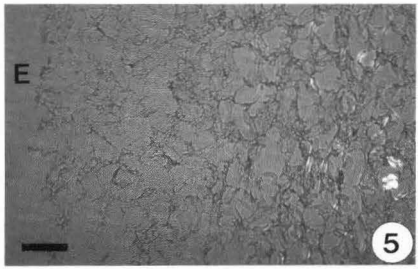
E
5

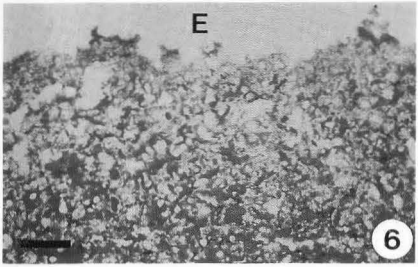
E
6

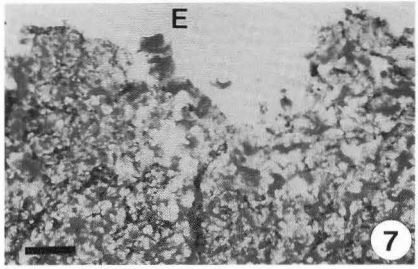
E
7

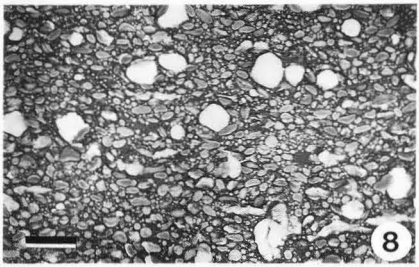
8

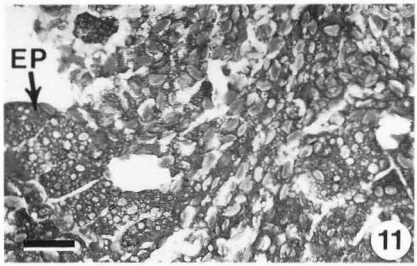
EP
11

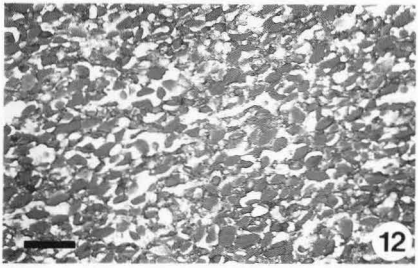
12

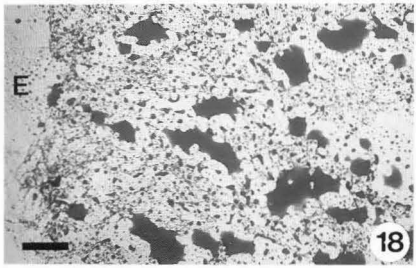
E
18

relatively smooth and not showing any sign of disruption (Fig. 6). The swelling of the starch, however, had stretched and partially disrupted the protein matrix in the outer zone. In the centre of the noodle the protein matrix was still continuous. After 4 min final cooking there was extensive disruption of the noodle surface due to excessive swelling of the starch granules (Fig. 7).

Effect of cooking water pH

Transverse sections of pre-cooked noodles containing either sodium hydroxide or kan swi were examined using phase contrast and polarisation microscopy. Cooking details and final pH of the pre-cooking water are given in Table 5.

Table 5 Hokkien Noodles

Effect of cooking water pH on cooking loss

Alkali	Pre-Cooking Water Initial pH	Final pH	Cooking Loss (g dry matter/ 100g raw noodles) Initial	Final
1% NaOH	8.5	11.0	2.67	3.00
1% Kan swi	8.8	9.5	2.62	2.70

It was apparent that both the size and general appearance of the central core was not influenced by the increase in pH of the pre-cooking water. However, the overall cross-sectional area of the partly cooked noodles increased with alkali build-up, being greatest in the case of sodium hydroxide, which was probably due to the higher pH of the latter. Thus it is only the periphery of the noodles that is affected by the build-up of alkali in the pre-cooking water. The more extensive swelling in the outer region of the noodle is associated with increased cooking loss (Table 5) and stickiness of the partly cooked noodle. The latter can be a problem in high volume, automated noodle plants if the flow of fresh water into the cooking bath is not adequate.

Cantonese Noodles

Effect of flour protein content

The three experimentally milled flours, of protein content 9.0%, 12.0% and 18.7% were chosen for this study. In all three samples the protein network in the raw, cut noodle strings surrounded all the starch. However, sections of the low protein noodles were more fragile than those from the other two samples, indicating that the protein network in the former was weaker. The protein matrix in the 18.7% protein noodles was noticeably thicker than that of the other two samples, and more air was trapped in the dough when compared to the other two samples (Fig. 8). In transverse sections all doughs showed disruption of the starch-protein matrix at the edge of the section, but the high protein sample showed the least contraction, suggesting that the protein matrix is more robust.

On cooking to optimum time (Table 4), the low protein sample had the smallest outer zone of gelatinization (300-400 µm wide) due to the shorter cooking time. However within this zone there was considerable surface disruption, due to the weaker protein network (Fig. 9). The starch granules in the central region of the noodle displayed a greater overall degree of swelling than was seen in the other two samples. The more extensive swelling was confirmed by the extremely pale colour of the starch granules when stained using the PAS reaction. The medium and high protein samples had similar, slightly wider outer zones of gelatinization (400-500 µm). The medium protein sample had a smooth outer surface indicating that the protein network was better able to hold the structure together (Fig. 10).

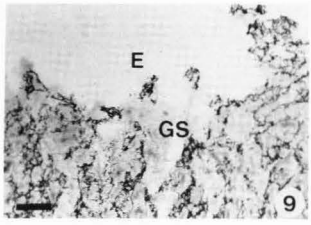

Fig. 9. Light micrograph of an optimally cooked (4.0 min.) Cantonese noodle made from the low protein (9.0%) flour. There has been considerable surface disruption due to the weaker protein network. Stain Ponceau 2R. Bar = 70 µm.

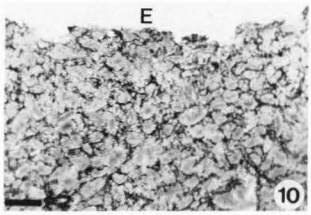

Fig. 10. Light micrograph of an optimally cooked (4.25 min.) Cantonese noodle made from the medium protein (12.0%) flour. There has been relatively little surface disruption due to the stronger protein network. Stain Ponceau 2R. Bar = 70 µm.

However, the high protein sample showed surface disruption equivalent to that of the low protein sample. This is partly due to the increased cooking time, but could also indicate some abnormality in the protein, since the protein content of the original wheat was abnormally high (19.6%). The eating quality of the noodles is shown in Table 4 and the differences in texture would appear to be related more to the protein network than the starch as the low protein sample had a larger central zone of less swollen starch than the other two samples. Cooking always

created voids in the central zone of the noodles, but for good, firm eating quality, the voids should be small (<50 μm diam). The voids are presumably created by forces imparted by the expanding, gelatinizing starch partially disrupting the structure. The more substantial protein matrix of the high protein sample was responsible for the rubbery texture and slowed down water penetration to such an extent that surface breakdown occurred if the centre of the noodle was to be adequately cooked.

When the three samples were cooked to the optimum time established for the high protein sample, the major difference was in the appearance of the starch in the centre of the noodle. The starch in the low protein sample was more swollen and less intensely stained by the PAS reaction than that in the other two samples, suggesting that the protein matrix in the low protein sample had allowed the water to penetrate into the noodle more rapidly and thus allowed the starch to absorb more water. In the centre of the other two samples the appearance of the starch was similar, being more intensely stained by the PAS reaction.

This conflict in cooking requirements at the high protein content meant that the flour was "out of balance" in terms of optimising quality. The protein matrix should be such that it allows the water to penetrate into the noodle so that the central starch granules are optimally gelatinised before surface breakdown occurs. However, the matrix must be sufficiently strong to hold the noodle together. The best "balance" was shown by the medium protein noodle.

Effect of flour particle size and starch damage on noodle quality

The microstructure of dough sheets made from flours of different particle size and starch damage (Table 1) was examined after the compression and reduction stages of processing. After the compression stage it was apparent that the larger the particle size, the slower was the rate of gluten development and fusion of endosperm particles (compare Figs. 11 and 12). However, the dough microstructure of the extremely fine, high starch damage sample was not as uniform as either the <85 μm or the 85-180 μm sample. This suggests that the extra milling had altered the properties of the gluten as well as the starch. It was also interesting to note that the high starch damage sample did not require any more water than the other samples. This again emphasises the different nature of gluten development of noodles compared to bread doughs. However Oh et al. (18) found that an increase in starch damage did increase water absorption of Japanese dried noodles. This anomaly may be due to different ingredients or processing techniques.

After the final reduction pass the microstructure of both the <85μm and the 85-180 μm samples was identical and totally uniform. The 2 coarser samples had progressively less uniform microstructures. This indicates that, in noodle doughs, for optimum gluten development the flour should be of relatively fine particle size, but below 180 μm particle size is not critical. The rollers used in noodle processing are therefore not as effective as a pasta press in developing the protein present in coarse endosperm particles. The protein structure in the high starch damage sample is more uniform than the two coarser samples, but less uniform than the two finer samples.

These differences in gluten development are reflected in terms of both eating quality and cooking loss (Table 1). Oh et al. (18) reported that decreasing particle size did not increase the firmness of cooked noodles, but they used pin-milled flour of fine particle size. The very poor eating quality and large cooking loss of the high starch damage sample would be mainly due to the starch damage, rather than the slightly impaired protein development. It would also appear that the high starch damage had slowed the rate of water penetration into the noodle, as indicated by the long cooking time.

Effect of alkali

The effect of alkali on the quality of Cantonese noodles was examined using the commercially milled flour of 12.5% protein. Alkali (sodium hydroxide or kan swi) is an essential ingredient in Cantonese noodles and the effect of alkali on gluten development and quality of noodles has been discussed elsewhere in relation to Hokkien noodles (11). Cantonese noodles showed a similar trend in the dough stages. Sodium hydroxide slowed down the rate of gluten development when compared to equivalent doughs containing either kan swi or sodium chloride. This effect was particularly noticeable at the upper and lower surfaces of the dough sheet. Even after the final reduction pass, the protein matrix in the sodium hydroxide noodle was not uniform and traces of endosperm particles could be discerned. However, the most obvious differences between the three samples after the final reduction stage were; firstly, that there were more voids in the sodium hydroxide dough sheet, and secondly, that the discontinuity of the protein matrix at the upper and lower surfaces of the noodle sheet was more apparent in the presence of sodium hydroxide. The high pH of the sodium hydroxide noodle (pH 11.5) did not alter the microscopic appearance of the majority of the starch granules, probably because of the low moisture content of noodle doughs.

Table 6 Cantonese Noodles

Effect of alkali on optimum cooking time and cooking loss.

	Treatment		
	1% NaCl	1% Kan swi	1% NaOH
Optimum cooking time (min)	4.5	5.5	6.0
Cooking Loss (g dry matter/ 100g raw product)	5.32	7.45	13.43

After cooking (Table 6), the voids were more plentiful in the sodium hydroxide noodle, partly due to the lack of continuity seen in the dough sheet. However, the toughening of the gluten in the dough by the sodium hydroxide may have prevented the gluten from expanding during cooking, thus increasing the lack of continuity.

The noodles containing either kan swi or sodium chloride had a more delicate, continuous protein matrix, but that of the latter was slightly more disrupted. This could be related to the firmer "bite" associated with the use of kan swi.

After optimum cooking, the starch granules in the centre of the sodium hydroxide noodles were more swollen than those in the other two samples. The surface continuity of the sodium hydroxide noodles was also less than that of the other two samples. The combination of more voids, greater swelling of the starch in the central zone, and more surface disruption resulted in the sodium hydroxide noodle having softer eating quality and surface stickiness. This could be due in part to the longer cooking time required by the sodium hydroxide noodles.

To gain a better understanding of the role of alkali during cooking, samples of sodium hydroxide and kan swi noodles were taken at intervals during the cooking process. It was apparent that the voids present at the dough stage in the sodium hydroxide noodle enlarged as the cooking proceeded, but did not appear to increase in number during cooking. In the sodium hydroxide noodles the size of the central core of less swollen starch granules was larger than that of the kan swi noodle at equivalent cooking times. This suggests that the water penetrates more slowly into the sodium hydroxide noodle, despite the lack of continuity of the protein matrix.

The increase in cooking time required to eliminate the uncooked core in the centre of the noodles meant that the outer surface of the noodle was subjected to the action of the boiling water for too long and it failed to maintain its integrity.

Effect of resting prior to reduction stage

Traditionally the noodle sheet is allowed to rest between the compression and reduction stages. This produces a smoother dough sheet and results in firmer eating noodles. However, a large number of Cantonese noodles are now produced in a continuous process with no provision for a rest period. Hence it was decided to compare the microstructure of noodles produced from both systems using the commercially milled 12.5% protein flour.

After the first reduction pass, the sample that had been rested had a more uniform protein matrix as the endosperm masses had started to fuse together more effectively. As a consequence, the rested sample also had fewer air spaces. The protein contraction at the upper and lower surfaces of the rested noodle sheet was also less than that in the unrested sample (compare Figs. 13 & 14). All these observations indicate that the protein becomes more extensible after resting. Further reduction passes lessened these differences in microstructure, but they were still apparent in the cut noodle strings.

There was no difference in cooking requirement between the two treatments, and after cooking, the internal appearance of both noodles was very similar. However there was a difference in the width and appearance of upper and lower outer zones of the noodles. In the non-rested sample the outer zone was wider (500 µm) and more clearly defined due to the gross swelling of the starch granules. This gross swelling had been allowed to take place because of the increased protein contraction seen in this zone of the raw noodles. In the cooked rested noodle the outer zone was narrower (200-300 µm) and there was a more gradual transition from the gross swelling seen at the surface to the more limited swelling in the central region. The improved eating quality which resulted from resting the noodles after the compression stage was thus due to the presence of a more continuous protein matrix in the raw, cut noodle string. Internally, the changes in microstructure that occurred due to cooking obscure these subtle differences, but at the outer surface they were magnified.

Instant Noodles

Instant (steamed and fried) noodles were made from the three flours of differing protein content (9.0%, 12.0% and 18.7%) and the structural differences at the dough stage were similar to those reported previously for Cantonese noodles.

After steaming, all the starch granules were fully gelatinised, but even the 9.0% protein noodle had no appreciable surface disruption and the starch granules had not ruptured or fused together (Fig. 15). This is in contrast to the cooking behaviour of the same flour when used for the production of Cantonese noodles. The lack of surface disruption was presumably due to the reduced water uptake during the steaming process compared to being placed in boiling water (the yield after steaming was 110%, compared to over 200% for the corresponding Cantonese noodles). The surface continuity of the 9.0% noodle was such that it was able to form large bubbles on the surface (Fig. 16). There were fewer such bubbles on the surface of the 12.0% protein noodle and none on the surface of the 18.7% noodle.

SEM examination showed that during frying, large voids were created inside all the noodles, but the internal structure of the low protein noodle was more uniformly open (Fig. 17). As the protein content increased, the voids became larger and the porosity less uniform. However, the use of aqueous reagents that are essential to the LM technique resulted in an expansion of the matrix and a marked reduction in the size of the voids. The surface of the low protein noodle showed some slight disruption after frying but this disruption decreased as the protein content increased. The shape of the starch granules was still much more clearly discernible than in boiled noodles, due to the low water content of the steamed instant noodles.

Fat up-take during frying is an important factor, as high up-take increases the cost of the finished product and may adversely affect shelf life. In the low protein noodle the fat was distributed as coarse globules and had penetrated uniformly throughout the noodle (Fig. 18). In the high protein noodle there was much less fat up-take, some areas had virtually no fat and there was less fat in the centre of the noodle. However the intermediate protein noodle had a similar fat up-take to the low-protein noodle. Thus protein content is not the sole factor influencing fat up-take. It was also surprising to observe that

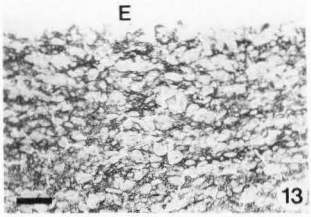

Fig. 13. Light micrograph of a Cantonese noodle after the first reduction pass. This sample has been rested for 30 min. after the compression stage. There is very little contraction of the darkly stained protein network at the surface of the noodle sheet. Stain Ponceau 2R. Bar = 70 µm.

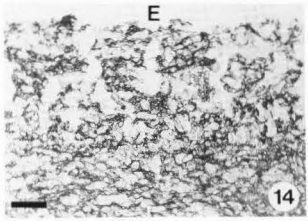

Fig. 14. Light micrograph of a Cantonese noodle after the first reduction pass. This sample has not been rested for 30 min. after the compression stage. There is some contraction of the protein network at the surface of the noodle sheet. Stain Ponceau 2R. Bar = 70 µm.

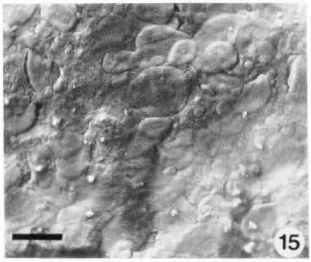

Fig. 15. SEM of the surface of an Instant noodle, made from the 9.0% protein flour, after the steaming process. The starch granules have not ruptured and fused together. Bar = 40 µm.

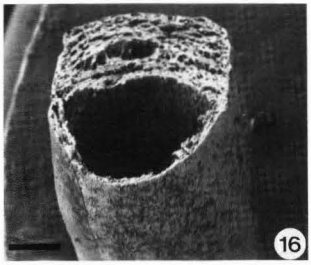

Fig. 16. SEM of a fracture surface of an Instant noodle, made from the 9.0% protein flour, after the frying process. The large blister on the surface was formed during steaming, and the internal voids were formed by steam generation during frying. Bar = 400 µm.

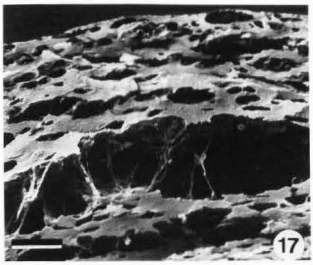

Fig. 17. SEM of a fracture surface of an Instant noodle, made from the 9.0% protein flour, before final cooking. Note the internal voids formed during frying. Bar = 100 µm.

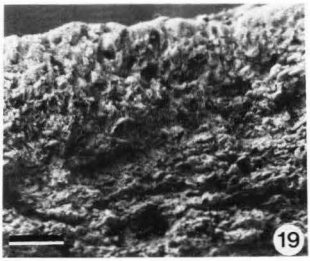

Fig. 19. SEM of a fracture surface of an Instant noodle, made from the 9.0% protein flour, after final cooking. The internal voids seen in the sample examined after frying have disappeared due to swelling of the starch granules on boiling. Bar = 100 µm.

there was no localised concentration of fat at the outer surface of the noodles.

When the noodles were re-cooked there was an increase in the area of the sections (32%) due to imbibition of water, but the most obvious change was in the condition of the voids. The starch-protein matrix had swollen to such an extent that the voids had virtually disappeared when examined using SEM (compare Figs. 17 and 19). However, light micrographs indicated that the internal cell walls that separated the voids had not fully fused together after the final cooking. The lipid in the central region appeared to have migrated from the body of the starch-protein matrix to line the walls of the former voids. However, the amount of lipid in this region was similar to that seen after frying, but the outer zone (250 um wide) was relatively free from lipid, presumably due to migration into the cooking water.

The sponge-like structure of the noodles after frying would be expected to facilitate water penetration and assist rapid reconstitution of the noodles in the final cooking process. However, if large voids remained in the noodles after reconstitution they would have an adverse effect on texture.

Conclusion

The eating quality of boiled noodles is influenced by the continuity of the protein matrix, the degree of starch swelling and the extent of surface disruption. Modern instant noodle quality is also influenced by these factors and by the formation of voids created by steam generation during the frying process. Microscopy provides a useful way of studying the manner in which ingredients and processing variables influence these quality parameters.

Acknowledgments

The authors wish to thank Miss S. Stiles for assistance with the SEM, and the Fuel Geoscience Unit of the Institute of Earth Resources, CSIRO, for the use of the SEM.

References

1. Cereal Laboratory Methods, 7th edn. (1978). American Association of Cereal Chemists, St. Paul, Minnesota.

2. D'Egidio M G, De Stefanis E, Fortina S, Galterio G, Nardi S, Sgruletta D, Bozzini, A (1982). Standardization of cooking quality analysis in macaroni and pasta products. Cereal Foods World, 27 (8): 367-368.

3. Dexter J E, Kilborn R H, Morgan B C, Matsuo R R, (1983). Laboratory compression tester : Instrumental measurement of cooked spaghetti stickiness. Cereal Chem., 60 :139-142.

4. Dexter J E, Matsuo R R, Dronzek B L, (1979). A scanning electron microscopy study of Japanese noodles. Cereal Chem. 56 (3) : 202-208.

5. Endo S, Hara H, Sato T, Nagao S, (1984). Effect of maturation on microstructure and rheological properties of Chinese noodles. Nippon Shokuhin Kogyo Gakkaishi. 31 (1) : 10-13.

6. Flint F O, Moss R, Wade P, (1970). A comparative study of the microstructure of different types of biscuits and their doughs. Food Trade Review 40 (4) : 32-39.

7. Gurr E, (1958). Methods of analytical histology and histochemistry. Leonard Hill, London. p 153.

8. Gurr E, (1958). Methods of analytical histology and histochemistry. Leonard Hill, London. pp 79-84.

9. Jacobsen J V, Knox R B, Pyliotis N A (1971). The structure and composition of aleurone grains in the barley aleurone layer. Planta (Berlin). 101: 189-209.

10. Miskelly D M, Moss H J (1985). Flour quality requirements for Chinese noodle manufacture. J. Cereal Sci. 3 (4) : 379-387.

11. Moss H J, (1984). Ingredient effects in mechanised noodle manufacture. Proc. fourth SIFST symp. Adv. in food processing, Singapore Institute of Food Science and Technology, Singapore, 71-75.

12. Moss H J, Miskelly D M, Moss R (1986). The effect of alkaline conditions on the properties of wheat flour dough and Cantonese-style noodles. J. Cereal Sci. 4 : 261-268.

13. Moss R, (1985). The application of light and scanning electron microscopy during flour milling and wheat processing. Food Microstruc. 4 : 135-141.

14. Moss R, (1973). Conditioning studies on Australian wheat II Morphology of wheat and its relationship to conditioning. J. Sci. Fd. Agric. 24 (9) : 1067-1076.

15. Oh N H, Seib P A, Deyoe C W, Ward A B, (1983). Noodles I. Measuring the textural characteristics of cooked noodles. Cereal Chem. 60 (6) : 433-438.

16. Oh N H, Seib P A, Deyoe C W, Ward A B (1985). Noodles II. The surface firmness of cooked noodles from soft and hard wheat flours. Cereal Chem. 62 (6) : 431-436.

17. Oh N H, Seib P A, Chung D S (1985). Noodles III. Effects of processing variables on quality characteristics of dry noodles. Cereal Chem. 62 (6) : 437-440.

18. Oh N H, Seib P A, Ward A B, Deyoe C W, (1985). Noodles IV. Influence of flour protein, extraction rate, particle size and starch damage on the quality characteristics of dry noodles. Cereal Chem. 62 (6) : 441-446.

19. Oh N H, Seib P A, Ward A B, Deyoe C W (1985).

Noodles VI. Functional properties of wheat flour components in oriental dried noodles. Cereal Foods World 30 (2) : 176-178.

20. Resmini P, Pagani M A (1983). Ultrastructure studies of pasta. A review. Food Microstruc. 2 : 1-12 and 98.

Discussions with Reviewers

D.D. Christianson: Could the authors elaborate on the production of the void spaces in noodles? Do the gliadin and glutenin contents influence void formation?

Authors: The gliadin and glutenin contents of the flours used in these trials were not measured and although this factor is known to influence extensibility in bread doughs it is not certain whether it plays the same role in noodle doughs where the moisture content is much lower. The protein does not necessarily have to be extensible to form a continuous matrix in noodle doughs as the matrix is formed by the fusion of the matrices already existing in the flour particles. However, on cooking, the expansion of the starch granules as they gelatinise puts a strain on the protein network. Voids are created when the protein network is torn apart at its weakest points by these forces.

D.D. Christianson: Does some chemical gelatinisation of the starch take place in the alkaline media? Barriers that reduce water penetration in NaOH noodles could be solubilized starch and/or degraded protein.

Authors: In isolated cases, some sections taken from sodium hydroxide doughs in the early stages of sheeting did occasionally contain streaks where the starch granules appeared to have suffered some chemical gelatinisation. However this fact was not emphasised in the text as it was not always observed. It would seem most likely that any chemically gelatinised starch would have arisen from the initial contact of the starch with the highly alkaline water at the start of the mixing.

P.A. Seib: In the Chinese style noodles, how does one determine the optimum moisture and alkaline agents to use?

Authors: For most trials water addition was not "optimised" but rather added at a standard level as determined through surveys carried out by the Bread Research Institute of noodle manufacturers and flour millers in the southeast Asian region. The type and amount of "kan swi" was also determined in this manner. Additional trials were carried out with the high starch damage flour to see if it required any extra water. However an additional 0.5% water caused the dough to become sticky and difficult to handle during sheeting.

R.R. Matsuo: Could the authors indicate whether the flours used for the trials were considered to be strong, medium or weak in terms of Farinograph characteristics?

Authors: The three Buhler milled flours of 9.0, 12.0 and 18.7% protein were milled from the hard grained, medium strength, Australian wheat variety Osprey. However,as descriptive interpretations of strength can be misleading, the authors have included Farinograph and Extensograph data for the three flours (Table 7).

Table 7

Flour Pr	Farinograph		Extensograph	
(%)	Water Abs (%)	Dev Time (min)	Max Resi (BU)	Ext (cm)
9.0	63.0	3.1	250	20.4
12.0	63.6	4.5	259	25.2
18.7	70.1	8.4	330	27.9

R.R. Matsuo: It is surprising that stickiness is noted in Hokkien noodles where the surface is coated with oil. Do the authors have a method for assessing surface stickiness?

Authors: As the reviewer has indicated, stickiness can be overcome in Hokkien noodle manufacture by the addition of oil. The stickiness referred to by the authors was observed in the un-oiled noodles. However application of extra oil to overcome excess stickiness imposes a cost penalty on the manufacturer.
The authors are currently evaluating two objective methods of measuring stickiness (2,3) but our estimates of stickiness in this work were subjective, being either stickiness as observed during mastication or handling.

R.R. Matsuo: The authors state that the less uniform microstructure of the high starch damage sample "suggests that the extra milling had altered the properties of the gluten as well as the starch". Is it not possible that differences noted may be due to the preferential water uptake by damaged starch rather than a change in gluten properties?

Authors: The authors wished to emphasise that both factors are important and did not intend to imply that starch damage was not an important factor. However the gluten damage which can occur as a consequence of the deliberate creation of starch damage in roller milling is often overlooked, and this can also influence dough properties as discussed elsewhere (13).

FOOD MICROSTRUCTURE, Vol. 6 (1987), pp. 75-79
Scanning Microscopy International, Chicago (AMF O'Hare) , IL 60666 USA

0730-5419/87$3.00+.00

EFFECT OF IONIZING IRRADIATION AND STORAGE ON MUSHROOM ULTRASTRUCTURE II. THE STIPE AND THE UPPER PART OF THE CAP OF AGARICUS BISPORUS (LGE. IMBACH)

Á. Keresztes[1] and E. Kovács[2]

[1]Department of Plant Anatomy, Eötvös Loránd University, 1088 Budapest, Muzeum krt. 4/A, Hungary

[2]Department of Microbiology, Central Food Research Institute, 1022 Budapest, Herman Ottó u. 15, Hungary

Abstract

After having investigated the ultrastructural effects of ionizing irradiation used for shelf-life extension, on the gills of Agaricus bisporus and Pleurotus ostreatus previously, it was of interest to examine how other parts of the fruit body were affected by the same treatment. Samples were taken from the lower and upper parts of the stipe and from the upper part of the cap of the control, stored, and irradiated (2.5 kGy) then stored A.bisporus fruit bodies. Transmission electron microscopy showed that irradiated samples generally retained plasm-content, which dramatically decreased in those without irradiation by the end of storing (6 days). However, irradiation also induced autophagy and necrosis in some cells of the lower part of the stipe.

Initial paper received July 28, 1986
Manuscript received December 01, 1986
Direct inquiries to E. Kovacs
Telephone number: 36-1-152028/157341

KEY WORDS: Mushroom, Agaricus bisporus, transmission electron microscopy, ultrastructure, irradiation, growth retardation, shelf-life extension, ripening

Introduction

In the course of our earlier investigation we found that gamma-irradiation of 2.5 kGy (applied for shelf-life extension) caused a substantial degradation or a total cell necrosis in the hymenium of Agaricus bisporus or Pleurotus ostreatus, respectively (Keresztes et al. 1985). This means that irradiation inhibits spore production by destroying basidia rather than conserving their juvenile stage. Destructive but much less pronounced changes were found in the hymenophoral cells.

Irradiation apparently also affects other parts of the fruit bodies in A.bisporus, since they remain closed and do not grow at an appreciable rate when irradiated at an early stage of development. It is known that opening is caused by the elongation of stipe cells (Bonner et al. 1956, Hagimoto 1964), accompanied by cell divisions to some extent (Craig et al. 1977). The question arises as to the cause of the growth retardation of carpophores. Does irradiation treatment destroy stipe cells (as seen in the hymenium), or does it act in another way?

In this paper we demonstrate that irradiation preserved the living content of the retarded cells in the upper parts of the cap and the stipe, while some cells below the annulus showed autophagy and necrosis.

Materials and Methods

Three groups of carpophores of A.bisporus obtained from Duna MgTSz (Budapest) were used: (1) fresh control; (2) stored control (6 days), and (3) irradiated (2.5 kGy) then stored (6 days) group.

Three kinds of samples were collected from a carpophore: (a) parts from the lower part of the stipe (about halfway between the base and the annulus); (b) from the upper part of the stipe (between the pileus and the annulus), and (c) from the pileus (about halfway be-

tween the brim and the center, above the gills).

In all cases samples were cut out close to the surface. For storing and irradiation treatment, see Keresztes et al. (1985).

Fixation was carried out in 6 % (v/v) glutaraldehyde (in 0.035 M K-Na phosphate buffer, pH 7.2) for 2 hours at 4°C. After thorough washing in the above buffer samples were postfixed in 1 % (w/v) OsO_4 for 1.5 hours, dehydrated in an acetone series and embedded in Spurr's resin.

Sections were made with a Porter-Blum ultramicrotome equipped with an LKB glass knife, and after contrast-staining with uranyl acetate and lead citrate, were examined in a Tesla BS 500 electron microscope operated at 60 kV.

Results and Discussion

The lower part of the stipe

In the fresh control the cells contain smaller or larger vacuoles (Fig. 1 A). In the latter case the cytoplasm forms a layer of variable thickness and medium density. In the more frequent former case the cytoplasm is less dense and apparently less compact. This kind of plasm is termed mictoplasm (Angeli-Papa and Eymé 1978) originating from the mixing of cytoplasm and the primary vacuole. Vacuoles seen at this stage are secondary ones derived probably from plasmalemmasomes.

The cells are multinucleate (Evans 1959, Craig et al. 1979), nuclei mostly being close to each other (not shown here). At higher resolution numerous glycogen rosettes can be observed in the cyto- or mictoplasm.

Cells of the stored control markedly differ from those of the fresh control, mainly in having a thin, low-density plasm layer along the walls (Fig. 1 B). The primary or secondary status of this cannot be readily discerned. Nuclei seem to be similar to those of the fresh control.

In the irradiated then stored samples the relative plasm-content of most cells is larger than that of the stored control. The vacuoles of these cells contain numerous small vesicles (Fig. 1 C), which may be a sign of autophagy, a process that has been observed also in irradiated Pleurotus subhymenium (Keresztes et al. 1985). Among the vesicles there are electron dense fuzzy, roundish bodies of unknown nature in the vacuoles. A part of the cells contains microplasm.

Cell walls are generally thicker than in any of the controls and also local thickenings occur (Fig. 1 C). This may be the reason for the increased consistency of tissue pieces experienced at excision. We have observed an imbalance between cell wall synthesis and extension also in neutron irradiated barley leaves (Kovács et al. 1979). Nuclei seem to be similar in size, shape and number to both controls.

Among the living cells, in contrast to the controls, there are necrotized and empty cells or groups of cells (Fig. 1 C). The walls of these remained thin. These may represent the end stage of an autophagic process induced by the irradiation. We have observed a similar phenomenon in the hymenium of Pleurotus ostreatus (Keresztes et al. 1985).

The upper part of the stipe

In the fresh control the shape of the cells seems to be more variable, the mictoplasm formation is less frequent than in the lower stipe (Fig. 2 A). The cells are multinucleate here, too.

In the stored control the relative plasm-content of cells is very low (Fig. 2 B). Cells of the irradiated then stored samples retain relatively more plasm, which is generally rich in glycogen (Fig. 2 C). In most cases these cells contain several smaller vacuoles instead of a single large one and show no obvious signs of autophagy.

The upper part of the cap

A general feature of these samples is that the cell shapes are variable and irregular with large intercellular spaces (lacunae) between them. In the fresh control the plasm-content of the cells is variable but generally less than in the fresh stipe (Fig. 3 A). Mictoplasm formation occurs. We have not seen more than two nuclei per cell.

In the stored control the plasm-content decreases as in the stipe (Fig. 3 B), while the irradiated and stored samples retain the plasm-content (Fig. 3 C).

Conclusions

In all investigated parts of the A.bisporus carpophores (with the exception of the hymenium, see Keresztes et al. 1985) we found that irradiation of 2.5 kGy preserved the plasm-content to a considerable extent, which decreased to a minimal amount during storing without irradiation. This demonstrates the merit of this method of shelf-life extension for the bulk of the fruit body at the ultrastructural level.

However, irradiation induced autophagy in the lower part of the stipe. This process may progress during prolonged storing causing cell necrosis, but in such a part of the fruit body which is not generally used in food technology.

Acknowledgements

We wish to thank Mrs. P. Petrovits, Mrs.G. Gácsi, Mrs. A. Gyurek and Mrs. J.Bencze-Böcs for their valuable technical help.

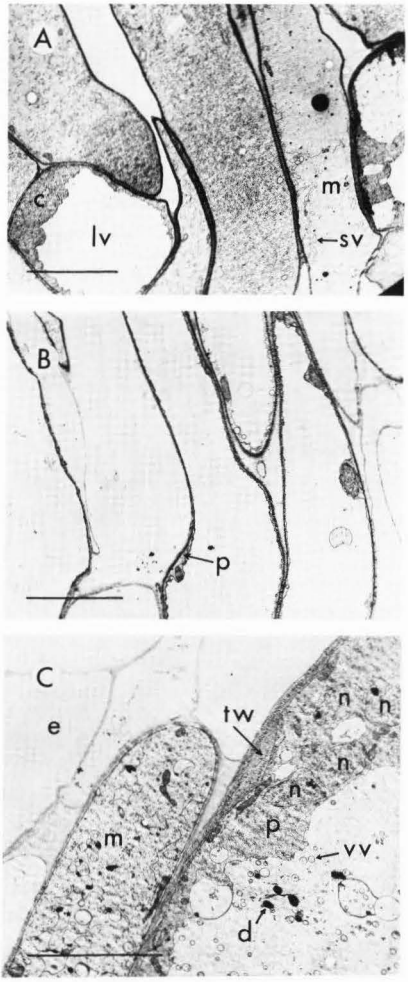

Fig. 1. Lower stipe cells. A: fresh control, B: stored control, C: irradiated then stored sample. Abbreviations: c=cytoplasm, m=mictoplasm, p=plasm, n=nucleus, tw=thickened wall, lv=large vacuole, sv=small vacuole, vv=vacuolar vesicle, d=dense body, e=empty cell. Bars equal lo µm.

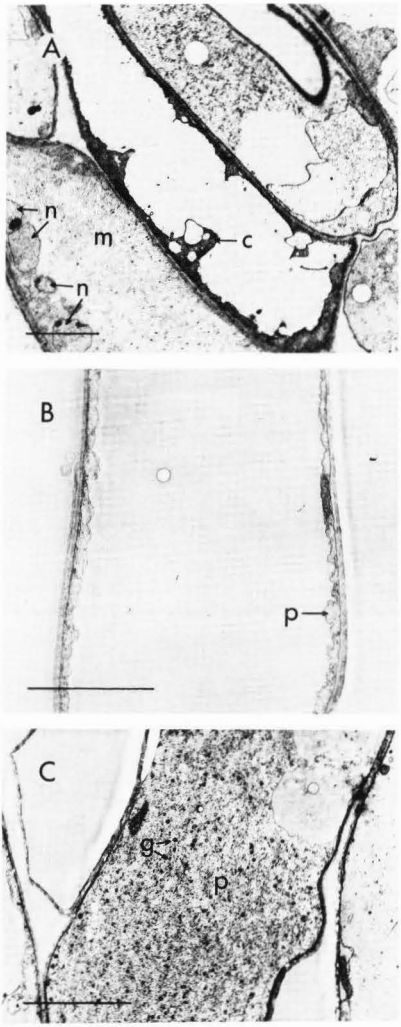

Fig.2. Upper stipe cells. A: fresh control, B: stored control, C: irradiated then stored sample.
Abbreviations: g=glycogen, for other symbols see Fig. 1. Bars equal 5 µm.

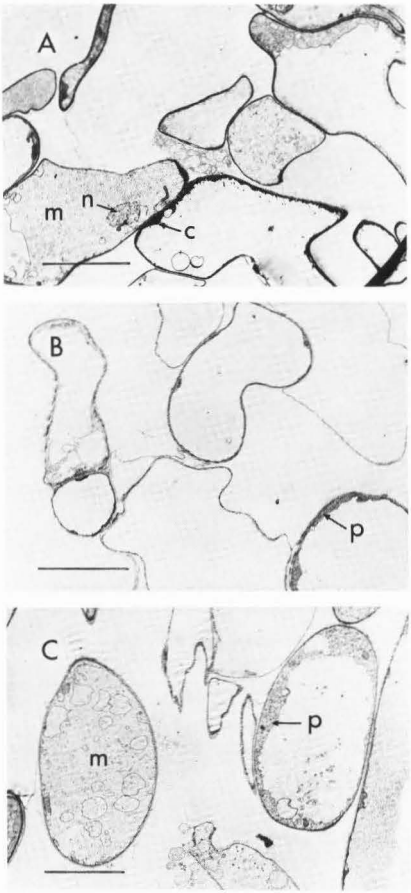

Fig. 3. Cells from the upper part of the cap. A: fresh control, B: stored control, C: irradiated then stored sample. For abbreviations see Fig. 1. Bars equal 10 μm.

References

Angeli-Papa J, Eymé J. (1978). Ultrastructural changes during development of Agaricus bisporus and Agaricus sylvicola. In: The biology and cultivation of edible mushrooms, ST Chang, WA Hayes (eds.), Academic Press, N.Y. 53-81.

Bonner JT, Kane KK, Levey RH. (1956). Studies on the mechanics of growth in the common mushroom Agaricus campestris. Mycologia 48,13-18.

Craig GD, Gull K, Wood DA, (1977). Stipe elongation in Agaricus bisporus. J. Gen. Microbiol. 102, 337-347.

Craig DJ, Newsam RJ, Gull K, Wood DA. (1979). An ultrastructural and autoradiographic study of stipe elongation in Agaricus bisporus. Protoplasma 98, 15-29.

Evans HJ. (1959). Nuclear behaviour in the cultivated mushroom. Chromosoma 10, 115-135.

Hagimoto, H. (1964). The growth of the fruit body of Agaricus bisporus (Lange) Sing. Trans. Brit. Mycol. Soc. 4, 158-164.

Keresztes Á, Kovács J, Kovács E. (1985). Effect of ionizing irradiation and storing on mushroom ultrastructure. I. The gills of Agaricus bisporus (Lange) Imbach and Pleurotus ostreatus (Jacq. ex. Fr.) Kummer. Food Microstructure 4, (2) 349-355.

Kovács V, Gyurján I, Keresztes Á, Virág E. (1979). Studies on the biological effect of fast neutrons. II. Variation of total nucleic acid content and ultrastructure in barley leaves vs. dose. Acta Biochim. et Biophys. Acad. Sci. Hung. 14, 103-109.

Discussion with Reviewers

D.L. Rinker: Shelf-life of mushrooms is not only a function of post-harvest manipulation but also reflects cultural practices, supplementation, and strain selection. How do these parameters affect shelf life of irradiated mushrooms? Authors: Mushrooms were a commercial product of Duna MgTSz, Budapest. The strain and the cultural practices have been constant for a long time, so we could not investigate the effect of their variation on shelf-life of mushrooms.

E.M. Jasinski: What were the storage conditions that the authors used, i.e. temperature, packaging material, length of time between harvest and storage? Authors: The samples were stored at 14-16°C, 90-95 % RH, without any packaging materials. The length of time between

harvest and storage was about 2-3 hours (spent by transportation and irradiation).

E.M. Jasinski: What was the maturity of the mushrooms at the time of harvest?
Authors: Mushroom caps were closed, the diameter of caps ranged from 4.2 to 4.9 cm. The mushrooms were picked from the second flush, which represents the best quality of mushroom.

E.M. Jasinski: Did the authors notice any bacterial degeneration of the mushroom tissue after/before storage?
Authors: No, we did not notice such signs.

E.M. Jasinski: How many of the mushrooms were tested in each of the groups? Are the pictures representative of the entire sample?
D.L. Rinker: How many samples were actually excised in order to draw the conclusions?
Authors: 50-50 carpophores were individually collected for irradiation and control. From these groups 3-3 carpophores were selected on the basis of average diameter for electron microscopy. From each sampling area on each fruit body 3-4 pieces were excised. Before the TEM investigations several thousand mushrooms had been individually measured studying the effect of irradiation on the cap opening and stipe elongation (Kovács E, Vas K. (1974). Acta Alimentaria 3, 19-25; Wahid, M. Kovács E. (1980). Acta Alimentaria 9, 357-366; Kovács E, Vörös Zs, Farkas, J. (1981). Acta Alimentaria 10, 379-388). We think the figures represent the samples.

FOOD MICROSTRUCTURE, Vol. 6 (1987), pp. 81-89
Scanning Microscopy International, Chicago (AMF O'Hare) , IL 60666 USA

0730-5419/87$3.00+.00

TEXTURAL PROPERTIES AND STRUCTURE OF STARCH-REINFORCED SURIMI GELS AS AFFECTED BY HEAT-SETTING

J.M. Kim[1], C.M. Lee[2], and L.A. Hufnagel[3]

[1]Department of Food Science
University of Maine, Orono, ME 04469;

[2] Department of Food Science and Nutrition;
[3] Department of Microbiology;
University of Rhode Island, Kingston,RI 02881

Abstract

The gel forming behavior of red hake (Urophycis chuss) surimi with and without starch and its relationship to the structure of the gel matrix were studied. For surimi gels without starch, a combination of preheat-setting at 40 C and cooking at 90 C resulted in significantly greater gel strength than cooking alone. However, preheat-setting of gels containing wheat or potato starch had no significant effect on gel strength demonstrating an opposite trend in gel strength due to the differences in swelling power, water holding ability and gelatinization temperature between potato and wheat starches. This difference in gel forming behavior due to the sources of starch and heat-setting prior to cooking correlated with changes in the structure of the matrix as evidenced by the results of image analysis. An examination of the microstructure of the gel matrix by light and electron microscopy showed that the structural differences may be due to the different protein matrix density as reflected in the increased gel strength.

Initial paper received October 06, 1986
Manuscript received May 06, 1987
Direct inquiries to J.M. Kim
Telephone number: 207 581 1624

KEY WORDS: Starch in surimi gel structure, wheat, potato, rheology, texture.

Introduction

Surimi is a Japanese term for mechanically deboned fish flesh which has been washed with water and mixed with cryoprotectants for a good frozen shelf life. It is used as an intermediate product for a variety of fabricated seafoods. Due to its high functionality, surimi can be substituted for a variety of traditional animal and vegetable proteins (Lee, 1984).

It has been reported that heat-setting at 40-50 C prior to cooking at 90 C resulted in a stronger gel than cooking alone (Okada, 1959a,b). Recently Wu and his coworkers (1985a) examined physical changes in a surimi-starch system during thermal processing by monitoring starch gelatinization and protein denaturation with a differential scanning calorimeter. They found that gelatinization temperature, degree of swelling and water uptake of starch granules influenced the textural properties of a cooked gel, and the addition of starch resulted in higher failure stress but no significant effect on failure strain.

Composite gel-reinforcing effect of starch has been suggested by several workers (Okada and Yamazaki, 1957; Wu et al., 1985b). Little is known, however, about the effect of cooking methods and ingredients on textural properties with respect to the microstructure of gels. This prompted us to investigate the gel forming behavior of surimi as affected by cooking methods and type of starch, with the focus on gel microstructure and its relationship to gel textural properties.

Materials and Methods

Preparation of surimi

Red hake (Urophycis chuss) caught off Galilee, Rhode Island was processed into surimi within 24 hours. Fresh red hake fillets were run through a deboner (Model 694, Baader North America, New Bedford, MA) with a drum having 5 mm diameter perforations and washed 3 times using 1 part fish meat to 4 parts water (w/w). Each washing was carried out at a water temperature of 10 C for 10 min and was followed by draining in a rotary rinser prior to the subsequent washing. The resulting slurry from the rinser was passed through a strainer (Model Bibun SUM 420, Ryan Engineering, Seattle, WA) to remove any residual dark connective tissue, black skin, bone and scale. The strained meat was then run through a screw dehydrator (Model Bibun SR 1000, Ryan Engineering, Seattle, WA) to remove

TABLE 1 - Types of surimi gels prepared

Types	Types of starch	Cooking methods used
I	Surimi paste without starch	cooked at 90 C for 40 min in a water bath and immediately cooled in running tap water for 20 min
II	Surimi paste without starch	heat-set at 40 C for 30 min and then treated in the same manner as Type I
III	Surimi paste with wheat starch	treated in the same manner as Type I
IV	Surimi paste with wheat starch	treated in the same manner as Type II
V	Surimi paste with potato starch	treated in the same manner as Type I
VI	Surimi paste with potato starch	treated in the same manner as Type II

water; chopped with sugar, sorbitol and sodium tripolyphosphate at 4%, 4% and 0.2%, respectively, in a 50 lb-capacity silent cutter (Model VCM 40, Hobart Manufacturing Company, Troy, Ohio) at a low speed (1,750 rpm) for 30 sec; and subsequently vacuum-packed (Model GK 120, Smith Equipment Co., Clifton, NJ) in cryobags to be stored at -20 C until used.

Preparation of heat-induced surimi gel

The thawed surimi (overnight in a refrigerator, -2 + 0.5 C, 78% moisture) was chopped with 2.5% salt (Morton plain salt, Morton Thiokol, Inc., Chicago, IL) in a silent cutter for 9 min. This was followed by additional chopping for 3 min with or without 5% wheat or potato starch and enough ice-chilled water to adjust the moisture level to 78%. The quantities of salt and starch added were based on a surimi weight basis. The chopped surimi paste was stuffed into 30 mm diameter cellulose casings and cooked. Six types of samples were prepared due to different cooking methods and types of starches incorporated as shown in Table 1. Wheat starch (Aytex P) and potato starch were obtained from Henkel Corporation (Minneapolis, MN) and Colby Starch Company (Caribou, ME), respectively.

Measurement of textural properties

The prepared gels were left overnight at room temperature to equilibrate to room temperature and were cut into cylindrical shapes (30 mm diameter and 25 mm long). Following the procedures proposed by Lee (1984) and using an Instron testing machine (Model 1122, Instron Engineering Corp., Canton, MA), compressive force, expressible moisture, compressive energy and penetration force were measured. Compression was done uniaxially at a crosshead speed and a chart speed of 50 and 100 mm/min, respectively, without having the specimen lubricated.

Compressive force with failure at 90% deformation was used as an index of the cohesiveness of the gel. The 90% deformation was sufficient to cause all samples tested in this study to rupture. At the same time, the amount of moisture expressed upon compression was measured by collecting the fluid on filter paper and recorded in terms of % expressible moisture on a sample moisture weight basis. The compressive energy (area of 2nd and 3rd compression peaks, Kg-mm) was measured as an index of chewiness during three repeated compressions at 90% deformation using a 10 cm dia compression head. Penetration force at 90% deformation was measured as an index of rigidity by using a plunger of 9.5 mm diameter.

Light microscopic study

For examination of surimi gels with a light microscope, small gel blocks (0.5 cm cubes) were frozen in liquid nitrogen and sectioned into 10-12 μm with a cryomicrotome (Model 3398, Damon/IEC Division, Needham Hts., MA). Prepared sections were mounted on slides by touching the sections with a slide at room temperature. In this manner, the cold sections freely adhered to the surface of the slide. They were then dehydrated by first dipping the specimen in 50% ethanol for 5 min and then in 70% ethanol for 5 min. The protein was stained with 0.1% Eosin Y in 70% ethanol (Humason, 1967) for 10 min. and the excess stain was rinsed off first with 70%, then with 50% ethanol and finally with water. Starch was stained by transferring the specimen while wet with water into the iodine staining dish containing finely ground iodine crystals and anhydrous $CaSO_4$, covered with a watch glass. Iodine vapor method was based on that used by Little (1957). When thoroughly dry, the slide was placed in xylene for 5 min and mounted in Cytoseal (Thomas Scientific, Swedesboro, NJ). The prepared specimens were examined with an Olympus microscope (Model CHBS, Olympus Optical Co., LTD., Japan).

For examination of starch gel, 15% potato starch slurry in distilled water (W/V) was cooked at 90 C for 40 min and placed at room temperature overnight and prepared in the same manner as surimi gels for a light microscopic study.

Image Analysis

A Hipad Digitizer (Houston Instrument, Austin, TX) connected to an IBM computer (Model 5160, IBM computer Inc., Armonk, NY) was used to measure volume fractions of starch granules in fish protein before and after cooking. The average area of the field examined was 0.25 mm^2. The result is an average of 3 replica.

Electron Microscopic Study

Small gel blocks (0.5-1.0mm) were fixed in 2% osmium tetroxide and 0.8% potassium ferricyanide (McDonald, 1984) in 0.1 M TRIS buffer (pH 7.2) for 4 hours at room temperature. The specimens were then block stained with 1% uranyl acetate and 1% DMSO in distilled water for 2 hours at room temperature, dehydrated in a series of increasing ethanol concentrations, infiltrated with propylene

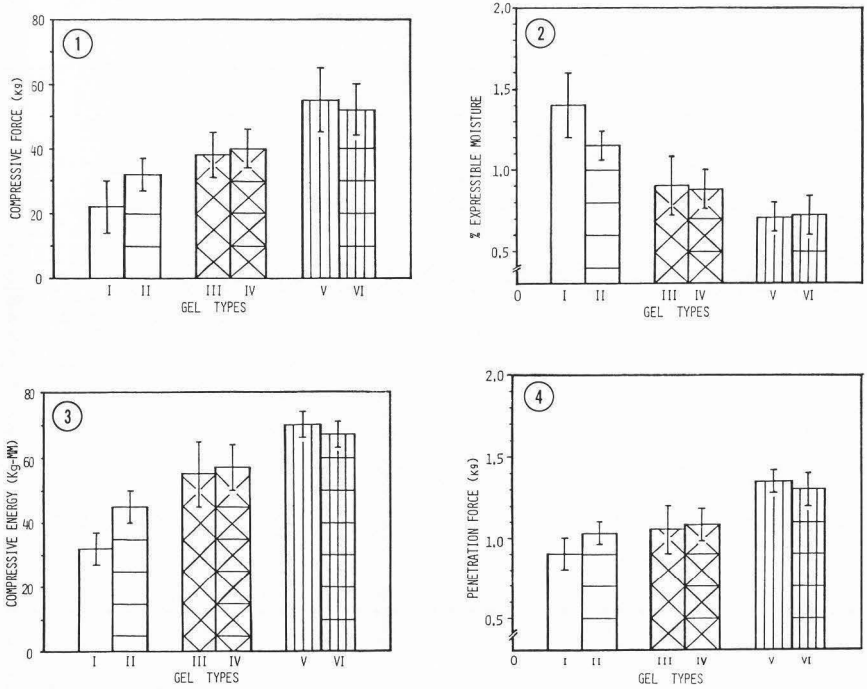

Figures 1 to 4. Effects of 5% starch and heat-setting on - **(Figure 1)** Compressive force of surimi gel; **(Figure 2)** percentage expressible moisture of surimi gel; **(Figure 3)** compressive energy of surimi gel; and **(Figure 4)** on penetration force of surimi gel.

oxide and embedded in Araldite 506 mixture (Luft, 1961). Sections of 60-90 nm thickness were mounted on carbon grids previously coated with parlodion, and stained with 2% uranyl acetate in 50% ethanol for 30 min. They were then treated with Reynold's lead citrate solution (Reynold, 1963) for 5 min., and rinsed with 0.02 N NaOH and with distilled water. The prepared specimens were examined with a JEOL 1200-EX electron microscope at 80 kV.

Statistical Analysis

Analysis of variance performed by the Statistical Analysis System (SAS, 1982) was used to determine differences in the physical properties among surimi gels due to different cooking methods and types of starches incorporated. Duncan's multiple range test (Duncan, 1955) was performed to determine the significance of the mean separation at 5% significance level.

Results and Discussion

Gel strengthening ability varies from starch to starch (Kim and Lee, 1987). In this experiment potato and wheat starches were used because they are most commonly used in commercial products. The textural properties, compressive force, % expressible moisture, compressive energy and penetration force of six different surimi gels are shown in Figs. 1 - 4, respectively.

Gels prepared with heat-setting (Type II) exhibited significantly ($P<0.01$) higher compressive force, water holding ability (lower % expressible moisture) and penetration force than those prepared without heat-setting (Type I) when starch was not incorporated. The structure of a protein gel matrix of Type II (Fig. 5b) was more uniform than that of Type I (Fig. 5a). Many areas of aggregated material were observed throughout the latter protein gel (Type I). These observed structural differences in the protein gels were reflected by the differences in gel strength (Figs. 1, 3 and 4) and water holding ability (Fig. 2).

Trends for all textural parameters of the gels prepared with wheat starch were similar to those of the gels prepared without starch, with no significant difference between the gels prepared with (Type IV)

TABLE 2 - Size of starch granules before and aftercooking of surimi paste

Types of starch incorporated	before cooking	After cooking: without heat-setting	After cooking: with heat-setting
wheat	0.29 ± 0.01	3.06 ± 0.24	4.50 ± 0.36
potato	2.24 ± 0.15	16.21 ± 2.85	10.69 ± 1.26

Values are mean volume ± S.D. of starch granules in $mm^3 \times 10^{-5}$

and without (Type III) heat-setting prior to cooking (Figs. 1 - 4). However, the gels prepared with potato starch showed an opposite trend in which the gel strength with heat-setting was lower than the one without heat-setting. But no significant difference was found between Type V and VI gels ($P < 0.05$). This may be explained by the fact that: 1) The fish protein starts to set at 40 C, which is substantially lower than the gelatinization temperature of potato starch, which ranges from 56 to 66 C (Leach, 1965) ; 2) The preset protein gel matrix prior to starch gelatinization could restrict the swelling of the starch granules during cooking. Water binding in the protein gel reduced the availability of water for the gelatinization of potato starch more in the protein gel cooked with (Type VI) than that cooked without (Type V) preheat-setting. The above reasoning explains why the gelatinized potato starch granules in the Type VI gel were slightly smaller than those in the Type V gel (Table 1). Accordingly, the Type VI gel had a slightly lower gel strength than did the Type V gel (Figs. 1 - 4). In contrast, the swelling power, water holding ability and solubility of wheat starch are much lower than those of potato starch (Leach, 1965). Therefore, the gelatinization of wheat starch during preheat-setting was not affected as much as that of potato starch by the amount of moisture held in the protein gel matrix. This was evidenced by the fact that the gelatinized wheat starch granules in the Type IV gel were slightly larger than those in the Type III gel. This also reflected the difference in gel strength between the Type III and Type IV gels, where the Type IV gel showed a slightly higher gel strength than the Type III gel. As mentioned above, the swelling power of starch plays an important role in the strengthening of a surimi gel. Wheat starch granules expanded an average of 10.5 times (average volume increase: 2.8 $mm^3 \times 10^{-5}$) after cooking without heat-setting, and an average 15.5 times (average volume increase: 4.2 $mm^3 \times 10^{-5}$) after cooking with heat-setting (Table 2). In contrast, potato starch granules expanded an average of 7.2 times (average volume increase: 14.0 $mm^3 \times 10^{-5}$) after cooking without heat-setting, and an average of 5 times (average volume increase: 8.5 $mm^3 \times 10^{-5}$) after cooking with heat-setting. This indicates that potato starch had a greater swelling power than wheat starch and explains the greater gel strengthening ability of potato starch (Figs. 1 - 4).

Before cooking, the compact amylose and amylopectin fractions in the intact wheat (Fig. 6a) and potato (Fig. 7a) starch granules in the surimi paste were dark blue-black and demonstrated their characteristic birefringence in polarized light (Figs. 6b and 7b). After cooking, the loosely arranged amylose fraction was light blue-black due to the swelling of the starch granules, while a small portion of the intact amylose fraction was dark blue-black in Figs. 8a, 8b, 9a and 9b (The red background is fish protein gel stained by Eosin Y). Based on the studies reported by Yamaguchi et al. (1979), and Christianson et al. (1982), most of amylopectin was assumed to remain in the gelatinized starch at the temperature used for cooking in this experiment. According to Rundle et al. (1944), the amylopectin forms an unstable red-purple complex with iodine. However, the complex is not seen in these figures because the amylose fraction stained by iodine covers the red amylopectin-iodine complex. Figs. 8 and 9 show that gelatinization of starch in starch-fish protein system is restricted due to the limited water, resulting from the competition of water between starch and protein systems during cooking. In contrast, starch granules in starch-water system cooked at 90 C for 40 min lost their shape completely and fused and adhered to one another (Fig. 10).

Figure 5. Surimi gel prepared without starch. (a) Cooked at 90 C for 40 min (Type I); (b) Prepared with heat-setting at 40 C for 30 min prior to cooking in the same manner as Type I (Type II).

Figure 6. Surimi paste with 5% wheat starch. ST: starch granules; FP: fish protein gel. (a) Before cooking; (b) same as Fig. 6a but photographed in polarized light.

Figure 7. Surimi paste prepared with 5% potato starch. ST: starch granules; FP: fish protein. (a) Before cooking; (b) same as Fig. 7a but photographed in polarized light.

Figure 8. Surimi gel prepared with 5% wheat starch. IA: intact amylose; FP: fish protein. (a) Cooked in the same manner as Type I (Type III); (b) cooked in the same manner as Type II (Type IV).

Figure 9. Surimi gel prepared with 5% potato starch. IA: intact amylose fraction; FP: fish protein. (a) Cooked in the same manner as Type I (Type V); (b) cooked in the same manner as Type II (Type VI).

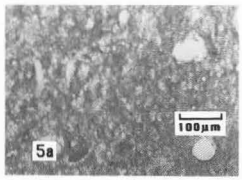
5a
100µm

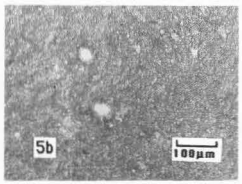
5b
100µm

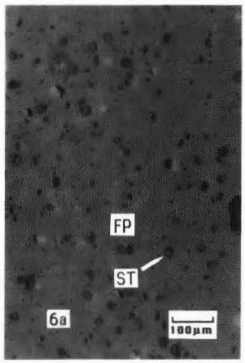
FP
ST
6a
100µm


6b
100µm

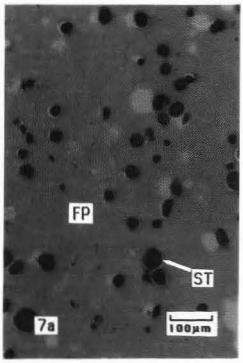
FP
ST
7a
100µm

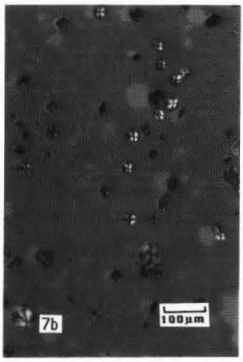
7b
100µm

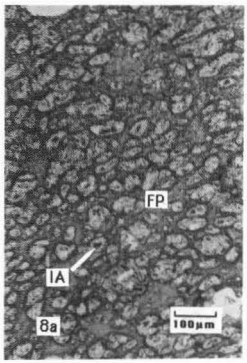
FP
IA
8a
100µm

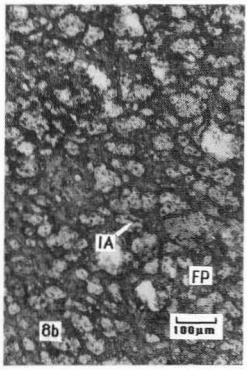
IA
FP
8b
100µm

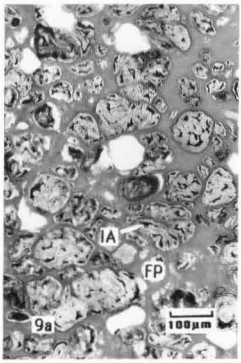
IA
FP
9a
100µm

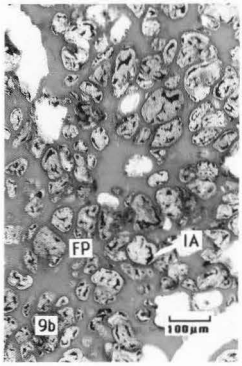
FP
IA
9b
100µm

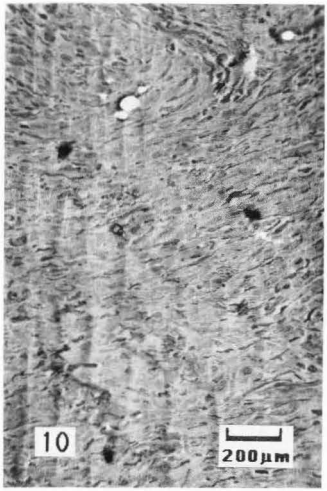

Figure 10. Potato starch gel (15% potato starch suspended in distilled water, W/V, was cooked at 90 C for 40 min and placed at room temperature overnight before the preparation in the same manner as for surimi gels for light microscopic study

Figure 11. Transmission electron micrographs of surimi gel. (a) Surimi Type I gel; (b) Surimi Type II gel; (c) Surimi Type III gel; (d) Surimi Type V gel.

The same result was previously observed after cooking at 80 C for 75 min. using a scanning electron microscope (Christianson et al., 1982).

The textural properties of gels determined by an Instron testing machine and the gross microstructure observed by light microscopy correlated with the fine microstructure of the gel examined by transmission electron microscopy. The following explanation for the composite reinforcing mechanism of starch in surimi gels has been proposed. The starch granules embedded in the protein gel absorb water from the matrix and push the matrix as they swell during cooking, and cause it to become more compact. This process has been visualized in the electron micrographs (Figs. 11a - 11d). The fine structure of surimi gels studied by a transmission electron microscope clarified the network structure which is composed of myofilaments and other protein components in myofibrils, and correlated gel strength with the network structure. The matrix with network structures of single myofilament and bundles of irregularly arranged filaments are seen to be random-

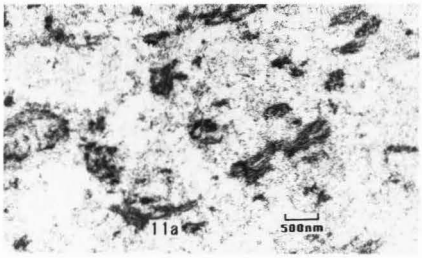

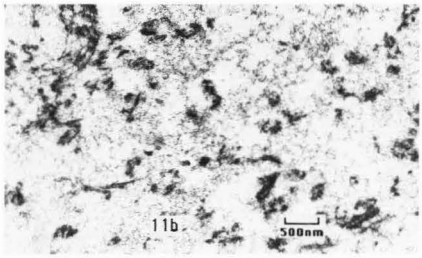

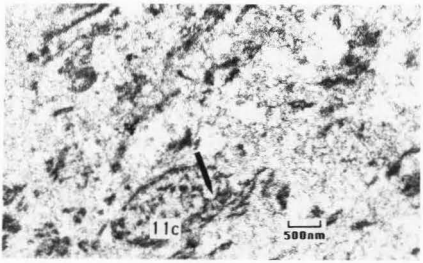

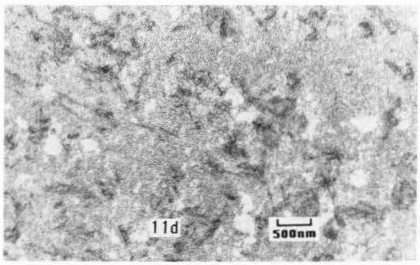

ly dispersed in all figures. Collagen-like dark objects (arrow) are illustrated in Fig. 11c. Some correlation was found between the microstructure profiles and gel strength. Gel strength increased with increased uniformity of the dispersed phase in the gel. This result was consistent with previous reports (Miyake, 1965; Miyake et al., 1971; Sato et al., 1984).

There seemed to be no significant difference in the uniformity of the dispersed phase between Type I (Fig. 11a) and Type II (Fig. 11b) gels. The differences in gel strength and water holding ability between these two gel types (Figs. 1 - 4) were attributed to the uniformity of the protein gel as mentioned earlier (Figs. 5a and 5b). The gel prepared with potato starch (Type V) (Fig. 11d) had a more uniform matrix distribution of the randomly dispersed phase than the gel prepared with wheat starch (Type III) (Fig. 11c). This resulted from the fact that potato starch increased in volume more than wheat starch (Table 2). In other words, potato starch produced less agglomerated protein gel matrix, and accordingly, a greater gel strength and water holding ability (Figs. 1 - 4) than wheat starch. Both starch-incorporated gels (Type III and V) had noticeably higher densities of the dispersed phase, which resulted in greater gel strength than the gels prepared without starch (Type I and II). Therefore, it can be concluded from these results that the presence or absence of starch and the type of starch clearly influence the density of the gel matrix and the gel strength.

Acknowledgements

This work was supported by Rhode Island Agricultural Experiment Station (Contribution Number 2335) and partly by the office of Sea Grant, NOAA, U.S. Department of Commerce under No. NA 81AA-D-00073. The authors would like to thank ICI America and Pfizer Chemicals as well as Henkel Corporation and National Starch Company for providing sorbitol and starch samples. The use of trade names in this publication does not imply endorsement of the products named.

References

Christianson DD, Baker FL, Loffredo AR, Bagley EB. (1982). Correlation of microscopic structure of corn starch granules with rheological properties of cooked pastes. Food Microstruct. 1, 13-24.

Duncan DB. (1955). Multiple range and multiple F tests. Biometrics, 11, 1-42.

Humason GL. (1967). Animal Tissue Technology, 2nd ed. W.H. Freeman and Company, San Francisco, 141-142.

Kim JM, Lee CM. (1987). Effect of starch on textural properties of surimi gel. J. Food Sci. 52(3), 722-725.

Leach HW. (1965). Gelatinization of starch. In: Starch: Chemistry and Technology, Vol 1, RL Whistler, EF Paschall (eds.), Academic press, New York, 289-307.

Lee CM. (1984). Surimi process technology. Food Technol. 38(11), 69-80.

Little RR. (1957). Permanent staining with iodine vapor. Stain Technol. 32, 7-9.

Luft JH. (1961). Improvement in epoxy resin embedding methods. J. Biophys. Biochem. Cytol. 9, 409-414.

McDonald K. (1984). Osmium ferricyanide fixation improves micro-filament preservation and membrane visualization in a variety of animal cell types. J. Ultrastruct. Res. 86, 107-118.

Miyake M. (1965). Studies on fish meat jellies (fish sausage) - VI. Electron microscopic observations on muscle destruction during the processing of fish sausage. Bull. Jap. Soc. Sci. Fish. 31, 464-470.

Miyake M, Hayashi K, Tanaka A, Niwa, E. (1971). Studies on fish meat jellies (Kamaboko) - X. Electron microscopic observations on dispersion of myofibrils in Kamaboko. Bull. Japan. Soc. Sci. Fish. 37, 534-539.

Okada M. (1959a). Application of setting phenomenon for improving the quality of kamaboko. Bull. Tokai Reg. Fish. Res. Lab. 24, 67-72.

Okada M. (1959b). Influence of cooking conditions on the jelly strength of kamaboko. Bull. Tokai Reg. Fish. Res. Lab. 24, 73-80.

Okada M, Yamazaki, A. (1957). Enhancing effect of starch on jelly strength of fish meat jelly. 1. Enhancing effect and gelatinization of starch. Bull. Jap. Soc. Sci. Fish. 22, 583-588.

Reynold ES. (1963). The use of lead citrate at high pH as an electron-opaque stain in electron microscopy. J. Cell Biol. 17, 208-212.

Rundle RE, Foster JF, Baldwin RR. (1944). On the nature of the starch-iodine complex. J. Am. Chem. Soc. 66, 2116-2120.

SAS Institute Inc. (1982). SAS User's Guide: Statistics. SAS Institute Inc., Box 8000, Cary, NC.

Sato S, Tsuchiya T, Matsumoto JJ. (1984). Electron microscopic study of fine structure of Kamaboko fish jellies. Bull. Jap. Soc. Sci. Fish. 50, 1869-1876.

Wu MC, Hamann DD, Lanier TC. (1985a). Rheological and calorimetric investigations of starch-fish protein systems during thermal processing. J. Text. Studies. 16, 53-74.

Wu MC, Lanier TC, Hamann DD. (1985b). Thermal transitions of admixed starch/fish protein systems during heating. J. Food Sci. 50(1), 20-25.

Yamaguchi M, Kainuma K, French D. (1979). Electron microscopic observations of waxy maize starch. J. Ultrastruct. 69, 249-261.

Discussion with Reviewers

E.B. Bagley: What is the swelling power you refer to?

Authors: The term swelling power in this paper is neither the degree of hydration nor a rate measure of swelling of the starch granules. It is an index of the increased volume during cooking.

D.D. Christianson: Can you clarify the compression force measurement at 90% deformation in relation to cohesiveness? What if the specimen does not rupture at 90% deformation? What if it ruptures at 30%? What if it does not rupture at all?

Authors: The measurement was made essentially to determine compressive force which results in failure or rupture of the specimen. In our experiment, all gel specimens that we tested ruptured before 90% deformation. Here 90% means that the instrument was set up to compress a specimen uniaxially to 90%. Previously, we observed that some low-moisture gels did not fail at 90% and required 95% deformation.

As the procedure says, we measured a force at failure regardless of the deformation applied. If the rupture occurred at 30%, we would simply measure the force corresponding to 30% deformation as a compressive force. Cohesiveness may be more correctly defined as the extent of deformation at failure, namely, a strain at failure. From our analysis of data, however, the strain at failure was not as discriminative as compressive force. Therefore, we decided to measure the compressive force at failure as an index of cohesiveness.

E.A. Davis: What criteria do the authors use to conclude that Fig. 11c was less dense than Fig. 11d?
Authors: Increased volume of potato starch was much greater than that of wheat starch resulting in greater decrease in the volume of gel matrix. This causes the gel prepared with potato starch to become more compact and consequently, to become less agglomerated and more uniform distribution of the dispersed phase.

D.P. Dylewski: What effect does preparing the various gels for TEM analysis (e.g., hydration, fixation, dehydration, ETOH) have on the density of the gel matrix?
Authors: Fish protein examined in this study has been solubilized while chopping with 2.5% salt and denatured by cooking (i.e., fixed). Therefore, little change in dimensions of protein gel matrix can be expected during dehydration with increasing concentrations of ethanol in the preparation. The protein gel was infiltrated with a liquid Araldite mixture embedding medium and polymerized to produce a solid plastic block. This block was, then, cut into thin sections. Therefore, the density of the gel matrix in the sections are not affected by hydration during staining.

T.C. Lanier: How can you be sure that an amylopectin-iodine complex has formed, if you cannot see it?
Authors: It has been reported that iodine molecules form a complex with amylose and amylopectin in a parallel orientation within the interior polar field of the helix of starch molecule: a stable blue complex with amylose and the less stable, red complex with amylopectin due to the short length of the branches. This unstable red complex was covered by the blue complex and cannot be seen in this preparation.

T.C. Lanier: What is the "dispersed phase" you refer to?
Authors: Preparation of surimi and heat-induced surimi gel involves a vigorous chopping process. Consequently, most of the myofilaments are chopped and fragmented, and dispersed in the gel.

FOOD MICROSTRUCTURE, Vol. 6 (1987), pp. 91-102
Scanning Microscopy International, Chicago (AMF O'Hare) , IL 60666 USA

SEED MICROSTRUCTURE AND ITS RELATIONSHIP TO WATER UPTAKE IN ISOGENIC LINES AND A CULTIVAR OF DRY BEANS (Phaseolus vulgaris L.)

George N. Agbo[1], George L. Hosfield[2], Mark A. Uebersax[1], Karen Klomparens[3]

[1]Department of Food Science and Human Nutrition
[2]Agricultural Research Service, USDA, Department of Crop and Soil Sciences
[3]Department of Botany and Plant Pathology and Entomology
Michigan State University, East Lansing, MI 48824

Abstract

Comparisons using scanning electron microscopy (SEM) were made among seeds of the isogenic bean strains, 'Nep-2' and 'San Fernando' and 'Sanilac', a navy bean cultivar, to ascertain interrelationships between seed microstructure and water absorption characteristics. During a 90 min soaking period 1:1 (v/v) tap and distilled water, 'San Fernando' hydrated at the slowest rate and imbibed water at only 60% and 78% of the percentages of water imbibed by 'Sanilac' and 'Nep-2', respectively. Among the three bean genotypes, 'Sanilac' hydrated the most rapidly and imbibed the most water (52.9%). 'Nep-2' was intermediate between 'Sanilac' and 'San Fernando' for water imbibition. The interpretation of SEM micrographs for 'Sanilac', 'Nep-2' and 'San Fernando' provided evidence for an association between microstructure and the water imbibition patterns observed. 'Sanilac' had an open and heart-shaped micropyle and prominent seed coat pores. The quality of these structures as observed by SEM favored rapid water uptake by 'Sanilac'. On the other hand, 'San Fernando' had an occluded micropyle and lacked seed coat pores. 'Nep-2' had a partially opened micropyle and a few prominent seed coat pores. The seed coat palisade cell layer was thicker in 'San Fernando' than the palisade layer thickness in the other two genotypes. Starch granules in 'San Fernando' viewed from SEM cross sections of cotyledons appeared smaller and more tightly enveloped by the protein matrix than the starch granules for 'Nep-2' or 'Sanilac'. 'Nep-2' tended to resemble a "hybrid" between 'San Fernando' and 'Sanilac' for microstructure of the seed. The microstructural differences observed between 'San Fernando' and 'Nep-2' are associated with the mutational induction of white seed coat ('Nep-2') by treating black seeds of 'San Fernando' with ethyl methane sulfonate. Manifold effects associated with an alternate state (e.g., white) of the major seed coat color locus in otherwise isogenic strains of beans are due to genetic linkage or pleiotropy.

Initial paper received October 31, 1986
Manuscript received February 26, 1987
Direct inquiries to G.L. Hosfield
Telephone number: 517 355 0110

Key Words: Seed coat, cotyledon, micropyle, hilum, scanning electron microscopy, cooking quality, plant breeding, 'Sanilac', 'Nep-2', 'San Fernando', genetic linkage, pleiotropy.

Introduction

Most plant seeds contain a relatively low water content when harvested. While this low moisture condition enables seeds to be stored for relatively long periods of time and still remain viable, seeds need to take up considerable amounts of water before germination can occur.

In addition to the requirement of water to germinate, seeds of grain legumes used for human food require hydration to prepare the seeds for cooking and eating. The imbibition of water by bean seeds during soaking leads to the softening of the seed coat and cotyledon because of cellular expansion (Deshpande, et al., 1983). Water in the seed also plays an important role in chemical reactions, heat transfer, and chemical transformations such as protein denaturation and starch gelatinization important in the cooking process (Davis and Gordon, 1982).

In dry edible beans (Phaseolus vulgaris L.), rapid water uptake in seeds is an important factor to the processing industry (Hoff and Nelson, 1965). Beans that do not hydrate properly during processing generally are of low textural quality (Morris et al., 1950). Beans prepared by traditional methods as in open kettles are generally soaked before cooking to decrease cooking time and eliminate toxic factors contained in the raw seed (Liener, 1962; Kakade and Evans, 1966).

It has long been known that dry beans differ in ability to imbibe water. Gloyer (1921) described two conditions in which beans failed to hydrate and remained dormant. One kind of failure of water imbibition called "hardshell" was due to the impermeability of the seed coat to water. The second condition of dormancy in bean seeds referred to as sclerema (Gloyer, 1921) was due to the inability of the cotyledon to take up water and expand. Snyder (1936) confirmed the condition of sclerema and observed beans that would not imbibe water even though the seed coat was scarified or removed.

Swanson et al. (1985) reviewed the literature of water imbibition in grain legume seeds and reported that seed coat and cotyledon microstructure appeared to be factors in water imbibition. Powrie et al. (1960) indicated that for dry beans of the navy commercial class, water migrated through the seed coat and hydrated the cotyledons during soaking. Water movement through seed coats was later addressed by Adams and Bedford (1973) who reported that a well-hydrated bean seed coat admitted water freely to the cotyledons resulting in softening of the whole seed. On the other hand, Snyder (1936)

showed for some beans other than "navies," the entrance of water at room temperature was largely through the micropyle and germinal area with little water entry occurring through the seed coat. Kyle and Randall (1963) reported that the micropyle was the principal area of water entry in Great Northern beans while the raphe and hilum areas freely admitted water in red Mexican beans. Korban et al. (1981a) studied sites of water entry among dry bean cultivars of diverse origin and concluded that little or no water uptake occurred through the seed coat. Adams and Bedford (1973) concluded that the hilum and micropylar areas usually admit water readily in beans, but, depending on the cultivar, seed coats differed strikingly for water absorption. Water absorption characteristics were shown to influence the textural characteristics of soaked legume seeds (Sefa-Dedeh and Stanley, 1979); hence, suggesting that microstructure of the seeds was important to water imbibition and movement throughout seed tissues.

Work by Hosfield and Uebersax (1980) showed 'San Fernando', a tropical black seeded dry bean genotype, and 'Nep-2', a white seed coat mutant derived from 'San Fernando' by ethyl methane sulfonate (EMS) treatment (Moh, 1971), differed strikingly in textural characteristics after cooking. The textural differences were of particular interest because both bean strains should be identical genetically except for the single gene determining seed coat color (Moh, 1971). Further examination of the bean genotypes revealed differences in water absorbing capacity (Agbo, 1982) and several physical-chemical traits related to culinary quality (Agbo, 1982; Wassimi, 1985).

Since water imbibition is a prerequisite to cellular changes in beans during processing and appears to be influenced by seed microstructure, the present study was undertaken. Specific objectives were to: (1) compare the microstructure of 'San Fernando', 'Nep-2', and 'Sanilac', a reference dry bean cultivar; and (2) examine the relationship between microstructure and water absorption rate.

Materials and Methods

'San Fernando', 'Nep-2', and 'Sanilac' dry bean genotypes were used in the study. 'San Fernando' is a black seeded bean of tropical origin. Seeds weigh between 18 to 20 g/100 and are round to ovoid in shape. 'Nep-2' has identical visible seed characteristics to 'San Fernando' except for a white seed coat (Moh, 1971). 'Sanilac' is a white pea bean of the navy commercial class. Seeds weigh between 18 to 20 g/100.

The three genotypes were planted in the nursery at East Lansing, Michigan, in the springs of 1978, 1979, and 1980. In planting the crops, seeds were precision drilled into four row plots that were 4.9 m long and spaced 50.8 cm apart. The experiments were replicated four times. Each year mature plants from 3 m of the middle two rows were harvested and threshed. After threshing the beans, samples were taken and handpicked to remove off-color, cracked, broken, or diseased seeds and sized using a 0.40 x 1.9 cm slotted metal sieve. Seeds were stored at $6^{o} \pm 2^{o}C$ until used.

Water uptake

The water uptake of seeds was determined by soaking 10 g of beans in a 1:1 (v/v) mixture of tap and distilled water at room temperature (ca $22^{o}C$) for 0, 15, 30, 45, 60, 75, and 90 min, followed by draining and blotting dry with a paper towel for 1 min and reweighing. Distilled and tap water were mixed to give a water solution with approximately 100 ppm of Ca^{++}. The increase in weight of the soaked beans was taken as due to water absorption. The initial weight of beans and weight after soaking were used to calculate percent water uptake.

Scanning electron microscopy

Dry and soaked beans were prepared for scanning electron microscope (SEM) examination by freeze-drying in a Virtis Unitrap II model freeze-dryer (Virtis Co., Gardiner, N.Y.). The length of time for lyophylization to occur was 4 to 8 h.

The freeze-dried beans were dry-fractured by hand using a razor blade to expose internal tissues and cells. After fracturing, the beans were mounted fracture side up on stubs with colloidal graphite cement (cathode ray tube coating and manufactured by GC Electronics, Rockford, IL) and sputter coated with approximately a 20 nm layer of gold. The coated samples were viewed with an International Scientific Instruments model Super III scanning electron microscope at an acceleration voltage of 15 kV.

Figure 2. Scanning electron micrographs of dry bean seed coat surfaces. Figs. 2a, b, c = abaxial surfaces (1000 x) of 'Sanilac', 'Nep-2', and 'San Fernando', respectively; orifice is denoted by O. Figs. 2d, e, f = adaxial surfaces (1000 x) of 'Sanilac', 'Nep-2', and 'San Fernando', respectively. The orientation (OR) of the roughened cellular surface as seen in Figs. 2d, e, f is denoted by the direction of the arrows.

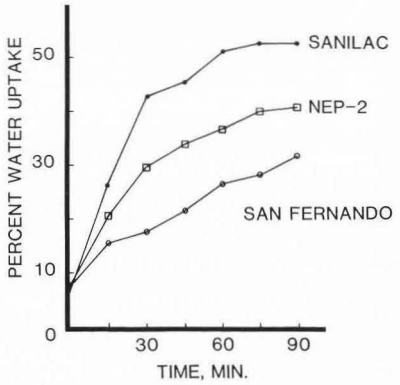

Figure 1. Mean water uptake of seeds of 'Sanilac', 'Nep-2', and 'San Fernando' at $22^{o}C$ and averaged over three growing seasons. Each mark is the average of nine observations.

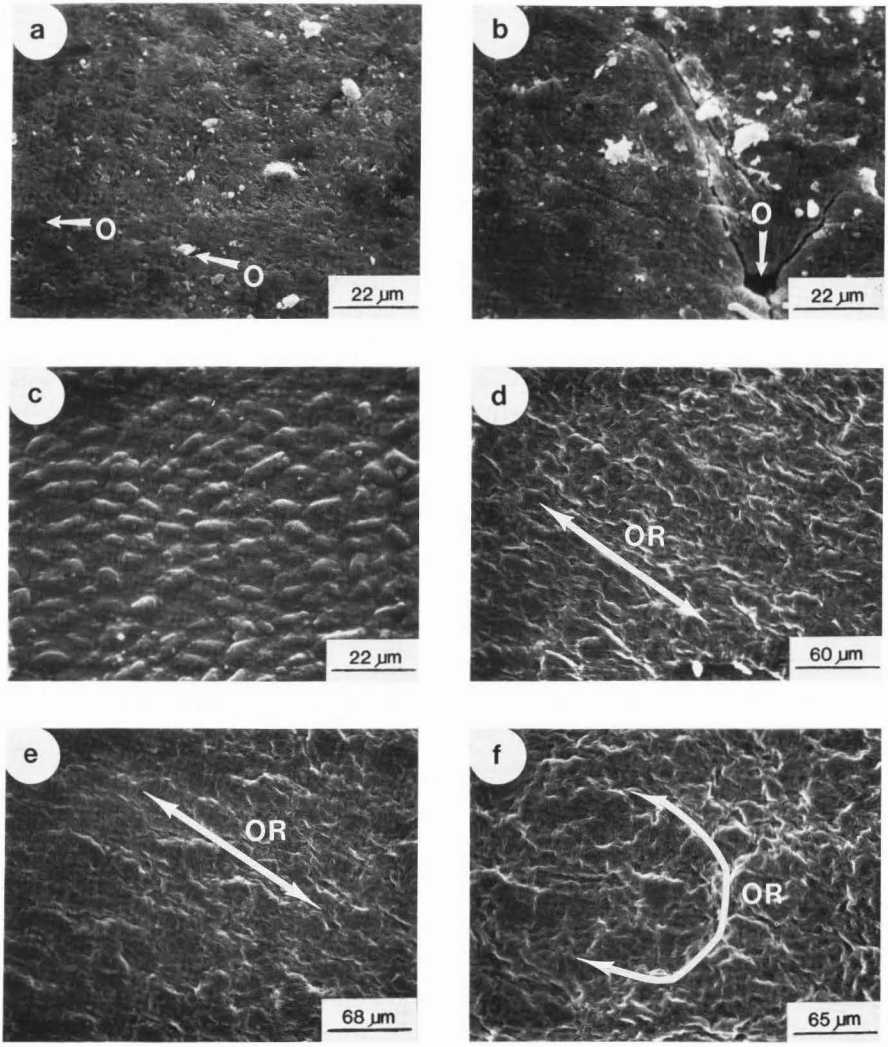
a
O
O
22 µm
b
O
22 µm
c
22 µm
d
OR
60 µm
e
OR
68 µm
f
OR
65 µm

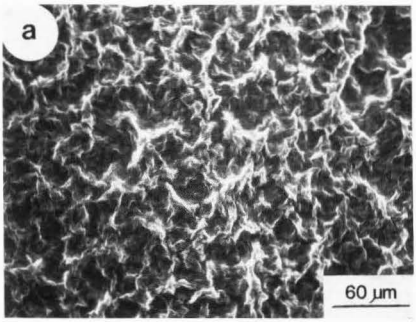

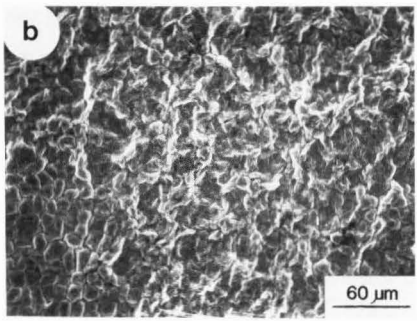

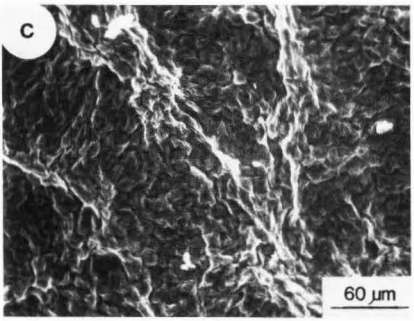

◆**Figure 3.** Scanning electron micrographs of raw bean seed cotyledon abaxial surfaces. Figs. 3a, b, c, show views for 'Sanilac', 'Nep-2', and 'San Fernando', respectively.

Figure 4. Scanning electron micrographs of the hilum, micropyle, and raphe of raw bean seeds. Figs. 4a, b, c show the hilum (H, oval-shaped scar-like structure), micropyle (M), and raphe (HC) for 'Sanilac', 'Nep-2', and 'San Fernando', respectively. Figs. 4d, e, f show the micropyle for 'Sanilac', 'Nep-2', and 'San Fernando', respectively. ➡

Results

'Sanilac' hydrated the fastest and to a greater extent than seeds of the other two genotypes (Fig. 1). During soaking for 90 min, 'San Fernando' imbibed the least amount of water of the three genotypes. Compared to 'Sanilac' and 'San Fernando', 'Nep-2' was intermediate in hydration characteristics.

Scanning electron microscopy of dry seeds

Numerous examinations of seeds of the three genotypes by SEM revealed a similarity in microstructure among the three years. However, fractures were clearly seen on the abaxial and adaxial surface of the cotyledon of 'Nep-2' grown in 1980, but apparently the fractures had little effect on water imbibition. Since differences were absent for seed microstructure among years and the differences observed among genotypes at high magnifications were consistent from year-to-year, the figures presented in this report are representative of the observations seen and photographed.

Examination of seed coat abaxial surfaces of the three genotypes illustrated that 'Sanilac' and 'Nep-2' possessed a rough and irregular cellular surface with occasionally occurring but noticeable structures appearing as pores (Figs. 2a and 2b). The seed coat pores were fewer but larger in size for 'Nep-2' compared to 'Sanilac' with some appearing sunken (Fig. 2b). The seed coat abaxial surface of 'San Fernando' was rough with prominent dimple-like structures arranged in a regular pattern (Fig. 2c). No openings were observed through the 'San Fernando' abaxial seed coat surface.

The micrographs indicated there were marked differences in microstructure among the three genotypes. SEM examination of the seed coat adaxial surface showed mostly an amorphous cellular layer with a roughened surface (Figs. 2d, 2e, and 2f). 'Sanilac' and 'Nep-2' more nearly resembled each other for microstructure of the adaxial seed coat surface than they resembled 'San Fernando'. This conclusion is supported by the orientation of cells seen in the micrographs (Figs. 2d, 2e, and 2f). For 'Sanilac' and 'Nep-2', the appearance and orientation of the roughened surface structures appeared organized in a linear fashion (Figs. 2d and 2e). On the other hand, 'San Fernando' did not show an orientation and the roughened surface structure appeared random (Fig. 2f).

Seed coats of the three genotypes were removed with a scalpel after soaking for 5 to 10 min in 1:1 (v/v) tap and distilled water held at room temperature (ca 22°C). The seed coat of 'Sanilac' was the easiest to remove but the presence of a membrane that adhered tightly to the cotyledon made removal of the 'Nep-2' and 'San Fernando' seed coat more

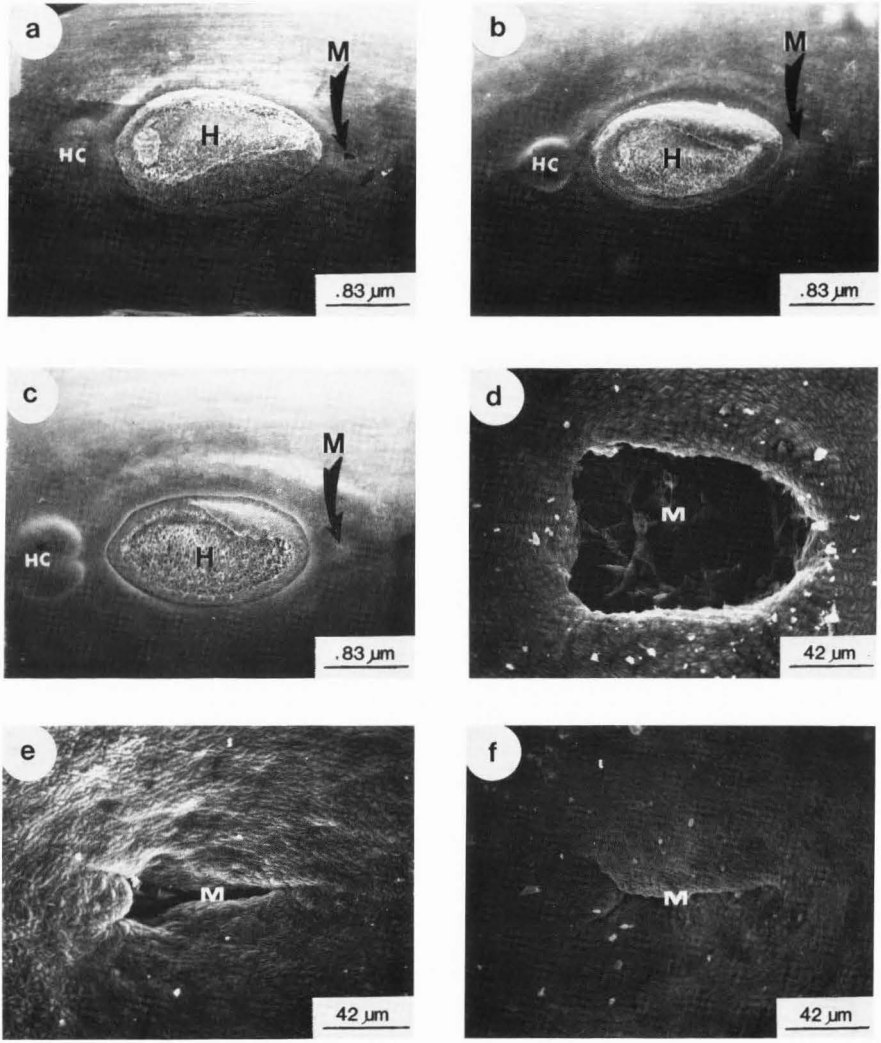
a
M
HC
H
.83 µm
b
M
HC
H
.83 µm
c
M
HC
H
.83 µm
d
M
42 µm
e
M
42 µm
f
M
42 µm

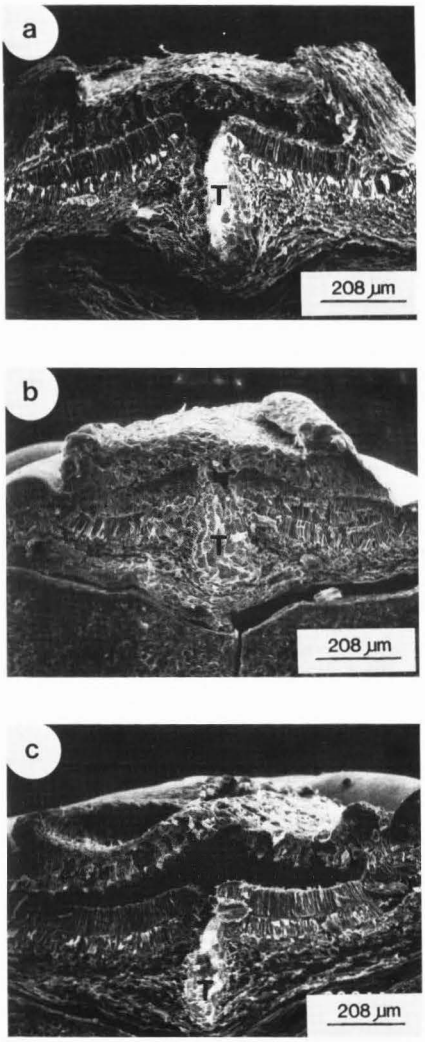

Fig. 5

Figure 5. Scanning electron micrographs of the hilum sectioned transversely for 'Sanilac' (a), 'Nep-2' (b), and 'San Fernando' (c). Tracheids (T) are visible.

Figure 6. Scanning electron micrographs of raw bean seed coats showing palisade (PAL) and hourglass (HGL) cells. Figs. 6a, b, c show transverse cross sectional views of 'Sanilac', 'Nep-2', and 'San Fernando', respectively.

Figure 7. Scanning electron micrographs of raw bean cotyledons showing the adaxial surface. The prominent feature is the bundle-like appearance of cells. Figs. 7a, b, c are for 'Sanilac', 'Nep-2', and 'San Fernando', respectively.

difficult.

A 700 x magnification of the abaxial cotyledonary surface of the three genotypes provided a detailed view of cellular surfaces (Figs. 3a, 3b, and 3c). The abaxial microstructure of the cotyledon was rough in appearance and showed no definite pattern of structures. The abaxial cotyledon surface of 'Sanilac' and 'Nep-2' were more alike in appearance than to the surface appearance of 'San Fernando'. It was interesting that the abaxial cotyledonary surface microstructure of each genotype appeared to complement the respective adaxial surface of the seed coat. The "ridge-like" structures seen for the abaxial cotyledon surface of each genotype (Figs. 3a, 3b, and 3c) appeared to fit into the "valley-like" structures seen for the respective adaxial seed coat surface (Figs. 2d, 2e, and 2f).

SEM of the abaxial surface of the bean seeds revealed the commonly observed anatomical structures of the hilum, micropyle, and raphe (Figs. 4a, 4b, and 4c). At 1000 x magnification, the three genotypes showed variability in size and shape of the micropyle Figs. 4d, 4e, 4f). 'Sanilac' had an open and heart-shaped micropyle with the horizontal dimension slightly larger than the vertical. On the other hand, the 'Nep-2' micropyle was much smaller than 'Sanilac' and the horizontal dimension was much greater than the vertical. The micropyle of 'San Fernando' was nearly occluded and resembled a narrow "y"-shaped opening.

The hilum of each genotype revealed a "spongy-like" amorphous microstructure. SEM at 200 x magnification of the hilum in cross section revealed structural differences among the bean genotypes (Figs. 5a, 5b, and 5c). 'Sanilac' had a flat hilum surface while the hilum surfaces of 'Nep-2' and 'San Fernando' were more elevated. The hilum in each of the three strains consisted of a double layer of macrosclerid (palisade) cells which are seen transversely. Immediately above the upper palisade cell layer were open spaces void of cellular structure. The dimensions of the spaces varied among the bean genotypes. Bisecting the palisade cells and just under the hilum surface layer of cells were tracheids. The tracheids of 'San Fernando' appeared narrower than tracheids for 'Sanilac' and 'Nep-2'.

The SEM of the beans, sectioned transversely, showed the characteristic structural cells of P. vulgaris seed coats. The cuticle can be seen in Figs. 6b, and 6c. Under the cuticle, three distinct cell layers are visible. The uppermost layer of cells are columnar in appearance and consist of palisade cells.

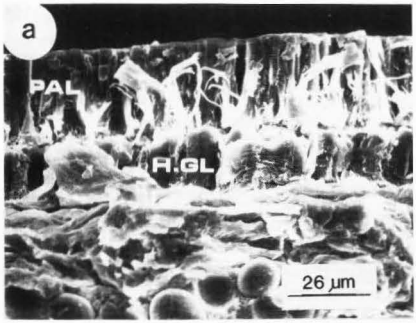
a
PAL
H.GL
26 µm

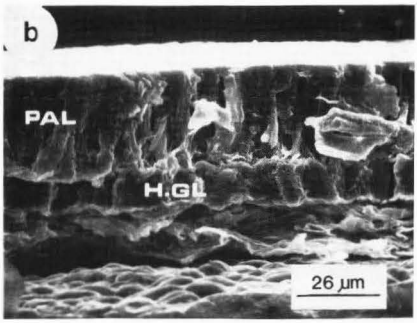
b
PAL
H.GL
26 µm

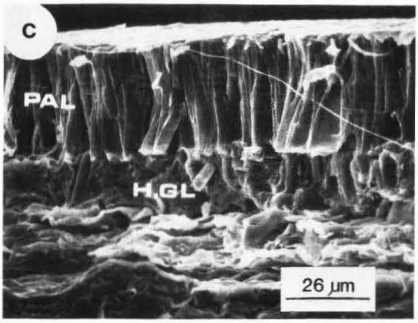
c
PAL
H.GL
26 µm

Fig. 6

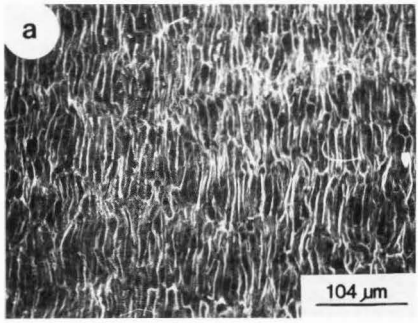
a
104 µm

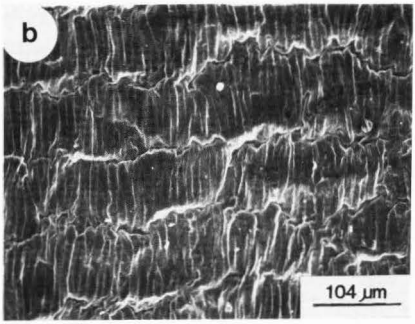
b
104 µm

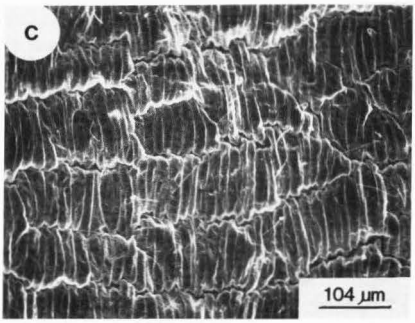
c
104 µm

Fig. 7

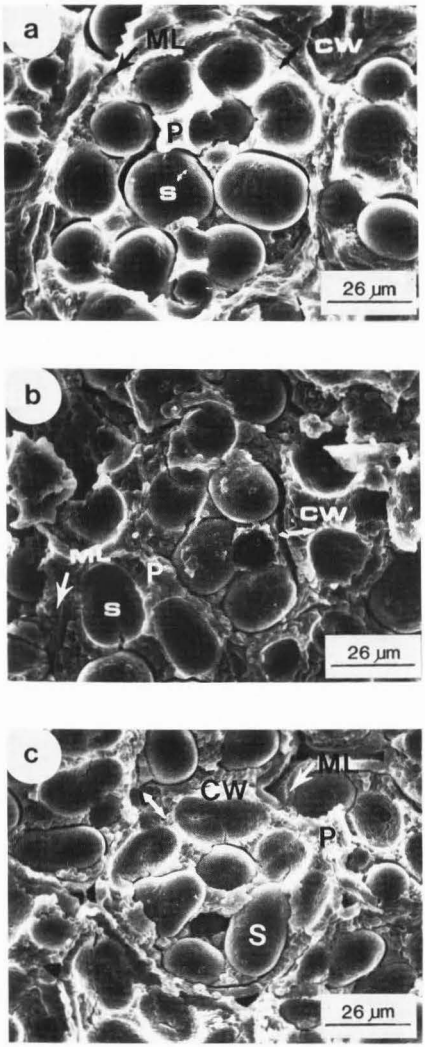

Figure 8. Scanning electron micrographs of raw bean cotyledons magnified 1,600 x. Figs. 8a, b, c, = transverse cross sections of 'Sanilac', 'Nep-2', and 'San Fernando', respectively. The structures identified are cell walls (CW and two-headed arrow) middle lamella (ML), protein bodies (P) and starch granules (S).

No spaces were observed between the cells in this layer. The thickness of the palisade cell layer measured on numerous samples were consistent and about 23 µm, 30 µm, and 32 µm for 'Sanilac', 'Nep-2', and 'San Fernando', respectively. The micrographs showed that the palisade cells of 'Nep-2' and 'San Fernando' were closer to each other in size than to the size of palisade cells of 'Sanilac' (Figs. 6a, 6b, and 6c).

The single layer of osteosclerid (hourglass) cells directly below the palisade cell layer was thinner then the palisade cells. The average hourglass cell layer thickness for 'Sanilac', 'Nep-2', and 'San Fernando' was 21 µm, 17 µm, and 13 µm, respectively. The separation of the seed coat cells from the cotyledon below the spongy parenchymatous layer can be clearly seen for 'Nep-2' and 'San Fernando' (Figs. 6b and 6c). The line of demarcation separating the seed coat from cotyledon for 'Sanilac' is not as apparent as for 'Nep-2' and 'San Fernando' although prominent starch granules are visible for 'Sanilac' (Fig. 6a).

The ultrastructures of the adaxial surface of cotyledons of the three genotypes were also examined. The embryonic axis was prominent and could be distinctly seen. Under 400 x magnification of the cotyledon adaxial surface a well organized layer of cells resembling a sheet of bundles stacked one on top of the other were noted (Figs. 7a, 7b, and 7c). The adaxial surface of the 'Nep-2' and 'San Fernando' cotyledon were similar in structure (Figs. 7b and 7c). Although 'Sanilac's' sheets of bundles were similar in morphology to 'Nep-2' and 'San Fernando', the 'Sanilac' "bundles" appeared thinner and more numerous (Fig. 7a).

SEM of cotyledon cross sections for the three genotypes revealed parenchyma cells of irregular shape; however, the parenchyma cells of 'San Fernando' were more circular in appearance than cells of 'Sanilac' and 'Nep-2' (Fig. 8). Embedded in the parenchyma cells were reserve materials in the form of starch granules. The majority of parenchyma cells examined ranged in length and width from 39 to 94 µm and 30 to 56 µm for 'Sanilac', 63 to 104 µm and 31 to 57 µm for 'Nep-2' and 46 to 68 µm and 29 to 42 µm for 'San Fernando'. A few cells were outside of this range. For example, in observing Fig. 8a, one can see a parenchyma cell of 'Sanilac' with dimensions of approximately 110 x 80 µm. Further SEM work has revealed the relative size of parenchyma cells for the genotypes to be 'Sanilac' $\simeq$ 'Nep-2' > 'San Fernando' (unpublished data). In the present study, the parenchyma cell dimensions of 'Sanilac' and 'Nep-2' were similar; however, 'Sanilac' had more variable dimensions and more irregular shape.

The smaller (length and width dimensions) cotyledon parenchyma cells observed for 'San Fernando' appeared surrounded by a densely appearing cell wall. 'Sanilac' and 'Nep-2' contrasted with 'San Fernando' in this regard and had a thinner

and more loosely appearing structure of parenchyma cell walls.

Starch granules of 'San Fernando' were embedded in a protein matrix and protein bodies (matrix) were seen to envelope the granules, thus, giving a tightly bound appearance (Fig. 8c). Starch granules of 'Sanilac' and 'Nep-2' were also embedded in a protein matrix. Loose granules were observed, but the envelopment of the granules by the protein bodies was not seen for 'Sanilac' and 'Nep-2' to the same extent as observed for 'San Fernando'.

Starch granules were mostly globoid; however, a few had irregular shapes. Starch granule dimensions along the longitudinal axis ranged from 16 to 29 μm, 11 to 30 μm, and 12 to 30 μm for 'Sanilac', 'Nep-2', and 'San Fernando', respectively.

Discussion

Seeds of the three dry bean genotypes as viewed by SEM had highly organized structures in seed coats and cotyledons. The structures have been observed in other food legumes (Sefa-Dedeh, 1978; Sefa-Dedeh and Stanley, 1979). The residual membrane attachment between the seed coat and cotyledon persisted even after complete removal of the seed coat. Visual observations indicated that the membrane was larger for 'San Fernando' than 'Nep-2'. Korban et al. (1981b) had difficulty removing the seed coat from seeds of a Great Northern bean cultivar because of the presence of a membrane. The double layer of hilum palisade cells, as seen in transverse cross sections of seeds, are similar to those found in soybean (Glycine max Merr., Kondo, 1913; Wolf and Baker, 1972). In legume seed coats, the cells immediately beneath the palisade layer are the hourglass cells (Corner, 1951; Sefa-Dedeh, 1978). Corner (1951) observed spaces between the hourglass cells in some legumes. We did not observe spaces in the present investigation. Our results agree with the dry bean SEM studies conducted by Swanson et al. (1985).

The palisade and hourglass cell layers of the three genotypes were measured, and the dimensions were similar to those reported by Swanson et al. (1985). In addition, there were differences noted among genotypes for the thickness of palisade and hourglass cell layers affirming the presence of phenotypic variability for cell layer thickness. Korban et al. (1981b) showed differences among diverse bean genotypes for the thickness of macrosclerid, osteosclerid, and parenchyma cell layers. In this experiment the ratios of palisade to hourglass cell layer thicknesses were 1.1, 1.8, and 2.5 for 'Sanilac', 'Nep-2', and 'San Fernando', respectively. It was interesting that the palisade to hourglass cell layer thickness for 'Nep-2' was about the same as the average of the respective layers for 'Sanilac' plus 'San Fernando' indicating that the ratio of cell layer thickness for 'Nep-2' lay midway between the cell layer thickness ratio of the other two genotypes.

Although the thickness of the palisade and hourglass cell layers varied among the three genotypes, the combined dimensions of the layers were 45 μm, 47 μm, and 45 μm for 'Sanilac', 'Nep-2', and 'San Fernando', respectively. Hence, the vertical space occupied by these cell layers were essentially the same in all three genotypes. Below the hourglass cells was the amorphous layer of parenchyma cells (Figs. 6a, 6b, and 6c) where the greatest swelling of bean seed coats during soaking occurs (Swanson et al., 1985).

Some aspects of bean seed anatomy may have regulated water imbibition and thus, may partly explain the soaking characteristics of the three genotypes (Fig. 1). For example, features of 'San Fernando's' microstructure suggested that this genotypes had a higher resistance to water uptake than the water uptake resistance of 'Sanilac' and 'Nep-2'. 'San Fernando' had an occluded micropyle (Fig. 4f) which Agbo (1982) suggested acted as a barrier to water uptake; his theory is supported by bean seed water entry and rate of water uptake studies (Kyle and Randall, 1963; and Korban et al., 1981a). Apparently, the hilum and micropyle, and raphe, to a lesser extent, function as the primary orifices for water entry into seeds of most dry beans (Kyle and Randall, 1963; Korban et al., 1981a; and Agbo, 1982). Although water uptake may occur through seed coat pores, this mechanism of water entry appears mainly a feature of white seeded beans of the navy commercial class (Powrie et al., 1960; Adams and Bedford, 1973). The presence of seed coat pores (Fig. 2a) and the prominent and open micropyle (Fig. 4d) noted for 'Sanilac' favored a more rapid water imbibition than water imbibition for 'San Fernando' or 'Nep-2'.

The thickness of seed coat palisade cell layers may have regulated the movement of water into the seed. Since 'San Fernando' had the thickest palisade cell layer and the slowest rate of water uptake during soaking (Fig. 1), it is implied that a slow hydration of the seed coat occurred which led to the slow hydration of seed cotyledonary structures. The effect on water movement of the sheet of cells resembling bundles observed on the adaxial cotyledon surface is not known (Figs. 7a, 7b, and 7c). The cell bundles may act as a barrier to the rapid migration of water throughout the cotyledon and, thus, regulate water uptake by the parenchyma cells.

Swanson et al. (1985) reported that 'San Fernando' had, on the average, smaller starch granules than 'Nep-2'. The smaller sized granules found in this study for 'San Fernando' suggested that 'San Fernando' had more densely packed structures than 'Sanilac' and 'Nep-2'. The envelopment of 'San Fernando' granules by a tough protein layer may have caused starches to hydrate to a lesser degree during soaking than the starches hydrated for the other two bean genotypes. Since 'Nep-2' was intermediate to 'Sanilac' and 'San Fernando' for the rate of water uptake, 'Nep-2's' resemblance to 'Sanilac' for the abaxial cotyledon surface (Figs. 3a, 3b) and 'San Fernando' for the adaxial surface (Figs. 7b, 7c) and micropyle appearance relative to the other two genotypes may partly explain the pattern of water imbibition observed.

The findings from the current study should be of interest to plant breeders, seedspersons, and bean processors who develop, market, and purchase dry beans. The bean industry requires cultivars that imbibe water readily and are free from hydration defects. Additional research is required to ascertain which soaking features, and to what degree, may be associated with the variable processing quality noted for the three bean genotypes. Of particular interest is the fact that 'Nep-2' was derived from 'San Fernando' as an EMS mutant supposedly involving a

single Mendelian factor affecting only white and black seed coat color (Moh, 1971). Yet, 'San Fernando' and 'Nep-2' differed markedly in water uptake and seed microstructure. "Qualitative" genes of classical Mendelian genetics may have more than a single phenotypic manifestation and, thus, show secondary effects. The secondary effects of the seed coat color genes that separate 'San Fernando' and 'Nep-2' grown in the same environment are due to genetic linkages or pleiotropy.

The current research could not distinguish between linkage effects and pleiotropy. Yet being able to make such a distinction could be of crucial importance to a breeder. Undesirable linkages can be separated through the use of breeding techniques that permit genetic recombination. On the other hand, pleiotropy is unpredictable, and undesirable pleiotropic effects cannot be separated from the major gene to which the effects are associated. When unfavorable gene side effects arise because of pleiotropy, the major genes exhibiting the unfavorable effects must be excluded from breeding programs.

Conclusions

Beans with black and colored seed coats are superior in disease resistance and yield to white seeded types (Moh, 1971; Deakin, 1974), but white seeded beans often command a higher price. Through the use of mutation breeding, white-seeded cultivars can be developed in a shorter time than by the conventional hybridization method followed by several years of selection and testing. Manifold effects associated with mutation breeding when the locus for a major gene is changed to an alternate state (for example, black to white seed coat) are generally ascribed to pleiotropy although linkage cannot be ruled out. If pleiotropy is at the root of the differences in seed coat and cotyledon characteristics between 'San Fernando' and 'Nep-2', mutation breeding in beans using EMS to develop white seeded strains from black or colored seeded types should proceed with caution. The outcome of such breeding programs in terms of seed characters important to consumer and processor quality may be unpredictable with pleiotropy. However, there is no indication to date that 'San Fernando' and 'Nep-2' differ in yielding ability and other favorable agronomic characteristics.

Acknowledgements

Part of a thesis submitted by the senior author (GA) in partial fulfillment of the requirements for the Ph.D. degree at Michigan State University. Approved for publication by the Michigan Agr. Expt. Sta. as Journal Article no. 12135. Partial financial support for this research was provided by a USAID Title XII Dry Bean/Cowpea CRSP.

General Material Disclaimer

Mention of a trade name, proprietary product or specific equipment does not constitute a guarantee or warranty by the U.S. Department of Agriculture and does not imply its approval to the exclusion of other products that may be suitable.

References

Adams MW, Bedford CL (1973) Breeding food legumes for improved processing and consumer acceptance properties. In: Nutritional Improvement of Food Legumes by Breeding (Proc. of a Symp. sponsored by PAG, Rome, July 1972). M. Milner (ed.) Protein Advisory, p. 299-309.

Agbo GN (1982) Genetic, physico-chemical and structural characteristics of dry beans. Ph.D. thesis, Michigan State University, East Lansing, MI.

Corner EJ (1951) The leguminous seed. Phytomorphology 1, 117-150.

Davis EA, Gordon J (1982) Food microstructure: An integrative approach. Food Microstruc. 1, 1-12.

Deakin JR (1974) Association of seed color with emergence and seed yield of snap beans. J. Amer. Soc. Hort. Sci. 99, 110-114.

Deshpande SS, Sathe SK, Salunkhe DK (1983) Dry beans of Phaseolus: A review. Part 3. Processing. CRC Critical Reviews in Food Sci. and Nutr. 21, 137-195.

Gloyer WO (1921) Sclerema and hardshell, two types of hardness of the bean. Proc. Assoc. Offic. Seed Anal. N.A. 13, 60-62.

Hoff JE, Nelson PE (1965) An investigation of accelerated water-uptake in dry pea beans. Purdue Agr. Expt. Sta. Res. Progress Rpt. 211, 13.

Hosfield GL, Uebersax MA (1980). Variability in physico-chemical properties and nutritional components of tropical and domestic dry bean germplasm. J. Amer. Soc. Hort. Sci. 105, 246-252.

Kakade ML, Evans RJ (1966) Effect of soaking and germinating on the nutritive value of navy beans. J. Food Sci. 31, 781-783.

Kondo M (1913) The anatomical structure of some common foreign legumes. Z. Unters. Nahr. U. Gen. Gebrauchsgegenstende. 15, 1-57.

Korban SS, Coyne DP, Weihing JL (1981a) Rate of water uptake and sites of water entry in seeds of different cultivars of dry bean. HortScience 16, 545-546.

Korban SS, Coyne DP, Weihing JL, Hanna MA (1981b) Testing methods, variation, morphological and genetic studies of seed-coat cracking in dry beans (Phaseolus vulgaris L.). J. Amer. Soc. Hort. Sci. 106, 821-828.

Kyle JH, Randall TE (1963) A new concept of the hard seed character in Phaseolus vulgaris L., and its use in breeding and inheritance studies. Proc. Amer. Soc. Hort. Sci. 83, 461-475.

Liener IE (1962) Toxic factors in edible legumes and their elimination. Amer. J. Clin. Nutr. 11, 281-298.

Moh CC (1971) Mutation breeding in seed coat colors of beans (Phaseolus vulgaris L.). Euphytica 20, 119-125.

Morris HJ, Olson RL, Bean RC (1950) Processing quality of varieties and strains of dry beans. Food Technol. 4, 247-251.

Powrie WD, Adams MW, Pflug IJ (1960) Chemical, anatomical and histochemical studies on the navy bean seed. Agron. J. 52, 163-167.

Sefa-Dedeh S (1978) Studies on the microstructure, texture, and proteins of cowpeas (Vigna unguiculata). Ph.D. thesis, Univ. of Guelph, Ontario.

Sefa-Dedeh S, Stanley DW (1979) Textural implications of the microstructure of legumes. Food

Technol. 33, 77-83.

Snyder EB (1936) Some factors affecting the cooking quality of the pea and great northern types of dry beans. Nebraska Agr. Expt. Sta. Res. Bul. 85, 31.

Swanson BG, Hughes JS, Rasmussen HP (1985) Seed microstructure: Review of Water Imbibition in Legumes. Food Microstruc. 4, 115-124.

Wassimi NN (1985) Genetic analyses of cooking times, nutritional and culinary quality in dry beans (Phaseolus vulgaris L.) Ph.D. thesis, Michigan State University, East Lansing, MI.

Wolf WJ, Baker FL (1972) Scanning electron microscopy of soybeans. Cereal Sci. Today 17, 125-130, 147.

Discussion with Reviewers

W.J. Wolf: You call attention to the fact that 'Nep-2' grown in 1980 was fractured. Were hydration properties measured for this lot of seed?
Authors: Fractures were seen on the abaxial and adaxial cotyledon surfaces of 'Nep-2' seed grown in 1980. The hydration properties of these seeds were similar to that shown in Figure 1 for 'Nep-2'. However, water uptake of the 1980 grown seed was more variable than for 'Nep-2' seed grown in 1978 and 1979.

B.G. Swanson: What do you believe is the physiological role of the hilum, micropyle and raphe? How does the physiological role relate to water imbibition in beans?
Authors: Most likely the physiological role of these structures is to facilitate gas exchange between the seed and surrounding environment and permit the entry of water to initiate germination. However, the hilum, micropyle, and raphe may differ in the degree to which they mediate gas exchange and water entry. K. Esau in her book, The Anatomy of Seed Plants, [Esau K (1977), John Wiley and Sons, 2nd Ed.] mentions that the hilum acts like a hydrostatic valve permitting the loss of water vapor from the seed but preventing moisture from entering. According to Corner (1951), cells in the hilum are interrupted along the mid-line by a very fine groove which is an air passage in the ripe seed. Presumably, the orifice-like nature of the hilum permits water to enter the seed when the seed is bathed in an aqueous medium. The water would have to penetrate the double layer of palisade cells and migrate to the parenchymatous cells overlying the cotyledon. The micropyle is an orifice that arises from the former point of entrance of the pollen tube into the ovule. One may envision the micropyle as a structure that permits rapid water entry into the seed. Since the raphe is a remnant of the funiculus, it probably also facilitates the exchange of gases and water between the seed and surrounding environment. Data obtained by several researchers (Snyder, 1936; Powrie et al., 1960; Kyle and Randall, 1963; Adams and Bedford, 1973; Korban et al., 1981a) support the idea that the hilum, micropyle, and raphe are important structures for the entry of water into the bean seed. We agree with the position taken by others regarding the relationship between structural function and water imbibition in beans because studies in our laboratory confirm the previous results.

B.G. Swanson: How do you relate phenotypic variation to differences in microstructure?
Authors: The phenotype of an organism is comprised of a component due to the genotype (assemblage of genes) and the environment (external stimuli). The phenotype is what one observes or to put it in other terms--the phenotype is the entity on which data is taken, measured, etc. Although the phenotype can be measured, the genotypic and environmental components can only be estimated. Only when causal components due to the environment are totally absent, can the genotype be measured, i.e., phenotype = genotype. In this study, 'Sanilac', 'Nep-2', and 'San Fernando' differed for particular aspects of microstructure, hence, the three strains exhibited phenotypic variation. The amount of this variation due to genetic causes and to environmental effects can be estimated from particular mating designs.

B.G. Swanson: How do palisade cell thickness and subepidermal cell thickness relate to water imbibition in beans?
Authors: This is difficult to say since we did not follow the mode of water penetration into beans nor did we attempt to observe structural regulation of imbibition. We did not measure thickness of cells per se in our study, but we determined the thickness of the palisade, hourglass, and parenchymatous cell layers of the bean seed coat. K. Esau (1977) reports that the palisade layer in Phaseolus is casually connected to the high degree of impermeability of hard seeds. From this standpoint, it is tempting to speculate that, in general, the sclerenchymatous palisade cells are less permeable to water movement than parenchymatous (subepidermal) cells that do not contain sclerids. Differential permeability could arise because, within a plant cell, the cell sap (vacuole), protoplasm, and cell wall each impose a diffusion pressure deficit (DPD). Since imbibition is the mass movement of water in response to the DPD in cells, thickening of palisade cells (this is due to the development of secondary walls encrusted with lignin) may lead to a lower cell DPD than the DPD of nonthickened (parenchymatous) cells. The thickness of the cell (palisade and hourglass) layers which we did measure in our study may have been causally related to water imbibition in a physical sense. In order to reach and hydrate the bean cotyledon, water has a greater distance to traverse a thick cell layer than a thin cell layer.

B.G. Swanson: Please define pleiotropy and explain how pleiotropy becomes an insurmountable problem for breeders.
Authors: Pleiotropy is the property of a gene having more than one phenotypic effect on an organism. If the gene with the quality of pleiotropy is segregating, it causes simultaneous variation in the characters it affects. Pleiotropic effects are unpredictable and should the effects be undesirable, they cannot be separated from a gene exhibiting pleiotropy by any known plant breeding strategy. Unpredictability and the inability to remove manifold effects are the qualities that exclude the use of pleiotropic genes by breeders. The failure to remove pleiotropic effects from an organism is an insurmountable breeding problem.

B.G. Swanson: What conclusions do you draw from

your results about water imbibition in 'Sanilac', 'Nep-2', and 'San Fernando' beans? What conclusions can you draw about water imbibition in other beans?
Authors: Beans of the 'Sanilac' variety hydrated the most rapidly and to a greater extent than seeds of the other two genotypes during a 90 minute soaking period. 'San Fernando' imbibed the least amount of water and 'Nep-2' was intermediate to 'Sanilac' and 'San Fernando' in water imbibition. We expected 'Nep-2' to be similar to 'San Fernando' for water imbibition because, presumably, 'Nep-2' and 'San Fernando' differ genetically by only a single Mendelian factor that imparts color to the seed coat. However, after SEM examination, marked structural differences among the three genotypes were noted. Based on previous work, our conclusion is that seed microstructure may be related to the water imbibition patterns observed. Perhaps, the most pronounced differences among the genotypes noted were the micropyle, seed coat, and parenchymatous cells of cotyledons. Since 'Nep-2' was derived from 'San Fernando' via a mutation using EMS, we suspected the gene for white seed coat in 'Nep-2' exhibited pleiotropy. We hoped these conclusions were conveyed lucidly in the text of the paper. We hesitate to make comparisons between our findings and findings in other beans because the genotypic effects in the current study are a fixed quantity. This imposes the restriction that results pertain only to the genetic materials studied. Nevertheless, pleiotropy is a quality of a gene that cannot be ignored. If pleiotropy accompanies an EMS mutation of the major color locus in beans, perhaps, breeders should proceed with caution when using the EMS technology in bean breeding.

FOOD MICROSTRUCTURE, Vol. 6 (1987), pp. 103-113
Scanning Microscopy International, Chicago (AMF O'Hare) , IL 60666 USA

INFLUENCE OF DELIGNIFYING AGENTS ON TISSUE STRUCTURE IN BERMUDAGRASS STEMS

D. E. Akin, L. L. Rigsby, F. E. Barton, II, P. Gelfand, D. S. Himmelsbach, W. R. Windham

Richard B. Russell Agricultural Research Center, ARS-USDA
P.O. Box 5677, Athens, Georgia 30613

Abstract

Permanganate, dioxane, ozone, and hydrogen peroxide, which delignify plant materials, were evaluated for their disruptive action on plant structure, their modification of histological reactions for lignins, and their change in in vitro digestibility by rumen microorganisms of young (second internode from top) and old (fourth and fifth internodes) bermudagrass stems. Epidermis, sclerenchyma ring, and vascular tissue (except phloem) gave positive reactions with acid phloroglucinol (AP) or chlorine-sulfite (CS) in all samples, whereas cortex and parenchyma in older stems gave a positive reaction with CS. Treatment with delignifying agents reduced the reactions for lignin, with permanganate-treated tissues having the least reaction. Gravimetric data indicated that $KMnO_4$ removed about 25% of the dry matter, with the other treatments resulting in no loss with ozone to 34% with hydrogen peroxide. Scanning electron microscopy (SEM) indicated that delignifying agents distorted parenchyma tissues, often resulting in collapsed cell walls. Permanganate especially disrupted parenchyma and the more rigid vascular bundle tissue and caused the most destruction of all the treatments. Ozone was effective in partially breaking down lignified vascular tissue in one sample set but not in a second, more mature set. Delignification resulted in improved in vitro dry matter digestibility by rumen microorganisms for the resultant fiber compared with neutral detergent fiber for all treatments, with permanganate causing the largest increase for both sample sets. SEM showed that chemical treatments improved degradation of the cortex and parenchyma, whereas the epidermis, sclerenchyma ring, and vascular tissue (except phloem) still resisted microbial breakdown.

Initial paper received October 13, 1986
Manuscript received January 12, 1987
Direct inquiries to D.E. Akin
Telephone number: 404 546 3482

Key words: Scanning electron microscopy, Lignin, Bermudagrass stems, Dioxane, Permanganate, Ozone, Peroxide.

Introduction

Electron microscopy has been useful in providing information on plant cell wall degradation by rumen microorganisms from a unique perspective (Akin, 1979; Harbers, 1985). The availabilities of specific tissues in many forages for rumen bacterial fermentation have been elucidated, and anatomical and structural factors which limit microbial degradation have been identified. Scanning electron microscopy (SEM) coupled with light histological techniques have shown that cell walls containing lignin are the least digested tissues in forages. Lignin, a polymer of phenylpropanoid units, is chemically associated with the structural carbohydrates of the plant fiber (Himmelsbach and Barton, 1980) and is recognized as a major limitation to forage utilization (Van Soest, 1973; Waldo et al., 1972).

Lignins vary in type based upon the predominant monomeric unit of the polymer, i.e., p-coumaryl, coniferyl, or syringyl units (Barton et al., 1983). Histochemical tests have also shown differences in types of lignin within cell walls, with the acid phloroglucinol test indicating cinnamaldehyde units and the chlorine-sulfite test indicating syringyl units (Vance et al., 1980).

Stems of grasses decrease in digestibility with increased maturity more than leaf materials (Hanna et al., 1976). Stem anatomy consists of a large proportion of highly lignified and poorly digested tissues, and increased maturity results in even more of the tissues becoming lignified and resisting microbial degradation (Akin et al., 1984; Hanna et al., 1976; Pigden, 1953). The result of increased age is a rigid plant residue in which only a small portion of the parenchyma is digested. It is likely that the rigid stem anatomy in grasses contributes to the lower feed consumption by ruminants generally noted for grasses vs. legumes (Demarquilly and Jarrige, 1974) and for grass stems vs. grass leaves (Laredo and Minson, 1973), possibly by influencing the retention time of undigested fiber in the rumen (Hendricksen et al., 1981). In another study the greatest result of KOH treatment to improve forage utilization was that the parenchyma, which reacts with chlorine-sulfite, was made available for digestion whereas acid phloroglucinol reacting-tissues, although disrupted, were still not available for microbial utilization (Spencer et al., 1984). Similarly, treatment of 100 µm sections of bermudagrass with $KMnO_4$ removed phenolic compounds preferentially from the parenchyma and made this tissue more

available for digestion (Akin et al., 1985). These data indicate that the lignin in parenchyma differs in a significant manner from that in the sclerenchyma ring or vascular tissues, such that the parenchyma cell walls are more susceptible to chemical treatment.

By oxidizing the lignin in cell walls, researchers have been able to make plant fiber more available to microbial fermentation (Barton and Akin, 1977; Ben-Ghedalia and Miron, 1981). However, it is clear that all lignified cell walls are not the same, and information is not available on the effect that oxidizing agents have on specific types of lignified fiber in stem. The influence that delignification has on specific plant structure and on cell wall digestibility by rumen microorganisms is important for developing strategies to improve forage utilization. Therefore, the objective of the present work was to evaluate the response of specific tissues of bermudagrass stems at two maturities to various delignifying agents. The stems were evaluated for the response to histochemical tests, the degree of structural alteration, dry weight loss due to extraction, and the improvement in in vitro degradation by rumen microorganisms.

Materials and Methods

Plant samples

Coastal bermudagrass (Cynodon dactylon) was grown in well managed fields near Athens, Georgia. Experiments were conducted on each of two cuttings (experiments 1 and 2) of six-week-old regrowth material harvested in the summer of 1982. Harvested material was stored at -10°C until used. Procedures and treatments were the same for samples in both experiments except that samples in experiment 1 were not treated with H_2O_2 and samples from experiment 2 were not treated with dioxane.

The second internodes from the top of plants (young internodes) and the combined fourth and fifth internodes (old internodes) were hand-separated from leaf blades and sheaths. For gravimetric studies, each sample of stem material was freeze-dried and ground through a 20 mesh (1mm) screen. For light microscopy, free-hand sections were cut from internodes representing five plants for each experiment. For scanning electron microscopy, 3mm sections were cut from 20 stems.

Histological tests for lignin

Free-hand sections were stained for lignin using the acid phloroglucinol (AP) and the chlorine-sulfite (CS) reactions as described by Jensen (1962), except that 2% Na_2SO_3 was used in the CS reaction. Reactions for lignin were scored as + (positive reaction), or O (no reaction).

Chemical delignification

Neutral detergent fiber (NDF) was prepared from ground or intact sections (3mm) of stem material (Van Soest and Wine, 1967, but without sodium sulfite) for subsequent delignification of plant cell walls. $KMnO_4$ delignification was carried out according to procedures of Van Soest and Wine (1967, 1968) as modified by Barton et al. (1976) and Barton and Akin (1977). Ground stems or intact sections of NDF material were extracted with neutral $KMnO_4$ for 3 h and demineralized with buffered oxalic acid in t-butanol for 1.5 h. The stem materials were washed with water and 80% ethanol and acetone 3 times each. The ground material was dried at 105°C overnight and the sections were air-dried at 28 mm Hg.

Dioxane delignification was carried out on 5 g of ground stems or 25 intact sections of NDF. Samples were preextracted with a benzene-ethanol (2.5:1 v/v) mixture at 39°C for 48 h to remove chlorophyll and waxes and freeze dried for 48 h. The samples were then treated with a 1% pepsin - 0.1 N HCl solution for 48 h at 39°C according to the procedure of Routley and Sullivan (1958) to remove protein, followed by centrifugation and freeze drying. The residue was then soxhlet-extracted with 150 ml of a 0.2 N (dry) HCl in dioxane/2, 2-dimethoxy propane solution (6.5:1 v/v) according to the procedure of Bolker and Teraschima (1966) in order to remove lignin. The resultant residue was then washed with fresh dioxane followed by ethylether and air dried.

For ozone delignification, NDF samples (5 g ground or 25 intact sections) were placed in a culture tube fitted with a septum and subjected to an ozone atmosphere generated by a glass micro-ozonizer (Supelco). The procedure was that of Beroza and Bierl (1967) except that the ozonization was performed on dried material. Ozone was introduced into the sample tube until the indicator solution (4 ml of 0.3% tetraphenylcyclopentadieone in CH_2Cl_2 solution) changed color (about 10 min). For experiment 1, the tube was let stand for 24 h and then flushed with nitrogen to remove excess ozone. For experiment 2 the ozone-treated material was not left in ozone for additional time or flushed with nitrogen.

Hydrogen peroxide delignification was carried out according to Gould (1985). One g of ground material or 20 to 40 stem sections were treated with 30 ml of 1% H_2O_2 at room temperature for 6 h. The pH was adjusted initially to 11.5 with 50% NaOH and every 30 min thereafter. After 6 h, samples were washed with distilled water and prepared as with $KMnO_4$ for future use.

In vitro fermentation

The dry weight loss of dried, ground material was determined in duplicate tubes after incubation with rumen microorganisms for 48 h followed by incubation with acidic pepsin for 48 h according to the Tilley and Terry (1963) in vitro dry matter digestibility (IVDMD) procedure. The digestibility of intact tissues in 3mm sections after in vitro incubation with rumen microorganism for 48 h was determined by SEM. For both gravimetric and SEM studies, rumen fluid was collected from a ruminally-cannulated steer fed Coastal bermudagrass hay plus 2 kg per day of grain concentrate (74% oats, 10% corn, 15% soybean meal, 0.5% trace minerals, and 0.5% defluorinated phosphate). The rumen fluid was strained through 4 layers of cheese cloth, then mixed with McDougal's (1948) carbonate buffer (1:2 rumen fluid to buffer), and 30 ml was dispensed into 50ml centrifuge tubes. The mixture was purged with CO_2 and the tubes were then capped with a one-way valve to exclude O_2. Fermentation tubes were incubated at 39°C.

Preparation for SEM

Stem sections that were not incubated with rumen fluid and those that were incubated with rumen fluid for 48 h were evaluated and included the following treatments: untreated; neutral detergent-treated fiber (NDF); and NDF sections delignified with $KMnO_4$, dioxane (experiment 1 only), ozone, or H_2O_2 (experiment 2 only). Sections were placed into 4% glutaraldehyde in 0.1 M cacodylate buffer, pH 7.4,

TABLE 1: Reactions of bermudagrass stem tissues for lignin with acid phloroglucinol (AP) and chlorine-sulfite (CS).

		Tissues[1]									
		Epidermis		Sclerenchyma Ring		Vascular Bundle		Cortex		Parenchyma	
Internode Age	Exp. No.	AP	CS	AP	CS	AP	CS	AP	CS	AP	CS
Young	1	+*	+**	+	+	+	+	0	0	0	0
Old	1	+	0	+*	+	+	+	0	+	0	+
Young	2	+	+	+	0	+	+	0	+	0	+
Old	2	+	0	+	0	+	+	0	+	+**	+

[1] + (positive reaction), 0 (no reaction) to stains.
*Reaction not present in all cells. **Slight Reaction in only a few sections.

TABLE 2: Reactions of bermudagrass stem tissues for lignin with acid phloroglucinol (AP) and chlorine-sulfite (CS) after chemical treatment (Experiment 1).

		Tissues[1]									
		Epidermis		Sclerenchyma Ring		Vascular Bundle		Cortex		Parenchyma	
Treatment	Internode Age	AP	CS	AP	CS	AP	CS	AP	CS	AP	CS
NDF	Young	+	+	+	+	+	+	0	+	0	+*
	Old	+	0	+	+	+	+	0	+	0	+
$KMnO_4$	Young	0	0	0	0	0	0	0	0	0	0
	Old	+	0	+	0	+	0	0	0	0	0
Dioxane	Young	0	+	0	+	0	+	0	0	0	0
	Old	0	+	0	+	0	+	0	+*	0	+*
Ozone	Young	+	+	+*	+*	+	+	0	0	0	0
	Old	+	+	+*	+*	+	+	0	0	0	+*

[1] + (positive reaction), 0 (no reaction) to stains. *Not all cells stained.

at 8°C and fixed for several days. Sections were then postfixed in 1.5% OsO_4 buffered as above for 4 h at 8°C. Sections in experiment 1 were rinsed with 0.1 M cacodylate buffer and air-dried. Because of partial collapse of the parenchyma cells noted in experiment 1, stem sections in experiment 2 were critical point dried in liquid CO_2 after dehydration in a graded ethanol series. Dried sections were adhered to aluminum stubs, coated with Au-Pd alloy, and examined in a Philips 505 T scanning electron microscope at 15 kV.

Results

Histological tests for lignin revealed differences between the young and old internodes in experiment 1 (Table 1). In young stems, the epidermis, sclerenchyma ring, and vascular bundle (except phloem) were positive (+) or slightly positive (±) for both AP and CS, whereas the cortex and parenchyma did not stain for lignin. In old stems, the epidermis, sclerenchyma ring, and vascular tissue (except phloem) were intensely positive for lignin with AP, with a CS+ reaction also occurring in the cortex and the centrifugal cells of the parenchyma. Although internodes from similar positions on the plants were chosen in experiment 2, the second internode samples gave reactions indicative of an older age than young stems of experiment 1, with a positive reaction for CS occurring in the cortex and parenchyma for both ages of stems (Table 1).

Internodes of experiment 1 that had been chemically treated to remove lignin were tested for histological reactions for lignin (Table 2). Reactions for NDF were similar to those in untreated stems, except that a slight or partial reaction with CS occurred in young cortex and parenchyma. All delignifying treatments reduced the reactions in

lignified tissues, but results varied for individual treatments. $KMnO_4$ resulted in the least reaction for lignin, with no reaction in young internodes and only AP+ reactions in epidermis, sclerenchyma ring, and vascular tissues in old stems. Dioxane resulted in CS+ reactions only, with reactions occurring mostly in the epidermis, sclerencyma ring, vascular tissue, and in old cortex and parenchyma tissues. Ozone reduced the lignin reactions in AP+ and CS+ tissues. A reaction with CS in the epidermis after dioxane or ozone treatment compared with the lack of a reaction in control material (Table 2) may indicate that a greater availability or different phenolic entities occurred after treatment, resulting in a stronger histological reaction. While not as rigorously evaluated, H_2O_2 - treated stem sections from experiment 2 showed that this delignifying agent also reduced the AP reaction for lignin compared with NDF samples.

TABLE 3: Dry weight loss of NDF due to chemical extraction.

Chemical treatment	Internode age	% dry weight loss Experiment 1	Experiment 2
$KMnO_4$	Young	23.3+0.3	28.7+0.7
	Old	20.2±0.6	27.7±0.9
Dioxane	Young	19.8[1]	ND
	Old	16.1	ND
Ozone	Young	0	0
	Old	0	0
H_2O_2	Young	ND	33.4+0.4
	Old	ND	34.9±0.2

[1]Bulked samples and no standard deviation.
ND = Not determined

The delignifying chemicals removed variable amounts of materials on a dry weight basis from the ground NDF sample (Table 3). $KMnO_4$ removed an average of 25% while H_2O_2 removed an average of 34% and dioxane an average of 18%; ozone resulted in virtually no dry weight loss. In all but the H_2O_2 treatment, old internodes gave up less dry matter during extraction than did young internodes, but differences were small (1 to 4 percentage units).

The dry matter digestibilities of untreated and delignified NDF by rumen microorganisms are shown in Table 4. The old stems in both experiments were less digestible than young ones, but material of each age in experiment 2 was less digestible than that for the corresponding position in experiment 1. All chemical treatments improved the IVDMD of the resulting fiber with old stems showing more improvement for all treatments. However, the degree of improvement varied markedly with treatments (Table 4) and further improvement might be possible under optimum conditions. $KMnO_4$ resulted in the greatest improvement in digestibility for both ages of samples and for both experiments.

SEM showed the responses of individual tissues to chemical treatment and to incubation with rumen microorganisms (Figs. 1-10). In experiment 1 (without critical point drying) most of the tissues in the top stems were intact and easily recognized; however, often the parenchyma tissues were collapsed. The NDF stems (Fig. 1a) were similar to untreated sections (not shown). Incubation with rumen fluid for 48 h resulted in loss of parenchyma, phloem, and cortex (Fig. 1b). $KMnO_4$ produced marked distortion and collapse of tissues such that only small parts of the stem could be recognized (Fig. 2a). That cell wall material had been markedly altered was confirmed by the substantial destruction of the stems and removal of all but the most rigid tissue after incubation in rumen fluid (Fig. 2b) and the recovery of mostly small pieces after fermentation. Treatment of top stems with dioxane (Fig. 3a) and ozone (Figs. 4a) produced distortion and collapse in tissues,

TABLE 4: IVDMD of NDF bermudagrass stems treated with delignifying agents.

Chemical treatment	Internode Age	IVDMD Experiment 1 %	% increase of NDF	Experiment 2 %	% increase of NDF
NDF	Young	58.7+9.5		49.6+0.8	
	Old	43.0±0.7		39.6±0.0	
$KMnO_4$	Young	73.5+0.6	25	66.0+2.6	33
	Old	59.6±2.6	39	69.2±1.1	75
Dioxane	Young	61.7+1.6	5	ND	ND
	Old	59.7±1.3	39	ND	ND
Ozone	Young	63.5+1.4	8	50.3+0.1	1
	Old	ND	ND	50.0±0.4	26
H_2O_2	Young	ND	ND	56.6+0.4	14
	Old	ND	ND	54.7±0.0	38

ND = Not determined

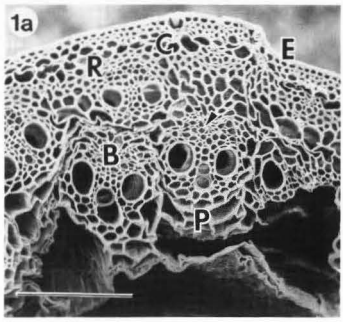

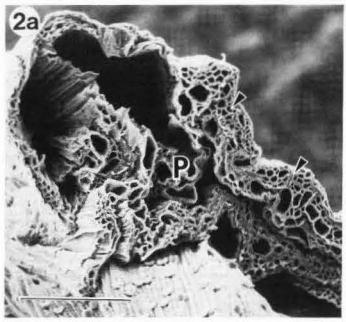

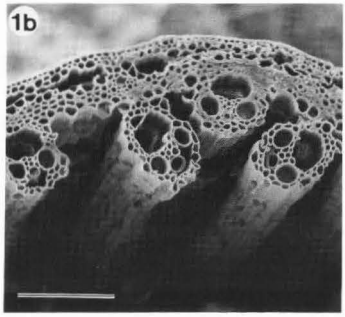

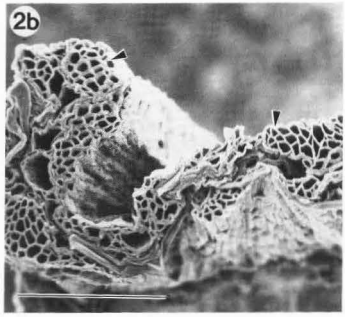

Figure 1. Young internode of NDF. (a). No incubation. All tissues are present but parenchyma is distorted. E = epidermis, C = cortex, R = sclerenchyma ring, B = vascular bundle, P = parenchyma, arrow points to phloem. (b). Incubated with rumen fluid. Parenchyma, phloem, and much of cortex is degraded leaving a residue of epidermis, sclerenchyma ring, and lignified vascular tissue. Bar = 100 μm.

Figure 2. Young internode of NDF treated with $KMnO_4$. (a). No incubation. Tissues are markedly distorted with portions of sclerenchyma ring (arrows) and parenchyma (P) distinguishable. (b). Incubated with rumen fluid. Sclerenchyma ring (arrows) is distinguished but other tissues are disrupted beyond recognition. Bar = 100 μm.

particularly in parenchyma. Microbial fermentation of stems treated with dioxane (Fig. 3b) and ozone (Fig. 4b) showed that only epidermis, sclerenchyma ring, and vascular tissue comprised the residue, with some parenchyma and cortex remaining in some of dioxane-treated stems. Ozone treatment followed by microbial fermentation produced a stem residue in which the extremely resistant xylem cells were partially broken down (Fig. 4b), indicating that this treatment resulted in more breakdown of the most resistant tissues than did dioxane. The H_2O_2 treatment (Figs. 5a,b) resulted in removal of phloem and portions of the parenchyma and appeared less disruptive than other treatments perhaps because of the more rigid nature of the parenchyma in this sample.

In old stems, NDF responded the same as the untreated sections. Microbial fermentation of NDF stems resulted in removal of the phloem and portions of the cortex and parenchyma (Figs. 6a,b). Parenchyma centrifugal to the stem center was less available than that near the center, and the lack of digestion in this tissue is consistent with CS+ reactions for lignin (Table 1). As in young stems, $KMnO_4$ of old stems resulted in marked distortion and collapse of tissues (Fig. 7a) and removal or partial destruction after microbial fermentation of all but the epidermis and sclerenchyma ring; the vascular bundles were especially affected (Fig. 7b).

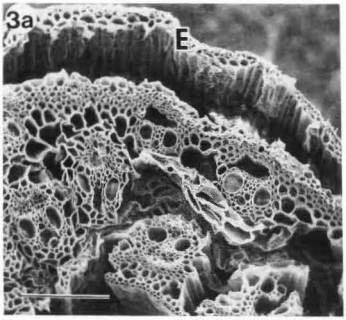
3a
E

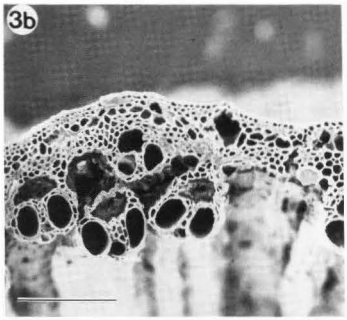
3b

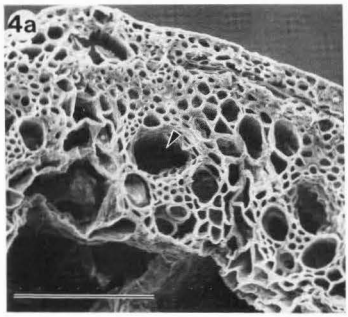
4a

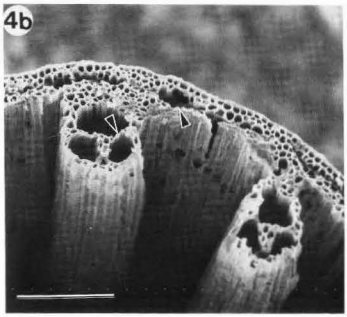
4b

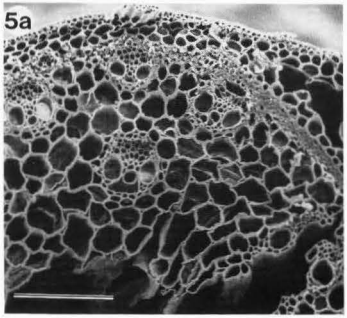
5a

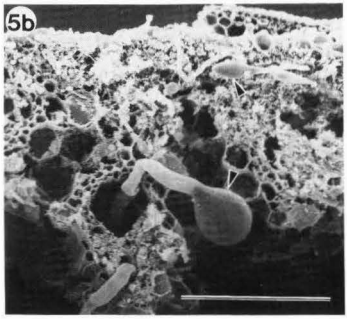
5b

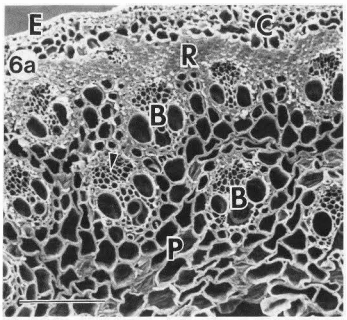

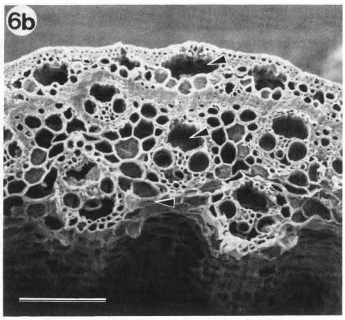

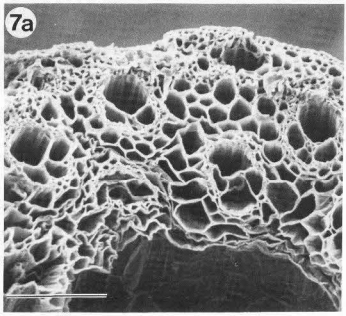

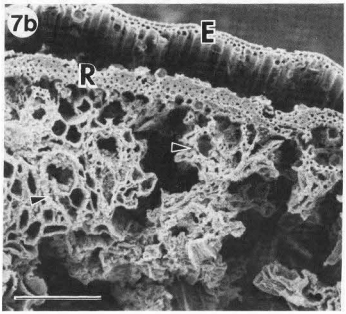

Figure 3. Young internode of NDF treated with dioxane. (a). No incubation. Tissues are mostly present, but parenchyma is collapsed. The epidermis (E) is separated from the remainder of the stem in places, and the whole section is cracked possibly due to air-drying and physical damage during handling. (b). Incubated with rumen fluid. Only epidermis, sclerenchyma ring, and lignified vascular tissue remain, and parenchyma, phloem, and cortex are removed. Bar = 100 μm.

Figure 4. Young internode of NDF treated with ozone. (a). No incubation. Tissues are distorted and phloem (arrow) and parenchyma are removed in some areas. (b). Incubated with rumen fluid. The residue consists of epidermis, sclerenchyma ring, and lignified vascular tissue; the latter two tissues show some evidence of attack (arrows). Bar = 100 μm.

Figure 5. Young internode of NDF treated with H_2O_2. (a). No incubation. All tissues are intact. (b). Incubated with rumen fluid. Degradation of phloem and parenchyma occurred. Rumen fungi are prevalent as shown by the sporangia (arrows). Bar = 100 μm.

Figure 6. Old internode of NDF. (a). No incubation. All tissues are intact, but the parenchyma is distorted. E = epidermis, C = cortex, R = sclerenchyma ring, B = vascular bundle, P = parenchyma, arrow points to phloem. (b). Incubation with rumen fluid. Degradation occurred in the phloem, parts of the cortex, and the centripetal regions of the parenchyma (arrows). Bar = 100 μm.

Figure 7. Old internode of NDF treated with $KMnO_4$. (a). No incubation. Tissues are distorted but intact, except for the loss of phloem. (b). Incubation with rumen fluid. Epidermis (E) and the sclerenchyma ring (R) are intact, but the lignified vascular tissue (arrows) is disrupted. The cortex and a large portion of the parenchyma is removed. Bar = 100 μm.

Marked destruction of tissues subjected to $KMnO_4$ and microbial fermentation occurred in both experiments. Treatment with dioxane (Fig. 8), ozone (Fig. 9), or H_2O_2 (Fig. 10) resulted in removal of phloem and partial degradation of cortex and parenchyma, leaving a residue of epidermis, sclerenchyma ring, vascular tissue, and parts of the parenchyma. Ozone treatment in experiment 1 (Fig. 9) resulted in marked destruction of parenchyma and a greater breakdown of the vascular bundle (Fig. 9b) than with all other treatments except $KMnO_4$. However, stems in experiment 2 did not show this marked destruction of vascular tissue but resembled more the tissue after dioxane or H_2O_2 treatment. The shorter time of treatment and more mature sample in experiment 2 could explain this variation in results.

Discussion

While delignifying agents have been used extensively to improve forage digestibility, the effects on plant structure have not been studied to a large extent. Our data showed that $KmnO_4$ resulted in the greatest reduction in histological staining for phenolic compounds, the greatest loss of dry matter, the greatest disruption of lignified tissues, and the greatest improvement in digestibility of resultant fiber from bermudagrass stems. Other workers (Darcy and Belyea, 1980) reported that treatment with permanganate resulted in an increased rate and extent of cellulose degradation in forage grass. $KMnO_4$ has been shown to preferentially extract phenolics from the CS+ tissues in bermudagrass stems, making them totally digestible (Akin et al., 1985). We have shown in this study that $KMnO_4$ disrupted the AP+ tissues even though some of them still resisted microbial utilization. All of the other three delignifying agents have been shown to improve fiber utilization (Han et al., 1975; Bunting et al., 1984; Kerley et al., 1985). SEM indicated that ozone disrupted parts of the AP+ tissues (i.e., vascular bundles), resulting in more apparent destruction of these lignified cell walls than dioxane or H_2O_2. It has been reported that ozone can oxidize lignin and thereby disrupt the lignocellulose complex (Bunting et al., 1984). Our data suggested that the more resistant AP+ tissues in bermudagrass stems, however, still were not made available to microbial digestion with our method of ozone treatment. Nonetheless, the destruction of vascular tissue with ozone in experiment 1 shows potential for this treatment and it should be explored further. Recently, alkaline peroxide delignification has been used to disrupt the lignocellulose complex (Gould, 1985) and the treatment increased the fermentability of wheat straw (Kerley et al., 1985). SEM of H_2O_2 - treated wheat straw indicates that the plant structure was extensively disrupted, and that bacterial colonization of fiber was improved (Kerley et al., 1985). However, as with dioxane and ozone for the most part, AP+ tissues were often resistant to microbial utilization in H_2O_2 - treated bermuda stems.

Conclusions

Bermuda stems increase in lignification with age, and an increase in the CS+ reaction in the cortex and parenchyma is the most notable change in histological reactions. Various chemical treatments to delignify fiber have resulted in marked improvement in degradation of the cortex and parenchyma, with total degradation in some treatments. The AP+ tissues (i.e., epidermis, sclerenchyma ring, and vascular tissue) are the most resistant tissues, and none of the delignifying agents resulted in total microbial breakdown of these tissues. Observations by SEM on plant cell wall destruction related closely to gravimetric losses for the delignifying agents.

Research to reduce the amount of AP+ tissues in stems or to delay CS+ lignification in parenchyma with maturity would appear to be profitable avenues to explore for improving forage quality. Research to optimize the ozone method might prove especially useful, since this treatment appeared to partially degrade the most resistant, AP+ tissues. Treatments that degrade lignin may produce soluble phenolic compounds that are toxic to rumen microorganisms, and this aspect should not be overlooked in studies to enhance forage utilization.

References

1. Akin DE. (1979). Microscopic evaluation of forage digestion by rumen microorganisms - a review. J. Anim. Sci. 48, 701-710.

2. Akin DE, Brown RH, Rigsby LL. (1984). Digestion of stem tissues in Panicum species. Crop Sci. 24, 769-773.

3. Akin DE, Willemse MTM, Barton II FE (1985). Histochemical reactions, autofluorescence, and rumen microbial degradation of tissues in untreated and delignified bermudagrass stems. Crop Sci. 25, 901-905.

4. Barton II FE, Akin DE. (1977). Digestibility of delignified forage cell walls. J. Agric. Food Chem. 25, 1299-1303.

5. Barton II FE, Akin DE, Windham WR, Himmelsbach DS. (1983). Methods of forage analysis - quantitative and qualitative aspects. In: Wood and Agricultural Residues, E.J. Soltes (ed.), Academic Press, NY, 167-202.

6. Barton II FE, Amos HE, Burdick D, Wilson RL. (1976). Relationship of chemical analysis to in

Figure 8. Old internode of NDF treated with dioxane. (a). No incubation. Tissues are intact, but parenchyma is distorted. (b). Incubation with rumen fluid. Only phloem and parts of the cortex and parenchyma are degraded. Bar = 100 μm.

Figure 9. Old internode of NDF treated with ozone. (a). No incubation. Tissues are intact, except for the loss of phloem. Starch granules are prevalent on the section surface. (b). Incubated with rumen fluid. Phloem Cortex, and parenchyma are virtually all degraded. The lignified cells of the vascular bundles also show partial degradation (arrows). Bar = 100 μm.

Figure 10. Old internode of NDF treated with H_2O_2. (a). No incubation. All tissues are intact. (b). Incubated with rumen fluid. Degradation occurred in the cortex and the centripetal parts of the parenchyma. An obvious microbial mat covers the stem surface. Bar = 100 μm.

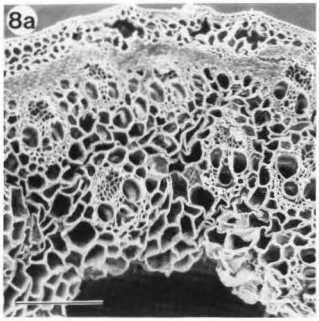
8a

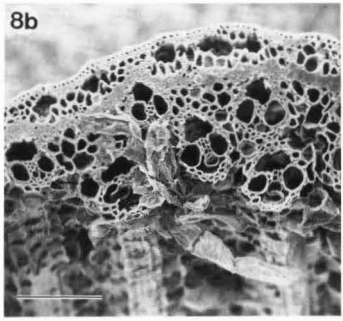
8b

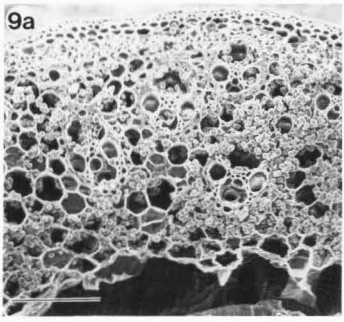
9a

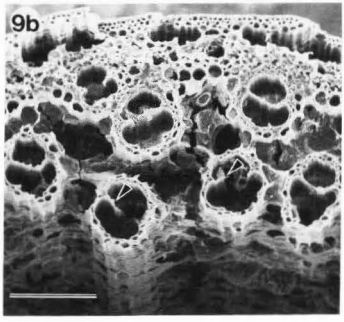
9b

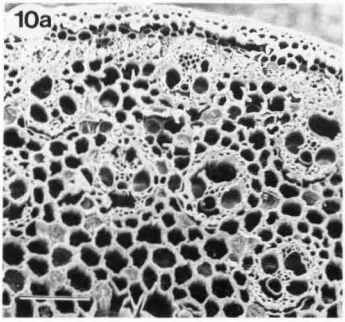
10a

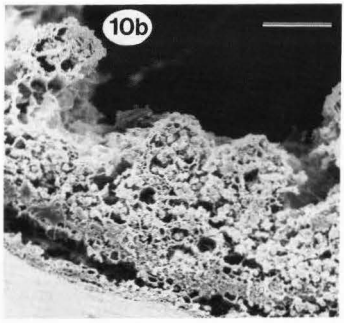
10b

vitro digestibility for selected tropical and temperate grasses. J. Anim. Sci. 43, 504-512.

7. Ben-Ghedalia D, Miron J. (1981). The effect of combined chemical and enzyme treatments on the saccharification and in vitro digestion rate of wheat straw. Biotech. Bioeng. 23, 823-831.

8. Beroza M, Bierl BA. (1967). Rapid determination of olefin position in organic compounds in microgram range by ozonolysis and gas chromatography. Anal. Chem. 39, 1131-1135.

9. Bolker HI, Teraschima N. (1966). Infrared spectroscopy of lignins. IV. Isolation of lignins by solvolysis in acetals. In: Lignin Structure and Reactions (Advances in Chemistry Series 59). American Chemical Society, Washington, DC, 110-124.

10. Bunting LD, Richardson CR, Tock RW. (1984). Digestibility of ozone-treated sorghum stover by ruminants. J. Agric. Sci., Camb. 102, 747-750.

11. Darcy BK, Belyea RL. (1980). Effect of delignification upon in vitro digestion of forage cellulose. J. Anim. Sci. 51, 798-803.

12. Demarquilly C, Jarrige R. (1974). The comparative nutritive value of grasses and legumes. Vaxtodling 28, 33-41.

13. Gould JM. (1985). Studies on the mechanism of alkaline peroxide delignification of agricultural residues. Biotech. Bioeng. 27, 225-231.

14. Han YW, Lee JS, Anderson AW. (1975). Chemical composition and digestibility of ryegrass straw. J. Agric. Food Chem. 23, 928-931.

15. Hanna WW, Monson WG, Burton GW. (1976). Histological and in vitro digestion study of 1- and 4-week stems and leaves from high and low quality bermudagrass genotypes. Agron. J. 68, 219-222.

16. Harbers LH. (1985). Ultrastructural utilization of plants by herbivores. Food Microstruc. 4, 357-364.

17. Hendricksen RE, Poppi DP, Minson DJ. (1981). The voluntary intake, digestibility and retention time by cattle and sheep of stem and leaf fractions of a tropical legume (Lablab purpureus). Aust. J. Agric. Res. 32, 389-398.

18. Himmelsbach DS, Barton II FE. (1980). ^{13}C nuclear magnetic resonance of grass lignins. J. Agric. Food Chem. 28, 1203-1208.

19. Jensen WA. (1962). Botanical Histochemistry, W H Freeman and Co., San Francisco, 205.

20. Kerley MS, Fahey Jr GC, Berger LL, Gould JM, Baker FL. (1985). Alkaline hydrogen peroxide treatment unlocks energy in agricultural by-products. Science 230, 820-822.

21. Laredo MA, Minson DJ. (1973). The voluntary intake, digestibility, and retention time by sheep of leaf and stem fractions of five grasses. Aust. J. Agric. Res. 24, 875-888.

22. McDougall EI. (1948). Studies on ruminant saliva. I. The composition and output of sheep's saliva. Biochem. J. 43, 99-109.

23. Pigden WJ. (1953). The relation of lignin, cellulose, protein, starch and ether extract to the "curing" of range grasses. Can. J. Agric. Sci. 33, 364-378.

24. Routley DG, Sullivan JT. (1958). The isolation and analysis of hemicellulose of bromegrass. J. Agric. Food Chem. 6, 687-692.

25. Spencer RR, Akin DE, Rigsby LL. (1984). Degradation of potassium hydroxide-treated 'Coastal' bermudagrass stems at two stages of maturity. Agron. J. 76, 819-824.

26. Tilley JMA, Terry RA. (1963). A two-stage technique for the in vitro digestibility of forage crops. J. Brit. Grassld. Soc. 18, 104-111.

27. Vance CP, Kirk TK, Sherwood RT. (1980). Lignification as a mechanism of disease resistance. Ann. Rev. Phytopathol. 18, 259-288.

28. Van Soest PJ. (1973). The uniformity and nutritive availability of cellulose. Fed. Proc. 32, 1804-1808.

29. Van Soest PJ, Wine RH. (1967). Use of detergents in the analysis of fibrous feeds. IV. Determination of plant cell wall constituents. J. Assn. Official Agric. Chem. 50, 50-55.

30. Van Soest PJ, Wine RH. (1968). Determination of lignin and cellulose in acid detergent fiber with permanganate. J. Assn. Official Agric. Chem. 51, 780-785.

31. Waldo DR, Smith LW, Cox EL. (1972). Model of cellulose disappearance from the rumen. J. Dairy Sci. 55, 125-129.

Discussion with Reviewers

M. J. Gould: Kerley et al. (1985) noted that delignification of wheat straw by alkaline hydrogen peroxide treatment resulted in a dramatic increase in the attachment of rumen microorganisms to the straw surface. The data in this paper seem to show a similar effect with peroxide treated bermudagrass (e.g., Fig. 10). From the micrographs presented, it appears that the other delignifying treatments tested do not cause a similar increase in bacterial attachment. To what factors do the authors attribute this difference, and is it likely to be of significance in vivo, where attachment of bacteria to cellulosic particles is thought to be important for efficient cell wall degradation?

Authors: In our study there was a difference between experiment 1 and 2 in the microbial mass that covered stem surfaces, probably due to the difference in inocula for these two studies. Sections delignified with other treatments and incubated with inocula from experiment 2 also were covered with microorganisms. In our study, the microbial mass on H_2O_2 treated bermudagrass does not appear to be significant for this treatment, and the IVDMD data (Table 4) appear to confirm this. It is our opinion that one should use care in interpreting a microbial cover as attached, active fiber-degrading microorganisms, because at times it may just indicate debris from the inoculum. Methods other than SEM should be used to verify true attachment of cells.

W. W. Hanna: Except for SEM pictures, how does permanganate stem digestion in this study differ from the Akin et al. (1985) paper? To me, both papers provide the same information.

Authors: $KMnO_4$ treatment did cause similar results in other studies. We felt that in order to have a true comparison of the methods to delignify stems, plant material from a common source should be used as we did for this study. We also felt that, since $KMnO_4$ delignification is widely used, information presented along with other treatments would permit a side-by-side comparison by the readers.

L. H. Harbers: The difference in histological reactions between samples for experiments 1 and 2 are interesting. Would environmental factors such as

temperature and rainfall influence rate of lignification?

Authors: Increased growth temperatures have been shown in several studies to result in lower forage digestibility, and often a concomitant increase in lignification occurs. Results of studies on moisture are less consistent. Extreme moisture stress has resulted in increased lignification and depressed digestibility, whereas moderate stress resulted in improved digestibility. With all aspects, it should be remembered that different plants may respond in different ways to environmental stress. It is likely that our bermudagrass samples from experiments 1 and 2 were exposed to different environmental stresses because internodes from experiment 2, even though from similar positions of 6 week old plants, appeared more mature and were 4 to 9 units lower in IVDMD.

L. H. Harbers: It is apparent from your studies that syringyl-type lignin is produced in mature stem parenchyma. Could this lignification be controlled genetically or will we have to rely on early harvest and/or chemical treatment of those types of grasses?

Authors: Some research has been done that suggests that plant cultivars can be developed with reduced lignin in the parenchyma and greater digestibility. It is possible that research which focuses on delayed maturity and reduced lignification in whole plants would result in hybrids of bioengineered plants in which the parenchyma is more digestible and that consumption by ruminants would be improved. Alternately, cultivars of some species have been developed with reduced numbers of vascular bundles in the stem with a resultant increase in stem digestibility. Therefore, it appears that lignin in stems can be manipulated genetically, and efforts to reduce lignin or lignified tissues should be pursued.

Scanning Microscopy International

(Previously Scanning Electron Microscopy, Inc.)

This not-for-profit organization pursues the following goals.
(a). Promotion of advancement of science of scanned image microscopy methods and related microscopy and microanalysis techniques. (b). Promotion of applications of these techniques in existing and new areas. (c). Promotion of these techniques so that their users obtain the best information of the highest quality.

The organization attempts to fulfill its goals by sponsoring meetings, including an annual meeting (in May, see below), and Pfefferkorn Conferences devoted to basic topics in electron microscopy (see below); and by publishing (i) the journal Scanning Microscopy (previously Scanning Electron Microscopy (Major Subject Indexes available on request), (ii) Food Microstructure (a semi-annual journal), (iii) the Proceedings of the Pfefferkorn Conferences (to be published as a supplement to Scanning Microscopy from 1987: 1st supplement on "Physical Aspects of Microscopic Characterization of Materials, in preparation), and (iv) related publications; (see current list of publications, over). Suggestions on other activities which may be undertaken to fulfill the above goals may be communicated to any one of the following persons:

John D. Fairing, President, Scanning Microscopy International
809 Westwood Drive, Ballwin, MO 63011 Phone: 314 227 8939
Robert P. Becker, Vice-President, Scanning Microscopy International
1S640 Brook Court, Glen Ellyn, IL 60137 Phone: 312 996 7215
Om Johari Secretary-Treasurer, Scanning Microscopy International, and Director of Meetings
AMF O'Hare (Chicago), IL 60666-0507 Phone: 312 529 6677
Godfried M. Roomans Advisor, and European Editor
Dept. Anatomy, Box 571, Univ. Uppsala, S-75123 Uppsala, Sweden (new address effective July 1, 1987).

1988 Annual Meeting

1988 Annual Meeting will take place from May 1 to 6 at Saint Louis, Missouri. Programs in most of the 1987 meeting areas (program available on request) will be planned; suggestions for new program topics are invited. The next Food Microstructure meeting will be at Reading, England, during Sept. 20-22, 1988.

Seventh Pfefferkorn Conference on Science of Biological Specimen Preparation

The 1988 Pfefferkorn Conference will take place from Sept. 11 to 16 in England. The **Organizers** are: **Ralph M. Albrecht., Ph.D**, Univ. - Dept. Vet. Sci., 1655 Linden Drive, Madison, WI 53706; **Gareth Griffiths, Ph.D.**, Euro. Molecular Biol. Lab., P.F. 102209, D-6900 Heidelburg 1, West Germany; **Prof. Edward Kellenberger**, Biozentrum der Univ., Klingelbergstr. 70, CH-4056 Basel, Switzerland; and **Richard L. Ornberg, Ph.D.**, National Institutes of Health, Bldg.8 - Room 420 - NIDDK, Bethesda, MD, 20892. For details of proceedings of the past conferences on this theme (1983 and 1985) see over.

SCANNING MICROSCOPY

A quarterly international journal of scanning electron microscopy, other scanning microscopies, related techniques, and applications

In recent years scanned image microscopy has reached unparalleled levels of use and recognition due to its versatile, interaction-dependent imaging and / or microanalysis facility. While the widest use of scanned image microscopy to date has been as scanning electron microscopy (SEM), investigators, in ever increasing numbers, are using the scanning function in conjunction with other probes (such as, protons and ions), and with imaging modes based on emissions of radiation other than electrons. One is cognizant, for example, of images based on ionic, X-ray, visible light, and acoustic signals emanating from samples. In keeping with the increased use of "other" scanning microscopies, this journal formally broadened its publishing purvey in 1987 to include all scanned image microscopies. This broadened editorial policy was, in part, manifested by the modification of the journal title from **Scanning Electron Microscopy** to simply **Scanning Microscopy** beginning with the March 1987 issue. We now solicit papers dealing with "scanning electron microscopy, other scanning microscopies, related techniques, and applications" (per instructions, available on request). This editorial change was celebrated by a change in the format from hard cover to soft cover, and a change in volume enumeration. The new organization name is: Scanning Microscopy International. The reviewing procedures and the "Discussion with Reviewers" features are retained, and as in the past, all efforts will be continually made to promptly publish papers with high quality reproduction of micrographs.

Volume 1, number 1 (for March 1987) and volume 1 number 2 (for June 1987) have been distributed. Major Subject Indexes are available on request. The new journal, beginning with this first issue, is also being **listed in Current Contents / Life Sciences.**

For Additional Information about programs and publications contact Om Johari or Godfried M. Roomans.

Scanning Microscopy International

(Previously Scanning Electron Microscopy, Inc.)

c/o Dr. Om Johari, Chicago (AMF O'Hare), IL 60666-0507, USA. Phone: 312 529-6677

COMPLETE CURRENT LIST OF PUBLICATIONS

(i) Journal "Scanning Microscopy" (ISSN: 0891-7035)

In 1987, publication of the quarterly journal Scanning Microscopy (with Vol. 1, No. 1) has begun. This journal was previously published as Scanning Electron Microscopy (see below).

The subscription price for 1987 is $109.00 per year (U.S. delivery), $119.00 (elsewhere).

(ii) Journal "Scanning Electron Microscopy" (ISSN: 0586-5581), now discontinued.

Up to 1986 the **quarterly** journal "Scanning Electron Microscopy" was published.

Tables of Contents are separately available at $1.00 **per part.** ($4.00 per year).

Prices for SEM/1980 to 1986, per year:	**U.S. Delivery**	**Elsewhere**
☐ Complete Set (Parts 1-4)	$109.00	$119.00
☐ any 2 different parts/same year	$ 84.00	$ 87.50
☐ any 1 part, also for 1979	$ 52.00	$ 55.00
SEM/1978 & 1979:		
☐ 1979(I+II) (Part III out of print)	$ 65.00	$ 71.50
☐ 1978/I (physical) or	$ 37.00	$ 41.00
☐ 1978/II (biology)	$ 40.00	$ 45.00
☐ 1978/2 part set	$ 67.50	$ 74.00

(iii) Proceedings of "Pfefferkorn Conferences" (hardbound):

1st — 1982: Electron Beam Interactions with Solids for Microscopy, Microanalysis and Microlithography. *31 Papers, 372 pages. Price: $51.00 (U.S. delivery), $54.00 (elsewhere).*

2nd — 1983: The Science of Biological Specimen Preparation for Microscopy and Microanalysis. *28 Papers, 246 Pages. Price: $40.00 (U.S. delivery), $43.00 (elsewhere).*

3rd — 1984: Electron Optical Systems for Microscopy, Microanalysis, and Microlithography. *27 Papers, 272 Pages. Price: $44.00 (U.S. delivery), $47.00 (elsewhere).*

4th — 1985: The Science of Biological Specimen Preparation for Microscopy and Microanalysis 1985. *30 Papers, 307 Pages. Price: $46.00 (U.S. delivery), $50.00 (elsewhere).*

(iv) Special Books Derived from SEM Volumes (soft cover):

1. Scanning Electron Microscopy Studies of Embryogenesis — 30 papers from SEM/1978 to 1985 (364 pages). *Price: $36.00 (U.S. delivery), $40.00 (elsewhere).*

2. The Integument: Scanning Electron Microscopy in Skin Biology — 31 papers from SEM/1978 to 1985 (294 pages). *Price $34.00 (U.S. delivery), $37.00 (elsewhere).*

3. Preparation of Biological Specimens for Scanning Electron Microscopy — 22 papers from SEM/1978 to 1984 (352 pages). *Price $32.00 (U.S. delivery), $35.00 (elsewhere).*

4. SEM of Cells in Culture — 30 papers from SEM/1978 to 1983 (320 pages). *Price $29.00 (U.S. delivery), $32.00 (elsewhere).*

5. Basic Methods in Biological X-ray Microanalysis — 20 papers from SEM/1979 to 1982 (284 pages). *Price $22.00 (U.S. delivery), $25.00 (elsewhere).*

6. Ultrastructural Effects of Radiation on Tissues & Cells — 17 papers from SEM/1981 & 1982. *Price $18.00 (U.S. delivery), $20.50 (elsewhere).*

7. Cell Surface Labeling — 10 papers from SEM/1979. *Price $10.00 (U.S. delivery), $12.00 (elsewhere).*

8. Clinical Applications of the SEM — 3 papers from SEM/1980. *Price $10.00.*

9. Brain Ventricular Surfaces — 18 papers from SEM/1978. *Price $14.95 (U.S. delivery) and $17.00 (elsewhere).*

(v) Food Microstructure (ISSN: 0730-5419)

The subscription to the **semi-annual** international journal "Food Microstructure" is $50.00 (U.S. delivery), $55.00 (elsewhere) for 1982 to 1987, per year.

Studies of Food Microstructure — A hardbound book with 36 papers from SEM/1979, 1980 and 1981. *Price $49.00 (U.S. delivery), $52.00 elsewhere.*

Reprints (or copies) of papers from SEM publications are available at $5.00.

REVIEWERS LIST

The help of the following reviewers with papers included in this issue of Food Microstructure is gratefully acknowledged.

Akin, D.E.	USDA Russell Agri. Res. Ctr., Athens, GA
Bagley, E.B.	USDA No. Reg. Res. Lab., Peoria, IL
Buchheim, W.	Bundes. Milchforschung, Kiel, West Germany
Carpenter, D.E.	Kraft Research & Dev. Lab., Glenview, IL
Carroll, R.J.	Retired from USDA Res. Lab., Philadelphia, PA
Christianson, D.D.	USDA No. Reg. Res. Lab., Peoria, IL
Coyne, D.P.	University of Nebraska, Lincoln
Davis, E.A.	University of Minnesota, Saint Paul
deMan, J.M.	University of Guelph, Ont., Canada
Dylewski, D.P.	Kraft Research & Dev. Lab., Glenview, IL
Emmons, D.B.	Agriculture Canada, Ottawa, Ont.
Gould, J.M.	USDA No. Reg. Res. Lab., Peoria, IL
Hanna, W.W.	USDA Coastal Plains Exp. St., Tifton, GA
Harbers, L.H.	Kansas State University, Manhattan
Heathcock, J.F.	Cadbury Schweppes, Reading, U.K.
Hermansson, A.-M.	Swedish Food Research Institute, Goteborg
Hernqvist, L.	University of Lund, Sweden
Holcomb, D.N.	Kraft Research & Dev. Lab., Glenview, IL
Holley, R.A.	Agriculture Canada, Ottawa, Ont.
Jasinski, E.M.	Pennsylvania State Univ., Univ. Park
Kalab, M.	Agriculture Canada, Ottawa, Ont.
Lanier, T.C.	No. Carolina State Univ., Raleigh
Larsson, K.	University of Lund, Sweden
Matsuo, R.R.	Agriculture Canada, Winnipeg, Man.
McDonald, I.J.	National Research Council, Ottawa, Canada
Nath, K.R.	Kraft Research & Dev. Lab., Glenview, IL
Rinker, D.L.	Ontario Min. Agr. & Food, Vineland Sta., Canada
Seib, P.A.	Kansas State University, Manhattan
Stemberger, B.H.	Pennsylvania State Univ., Univ. Park
Swanson, B.G.	Washington State Univ., Pullman
Tung, M.A.	Technical Univ. Nova Scot., Halifax, Canada
Van Soest, P.J.	Cornell University, Ithaca, NY
Walstra, P.	Agriculture Univ., Wageningen, Netherlands
Wolf, W.J.	USDA No. Reg. Res. Lab., Peoria, IL
Yiu, S.H.	Agriculture Canada, Ottawa, Ont.

Call for Reviewers

The contributions of reviewers to the quality and content of this journal are very significant. We invite qualified reviewers in the areas covered by our journal [see Table of Contents of this issue; Major Subject Index for vol. 5 in vol. 5, no. 2 (1986); and Major Subject Index in vol 4, no. 2 (1985) for all food related papers published during 1979 to 1985 by our organization] to request a mailing list form for suggesting themselves as reviewers.

FOOD MICROSTRUCTURE
INSTRUCTIONS TO AUTHORS

Papers for publication in the international journal Food Microstructure are invited. Papers can cover all types of foods, including vegetables, grains, sea foods, meat, dairy products and others. Topics of interest are: Fundamental aspects of food microstructure such as the molecular and colloidal forces which determine it, and the practical relationship between food microstructure and processing, ingredient changes, shelf life, consumer acceptability, and other food-related areas. Techniques used may include transmission and scanning electron microscopy, light microscopy, x-ray microanalysis, or other related microscopy/microanalytical methods.

Papers for Food Microstructure (FM) may be offered at any time. Papers can be for publication only, or intended for oral presentation at the Annual Food Microstructure meeting in early spring. The latter papers are due two months prior to the start of the meeting; only papers acceptable for publication are allowed oral presentation. Oral presentation of a paper at some other meeting or publication as unreviewed abstract (e.g., in proceedings, etc.) does not preclude consideration of a paper by FM.

The letter accompanying the paper should contain names and complete addresses of at least **four persons competent to review the paper**. Suggested reviewers: **a.** must neither be from author's current or recent affiliations, nor coworkers; **b.** should preferably be active researchers in the field (e.g., whose work is being extensively referred to); and **c.** need not be personally known or contacted by the authors. The editors **will select** the most suitable reviewers irrespective of their location. Each paper will be intensely reviewed by at least three reviewers.

The **initial paper (hereafter referred to as "paper")** should conform to **these Instructions.** However, to be published after reviewing, **the final manuscript (hereafter referred to as "manuscript") should be either a. submitted on the model sheets conforming to the Manuscript Preparation Guidelines (mailed along with the reviewers' comments), or b. sent to SEM Inc. for preparation at a nominal cost (per details mailed with reviews).** In addition to all the text, the **manuscript** may have to contain the author's publishable responses to questions raised by the paper's reviewers (see the Discussion with Reviewers in papers published in FM).

The following types of contributions can be offered. A length limit is not imposed on papers. Short, but complete, papers are welcome.

RESEARCH PAPER: Presents new unpublished findings.

REVIEW PAPER: Includes an extended literature review and complete bibliography, **emphasizes author's new unpublished findings** and in an extended discussion puts the topic in proper perspective.

TUTORIAL PAPER: Contains an **organized comprehensive review** of **ALL** relevant published material as for a teaching lecture.

TECHNICAL TIP: Paper should have no more than 1000 words.

LETTER TO THE EDITOR: Commenting on paper already published in FM.

The author should indicate the type of paper and carefully adhere to the applicable definition, since the reviewers and editors judge the paper accordingly.

INSTRUCTIONS FOR SUBMISSION OF PAPERS

Type paper in **double-spaced** format on standard size paper.

The paper should include title page, abstract, all headings and text. On the **title page** include: **a.** a **short title** which accurately represents the contents of the paper; **b.** an **informative running head** consisting of no more than 50 characters; **c. names and affiliations** of all authors, **name and complete work and home addresses and phone numbers of the person to contact; d. 10 key words/phrases** suitable for subject index; and **e. for review papers, indicate page numbers containing new material** (e.g., "new material will be found on pages __.").

An **Abstract** (of 100-250 words) is required for all papers. The Abstract should be concise and include the purpose of the paper, major results obtained and conclusions. Phrases such as "will be described," "is discussed," "are presented" etc. should be avoided.

The **Introduction** of the paper **must** contain a clear, concise statement of the purpose of the paper and the relationship of this paper to what is already in the literature. As applicable, a **Materials and Methods** section with **complete specimen preparation** information must be included (even if already published elsewhere), so that the work can be duplicated by others.

Equations should be numbered consecutively, using arabic numerals. Each **symbol and abbreviation** should be defined when first used. **SI units must be used;** other metric units or U.S. customary units (English), if used, must be given in parentheses.

REFERENCES

Include all references relevant to paper which are either readily available published works or papers in press. Work in progress, manuscripts submitted or in preparation, unpublished findings, personal communications etc. must be excluded from the reference list but may be acknowledged in the text (in parentheses).

The reference list at the end of the paper must be organized in alphabetical order by the first authors' names. Names of all authors (last names and initials only, with a comma between names and no other punctuation), full titles of papers, appropriate bibliographic information (with standard abbreviations for journals, and editors and publishers for books and proceedings), and inclusive pagination must be included. Availability information must be included for all non-journal references.

When referencing **SEM Inc. publications**, use the following formats only:

SEM Journal: Frederik PM, Busing WM, Persson A. (1984). Surface defects on thin cryosections. Scanning Electron Microsc. 1984; I:433-443.

Food Microstructure: Elgasim EA, Kennick WH. (1982). Effect of high hydrostatic pressure on meat microstructure. Food Microstruc. 1, 75-82.

In the **text, cite references** in one of the following two styles:

a. Cowley (1967) or (Cowley, 1967) or Crewe and Wall (1970). If there are three or more authors, use the form Venables et al. (1978). If more than one paper is published in the same year by the same author (or group of authors) use the form (Rose, 1974a), etc.

b. As long as there is consistency, either superscript[1] or full-size numerals in brackets [1] can be used. In this case, the numbering must be in sequence in the reference list, but the references will generally not appear in sequence in the text.

ILLUSTRATIONS AND TABLES

Number each figure and table with **an arabic numeral and refer to them in sequence in the text.** Several illustrations within a figure must be designated a, b, c, etc. Each table must have a title. ***Each figure must have a caption*** – either on its own page or all captions should be placed together on separate pages. **Very important: Use arrows or letters to identify features referred to, and so indicate in the caption.** Illustrate text with the fewest photographs possible. Indicate magnification on photos by a line of, e.g., 1μm, 10μm, 100μm, or 1 mm length; identify either on the photo or in the caption. Use nm, μm, or mm, not μ, u or -X.

Quality of Illustrations. *Photos should be clear, clean, unscreened* (screened photos are not acceptable), *black and white glossy prints.* **Color photographs** can be published by prior arrangement between author and the managing editor, whereby the author will be asked to pay the additional cost.

Size. For the *manuscript*, illustrations and tables should preferably be 10.5 cm wide. The maximum permissible length for photographs will be 9 cm (3.5"); line drawings and tables may be longer than 9 cm but not wider than 10.5 cm. All letters and symbols on illustrations and tables must be larger than 2.0 mm. **THE ILLUSTRATIONS, TABLES AND LETTERING INCLUDED WITH THE PAPER MUST CONFORM TO THESE SIZES.** *Permission for larger illustrations and/or tables must be requested when the paper is submitted.*

SUBMISSIONS AND COMMUNICATIONS

Submit 4 copies of the paper. Each of the 4 copies must include its own set of illustrations and clear glossy prints of all photographs. (Retain the best set of prints for your manuscript, since illustrations sent with paper may not be returned.) Papers containing photocopies (Xerox, etc.) of photographs will not be processed for reviewing; manuscripts containing photocopies of tables and illustrations are not accepted. All illustrations must be organized in sequence (must not be mounted on cardboards) and placed in separate envelopes. Place each copy of the paper *(together with its envelope of illustrations) in a separate, unsealed, ready-to-mail envelope,* so that the paper can be sent directly to its reviewers.

For **submission** of papers and **inquiries** contact: one of the editors or **Dr. Om Johari**, Managing Editor, **(phone 312-529-6677)**, P.O. Box 66507, AMF O'Hare, IL 60666 USA. (**Street address,** if needed, is: 1034 Alabama Dr., Elk Grove Village, IL 60007, USA).

OTHER IMPORTANT ITEMS

Reprints. 15 complimentary tear sheets are provided. Information for ordering additional reprints is sent with the proofs.

Copyright. Food Microstructure is a copyrighted publication. Letters granting permission to use other copyrighted material must accompany the **manuscript.**

Continued from outside back cover

FOOD MICROSTRUCTURE

An International Journal on the Microstructure and Microanalysis of Foods, Feeds and their Ingredients

VOL. 6, NO. 1 (1987)

TABLE OF CONTENTS

Continued on inside back cover